DOCUMENT RESUME

ED 211 337 SE 035 947

AUTHOR Maxwell, Eugene L.
TITLE Active Remote Sensing of Natural Resources: Course Notes. Science Series No. 5. Final Technical Report.
INSTITUTION Colorado State Univ., Ft. Collins. Coll. of Forestry and Natural Resources.
SPONS AGENCY National Science Foundation, Washington, D.C.
PUB DATE Jun 72
GRANT NSF-GZ-1760
NOTE 304p.; Contains occasional light and fricken type.

EDRS PRICE MF01/PC13 Plus Postage.
DESCRIPTORS College Science; *Course Content; Energy; *Environmental Education; Higher Education; *Interdisciplinary Approach; *Natural Resources; Optics; Physical Environment; Science Curriculum; Science Education; Spectroscopy
IDENTIFIERS *Remote Sensing

ABSTRACT

Presented is a portion of a research project which developed materials for teaching remote sensing of natural resources on an interdisciplinary basis at the graduate level. This volume contains notes developed for a course in active remote sensing. It is concerned with those methods or systems which generate the electromagnetic energy "illuminating" the target or resource to be detected. It attempts to provide guidance in the development of theories to support experimental results, and to bring together information useful to both the engineer and the resource manager. A primary aim of the course is to train students to use their own judgment about the value of a remote sensing system for a particular application. The notes include a short course in electromagnetics and a review of electromagnetic properties of natural materials. These tools are used to study the interaction between natural resource targets and the electromagnetic energy from active systems. Typical images and other types of data are examined to understand experimental results. (Author)

Department of Watershed Sciences
College of Forestry and Natural Resources
Colorado State University
Fort Collins, Colorado 80521

June, 1972

ACTIVE REMOTE SENSING OF NATURAL RESOURCES - COURSE NOTES

Science Series No. 5

Eugene L. Maxwell

This report results from support of NSF Special Projects in Graduate Education Grant GZ-1760

WATERSHED SCIENCES

RELATED MAJOR REPORTS ON REMOTE SENSING OF NATURAL RESOURCES

by Department of Watershed Sciences

DESIGN OF A FIELD SPECTROMETER LABORATORY. R. L. Pearson and L. D. Miller. 1971. Science Series 2, Department of Watershed Sciences, Colorado State University, Fort Collins, Colorado, 102 p. ($5).

THE IMPACT OF REMOTE MULTISPECTRAL SENSING ON URBAN WATERSHED WATER YIELD SIMULATION. R. R. Root and L. D. Miller. 1972. Office of Water Resources Research Completion Report, Environmental Resources Center, Colorado State University, Fort Collins, Colorado, 105 p. ($10 - four color photos).

(In Preparation)

PATTERN RECOGNITION ROUTINES FOR GRADUATE TRAINING IN THE AUTOMATIC ANALYSIS OF REMOTE SENSING IMAGERY - RECOG. J. A. Smith, L. D. Miller, and T. Ells. 1972. Science Series 3A, Department of Watershed Sciences, Colorado State University, Fort Collins, Colorado, 50 p. ($2).

USER'S MANUAL FOR RECOG (Pattern RECOGnition Programs). T. Ells, J. A. Smith, and L. D. Miller. 1972. Science Series 3B, Department of Watershed Sciences, Colorado State University, Fort Collins, Colorado, 75 p. ($3).

PROGRAMMER'S MANUAL FOR RECOG (Pattern RECOGnition Programs). T. Ells, J. A. Smith, and L. D. Miller. 1972. Science Series 3C, Department of Watershed Sciences, Colorado State University, Fort Collins, Colorado, 200 p. ($10).

PASSIVE REMOTE SENSING OF NATURAL RESOURCES/COURSE NOTES. L. D. Miller. 1972. Science Series 4, Department of Watershed Sciences, Colorado State University, Fort Collins, Colorado, 220 p. ($4).

ACTIVE REMOTE SENSING OF NATURAL RESOURCES/COURSE NOTES. E. Maxwell. 1972. Science Series 5, Department of Watershed Sciences, Colorado State University, Fort Collins, Colorado, 200 p, ($4).

RELATED OTHER REPORTS

ANALYSIS OF ENVIRONMENTAL AND VEGETATIVE GRADIENTS IN YELLOWSTONE NATIONAL PARK FROM REMOTE MULTISPECTRAL SENSING. L. D. Miller and C. C. Cooper. 1969. In Remote Sensing in Ecology, University of Georgia Press, Athens, Georgia, pp. 180 - 131 (n.a.).

THE DESIGN OF A LANDSCAPE MODEL, CENTRAL BASIN WATERSHED, R. E. Oliver and L. D. Miller. 1971. International Biological Program, Grassland Biome, Technical Report 89, Colorado State University, Fort Collins, Colorado, 19 p. (n.c.).

n.c. - no charge
n.a. - not available from Watershed Sciences Department
charges shown are for reproduction costs only

RELATED OTHER REPORTS cont.

A FIELD LIGHT QUALITY LABORATORY -- INITIAL EXPERIMENT. L. D. Miller and R. L. Pearson. 1969. Colorado State University, Department of Watershed Sciences, Incidental Report 1, Fort Collins, Colorado, 16 p. (n.c.)

A FIELD LIGHT QUALITY LABORATORY -- INITIAL EXPERIMENT: THE MEASUREMENT OF PERCENT OF FUNCTIONING VEGETATION IN GRASSLAND AREAS BY REMOTE SENSING METHODOLOGY. R. L. Pearson and L. D. Miller. 1971. International Biological Program, Grassland Biome, Technical Report 90, Colorado State University, Fort Collins, Colorado, 24 p. (n.c.).

REMOTE SENSING OF NATURE -- TECHNICAL DOCUMENT LIBRARY/A DETAILED DESCRIPTION OF THE SOFTWARE UTILIZED. J. C. Tucker and L. D. Miller. 1971. Colorado State University, Department of Watershed Sciences, Incidental Report 2, Fort Collins, Colorado, 157 p. ($3).

AERIAL MAPPING PROGRAM OF THE IBP GRASSLAND BIOME: REMOTE SENSING OF THE PRODUCTIVITY OF THE SHORTGRASS PRAIRIE AS IMPUT INTO A BIOSYSTEM MODEL. L. D. Miller and R. L. Pearson. 1971. Proceedings of the Seventh International Symposium on Remote Sensing of the Environment, University of Michigan, Willow Run Laboratories, Ann Arbor, Michigan, pp. 165-207 (n.c.)

REMOTE SPECTRAL MEASUREMENT AS A METHOD FOR DETERMINING PLANT COVERS. R. L. Pearson and L. D. Miller. 1972. International Biological Program, Grassland Biome, Technical Report ?, Colorado State University, Fort Collins, Colorado, 46 p.

(In Preparation)

SPECTRO-OPTICAL CHARACTERISTICS OF SELECTED PLANTS OF THE PAWNEE INTENSIVE SITE MEASURED 'IN SITU'/THE FLOW OF SOLAR ENERGY INTO THE PRIMARY PRODUCERS. C. J. Tucker and L. D. Miller. March, 1972. International Biological Program, Grassland Biome, Technical Report ?, Colorado State University, Fort Collins, Colorado, 70 p.

FIELD SPECTROMETER EXPERIMENTAL DATA -- 1971: SPECTRORADIANCE, SPECTROREFLECTANCE, SPECTROABSORBANCE, AND SPECTROTRANSMISSANCE OF SHORTGRASS PRARIE VEGETATION. L. D. Miller, R. L. Pearson, and J. Tucker, March, 1972. International Biological Program, Grassland Biome, Technical Report ?, Colorado State University, Fort Collins, Colorado, 1200 p.

A WATERSHED TERRAIN MODEL -- LITTLE SOUTH FORK, CACHE LA POUDRE RIVER. R. E. Oliver. March, 1972. Colorado State University, Department of Watershed Sciences, Incidental Report 3, Fort Collins, Colorado, 75 p.

n.c. - no charge
n.a. - not available from Watershed Sciences Department
charges shown are for reproduction costs only

ACKNOWLEDGEMENTS

These course notes resulted from research conducted by the author and others on how to teach remote sensing of natural resources on an interdisciplinary basis at the graduate level. The total program, of which this is a portion, has been sponsored by a National Science Foundation grant of $104,000, GZ-1760, which was matched by a contribution of $20,000 by the College of Forestry and Natural Resources of Colorado State University. The program has been administered by the NSF's Advanced Science Education Program, Division of Graduate Education in Science with Dr. Terrance Porter as contracting officer.

PREFACE

During the first year development of the graduate level course, "Active Remote Sensing of Natural Resources", a set of course notes were prepared for use by the instructor. The second year this course was taught, the notes were expanded for use by the students and the instructor. This expanded set of course notes is contained herein. Eventually these notes will be used to prepare a textbook on the subject.

Certain sections of these notes are quite complete, with descriptive text, illustrations and problems. Other sections are little more than a detailed outline with disconnected comments. The student will find it necessary, therefore, to attend lectures and/or study the references given to obtain a thorough knowledge of the subject.

The course, and therefore these notes, has been prepared for the natural scientist with little background in electromagnetic (EM) theory. An electrical engineer could probably skip by the first four sections and delve immediately into the later material. Engineers who have taken the course, however, have found a review of this material beneficial, and have found some new concepts to be of value. The natural resource scientist may find the EM theory somewhat onerous and initially confusing. Our emphasis is on the concepts, not the mathematical detail, however, and we believe these concepts are vital to an understanding of active remote sensing systems and the data they produce.

Numerous examples of radar imagery and other data are used in teaching this course. These materials could not be included in these notes but are available to those attending lectures. Some of these materials can be made available to others upon request.

TABLE OF CONTENTS

Active Remote Sensing Of Natural Resources

1. INTRODUCTION TO THE SUBJECT

Active remote sensing denotes those methods or systems which generate the electromagnetic energy "illuminating" the target or resource to be detected. A searchlight, probing the sky for airplanes, is just as much an active remote sensor as is a radar system. Most active systems, however, operate below the visible and infrared frequency range. We find, therefore, that dividing the subject of remote sensing into active and passive systems, results in a frequency/wavelength division centered at about 10^{12} Hertz/300 micrometers. In other words, most active systems operate below 10^{12} Hertz and most passive systems operate above this frequency, which corresponds to a wavelength of 300 micrometers. An important exception to this division are the passive microwave systems which we will be considering in this study.

1. 1. Remote Sensing Defined

1. Remote sensing is the detection and use of energy, waves or substances emanating from objects or materials.
2. Remote sensing of environment is defined as the utilization of various systems that bring us information at a distance concerning physical-chemical phenomena.

Examples

Eye-Brain System

Our eyes and brain form the best remote sensing system in existance. They provide information concerning location, size,

color, material type; and through information storage, comparison and pattern recognition within the brain, complete identification may be possible. This is a passive system which detects EM energy which is radiated or reflected from the objects seen. The brain uses or interprets the energy detected by the eyes.

The blind person must touch an object to know of its existence, to identify it, etc. He must even touch to read. He may, however, develope his ears and brain to form a poor substitute remote sensing system.

The Bat's Sonar System

Some bats use an active remote sensing system to detect and identify objects. They emit high-pitched, repetitive squeaks (the source) which are reflected by nearby objects. From the echoes, the bat can determine distance and apparently something about the nature of the object.

Note

Nature has provided very few active remote sensing systems but she has provided many passive systems.

Table 1. 1. compares methods for finding skunks and uranium ore to further define remote sensing and to compare remote with direct sensing. Note that the detection of gamma rays from U_3O_8 with a down-hole device, does not qualify as a remote sensor since the device is in close proximity with the material being detected.

TABLE 1. 1.

REMOTE SENSING COMPARED TO DIRECT SENSING SYSTEMS

Target	Sense	Emanation	Type
Skunk	Smell	Odorous liquid	Remote
U_3O_8	Spectrometer (surface or airborne)	Helium	Remote
Skunk	Touch (long pole)	None used	Direct
U_3O_8	Radioactivity (down-hole)	Gamma rays	Direct
U_3O_8	Drill cuttings	None used	Direct

What should you expect to learn from remotely obtained data

Often: Remote sensing systems tell you part of what you would know if you were on site.

Sometimes: They tell you everything that you could determine on site.

Occasionally: They will tell you more than you can determine (readily) on site.

Almost Always: The remote sensing system will collect whatever data it does provide more rapidly and at lower cost than the same data collected by direct methods.

Some general comments about data interpretation

It is worth noting that the human eye and brain are an important part of most data interpretation systems. Not in the sense of just reading results, but more often than not, the eye-brain system does some of the data processing, e.g., smoothing, averaging, integrating, noise reduction, etc. In addition the

final interpretation of the results is usually done by the eye-brain system. Computer processing and data interpretation are playing an increasingly important role, but they almost always require some assistance from the human. Only when the computer system reaches the point that it prints out full identifying data can we say that we have eliminated the need for the eye-brain system. Except in rare cases, this may not be possible or desirable.

Do not sell short, however, the value of the computer to handle large quantities of data and to put it into a form which makes it more "visible" and meaningful to the eye-brain.

1. 2. Applications of Active Remote Sensing Systems

One of the primary aims of this study is the preparation of a student to make his own judgment of the value of a remote sensing system for a particular application. Some of the general considerations which the student should keep in mind throughout his studies are listed below.

1. Sensors should be applied to a natural resource problem if:
   a. Direct samples of the material are not required.
   b. The information needed can be obtained from a property of the material affecting the phenomena detected. (see Table 1. 1.).
   c. The sensor can "see" through interference, e.g., clouds, foliage, overburden.
   d. The interpretation of the data is unambiguous (relatively).
   e. The cost is reasonable compared to the value of the natural

resource and compared to the cost of other data collection techniques.

2. Remote sensed data from aircraft or spacecraft are particularly valuable if:

   a. The problem is on a regional to global scale.

   b. Repeated observations can detect time-dependent changes.

   c. The process is economical.

3. Multiple sensors:

   a. May be required to reduce ambiguity.

   b. Will be most valuable if they detect phenomena related to different properties of the materials. (See Figure 1-1).

The material presented in this section should be briefly perused now to obtain a "feel" for the systems and their application. The reader will want to refer back to this section later, however, to see how well these proposed applications are supported by analyses of the systems and the targets.

1. 2. 1. Side Look Radar

   a. SLR is capable of seeing through clouds. This is particularly valuable in regions having cloud cover a high percentage of the time. Darien Province, Panama (10,000 sq. km.) was covered in six hours flying time (six operating days), whereas, during a 15 year period, only 40 percent of the Province had been photographed.

   b. The uniform, constant illumination afforded by this active system results in certain advantages over

photographic images.

c. The system is very good for large, regional coverage, particularly because of the uniform illumination.

d. Studies of geologic structure have been quite effective.

e. SLR sees through foliage, sometimes more effectively than others.

f. SLR is generally too expensive for surveys covering less than 1000 square miles. Exception, of course, could occur; for instance, areas continually cloud covered might not be mappable any other way.

g. Use of vertical and horizontal polarizations of the scattered energy may result in unique interpretation.

1. 2. 2. Microwave Radiometers

a. These passive systems also see through clouds.

b. Because of the lower frequency, compared to IR, the temperature below the surface of objects is seen. The overall, effective temperature of an entire tree or forest may be seen.

c. This system has been used effectively for vulcanology and fault location work.

d. Resolution is not too good and is one of the more significant limitations of these radiometers.

1. 2. 3. Low Frequency (LF) Systems

a. These systems typically see to depths of 10's to 100's of meters.

b. Their depth of penetration makes LF systems particularly useful for mineral exploration.

c. May be useful for study of subsurface geologic structure.

d. Application has been made for mapping of subsurface groundwater.

e. These systems do not form images, the data is either obtained point by point or as individual scan lines across the region of interest.

1. 2. 4. Checkerboard Guesstimates

Several checkerboards have been made which show proposed, anticipated or potential applications of various remote sensing systems. These are reproduced on Figures 1. 2, 1. 3, and 1. 4. These represent, at times, experience, theory and guesses. Some disagreement will be found between these checkerboards, and they all should be taken with a grain of salt, until experience or good theory can be used to support these projections. As the student becomes more familiar with the systems, and with natural resource parameters, he will be able to support or refute some of the guesses.

1. 3. Approach and Aims of This Study

Historically, much remote sensing data has been taken to "sell" remote sensing. NASA, for instance, has sponsored the collection of thousands of miles of side look radar images. These images were then given out to various organizations and individuals for evaluation. Ground truth was virtually nonexistant, and the evaluations for the most part were very perfunctory.

Industry has taken a similar approach. In effect, their calling cards read, "Have Radar -- Will Travel." From that point on, its up to the buyer to call the shots. Industry has even gone so far as to fly areas on a "wildcat" basis, in the hope the imagery would be marketable. The entire Vancouver Island has been flown and the resultant imagery can be obtained at about $5 per square mile.

Scientific development has always consisted of alternate surges of experimental and theoretical advances; but without both, development will cease. Several of the key speakers at the 7th International Symposium of Remote Sensing (1971) expressed concern over the lack of the development of theories to support experimental results. The field of remote sensing is long overdue, at least in terms of effort expended, for this change in direction. This course of study is designed to help you to become prepared to assist in this effort.

Advances in the field of remote sensing must have multidisciplinarians. It is not sufficient for the engineer to design systems without regard for the needs of the forester or agriculturalist. Nor is it sufficient for the resource manager to call for the use of systems or the development of new systems without a knowledge of the basic physics involved and the limitations imposed by hardware and the real world. This course is an attempt, however feeble, to bridge the gap. The engineer will not become a resource manager as a result of this study, now will the forester turn into an engineer. Both will be better prepared to assess the

proper application of active remote sensing systems to the collection of natural resource information. Both will be able to participate more effectively in research to advance the state-of-the art. They will speak and listen to each other with greater understanding.

We have included, therefore, a short course in electromagnetics and a review of the electromagnetic properties of natural materials. With these tools we study the interaction between natural resource targets and the EM energy from active systems. Finally, we examine typical images or other types of data and attempt to understand the experimental results in terms of the natural resource properties.

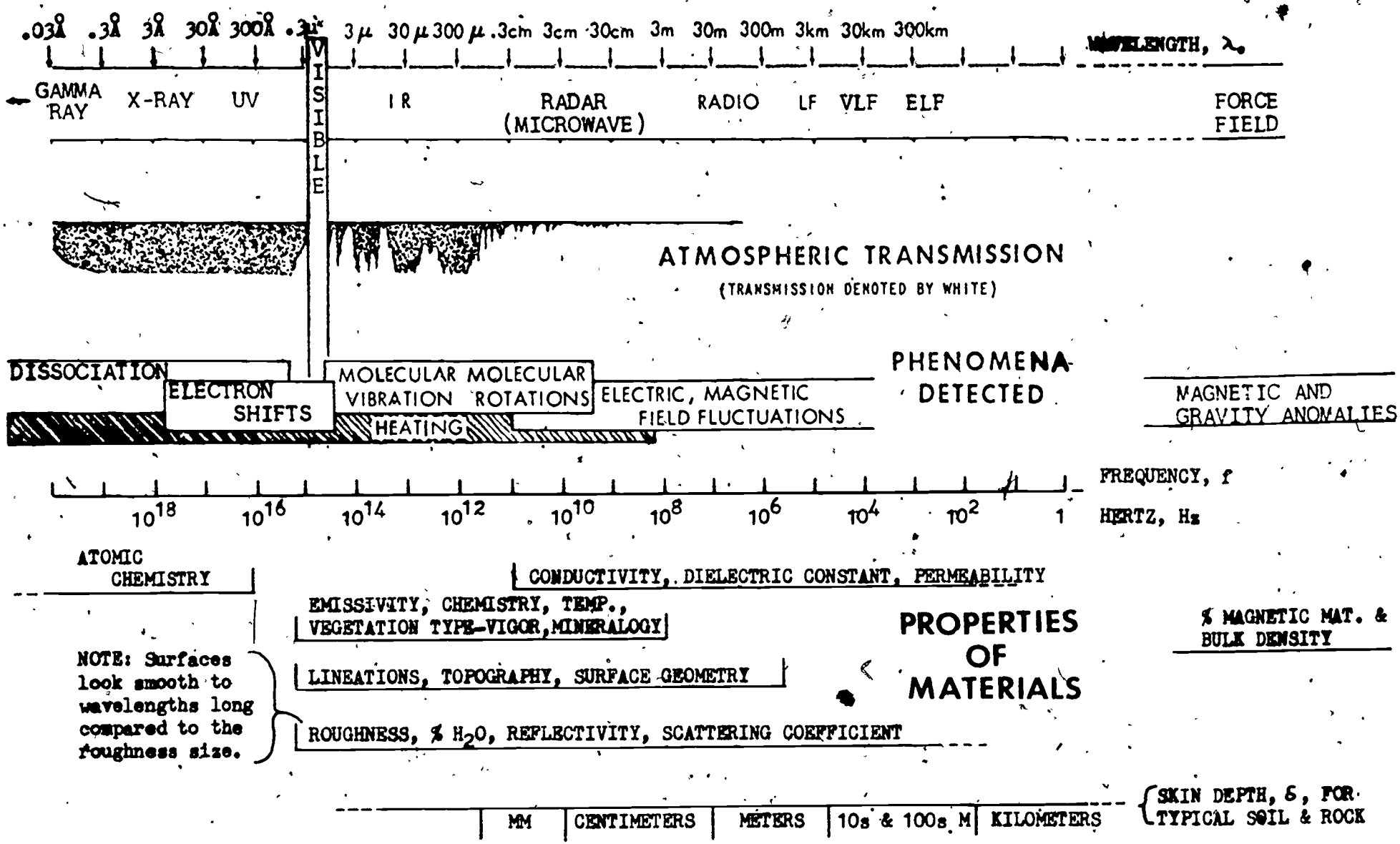

FIGURE 1-1 - ELECTROMAGNETIC SPECTRUM AND A SUMMARY OF PHYSICAL PROPERTIES RELATED THERETO.

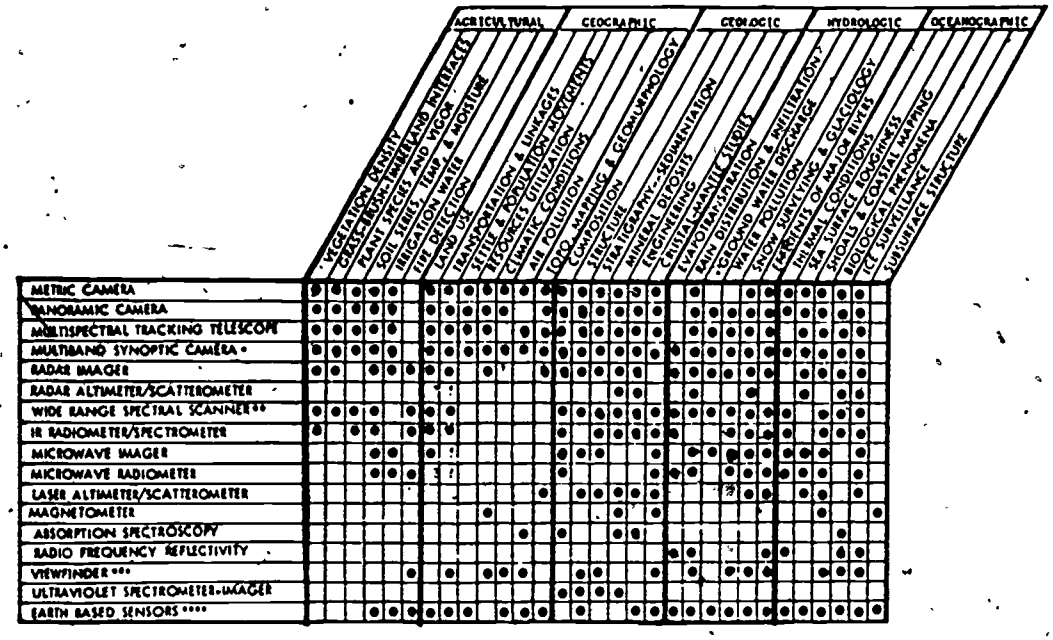

* Defined for both film return and telemetry modes.

** 0.32 - 14.0 microns.

*** This instrument augments an astronaut's vision with optical power and directional data. The astronaut can utilize the viewfinder by itself or in conjunction with other directional type sensors.

**** These earth-based sensors may include a number of fixed and mobile instruments, such as buoys, seismographs, stream gauges, and so forth, placed on or near the earth's surface for detecting, recording, and transmitting a variety of earth resources phenomena of interest to a large number of users.

*This table has been summarized from more detailed tables for each discipline and, therefore, does not include all the anticipated applications which have been identified to date.

FIGURE 1-2- Potential applications of earth resources data gathering systems.

FIGURE 1-3
ANTICIPATED
GEOLOGIC APPLICATIONS
OF REMOTE SENSORS

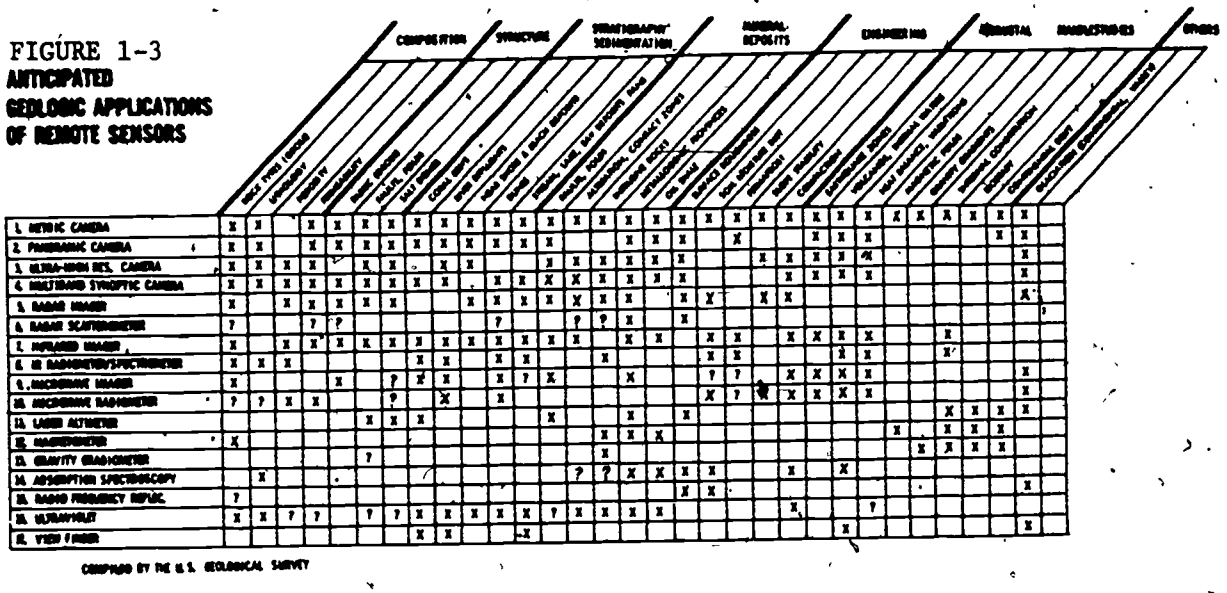

COMPILED BY THE U.S. GEOLOGICAL SURVEY

FIGURE 1-4 - RELATIVE PRIORITY OF REMOTE SENSING INSTRUMENTS FOR HYDROLOGIC PURPOSES (A WEIGHTED CHART)

		EVAPOTRANSPIRATION	WATER SURFACE ROUGHNESS	RAINFALL AND INFILTRATION	GROUND-WATER DISCHARGE	SUBAQUEOUS FEATURES	LIGHT ABSORPTION BY WATER	WATER POLLUTION	RESERVOIR SEDIMENTATION	EFFLUENTS OF RIVERS	DRAINAGE BASIN CHARACTERISTICS	VALLEY GLACIERS	LAKE AND RESERVOIR LEVELS	SNOW SURVEYING	EROSION AND SEDIMENTATION	TOTAL WEIGHT	GROUP WEIGHT	PRIORITY
PHOTO	1. METRIC MAPPING CAMERA		X	X		X			X		X	X		X	X	5	130	1
	2. PANORAMIC HIGH RESOLUTION CAMERA			X	X	X		X	X	X	X	X	X	X	X	5		
	3. ULTRA-HIGH RESOLUTION CAMERA		X	X	X	X	X	X	X	X	X	X	X	X	X	5		
	4. MULTIBAND SYNOPTIC CAMERA	X		X	X	X	X	X		X	X	X			X	5		
RADAR	5. RADAR IMAGER	X		X	X			X			X	X		X	X	2	38	4
	6. RADAR ALTIMETER/SCATTEROMETER			X							X			X		2		
IR	7. INFRARED SCANNER	X		X	X			X		X	X	X		X		4	45	2
	8. INFRARED SPECTROMETER	X	X					X			X	X		X		4		
UV	9. ULTRAVIOLET CAMERA	X		X							X					2	15	4
MICRO-WAVE	10. MICROWAVE IMAGER			X	X			X			X	X		X	X	3	40	3
	11. MICROWAVE SPECTROMETER	X		X				X			X	X		X		3		
	12. LASERS												X				2	5
	WEIGHTING	3	1	5	2	2	1	4	1	1	5	2	1	3	3			

2. BASIC ELECTROMAGNETIC THEORY

A general understanding of basic electromagnetic theory is necessary for a full appreciation of the interaction of natural resources and electromagnetic (EM) fields. Similarly, an appreciation of this interaction is important for proper interpretation of Radar and Low Frequency data. Hence, the material in this section should be carefully studied before proceeding.

The emphasis here is toward understanding, not proofs and derivations. Some familiarity with general physics, calculus, and vector analysis will aid in obtaining a full appreciation of this material.

For the student desiring a more thorough and rigorous treatment of EM theory, we recommend Hayt, 1958, and Jordan, 1950.

2. 1. Electric Charge -- The EM Field Maker

1. All electric charge comes from electrons or ions. Charge of an electron:

$$Qe = 1.6019 \times 10^{-19} \text{ coulomb.}$$

Ions have a charge of multiples of Qe.

2. All EM Fields originate from:

   a. Charges at Rest -- Static Electric Fields

   b. Charges in Motion -- Magnetic Fields and Electric Fields

      A magnet results from electron motion within the atoms, the earth's magnetic field results from electric current within the mantle and core.

   c. Charges in Motion, Varying With Time -- Electromagnetic Fields And Waves

3. Once generated, a radiating EM Field is self perpetuating. This results from the fact that a changing electric field,

$\frac{dE}{dt}$, generates a magnetic field and a changing magnetic field, $\frac{dH}{dt}$, generates an electric field. Hence, the electric and magnetic fields regenerate each other as an EM wave propagates through space (or any medium).

2. 2. Electro Magnetic Units

We will use the MKS system of units almost exclusively. Lengths will be measured in meters, mass in kilograms, and time in seconds. We will show the relationship between the units of length, mass, time, and electrical units. This should also help the student to recognize that we are still dealing with forces and the results of forces.

Newton's first law might be considered the defining equation for force

$$F = ma \qquad (2.1)$$

where F is force in newtons

m is mass in kilograms, and

a is acceleration in meters per second^2.

The defining equation for work or energy is

$$W = FL \qquad (2.2)$$

where W is work or energy in Joules and L is length in meters. Similarly, the defining equation for power is

$$P = \frac{W}{t} \qquad (2.3)$$

where P is power in watts and t is time in seconds. It will be seen that electric units have been chosen such that a direct unit for unit relationship with work and power exists. In otherwords, when computing work and power using electric units, the constant

of proportionality is equal to one. Therefore, the equation for electric power is

$$P = VI \tag{2.4}$$

where P is power in watts, V is electromotive force in volts, and I is electric current in amperes.

Electric current is the movement of electric charge. By definition, therefore,

$$Q = It \tag{2.5}$$

where Q is electric charge in coulombs.

All circuits and all materials offer a resistance to the movement of charge, i.e., the flow of current. The defining equation for resistance is given by Ohm's Law

$$R = V/I \tag{2.6}$$

where R is resistance in ohms.

Before proceeding with our definition of electromagnetic units, it will be informative to show the relationship between mechanical and electrical forces. There are no simple one to one relationships between electric and mechanical forces, as there are between electric and mechanical units of power and energy, because of the basic difference in the nature of the forces at work. Mechanical forces are due to the presence of mass and mass in motion. Electrical forces are due to the presence of charge and charge in motion. For instance, the equation for gravitational force (forces due to the presence of mass) is

$$F = G\frac{m_1 m_2}{r^2} \tag{2.7}$$

where G is the gravitational constant, m_1, and m_2 are the masses of the objects in kilograms and r is the distance between the objects. Note that two one-kilogram masses separated one meter exert a force on each other of 6.67×10^{-11} newtons. The number 6.67×10^{-11} is, of course, the gravitational constant. This constant cannot be computed from any theoretical physical considerations but has been determined from experimental measurements.

Similarly, the force between two charges is given by the expression

$$F = K \frac{Q_1 Q_2}{r^2} \qquad (2.8)$$

where K is a constant equal to 9×10^9, Q_1, Q_2 are the quantities of charges in coulombs and r is the distance between the charges in meters. Note that the force between two charges of one coulomb separated one meter is 9×10^9 newtons. This is equivalant to about one million tons. We see that the forces associated with electric charges are many orders of magnitude greater than the gravity forces associated with mass. It is interesting to note that the tremendous forces of the atomic bomb are due mostly to coulomb forces which result from the splitting of the electric charges within the atoms.

We are now ready to derive the expressions for electric field intensity. An electric field is a force field similar in every way to a gravity field as evidenced by the similarity in the force equations (2.7) and (2.8). We express electric field intensity in terms of the change in electromotive force with distance, i.e., the electric field units should be volts per meter. We can show

the relationship between electric field intensity, E, and the forces produced by charges in the following manner. From equations (2.4) and (2.5) we obtain an expression for electric power

$$P = \frac{VQ}{t} \tag{2.9}$$

and from equations (2.2) and (2.3) we obtain an expression for mechanical power

$$P = \frac{FL}{t} \tag{2.10}$$

therefore,

$$\frac{VQ}{t} = \frac{FL}{t} \tag{2.11}$$

and,

$$\frac{V}{L} = \frac{F}{Q} \tag{2.12}$$

or

$$E = F/Q \tag{2.13}$$

Finally, if we combine (2.13) and (2.8) we obtain the desired expression for electric field intensity

$$E = K\frac{Q}{r^2} \tag{2.14}$$

Now, since many of the expressions of greater significance and more frequent use involve, in one way or another, a summation over the surface area of a sphere (consider the intensity of light in lumens per square meter from a point source), workers in this field have found it more convenient to introduce a $\frac{1}{4\pi}$ term in the expressions for coulomb forces and electric field intensities. In otherwords, we will now let

$$K = \frac{1}{4\pi\epsilon} \tag{2.15}$$

and we have the more common expression for electric field intensity from a point charge

$$E = \frac{-Q}{4\pi\varepsilon r^2} \qquad (2.16)$$

where ε is the dielectric constant of the medium surrounding the point charge. Since $K = 9 \times 10^9$ for free space we find that ε for free space $= 8.85 \times 10^{-12}$.

The student should be aware that electric field intensity, E, is a vector quanitity, i.e., it should properly be expressed in terms of magnitude and direction. For the point charges considered so far the electric field intensity is equal in all directions and the directionality of the field has not been significant. This is not the case for other electric field generators as will be seen later.

If we integrate (2.16) over the range r, we obtain the expression

$$V = \frac{Q}{4\pi\varepsilon r} \qquad (2.17)$$

which is the potential with respect to infinity at a position r meters from a point charge. From this we see that electric field is the gradient of potential.

There are not many practical sources of electromagnetic energy which may be represented as a single point charge. We will consider next, therefore, the most common source of electromagnetic energy, the electric dipole.

2. 3. The Field of an Electric Dipole

Most electromagnetic dipoles result from electric charge

back and forth along a wire. In order to maintain the continuity and the relative simplicity of our discussion, we will continue to deal with static electric charges. Although simplified, the results will adequately disclose the electric dipole characteristics of importance at this time. Figure 2-1 gives the geometry of the situation. Note that we have positive and minus electric charges along the Z axis, equidistant from the origin. Using equation (2.17) we solve first for the potential at P:

$$V = \frac{Q}{4\pi\varepsilon}\left[\frac{1}{R_1} - \frac{1}{R_2}\right] = \frac{Q}{4\pi\varepsilon}\frac{R_2 - R_1}{R_1 R_2} \qquad (2.18)$$

For a distant point ($r > 10\ d$) we can simplify equation (2.18) with the approximations

$$R_1 R_2 \approx r^2$$

$$R_2 - R_1 \approx d\cos\theta$$

The simplified expression for the potential from an electric dipole is

$$V = \frac{Qd\cos\theta}{4\pi\varepsilon r^2} \qquad (2.19)$$

We would like now to obtain the equation for the electric field intensity of an electric dipole. From equation (2.19(and Figure 2-1, it is apparent that the electric field from a dipole source is not omnidirectional. We will, therefore, need the vector operator ∇ to determine E, the gradient of V. In Cartesian coordinates, this is

$$\nabla = \frac{\partial}{\partial x}\bar{a}_x + \frac{\partial}{\partial y}\bar{a}_y + \frac{\partial}{\partial z}\bar{a}_z \qquad (2.20)$$

In spherical coordinates, this becomes

$$\nabla = \frac{\partial}{\partial r}\,\bar{a}_r + \frac{1}{r}\frac{\partial}{\partial \theta}\,\bar{a}_\theta + \frac{1}{r \sin\theta}\,\frac{\partial}{\partial \phi}\,\bar{a}_\phi \qquad (2.21)$$

Because of the geometry of the problem, it is easier to compute the electric field in spherical coordinates. Subjecting equation (2.19) to the partial derivatives called for by equation (2.21) we obtain

$$\bar{E} = -\nabla V = -\left(-\frac{Qd\cos\theta}{2\pi\varepsilon r^3}\,\bar{a}_r - \frac{Qd\sin\theta}{4\pi\varepsilon r^3}\,\bar{a}_\theta\right) \qquad (2.22)$$

which may be simplified to become

$$\bar{E} = \frac{Qd}{4\pi\varepsilon r^3}\,(2\cos\theta\,\bar{a}_r + \sin\theta\,\bar{a}_\theta) \qquad (2.23)$$

where all of the terms have been previously defined or are defined on Figure 2-1. Note particularly that whereas the electric field from a single point charge varied as a function of distance squared, that the electric field from the dipole varies inversely with distance cubed. This is the same variation which we will find later for the near or electrostatic field from a radiating antenna. These fields are of importance primarily when dealing with very low frequency signals, such as used in the exploration for minerals.

2. 4. The Steady Magnetic Field

Magnetic fields are generated by electric currents or charges in motion. We will not have a point source for a magnetic field, therefore, since it is impossible to have current flow restricted to a single point in space. The student might consider the possibility of obtaining an infinitely small, permanent magnet and consider this to be a point source for magnetic fields. Even if we consider the magnetic field set up by electron rotation about the nucleus of an atom, we find we are not dealing with a point

source since the movement of the electrons take place over a finite distance.

Relating magnetic fields to their source and to the basic mechanical system of units is quite difficult. We shall, therefore, find it necessary to accept the laws governing magnetic fields on faith alone. It is the author's feeling that the student can obtain a good understanding of magnetic fields and their effects without going through a series of rigorous proofs. For a student interested in a more in-depth treatment of this subject, we recommend Chapter 8 from Hayt (1958).

The source of the steady magnetic field may be a permanent magnet, a direct current, or an electric field changing linearly with time. Our immediate concern will be the magnetic field produced by a differential current element. The geometry relating the current element, $d\bar{L}$, and the differential magnetic fields, $d\bar{H}$, produced thereby is shown in Figure 2-2.

The experimental law of Biot-Savart states that at any point P the magnitude of the magnetic field intensity from the differential current element is proportional to the product of the current and the differential length. The entire Biot-Savart Law is written in concise mathematical notation as

$$d\bar{H} = \frac{I\, d\bar{L} \times \bar{a}_R}{4\pi R^2} \tag{2.24}$$

or

$$d\bar{H} = \frac{I\, dL \sin\theta}{4\pi R^2}\, \bar{a}_H \tag{2.25}$$

where $\bar{H}$ is magnetic field intensity in amperes per meter and is perpendicular to the paper and directed into it. Note that the

magnetic field intensity for this differential current element is varying inversely with distance squared.

A simple application of the Biot-Savart Law may be made by considering the fields produced by steady-state current flow in an infinitely long wire. This problem is simplified by redefining the geometry in terms of a cylindrical coordinate system as indicated in Figure 2-3. Equation (2.24) then becomes

$$\overline{dH} = \frac{I\, dz\, \overline{a}_z \times (r\, \overline{a}_r - z\, \overline{a}_z)}{4\pi (r^2 + z^2)^{3/2}} \tag{2.26}$$

where the vectors and distances are defined by Figure 2-3. Solution to the problem requires integration over the infinitely long wire or

$$\overline{H} = \int_{-\infty}^{\infty} \frac{I\, dz\, \overline{a}_z \times (r\, \overline{a}_r - z\, \overline{a}_z)}{4\pi (r^2 + z^2)^{3/2}} \tag{2.27}$$

which becomes

$$\overline{H} = \frac{I}{4\pi} \int_{-\infty}^{\infty} \frac{r\, dz\, \overline{a}_\phi}{(r^2 + z^2)^{3/2}} \tag{2.28}$$

Carrying out this integration, we obtain the results

$$\overline{H} = \frac{I}{2\pi r}\, \overline{a}_\phi \tag{2.29}$$

which indicates that the magnitude of the field is not a function of ϕ or Z and varys inversely as the distance from the infinitely long wire. The direction of the magnetic field intensity vector is, of course, circumferential.

2. 5. Conductors, Dielectrics, and Magnetic Materials

Electric and magnetic fields exert forces on charges and charged particles and are, therefore, properly defined as force fields.

Electric fields exert forces on charges at rest or in motion. Magnetic fields can exert forces only on charges in motion. Keep in mind, however, that the orbit and spin of electrons in individual atoms constitute charges in motion. The forces produced by the electric and magnetic fields result in movement of the charges. This results in the generation of electric and magnetic flux fields.

In a conducting medium the flux field is the current density, J. This is a physically real flux consisting of the movement of electrons or ions in response to the electromagnetic force field. If we draw isofield lines representing equipotential surfaces in the media and flux lines representing the movement of the charges we find that they are everywhere equally perpendicular. This is illustrated in Figure 2-4 and is the natural result of charges seeking the shortest path between positions of different potential.

Although the dielectric and magnetic properties of materials are a result of the movement of charge, this movement is not a continuous flow along flux lines and we find that electric flux (displacement currents) and magnetic flux are mathematical and perceptual conveniences.

We will now discuss the basic characteristics of conductors, dielectrics and magnetic materials and their relation to force and flux fields.

2. 5. 1. Conductors

Conductors have free electrons or ions, i.e., the electrons or ions may move freely about within the material, whereas, dielectrics (insulators) do not.

Just as resistance is a defined quantity relating voltage and current in a specific circuit or object, the

conductivity, σ is by definition the property of a material relating electric field intensity and current density

$$\sigma = \frac{\bar{J}}{\bar{E}} \tag{2.30}$$

We can obtain additional insight into the significance of conductivity and its relationship to specific materials and circuits through an examination of Figure 2-5. For a constant uniform electric field in a homogeneous medium, the electric force field and current density field vectors are parallel and are related in magnitude by equation (2.30). This is illustrated in Figure 2-5A. Figure 2-5B illustrates current flow through a cylindrical rod. The development of the relationship between the resistance from one end of the rod to the other and the conductivity of the material from which the rod was formed is given on the figure. Noting that the resistivity of the material is the inverse of conductivity we can express the resistance across the ends of any cylinder of any material as follows:

$$R = \frac{\ell}{\sigma A} = \frac{\rho \ell}{A} \tag{2.31}$$

where ℓ is length of the cylinder in meters, A is the cross-sectional area of the cylinder in square meters, σ is the conductivity of the material in mhos per meter, and ρ is the resistivity of the material in ohm meters.

We will refer to the flow of charge through a conductor as conduction current flow.

2. 5. 2. Dielectrics

For a pure dielectric material, there would be no conduction current flow, i.e., there would be no transfer of charge through the material. Although this pure dielectric does not exist, there are many materials classed as dielectrics for which conduction current flow is negligible. The electric charges in a dielectric undergo a physical displacement resulting from a force of an electric field. This displacement of charge (called displacement current) results in a polarization of the material, i.e., the charges are displaced or oriented such that the material exhibits an electric polarity opposite to the electric force causing the original displacement. The subject of polarization will be treated in great detail in later sections.

We now introduce the fictitious electric flux density which is defined by the expression

$$\overline{D} = \varepsilon \overline{E} \qquad (2.32)$$

where $\overline{D}$ is electric flux density in coulombs per meter squared. It is apparent from the units of electric flux density that we can also express it in terms of the charge per unit area on the surface of the dielectric:

$$D = \frac{Q}{A} \qquad (2.33)$$

This surface charge is not the same as the surface charge on a conductor, for the latter consists of the presence or absence of free electrons. The effect of this surface charge, however, is just the same as that of free surface

charge, and this effect may be used to show that the displacement of charge results in a storage of energy within the dielectric. This energy storage is related to the capacity for storage of charge between electric plates separated by a dielectric as shown in Figure 2-6. Capacity is defined by the equation

$$C = Q/V \qquad (2.34)$$

The development of the relation between capacity, the dielectric constant of the material separating the plates, the area of the plates and their separation is given in Figure 2-6. The resulting expression is

$$C = \frac{\varepsilon A}{d} \qquad (2.35)$$

where C is capacitance in farads, ε is dielectric constant in farads per meter, A is the area in meters squared, and d is the plate separation in meters. Note from equation (2.34) that one farad equals one coulomb per volt.

2. 5. 3. Magnetic Materials

We will begin with the defining equation which relates magnetic field intensity, H, to magnetic flux density, B, and the magnetic permeability, μ, of materials:

$$\overline{B} = \mu \overline{H} \qquad (2.36)$$

where $\overline{B}$ is magnetic flux density in Webers per meter squared, μ is permeability in Henrys per meter, and $\overline{H}$ is magnetic field intensity in amperes per meter.

We will use the atomic model consisting of a central

positive nucleus surrounded by electrons in various orbits to obtain some appreciation of the difference in behavior of various materials in magnetic fields. An electron in an orbit is analogous to a small current loop and, as such, experiences a torque in an external magnetic field. This torque tends to align the magnetic field produced by the orbiting electron with the external field. This is the same effect as the tendency of magnets to align themselves. Since the magnetic field of the electron adds to the external field, this simple picture would lead us to believe that the magnetic field in any material would be greater than without the material present. This is not true in most materials, however, because of electron spin. The spinning electron is the equivalent of a second current loop, and the torque on this loop must also be considered. It turns out that these effects very nearly cancel each other in most atoms, the notable class of exceptions being ferromagnetic materials. In this class of materials, orbital motion and electron spin fail to counteract each other. Each atom has a relatively large magnetic moment and in a magnetic field, the magnetic flux density increases to many times the value it would have in free space.

There are no simple circuit components which would shed any more light on the nature of the magnetic properties of materials and since most natural resource materials are non-ferromagnetic, we will not spend any more time on this subject. We should note, however, that the alignment

of electron orbits and electron spin result in storage of energy within the magnetic material much as the displacement of charge resulted in the storage of energy in a dielectric.

2. 5. 4. Energy and Other Relations

In the interest of imparting as much understanding on this subject as possible, we would like the student to note that current density consists of actual electric charges in motion, electric flux (displacement current) may be viewed as lines terminating on electric charges and magnetic flux may be viewed as lines which form closed loops, since there is no magnetic charge. If a little bit of contemplation does not make the reason for this statement clear, we would recommend further reading in the references.

It should be instructive to consider the similarity of the three equations which relate force fields and flux fields to the properties of the materials:

$$\overline{J} = \sigma \overline{E} \qquad (2.30)$$

$$\overline{D} = \varepsilon \overline{E} \qquad (2.32)$$

$$\overline{B} = \mu \overline{H} \qquad (2.36)$$

It would be well to commit these three expressions to memory since they will be used frequently in the material which follows.

Although we don't consider it worth the effort to show their development, it may provide further insight to

give the equations for energy dissipation and storage associated with the electromagnetic fields and the properties of materials which have been discussed.

Energy Stored in a Magnetic Media

$$W_H = 1/2 \int_{vol} \bar{B} \cdot \bar{H} \, dv \qquad (2.37)$$

$$= 1/2 \int_{vol} \mu H^2 \, dv \qquad (2.38)$$

Energy Dissipated in a Conductive Media

$$W_{E_R} = 1/2 \int_{vol} \bar{J} \cdot \bar{E} \, dv \qquad (2.39)$$

$$= 1/2 \int_{vol} \sigma E^2 \, dv \qquad (2.40)$$

Energy Stored in a Dielectric Media

$$W_E = 1/2 \int_{vol} \bar{D} \cdot \bar{E} \, dv \qquad (2.41)$$

$$= 1/2 \int_{vol} \varepsilon E^2 \, dv \qquad (2.42)$$

In this section we have covered the basics of static, non-time varying fields. We have done very little development of the field equations since our interest has been to convey understanding and not develop mathematical detail. The material is designed to acquaint you with electromagnetic fields, their variation with distance from the source, and effect of the electromagnetic properties of materials of these fields. In the next section we will allow the fields to vary with time, which opens up a whole new category of subjects and introduces us to the field of particular interest to the subject of remote sensing.

REFERENCES

Hayt, William H., Jr., 1958. Engineering Electromagnetics. McGraw Hill Book Company, Inc.

Jordon, E. C., 1950. Electromagnetic Waves and Radiating Systems. Prentice Hall, Inc.

Note: There are probably more-recent editions of both of these books, but any edition will serve the purposes of this course.

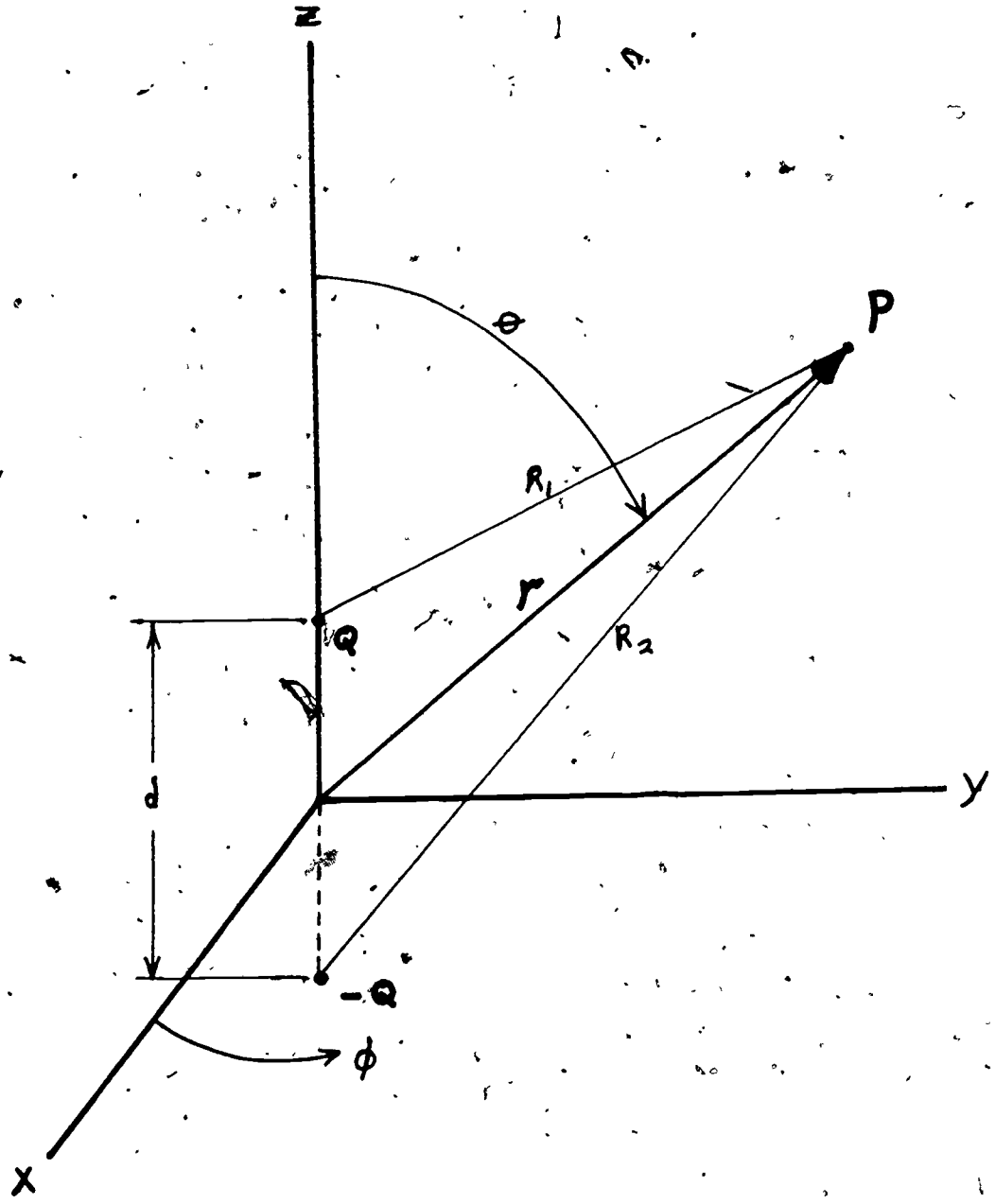

FIGURE 2-1 -- Geometry for Computing the Field from an Electric Dipole

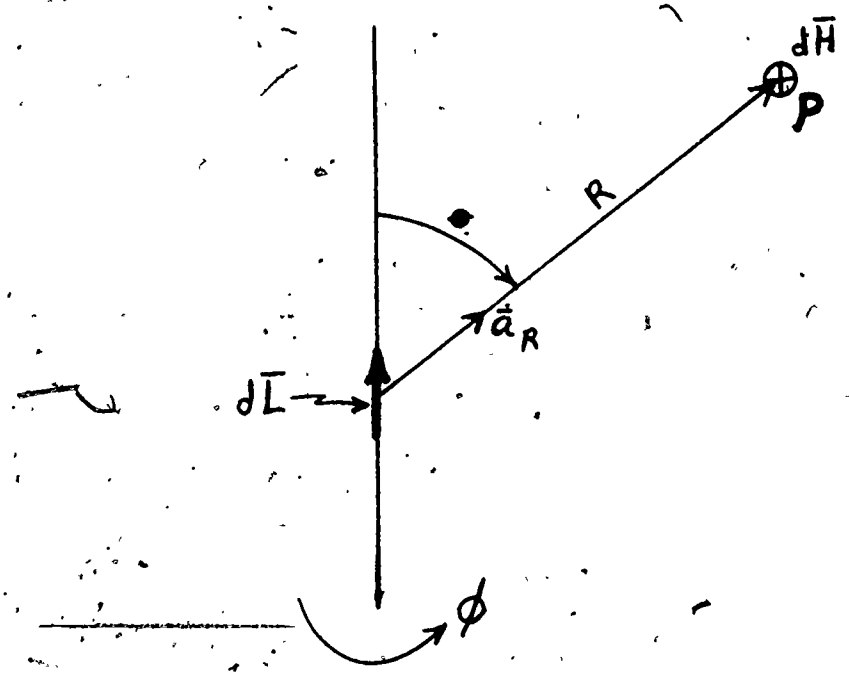

FIGURE 2-2 -- Geometry for the Magnetic Field from a Differential Current Element

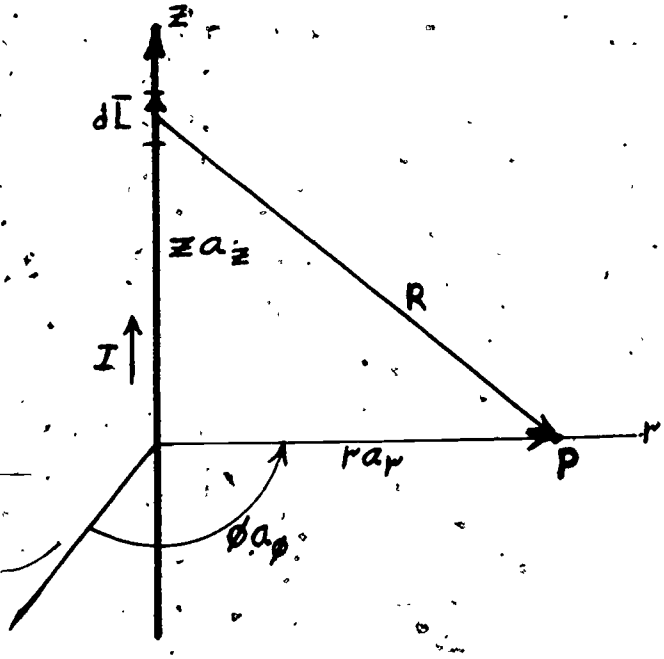

FIGURE 2-3 -- An Infinitely Long Straight Wire Carrying a Current I

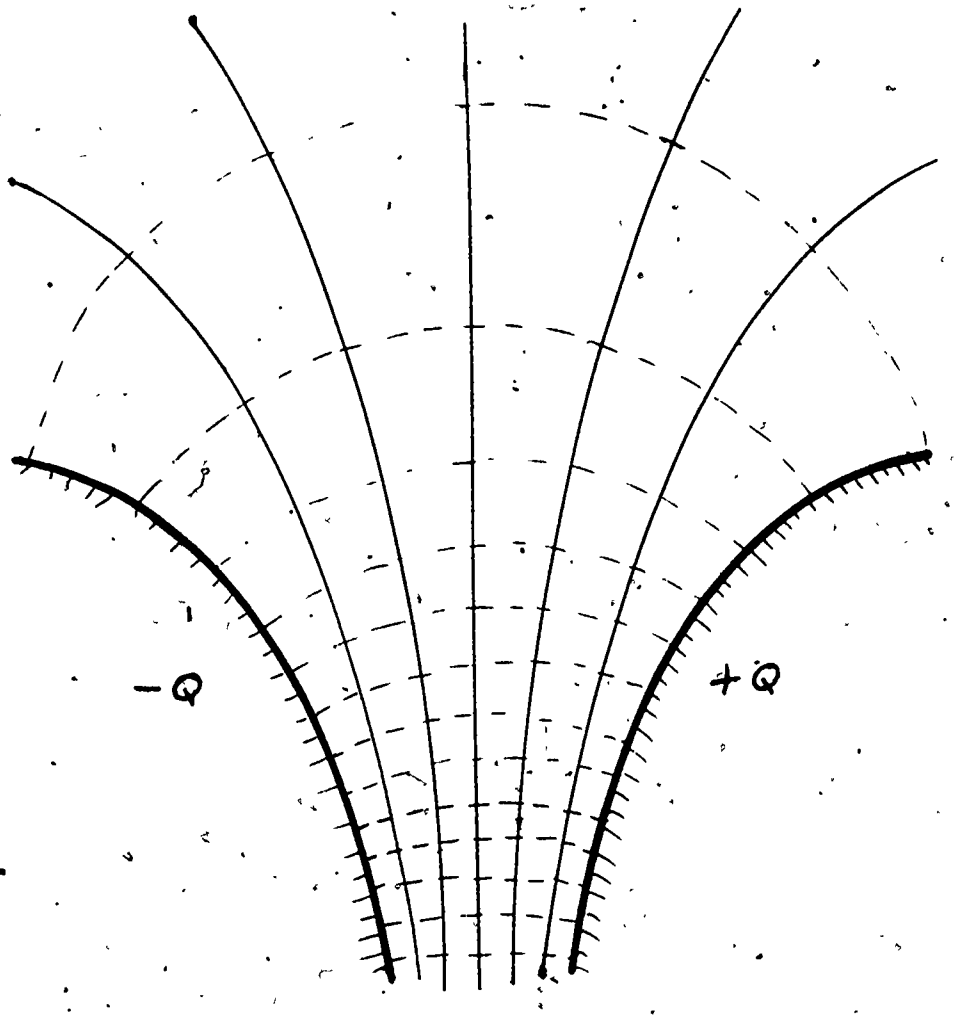

FIGURE 2-4 -- Equipotential Field Lines (Solid) and Electric Flux Lines (Dashed) Between Two Charged Objects

A

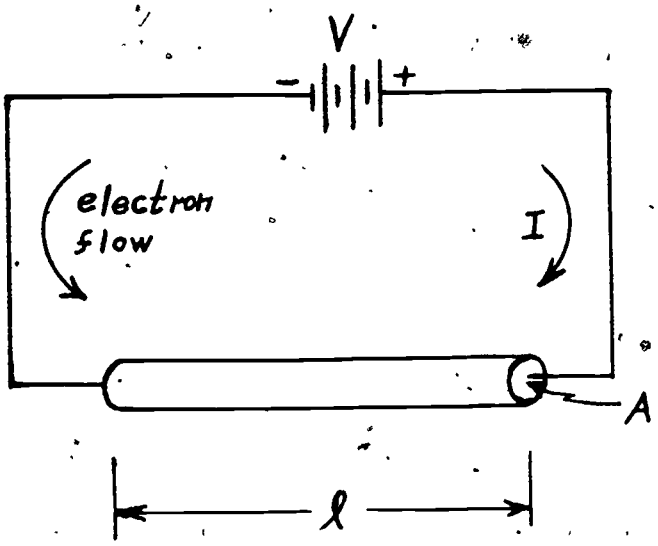

$\sigma = \bar{J}/\bar{E}$

$\bar{E} = V/\ell$

$\bar{J} = I/A$

$R = V/I = \frac{\bar{E}\ell}{\bar{J}A}$

$R = \frac{\ell}{\sigma A} = \frac{\rho\ell}{A}$

(finite conductor)

B

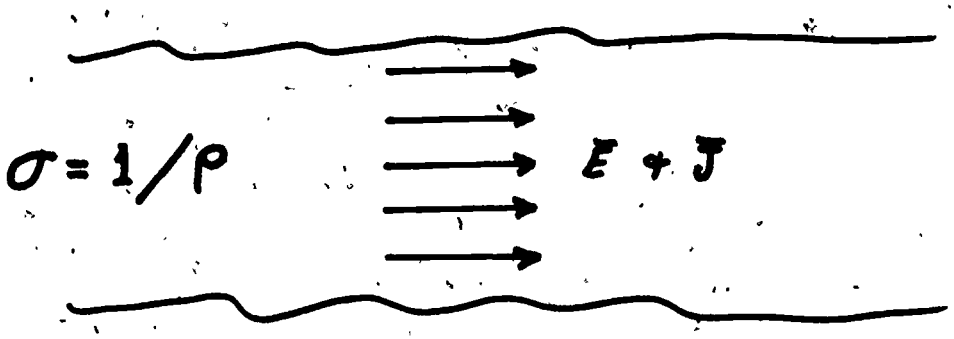

$\bar{J} = \sigma \bar{E}$

(infinite, homogenous medium in a uniform field)

FIGURE 2-5 -- Fields and Properties of Conductors.

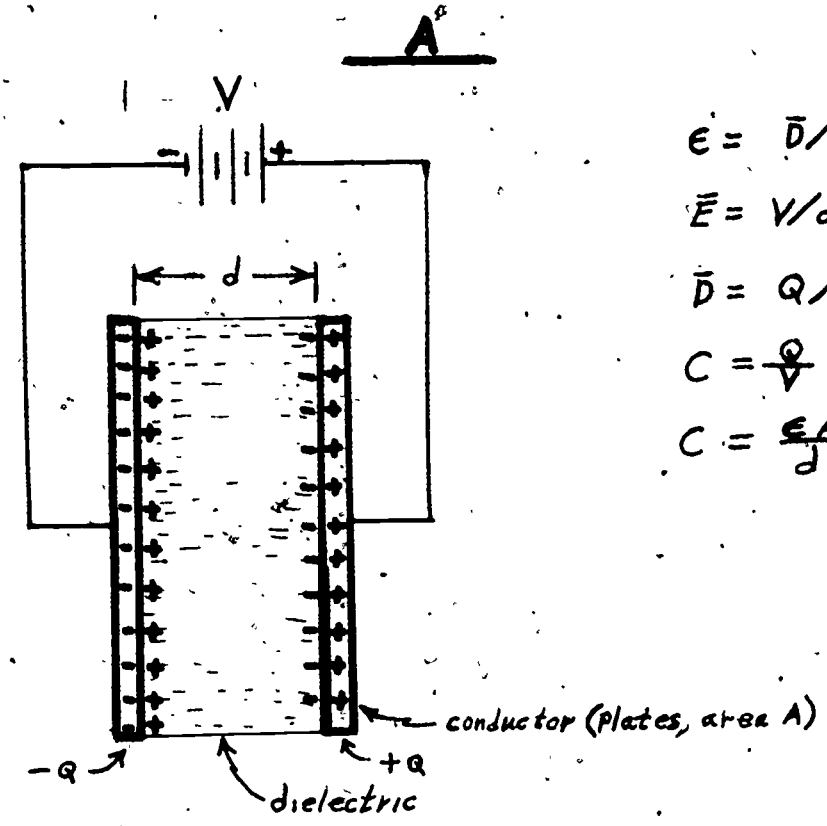

$\epsilon = \bar{D}/\bar{E}$

$\bar{E} = V/d$

$\bar{D} = Q/A$

$C = \frac{Q}{V} = \frac{\bar{D}A}{\bar{E}d}$

$C = \frac{\epsilon A}{d}$

(parallel plate capacitor)

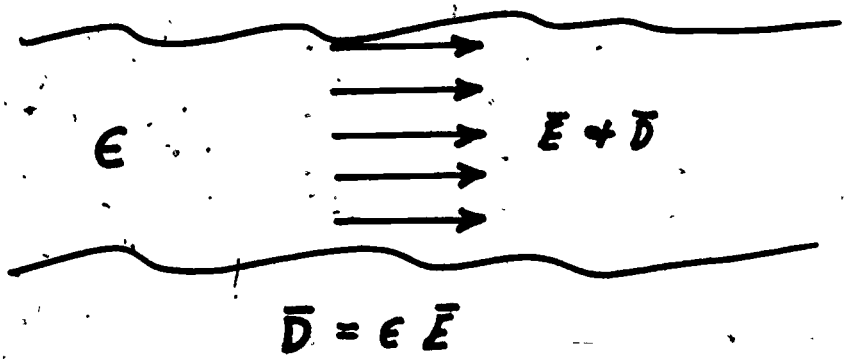

$\bar{D} = \epsilon \bar{E}$

(infinite, homogenous medium in a uniform field)

FIGURE 2-6 -- Fields and Properties of Dielectrics

PROBLEMS

2. 1. Compute the electric field intensity, E, at a distance of 33 feet from a point charge of 10^{-2} coulombs.

2. 2. Calculate the capacity of two metal plates, one foot square, separated one inch: (a) in a vacuum, (b) immensed in water ($\varepsilon/\varepsilon_0 = 80$).

2. 3. Calculate the resistance of a one mile length of copper wire having a diameter of 1/10 inch (the conductivity of copper is about 5.8×10^7 mhos/meter).

2. 4. Compute the electric field intensity, E, and the potential, V, at distances of 10, 100, and 1000 meters from the center of an electric dipole consisting of one coulomb charges separated one meter. Let θ (Figure 2-1) be 0^0, 45^0, and 90^0.

3. TIME VARYING FIELDS AND ELECTROMAGNETIC WAVES

From the material in the previous section, you have been introduced to the symbols, terminology, and the general concepts of electromagnetic fields and the electromagnetic properties of materials. We now wish to expand your understanding of EM fields with a consideration of time varying fields and electromagnetic waves. A comprehensive text in EM theory would spend several chapters in the development of the four field equations which are generally referred to as Maxwell's Equations. This material is meant to provide you with a general understanding of electromagnetic fields and their interaction with natural resource materials and is designed for the natural resource specialist, not for the physicist or electrical engineer. We begin our discussion, therefore, by presenting these equations in their most common form:

$$\text{curl } \bar{H} = \bar{J} + \frac{\partial \bar{D}}{\partial t} \quad \text{or} \quad \nabla \times \bar{H} = \bar{J} + \frac{\partial \bar{D}}{\partial t} \tag{3.1}$$

$$\text{curl } \bar{E} = -\frac{\partial \bar{B}}{\partial t} \quad \text{or} \quad \nabla \times \bar{E} = -\frac{\partial \bar{B}}{\partial t} \tag{3.2}$$

$$\text{div } \bar{D} = \rho \quad \text{or} \quad \nabla \cdot \bar{D} = \rho \tag{3.3}$$

$$\text{div } \bar{B} = 0 \quad \text{or} \quad \nabla \cdot \bar{B} = 0 \tag{3.4}$$

The symbols and units for these equations are the same as those developed in Section 2 with the exception that ρ is used here as electric charge density in coulombs per meter^3. In order to avoid confusion between the use of ρ for resistivity, we will try to use the inverse of resistivity, conductivity, when referring to the electrical properties of materials.

As is obvious from quick inspection, the four field equations establish the relationship between force fields and flux fields and electric fields

and magnetic fields. The equations express mathematically and exactly that, (3.1), a current generates a magnetic field that curls around the current, (3.2), a magnetic field that changes with time generates an electric field that curls around the magnetic field, (3.3), the net electric displacement current (flux) through the surface enclosing a volume is equal to the total charge within the volume and (3.4), the net magnetic flux emerging through any closed surface is zero.

The solution of any electromagnetic problem requires satisfaction of the four field equations. Also, the three relations concerning the electfo-magnetic properties of the medium in which the fields exist must be satisfied. These three equations are repeated here for convenient reference:

$$\overline{J} = \sigma\overline{E} \qquad (2.30)$$

$$\overline{D} = \varepsilon\overline{E} \qquad (2.32)$$

$$\overline{B} = \mu\overline{E} \qquad (2.36)$$

These equations assume the medium to be homogeneous, isotropic, and source free. The medium is homogeneous if ε, μ, & σ are the same at any position within the medium. The medium is isotropic if ε, μ, and σ are not functions of direction. This might be clarified by stating that a medium is anisotropic if the conductivity, dielectric constant, or magnetic permeability is different in one direction compared to another. Although many natural resource materials exhibit a certain degree of anisotropy, the effect is usually small, making results based on an assumption of isotropy reasonable. A source free medium is one which contains no source of electromagnetic fields within the medium. This is an accurate assumption for most conditions of interest.

The assumption of homogeneity is probably the most inaccurate since natural resource materials are generally a mixture of materials or ingredients having different electrical properties. Results obtained using this assumption, however, are often quite useful since the material may be homogeneous when viewed macroscopically.

3. 2. Electromagnetic Waves

The fact that electromagnetic energy travels through space (or any media) in the form of waves is the basis for all radio communications, most remote sensing techniques, and the propagation of energy from the sun to the earth. In order to understand why these natural and man-made systems work as they do, we must develop the equations for electromagnetic wave motion.

Virtually any kind of wave motion can be described with the general wave equation:

$$c^2 \nabla^2 \phi = \frac{\partial^2 \phi}{\partial t^2} \qquad (3.5)$$

where ϕ is the wave height or amplitude and c is the wave velocity in meters per second. From the expansion of $\nabla^2 \phi$,

$$\nabla^2 \phi = \frac{\partial^2 \phi}{\partial x^2} + \frac{\partial^2 \phi}{\partial y^2} + \frac{\partial^2 \phi}{\partial z^2} \qquad (3.6)$$

we see that the wave equation provides the relation between the space and time variations of the wave amplitude. If electromagnetic energy does propagate in the form of waves, we should be able to show this from the four field equations and the three media equations given

above. We will first develop the wave equations for free space, i.e. $\sigma = 0$. This media is, of course, ideally homogeneous, isotropic, and source free.

Under these conditions, we may substitute the appropriate terms from the media equations into the field equations and obtain:

$$\nabla \times \bar{H} = \varepsilon_0 \frac{\partial \bar{E}}{\partial t} \tag{3.7}$$

$$\nabla \times \bar{E} = -\mu_0 \frac{\partial \bar{H}}{\partial t} \tag{3.8}$$

$$\nabla \cdot \bar{E} = 0 \tag{3.9}$$

$$\nabla \cdot \bar{H} = 0 \tag{3.10}$$

Taking the curl of equation (3.7) we obtain

$$\nabla \times \nabla \times \bar{H} = \varepsilon_0 \nabla \times \frac{\partial \bar{E}}{\partial t} = \varepsilon_0 \frac{\partial}{\partial t} (\nabla \times \bar{E}) \tag{3.11}$$

A vector identity provides us with an expansion for equation (3.11) and we have

$$\nabla \times \nabla \times \bar{H} = \nabla(\nabla \cdot \bar{H}) - \nabla^2 \bar{H} = \varepsilon_0 \frac{\partial}{\partial t} (\nabla \times \bar{E}) \tag{3.12}$$

Now if we substitute equations (3.8) and (3.10) into (3.12) we see that

$$\nabla^2 \bar{H} = \mu_0 \varepsilon_0 \frac{\partial^2 \bar{H}}{\partial t^2} \tag{3.13}$$

Through a similar procedure, which leaves an exercise for the student, we can obtain

$$\nabla^2 \bar{E} = \mu_0 \varepsilon_0 \frac{\partial^2 \bar{E}}{\partial t^2} \tag{3.14}$$

Comparing (3.13) and (3.14) with equation (3.5) for general wave motion, we see that the velocity for an electromagnetic wave in free space is equal to

$$C = \frac{1}{\sqrt{\mu_0 \epsilon_0}} \tag{3.15}$$

Inserting the values for the dielectric constant and magnetic permeability of free space ($\epsilon_0 = 8.85 \times 10^{-12}$ and $\mu_0 = 4\pi \times 10^{-7}$) we obtain the familiar value for the velocity of light, $3 \times$ [illegible] meters per second.

If $\overline{E}$ is independent of y and z,

$$\nabla^2 \overline{E} = \frac{\partial^2 \overline{E}}{\partial x^2} \tag{3.16}$$

and the Wave Equation becomes:

$$\frac{\partial^2 \overline{E}}{\partial x^2} = \mu\epsilon \frac{\partial^2 \overline{E}}{\partial t^2} \tag{3.17}$$

For sinusoidal time varying fields:

$$\overline{E} = \overline{E}_0 \, e^{j\omega t} \tag{3.18}$$

$$= \overline{E}_0 \, (\cos \omega t + j \sin \omega t) \tag{3.19}$$

where $\omega = 2\pi f$ and is radian or angular frequency, f is frequency in Hertz. If $\overline{E} = \overline{E}_0 \, e^{j\omega t}$ then (3.17) becomes:

$$\frac{\partial^2 \overline{E}}{\partial x^2} = -\mu\epsilon\omega^2 \, \overline{E} \tag{3.20}$$

Taking only the y term of $\overline{E}$ we get

$$\frac{\partial^2 \overline{E}_y}{\partial x^2} = -\mu\epsilon\omega^2 \, \overline{E}_y \tag{3.21}$$

This represents a plane wave propagating in the x direction. From the general solution to linear second order differential equations we obtain

$$E_y = A_1 e^{-j\beta X} + A_2 e^{j\beta X} \tag{3.22}$$

where the first term is an outward propagating wave and the second term represents a wave returning to the source. Adding the time variation $e^{j\omega t}$ and concerning ouselves with only the outward going wave we get:

$$E_y = A_1 e^{j(\omega t - \beta X)} \tag{3.23}$$

Where $\beta = \omega\sqrt{\mu\varepsilon}$.

Equation (3.23) is the general solution for a plane wave propagating in a source free dielectric medium. Note that it does not attenuate with time or distance. (Free space if $\varepsilon = \varepsilon_0$ and $\mu = \mu_0$).

To determine velocity, note that E_y is maximum when $\omega t - \beta X = 0$. In order to always remain on a crest we must move in the X direction with a velocity

$$v = \frac{X}{t} = \frac{\omega}{\beta} = \frac{1}{\sqrt{\mu\varepsilon}} = c \tag{3.24}$$

which agrees with our previous result. From the definition of wavelength and frequency we have

$$v = \lambda f \tag{3.25}$$

where λ is wavelength in meters and f is frequency in Hertz. Combining (3.25) and (3.24) we obtain:

$$\beta = \frac{2\pi}{\lambda} \tag{3.26}$$

(Remember, $\omega = 2\pi f$).

And we see that β, the phase shift constant is a measure of radians* per meter.

Our solutions so far have dealt with EM waves propagating in a pure dielectric (non-conducting) medium. The medium is homogeneous, isotropic and source free. All other conditions result in a complication of the solutions.

3. 2. 1. General Solutions of Field Equations

Note: The medium now has finite conductivity, it is still homogeneous, isotropic and source free. Assuming sinusoidal time variations, $e^{j\omega t}$, the field equations may now be solved to obtain the general wave equations:

$$\nabla^2 \overline{E} = j\omega\mu(\sigma + j\omega\epsilon)\ \overline{E} \qquad (3.27)$$

$$\nabla^2 \overline{H} = j\omega\mu(\sigma + j\omega\epsilon)\ \overline{H} \qquad (3.28)$$

which are often written in the form

$$\nabla^2 \overline{E} = \gamma^2\ \overline{E} \qquad (3.29)$$

$$\nabla^2 \overline{H} = \gamma^2\ \overline{H} \qquad (3.30)$$

where γ is the propagation constant and equals

$$\gamma = \sqrt{(j\omega\mu)(\sigma + j\omega\epsilon)} \qquad (3.31)$$

The propagation constant is complex and may be written in terms of real and imaginary parts according to the relation

$$\gamma = \alpha + j\beta \qquad (3.32)$$

*All equations use radians for angular measure. One radian = 57.3°.

where α is the attenuation factor in Nepers per meter and β is the phase shift factor in radians per meter. Note:

$$\text{A Neper} = \frac{1}{e} = \frac{1}{2.71828....}$$

3. 2. 2. Plane Wave Solution

Again we will consider a uniform plane wave propagating in the X direction and (3.29) becomes

$$\frac{\partial^2 \overline{E}}{\partial x^2} = \gamma^2 \overline{E} \tag{3.33}$$

The solution of which takes the familiar form

$$\overline{E} = A_1 e^{\gamma X} + A_2 e^{-\gamma X} \tag{3.34}$$

Taking the outward propagating wave we write

$$\overline{E} = A_2 e^{-\gamma X} \tag{3.35}$$

and if we again introduce sinusoidal time variation we get

$$A_2 = A_0 e^{j\omega t}$$

then

$$\overline{E} = A_0 e^{j\omega t} e^{-\gamma X}$$

$$= A_0 e^{j\omega t} e^{-(\alpha+j\beta)X}$$

$$= A_0 e^{j\omega t} e^{-\alpha X} e^{-j\beta X}$$

and finally

$$\overline{E} = A_0 e^{-\alpha X} e^{j(\omega t - \beta X)} \tag{3.36}$$

Comparing (3.36) with (3.23) we see that the conducting medium has resulted in the added term, $e^{-\alpha X}$. Also, as we will soon see, the value for β has been changed. Equation (3.36) represents a wave propagating in the X direction at a velocity ω/β. It is attennated according to the factor $e^{-\alpha X}$. Note that α and β are the real and imaginary parts of

$$\gamma = [(j\omega\mu)\ (\sigma + j\omega\varepsilon)]^{1/2}$$

and that

$$\alpha = \omega[\frac{\mu\varepsilon}{2}((1 + \frac{\sigma^2}{\omega^2\varepsilon^2})^{1/2} - 1)]^{1/2} \qquad (3.37)$$

and

$$\beta = \omega[\frac{\mu\varepsilon}{2}((1 + \frac{\sigma^2}{\omega^2\varepsilon^2})^{1/2} + 1)]^{1/2} \qquad (3.38)$$

3. 2. 3. Intrinsic Impedance, η

For now we will simply introduce this parameter and define it as

$$\eta = \frac{\bar{E}}{\bar{H}} \qquad (3.39)$$

This is analogous to $R = \frac{V}{I}$, but do not confuse with $\rho = \frac{\bar{E}}{\bar{J}}$. η is the ratio of the $\bar{E}$ and $\bar{H}$ fields for a propagating plane wave and is related to the properties of the medium for the general case by the equation:

$$\eta = [\frac{j\omega\mu}{\sigma + j\omega\varepsilon}]^{1/2} \quad \text{ohms} \qquad (3.40)$$

Intrinsic impedance is a useful parameter because, as is evident from equation (3.40), it is a function of the

basic electromagnetic properties of the media and the frequency of the electromagnetic energy. Intrinsic impedance should be considered as undefined at both zero (DC) and infinite frequency. It must be used with considerable care since equation (3.40) is not valid when very close to the source of energy. This parameter is found to be quite useful for certain low frequency exploration systems, however, and it will be discussed in greater detail under the subject, Low Frequency Systems.

3. 2. 4. Depth of Penetration (Skin Depth)

The skin depth, δ, is defined as that depth in a medium at which waves are attenuated to 1/e or approximately 37 percent of their original value. Remember, 1/e is one Neper or 8.68 dB (see Appendix A for a discussion of decibels and nepers). Skin depth is finite only for media having finite conductivity since a wave in a pure dielectric, $\sigma = 0$, suffers no attenuation.

In a conducting medium, the wave amplitude decreases by the factor $e^{-\alpha X}$. We see, therefore, that when $\alpha X = 1$, the amplitude has decreased to 1/e of its value at $X = 0$. Therefore,

$$\delta = \frac{1}{\alpha} \quad \text{meters} \tag{3.41}$$

and for the general case of an homogeneous, isotropic medium,

$$\delta = \frac{1}{\omega\left[\frac{\mu\varepsilon}{2}\left(\left(1 + \frac{\sigma^2}{\omega^2\varepsilon^2}\right)^{1/2} - 1\right)\right]^{1/2}} \tag{3.42}$$

3. 2. 5. Conductors and Dielectrics

Maxwell's first equation may be written

$$\nabla \times \overline{H} = \sigma\overline{E} + j\omega\varepsilon\overline{E} \qquad (3.43)$$

conduction current ↑ displacement current ↑

From the above, it is evident that the ratio of conduction current to displacement current is

$$\frac{\sigma}{\omega\varepsilon} \qquad (3.44)$$

and therefore,

$$\frac{\sigma}{\omega\varepsilon} = 1$$

marks the dividing line between conductors and dielectrics. We may now write or define:

Perfect conductors -- $\sigma/\omega\varepsilon = \infty$

Good conductors -- $\sigma/\omega\varepsilon >> 1$

Good dielectric -- $\sigma/\omega\varepsilon << 1$

Perfect dielectric -- $\sigma/\omega\varepsilon = 0$

Note: 1) For copper, $\sigma/\omega\varepsilon \sim 3.5 \times 10^8$

2) For Mica, $\sigma/\omega\varepsilon \sim 0.0002$

3) For good conductors σ and ε are not functions of frequency.

4) For good dielectrics and most material in between, σ and ε are a function of frequency. This is true for most natural resources, soil, and rocks.

For good conductors and good dielectrics the general expressions for α (3.37), β (3.38), η (3.40), and δ (3.42)

may be simplified.

The student should try to arrive at some of the simplifications given in Tables 3.1, 3.2, and 3.3 to see why they are reasonable approximations. Note, the better the conductor or dielectric, the better is the approximation.

Table 3. 1 Wave Propagation in a Good Dielectric

$$\alpha \simeq \frac{\sigma}{2}\sqrt{\frac{\mu}{\varepsilon}} = \frac{1}{\delta}$$

$$\beta \simeq \omega\sqrt{\mu\varepsilon}\left(1 + \frac{\sigma^2}{8\omega^2\varepsilon^2}\right)$$

$$\eta \simeq \sqrt{\mu/\varepsilon}\left(1 + j\,\frac{\sigma}{2\omega\varepsilon}\right)$$

$$\delta \simeq 2/\sigma\sqrt{\frac{\mu}{\varepsilon}}$$

$$v \simeq v_0\left(1 - \frac{\sigma^2}{8\omega^2\varepsilon^2}\right)$$

Table 3. 2 Wave Propagation in a Perfect Dielectric

$$\alpha = 0$$

$$\beta = \omega\sqrt{\mu\varepsilon}$$

$$\eta = \sqrt{\frac{\mu}{\varepsilon}}$$

$$\delta = \infty$$

$$v = \frac{1}{\sqrt{\mu\varepsilon}}$$

Table 3.3 - Wave Propagation in a Good Conductor

$$\alpha = \beta \simeq \sqrt{\frac{\delta\mu\sigma}{2}}$$

$$\gamma \simeq \sqrt{j\omega\mu\sigma} \simeq \sqrt{\omega\mu\sigma}\ \angle 45^\circ$$

$$\eta \simeq \sqrt{\frac{j\omega\mu}{\sigma}} \simeq \sqrt{\frac{\omega\mu}{\sigma}}\ \angle 45^\circ$$

$$\delta \simeq \sqrt{\frac{2}{\omega\mu\sigma}}$$

$$v \simeq \frac{\omega}{\beta} \simeq \sqrt{\frac{2\omega}{\mu\sigma}}$$

The student should remember that we have been dealing with plain with plain electromagnetic waves in an homogeneous, isotropic, and source free medium.

PROBLEMS

3. 1. Compute the skin depth of a material having,

$$\sigma = 10^{-4} \text{ mhos/meter}$$

$$\varepsilon/\varepsilon_0 = 80$$

$$\mu = \mu_0$$

for frequencies of 10^4, 10^6, and 10^8 Hertz. Discuss your results.

3. 2. Derive the general equations for α and β from the general equation for γ.

3. 3. Calculate the wave impedance for a material having properties of,

$$\sigma = 10^{-2} \text{ mhos per meter}$$

$$\varepsilon/\varepsilon_0 = 1000$$

$$\mu = \mu_0$$

for frequencies of 10^4, 10^5, and 10^6 Hertz using the exact equation and the equation for a good conductor. Discuss your results.

3. 4. Using the four field equations (Maxwell's equations) and the three media equations, (2.30), (2.32), and (2.36), derive equation (3.14).

4.0 RADIATION

At the time of this printing, June, 1972, this section was still in preparation. When completed, this section will discuss the concepts of radiation, that phenomena whereby an electromagnetic field propagates away from its source at the speed of light. For the time being the student must obtain this information from lectures and from the references given at the end of Section 2.

5.0 ELECTROMAGNETIC PROPERTIES OF MATERIALS -- GENERAL

We have seen how the electromagnetic properties of materials effect current flow (conduction and displacement), electric and magnetic fields, and *EM* wave propagation.

We will now shift our viewpoint 180° and consider the effect of *EM* fields (forces) on materials, and attempt to determine the ease with which three phenomena take place in materials. These phenomena are:

Electric polarization

Magnetization

Conduction

The physical constants defined by these phenomena are, of course:

ε -- dielectric constant

μ -- magnetic permeability

σ -- electric conductivity

These constants, along with the shape and size of an object, control the scattering or reradiation of energy. This, in turn, determines the characteristics of a radar image of the object.

5.1 Conversion of Conductivity Units

If not already, you will inevitably run across other units of conductivity and resistivity. We will work with *mks* units so you should know how to convert other units to *mks*.

Resistivity, ρ, may be defined by

$$R = \frac{\rho \ell}{A}$$

from which we see that the resistance of a 1 meter cube of material having a resistivity of 1 ohm -- meter is

$$R = \frac{1 \times 1}{1} = 1 \text{ ohm}$$

In *cgs* units ℓ and A are in *cm* and cm^2 and we define resistivity as the resistance across a 1 *cm* cube. In *mks* units, for a 1 *cm* cube of the same material

$$R = \frac{1 \times 10^{-2}}{10^{-4}} = 100 \text{ ohms}$$

In *cgs* units

$$R = \frac{\rho \times 1}{1} = 100 \text{ ohms}$$

and therefore,

$$\rho = 100 \text{ ohm-cm}$$

and we may write

$$\rho \text{ mks} = \rho \text{ cgs}/100 \qquad (5.1)$$

and

$$\sigma \text{ mks} = 100\ \sigma \text{ cgs} \qquad (5.2)$$

similarly we find

$$\rho \text{ mks} = \rho\Omega - \text{ft}/3.281 \qquad (5.3)$$

$$\sigma \text{ mks} = 3.281\ \sigma \text{ mhos/ft} \qquad (5.4)$$

Physics handbooks and other references will often give σ *esu* (electrostatic units) values. Now, the units for voltage and current are also different and we would need to use the equation

$$V/I = \frac{\rho \ell}{A} = \frac{\ell}{\sigma A}$$

to determine the conversion factors

$$\rho\ mks = 9 \times 10^9\ \rho\ esu \qquad (5.5)$$

$$\sigma\ mks = \sigma\ esu/9 \times 10^9 \qquad (5.6)$$

5.2 Conduction in Metals

Materials are generally classed as:

a) metallic conductors if -- $\sigma > 10^5$ mhos/meter

b) semiconductors if -- $10^5 > \sigma > 10^{-8}$ mhos/meter

c) insulators if -- $\sigma < 10^{-8}$ mhos/meter

The use of the term semiconductor, to describe something in between a metallic conductor and an insulator, should not be confused with the common use of the same term to describe solid state devices and materials which conduct better in one direction than the other.

Most natural resources can be classed as semiconductors (as defined above). Nevertheless, it will be instructive to consider conduction in metals before progressing to other materials.

The free electron model of metals is based on valence electrons being able to move about freely through the volume of the specimen.

In the absence of an electric field the electrons move about randomly and

$$v_D = \frac{1}{N} \sum_{i=1}^{N} v_i = 0 \qquad (5.7)$$

where v_D is average or drift velocity of the electrons, v_i is velocity of individual electrons, and N is the total number of electrons per unit volume.

and is about equal to the total number of atoms. When an electric field is applied, the electrons experience an average force . The electrons will then accelerate according to the well known relation, $F = ma$ which, for the free electron model should be written,

$$F = m\left(\frac{dv_D}{dt} + \frac{v_D}{\tau}\right) \qquad (5.8)$$

where, τ, is the Relaxation Time, which is closely related to the time between collisions with other electrons. Note: if $\tau = 0$, $I = 0$, but if $\tau = \infty$, the electrons accelerate with little force and maintain the current indefinitely, e.g., for superconductors, $\tau = \infty$. τ is the time required for the electrons to approach rest conditions after having been accelerated to some value v_D. $\frac{mv_D}{\tau}$, is equivalent to a frictional or damping force. $m\frac{dv_D}{dt}$, is acceleration due to external forces. For an electric field, $F = eE$, where e is the electron charge, 1.6019×10^{-19} coulombs, we write,

$$eE = m\frac{dv_D}{dt} + \frac{v_D}{\tau} \qquad (5.9)$$

where m is the mass of the electron, 9.1×10^{-31} kgm. Under steady state conditions (for frequencies where $1/f >> \tau$. And

$$\frac{dv_D}{dt} \approx 0.$$

$$v_D = \frac{e\tau E}{m} \qquad (5.10)$$

We are now ready to show the relation between drift velocity, electron charge, etc., and the conductivity of a metal. The free charge density in a metal is obviously

$$\rho_q = Ne \qquad (5.11)$$

where ρ_q is charge density in coulombs/m^3, N is the number of free electrons per meter^3, and e is the electron charge in coulombs, or,

$$\rho_q = \frac{electrons}{meter^3} \cdot \frac{coulombs}{electron} = \frac{coulombs}{meter^3}$$

If we now introduce drift velocity we obtain,

$$Nev_D = \frac{coulombs}{meter^3} \cdot \frac{meters}{second}$$

equals,

$$\frac{coulombs}{meter^2\text{-}sec}$$

but,

$$\frac{coulombs}{second} = amperes$$

so,

$$Nev_D = \frac{amperes}{meter^2}$$

and we may write,

$$J = Nev_D \qquad (5.12)$$

and with (5.10) we obtain,

$$J = \frac{Ne^2\tau}{m} E \qquad (5.13)$$

Which from,

$$J = \sigma E$$

yields,

$$\sigma = \frac{Ne^2\tau}{m} \qquad (5.14)$$

In equation (5.14) note the terms Ne, charge density and e/m, which results from acceleration being proportional to e and inversely proportional to m.

For copper, Quantum Theory tells us,

$$\tau \approx 2 \times 10^{14} \text{ second}$$

Assuming each atom contributes one electron and since there are 6.025×10^{23} atoms per molecule and since one molar volume (volume occupied by one gram-molecule-weight) for copper is 7.1 cm^3, we obtain N as,

$$N = 10^6 \, (6.025 \times 10^{23})/7.1$$

equals

$$8.5 \times 10^{28} \text{ electrons}/m^3$$

Therefore for copper,

$$\sigma = \frac{(8.5 \times 10^{28}) \, (2.56 \times 10^{-38}) (2 \times 10^{-14})}{9.1 \times 10^{-31}}$$

$$4.8 \times 10^7 \text{ mhos/meter}$$

which is reasonably close to handbook values of 5.7×10^7.

We now introduce mobility, υ (upsilon), which by definition is,

$$\upsilon = \frac{v_D}{E} = \frac{e\tau}{m}, \quad \frac{\text{meters}^2}{\text{volt-sec}} \qquad (5.15)$$

Mobility is a measure of the ease with which a particle is accelerated by an electric field. We may now write, by combining (5.14) and (5.15),

$$\sigma = Nev \qquad (5.16)$$

or for the more general case,

$$\sigma = N_1 \, q_1 \, v_1 + N_2 \, q_2 \, v_2 + \ldots N_\eta \, q_\eta \, v_\eta \qquad (5.17)$$

where N_i is the number of free charge carriers/m^3 of the i^{th} type, q_i is the charge/carrier, v_i is the mobility of the i^{th} charge carrier. This brings us to the point that we may consider conduction in any media containing free charge carriers.

5.3 Conduction in Electrolytes

Conduction in most natural resources is due to the presence of salts in solution. Salts in solution form an electrolyte, and conduction takes place via the movement of ions. Changes in the chemical makeup of plants, soils, water, etc., will, therefore, effect the conductivity of the materials. This change in conductivity may then be detectable with a remote sensing system. If we can estimate the magnitude of the change in conductivity which will result from some change in a resource of interest, then we can determine the probability of detecting the change remotely. In very dilute solutions, we may use equation (5.17) to compute conductivity, where each term represents an ion in solution.

The equation is usually written in the form,

$$\sigma = F\,(C_1\,\eta_1\,\upsilon_1 + C_2\,\eta_2\,\upsilon_2 + \ldots + C_\eta\,\eta_\eta\,\upsilon_\eta) \qquad (5.18)$$

where F is Faraday's number = 96,500 coulombs/gram equivalent weight, C_i is the concentration of the i^{th} ion in gram molecular weights per meter^3, η_i is the absolute value of the valence of the i^{th} ion, and υ_i is the mobility of the i^{th} ion. Note: υ_i is a function of C_i and temperature.

We will leave it up to the student to show the equivalence of (5.17) and (5.18). Example:

The conductivity of a one percent (by weight) NaCl solution (also given as 10 grams/liter and 10 0/00) calculates to be (at 25° C): The number of gram molecule weights/m^3 is,

$$c = \frac{10^4\ (grams\ NaCl)}{58.43\ (MW\ of\ NaCl)} = 171$$

$$c_{Na} = c_{Cl} = 171$$

$$n_{Na} = n_{Cl} = 1$$

$$\upsilon_{Na} = 5.2 \times 10^{-8} \text{ (dilute solution at 25° C)}$$

$$\upsilon_{Cl} = 7.9 \times 10^{-8} \text{ (dilute solution at 25° C)}$$

Now,

$$\sigma = 96{,}500\ (171\ (5.2 \times 10^{-8}) + 171\ (7.9 \times 10^{-8})) =$$

$$2.16 \text{ mhos/meter}$$

The following comparisons between calculated and measured σ for *NaCl* solutions shows the reduction of υ for concentrated solutions (the value of υ for a dilute solution was used).

Table 5.1 -- NaCl Solutions at 25° C

Salinity (gm/liter)	σ calc. (mhos/m)	σ meas. (mhos/m)
0.01	0.00216	0.0021+
0.1	0.0216	0.02
1.0	0.216	0.185
10.0	2.16	1.7
100.0	21.6	11.0

Table 5.2 – Mobility of Ions at 25° C

Ion	Mobility	
H^+	36.2×10^{-8}	m^2/volt-second
OH^-	20.5	
$SO_4^=$	8.3	
Na^+	5.2	
Cl^-	7.9	
K^+	7.6	
NO_3^-	7.4	*(From Keller)*

The conductivity of solid electrolytes and electronic semiconductors will not be studied in detail because these methods of conduction are not important for most natural resources.

5.4 The Electric Polarization of Materials

Polarization involves the displacement of charge, or the alignment of particles having a permanent displacement of charge, i.e., electric dipoles. Polarization does not involve the transportation of charge through the sample.

All materials are polarizable to a greater or lesser degree. The total polarizability of a material may be divided into five parts: 1) electronic; 2) ionic; 3) orientational or dipolar; 4) interfacial; and 5) electrochemical (overvoltage effect). A brief description of these five polarization processes follows.

1) Electronic. This process involves the displacement or deformation of electron orbits or spins about atomic nuclei,

this is effective at optical frequencies and down.

2) Ionic. This involves the displacement or deformation of ions and is effective below optical frequencies.

3) Dipolar. This is due to the alignment of molecular dipoles,

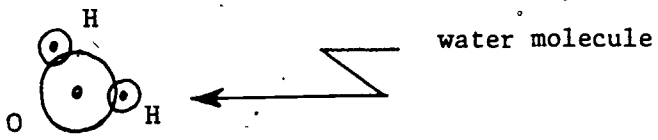

Water is the most important; its dipole structure makes it a solvent. For water at room temperature, $\tau \approx 0.25 \times 10^{-10}$ *second.*

4) Interfacial. Caused by small capacitors formed by structural interfaces, i.e., conducting regions separated by insulators.

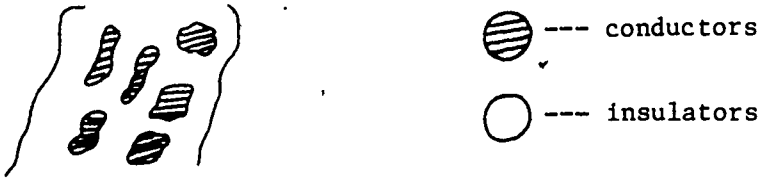

The frequency range is limited by the mobility of conducting particles.

5) Electrochemical. This process is very important in the search for sulfide minerals. It is associated with ionic transfer from solid to liquid and a difference in potential required to go from liquid to solid vs. solid to liquid. Very low frequency effect -- 0.1 to 1000 Hz. We will study in more detail later.

For materials exhibiting both conduction and polarization processes, the expression for current density becomes,

$$J = (\sigma + j\omega\varepsilon)\, E \qquad (5.19)$$

which indicates that conduction current is in phase with E and that displacement current leads E by 90°, or in other words, is a quadrature component of current. Displacement or quadrature currents do not result in any power loss, they do instead, represent energy stored.

The slight movement of charge or rotation of a dipole, does take a small amount of energy, however, which results in an energy loss, or in-phase component of current. The higher the frequency, relative to $1/\tau$, the more significant becomes this in-phase current. When the frequency becomes so high that the dipole rotation, ion movement, electron pattern, etc., cannot respond appreciably in a 1/2 cycle, then the dielectric looks like a poor conductor.

This results in a complex relative dielectric constant:

$$\hat{\varepsilon} = \varepsilon^1 - j\varepsilon''$$

Note:

$$\varepsilon = \varepsilon^1 \varepsilon_0$$

The student should become familiar with the terms Relaxation Time, τ, Relaxation Frequency, f_c, Loss Tangent and Loss Angle, all of which are interrelated as shown below,

$$f_c = \frac{1}{\tau} \qquad (5.20)$$

$$\tan\phi = \frac{\varepsilon''}{\varepsilon'} = \frac{f}{f_c} \qquad (5.21)$$

When $\tan\phi = 1$, $f = f_c$ and $\varepsilon'' = \varepsilon'$, which means simply that conduction and displacement components of current are equal.

Note that we may write the general equation (5.19) as,

$$J = (\sigma_{DC} + j\omega\ (\varepsilon' - j\varepsilon'')\varepsilon_0)\ E \qquad (5.22)$$

and if

$$\sigma_{DC} = 0$$

then an *ac*, σ_{eff} may be obtained from

$$j\omega\varepsilon'\ \varepsilon_0 + \omega\varepsilon''\ \varepsilon_0$$

When σ_{DC} is not equal to *0*, the situation becomes more complex.

5.5 Magnetic Permeability

The magnetic permeability of most (virtually all) natural resources is equal to that of free space, i.e.,

$$\mu_0 = 4\pi\ x\ 10^{-7} \quad \textit{Henrys/meter}$$

The only significant exception are iron ore minerals and nickel ore. Values for ferromagnetic minerals and other common minerals are given in Table 5.3 and Figure 5.3.

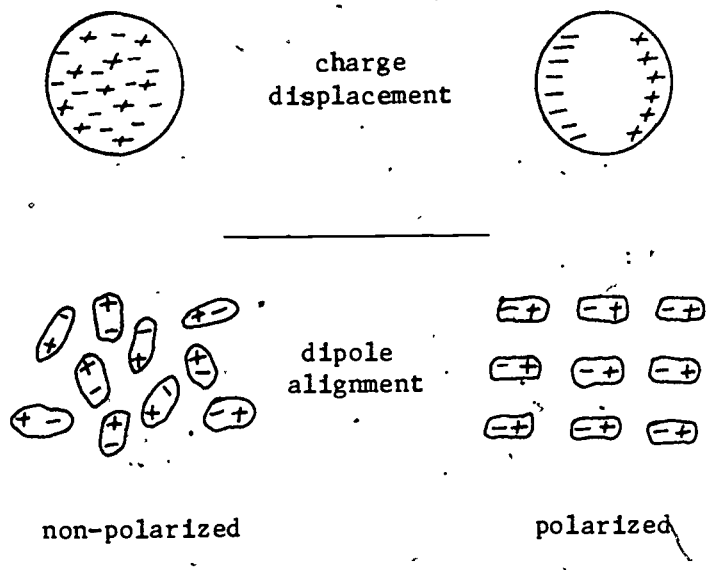

FIGURE 5.1 Illustration of Polarization from Charge Displacement and Dipole Alignment.

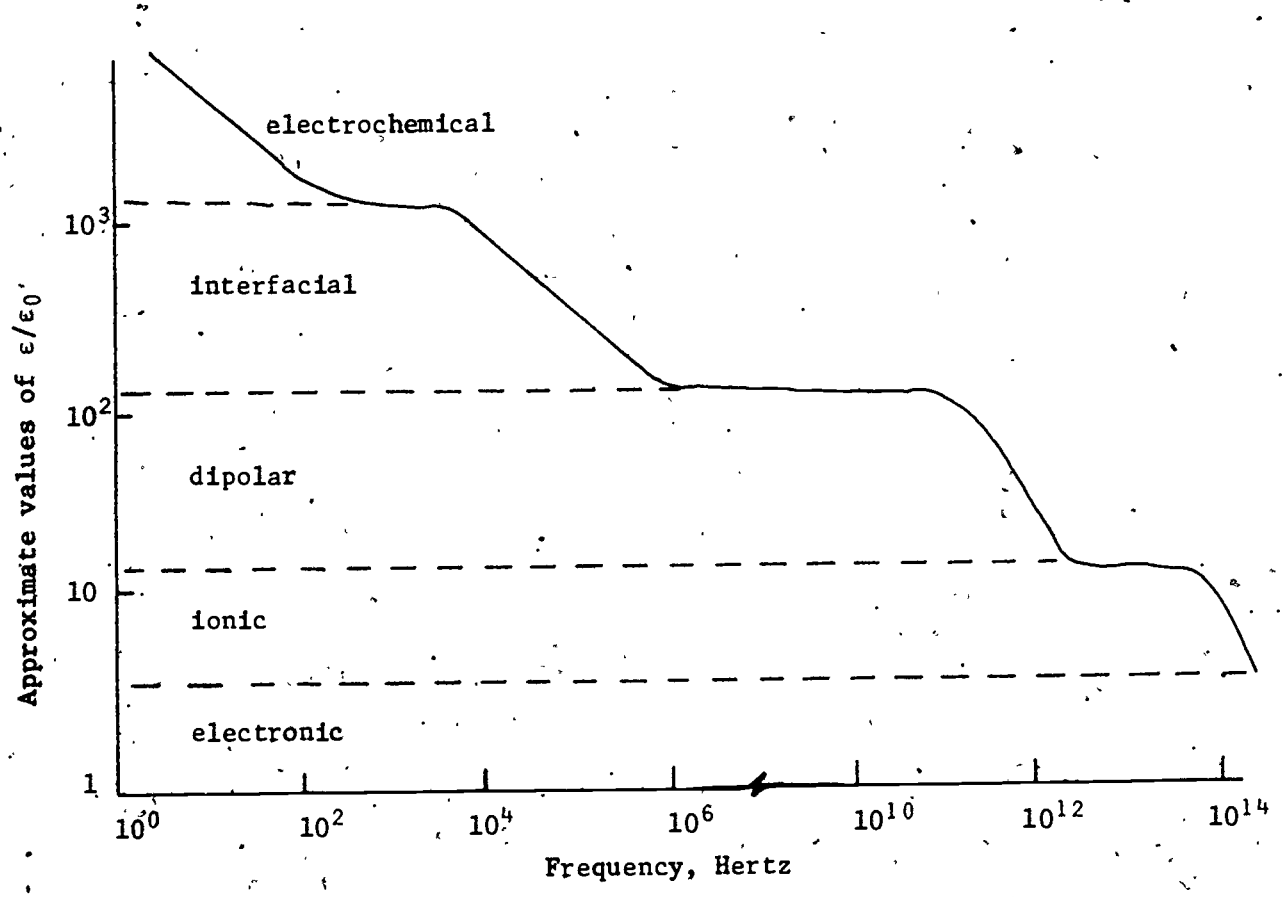

FIGURE 5.2 General Frequency Dependence of the Several Contributions to Polarization of Materials.

Table 5.3 Relative Magnetic Permeability of Some Common Minerals

Mineral	
Magnetite	5.0
Pyrrhotite	2.55
Ilmenite	1.55
Hematite	1.053
Pyrite	1.0015
Rutile	1.0000035
Calcite	0.000087
Quartz	0.999985

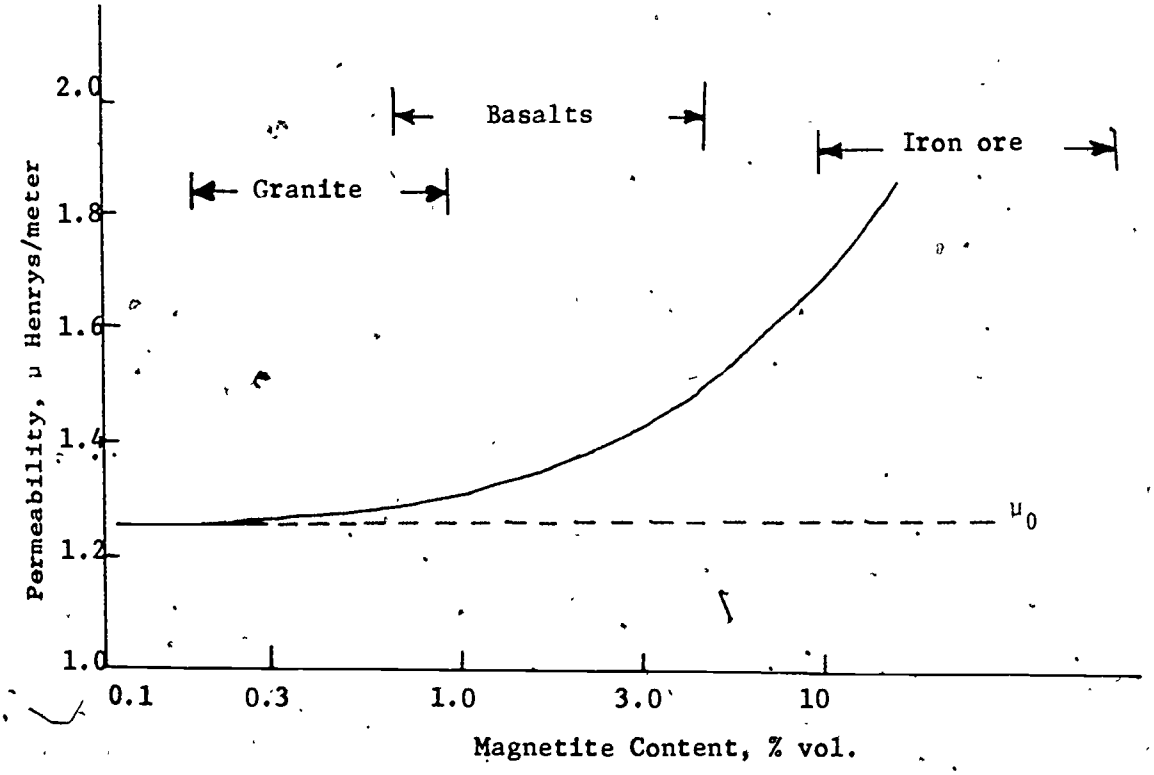

FIGURE 5.3 Relation Between Percent Magnetite and Permeability

Problems for Section 5.0

5.1 Show that equations (5.17) and (5.18) are equivalent and that units do reduce to mhos per meter.

5.2 Compute the conductivity of a 0.01 percent solution of sulfuric acid.

5.3 Compute the acceleration (meters per second^2) of an electron in a vacuum, in an electric field of 1000 volts per meter.

5.4 Given a 10 foot length of one inch plastic tubing filled with a 0.1 percent solution, compute the conductivity of the solution in mhos per foot and mhos per meter and compute the resistance from one end to the other. The solution is Hydrochloric Acid.

6. Electromagnetic Properties of Water, Snow, and Ice

The characteristics of water, snow, and ice are very important because the electrical properties of most natural resources are controlled by their water content. Water itself is, of course, one of our most important natural resources and any means capable of providing better information as to its availability and purity is of considerable importance.

6. 1. Water

Very pure water has a conductivity in the order of 4×10^{-6} mhos per meter. Lake Superior, noted for its relative purity, has a conductivity of 9×10^{-3} mhos per meter. This is equivalent to a total dissolved salt content of about 50 parts per million. Rivers and lakes in general have conductivities between 10^{-1} and 10^{-3} mhos per meter. The oceans, on the other hand, have conductivities of 2.5 to 5.5 mhos per meter with an average value of 4 mhos per meter. Figure 6-1 shows the electrical conductivity of water as a function of temperature and salinity.

Figure 6-2 shows the dielectric constant of water at room temperature as a function of frequency. The high dielectric constant of water is, of course, due to the dipolar nature of the water molecule. The relaxation time and relaxation frequency for water are respectively 0.25×10^{-10} seconds and 4×10^{10} Hertz.

6. 2. Snow and Ice

Since the conductivity and dielectric constant of water are controlled by ions in solution and the dipolar nature of the water molecule, freezing drastically alters the electrical properties. This change is due primarily to two factors: 1) ions tend to remain in

solution as the water freezes; and 2) the water molecule in the solid state cannot rotate as easily as it does in the liquid state. From Auty and Cole, 1952 (See Figure 6-3), we see that for pure ice, relaxation frequencies are very low. It is interesting to note that as the ice becomes colder, the relaxation frequency is reduced quite drastically.

The following material is taken almost verbatim from Watt and Maxwell, 1960.

The electrical and physical properties of ice have been discussed in considerable detail by Dorsey, 1940. He presents tabulations of permittivity and conductivity as reported by numerous observers. A more recent paper by Auty and Cole, 1952, has analyzed the lack of close agreement between measured dielectric constants of ice and has found that in general they appear to be attributable to the formation of voids or cracks in the samples being measured.

For a material with a single relaxation frequency, the simple theory of dielectric relaxation predicts a complex dielectric constant $\bar{\varepsilon}$

$$\bar{\varepsilon} = \varepsilon' - i\varepsilon'' = \varepsilon_\infty + (\varepsilon_{dc} - \varepsilon_\infty)/(1 + if/f_c) \qquad (6.1)$$

where the time factor is $e^{i\omega t}$, ε_{dc}, and ε_∞ are the so-called equilibrium and limiting high-frequency values of relative dielectric constant, f is the frequency at which the electrical properties are being measured, and f_c is defined as the relaxation frequency, which is equal to $1/\tau$, where τ is the relaxation time. The complex plane presentation of $\bar{\varepsilon}$ forms semi-circles as shown in Figure 6-3. This type of presentation is known as the Argand diagram. Auty and Cole, with carefully designed equipment and experimental procedures, found

that pure ice does in fact adhere very closely to the form predicted by this simple theory, and they were able to obtain results with a high degree of repeatability. From their data we have obtained the relaxation frequency f_c as a function of temperature as shown in Figure 6-4. The high frequency dielectric constant ε_∞ was found to be very close to 3 for all temperatures ranging from -0.1° C to -65.8°C. Equilibrium values, ε_{dc}, also shown in Figure 6-4, range from approximately 90 to 114 over the temperature range indicated. The value of ε corresponding to the relaxation frequency, ε_c, permits a rapid construction of Argand diagrams since this point represents the center of the semi circular diagram. Frequencies at other points on this diagram can readily be obtained by the relationship

$$\tan \phi = f/f_c \qquad (6.2)$$

where ϕ is the angle indicated in Figure 6-3. The relative dielectric constant $\varepsilon' = \varepsilon/\varepsilon_o$ can be readily obtained from diagrams such as Figure 6-3 and the results presented as a function of frequency for various temperatures as shown in Figure 6-5.

The conductivity of pure ice can be obtained from the Argand diagram of Figure 6-3 by means of the relationship

$$\sigma = \varepsilon'' \omega \varepsilon_o \qquad (6.3)$$

which can also be written as

$$\sigma = 5.56 \times 10^{-11} \varepsilon'' f \qquad (6.4)$$

where f is the frequency in Hertz and σ is the conductivity in mhos per

meter. The results of these calculations, shown in Figure 6-6, indicate that for a given temperature and at frequencies below the relaxation frequency, that conductivity is directly proportional to the square of the frequency.

The properties of drifted snow were measured at two locations in the mountains of Colorado. The resulting Argand diagrams are shown in Figure 6-7 where it is obvious that the characteristics are different from those of pure ice. Four electrode methods of measuring the absolute magnitude of the complex conductivity are also employed and a comparison of results is shown in Figure 6-8. Relatively good agreement exists between the two types of measurements. It should be pointed out that the rather large values of ε'', which result from an increase in conductivity, are probably due to the presence of impurities in the snow.

Observations made on the Athabasca glacier near Jasper, Alberta, Canada produced the Argand diagram shown in Figure 6-9. Note that the general circular form expected for pure ice having a simple dielectric relaxation is obtained for frequencies down to approximately 2 kHz. Below this the ε'' values increase quite rapidly, indicating an appreciable amount of conductivity.

A comparison of the magnitude of the complex conductivyt as obtained by bridge and four-electrode Eltran measurements, Figure 6-10 shows close agreement. This may be due to the fact that the rods were surrounded by a very thin interface of water. These sets of observations were obtained in the same general area on the glacier, and would indicate that the large observed values of ε' and ε'' are probably real. It should be pointed out that some dispersion was found between observations

in different areas on the glacier, due possibly to cracks and crevasses.

The parallel plate observations of Figure 6-9 were made near the surface of the ice which was rather porous and wet at the time of measurement. The rods on the ridge were placed in the same general area as the parallel plate measurements, but being 4 feet long are expected to give results typical for ice several feet below the surface which was observed to be much more solid than the surface ice. The third curve for rods in a crevasse represents measurements made some 30 feet below the surface of the glacier where the ice was less disturbed by wind action, and in addition, it was expected to be slightly colder than the surface ice. This reduction in temperature with depth is indicated by the fact that rods in or near the surface caused melting around them while rods a hundred feet or so below the surface would freeze in place.

Figure 6-11 shows $|\overline{\sigma}|$ as a function of frequency for three different electrode spacings on the Athabasca glacier. It is interesting to note the reversal in magnitude at the 100 Hz region. It is obvious from these results that the properties of the glacier change with depth and that this change has an inverse effect at frequencies above and below the 100 Hz region.

It is instructive to observe the manner in which the conductivity, admittivity, and loss tangent vary as a function of frequency. A typical example taken from the Athabasca glacier for 0° C glacial ice is shown in Figure 6-12 where it can be seen that the loss tangent increases below one kc rather than continuing to decrease as it does for pure ice.

Additional measurements were made on the Greenland ice cap some 10 miles from the coast in the vicinity of Thule. Ice temperatures

ranged from -5.5° C to -8° C. The results of these measurements are shown in the Argand diagram of Figure 6-13. It would appear that the conductivity is appreciably higher than was observed on the Athabasca glacier. The data at -8° C was taken in an ice tunnel several hundred feet below the surface of the ice cap so that any local contamination due to salt from sea spray being carried inland is not expected to be important. The wide range of electrical properties of snow and glacial ice can be seen in Figure 6-14 which summarizes many of the results presented.

From these results, it would appear that further observations should be made on the colder glacial ice, and that bridge measurements under such conditions should include several larger spacings, i.e., larger d/A ratios.

6. 3. Sea Ice

The electric properties of sea ice are very complex and variable. Sea ice is a mixture of ice, brine, salts, and air in proportions and spacial arrangements determined by the temperature, thermal history, and conditions during formation. A wide range of conductivity and dielectric constant values are found. Unfortunately, almost no good data, correlating conductivity and dielectric constant with salinity temperature, age, etc. is available.

Figure 6-15, a phase diagram of sea ice, shows the temperature at which various salts begin to crystalize from the solution. The arrows on the right hand side of this Figure indicate the probable ice, salt, brine ratio at -60° centigrade. Obviously, as the percentage of brine is reduced in relation to ice and solid salts, the conductivity of the ice will be lowered.

Figure 6-16 from Anderson and Weeks, 1958, shows the cellular structure of sea ice. The cylindrical brine cells shown tend to migrate toward the warm side of the ice formation. Thus, they migrate upward in summer and down in winter. Old sea ice tends, therefore, to be more resistive since much of the brine has escaped during several up and down migrations.

The only data available on the conductivity of sea ice have been taken at either very low frequencies, below 100 Hertz or very high frequencies, 10^8 Hertz. This data, obtained by Cook, 1960, Dichtel and Lundquist, 1951, and Pounder and Little, 1959, is shown in Table 6-1.

Table 6-1

Electrical Properties of Sea Ice

Source	Frequency	Temperature, ^oC	σ, mhos per meter
Dichtel	~ 10 H_z	-8	$\sim 10^{-3}$
Dichtel	~ 10 H_z	-24	$\sim 10^{-4}$
Pounder	~ 10 H_z	0^o to -10^o	10^{-1} to 10^{-3}
Cook	10^8 H_z	-20^o	10^{-1}
Cook	10^8 H_z	-30^o	10^{-2}

As would be expected, the electrical properties of sea ice are a function of temperature and frequency. It will require considerably more data to obtain a reasonable understanding of these functions.

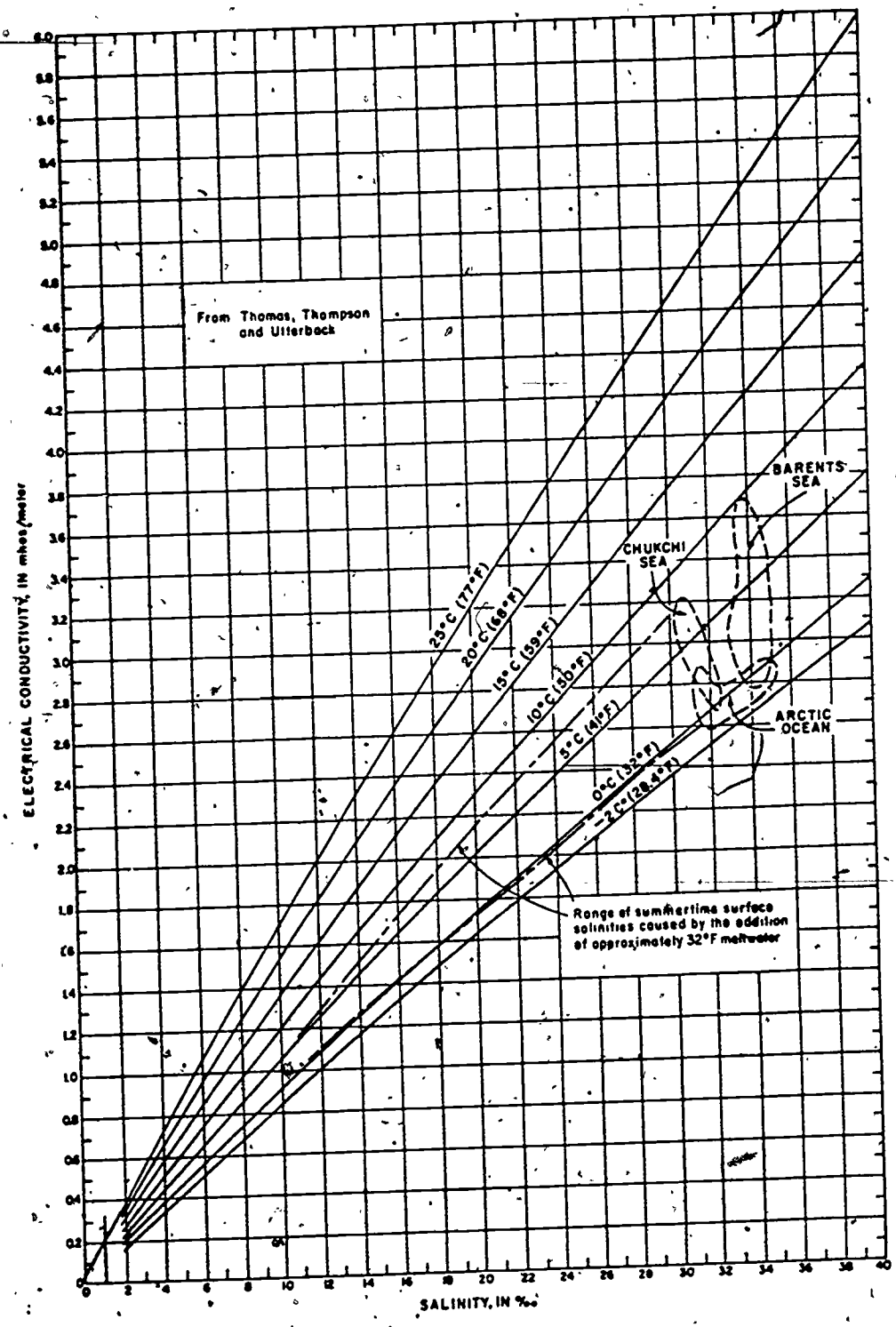

FIGURE 6-1: ELECTRICAL CONDUCTIVITY OF SEA-WATER VS TEMPERATURE AND SALINITY

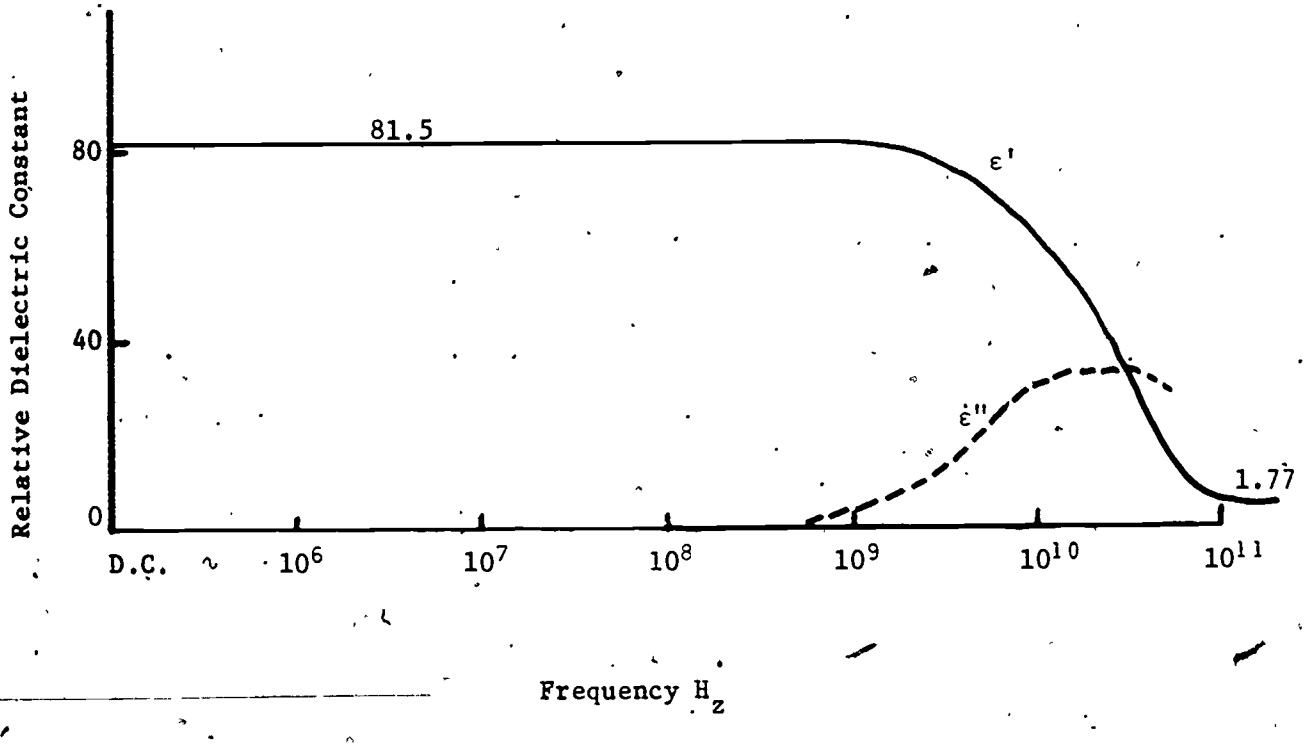

FIGURE 6-2: Dielectric Constant at Room Temperature For Water

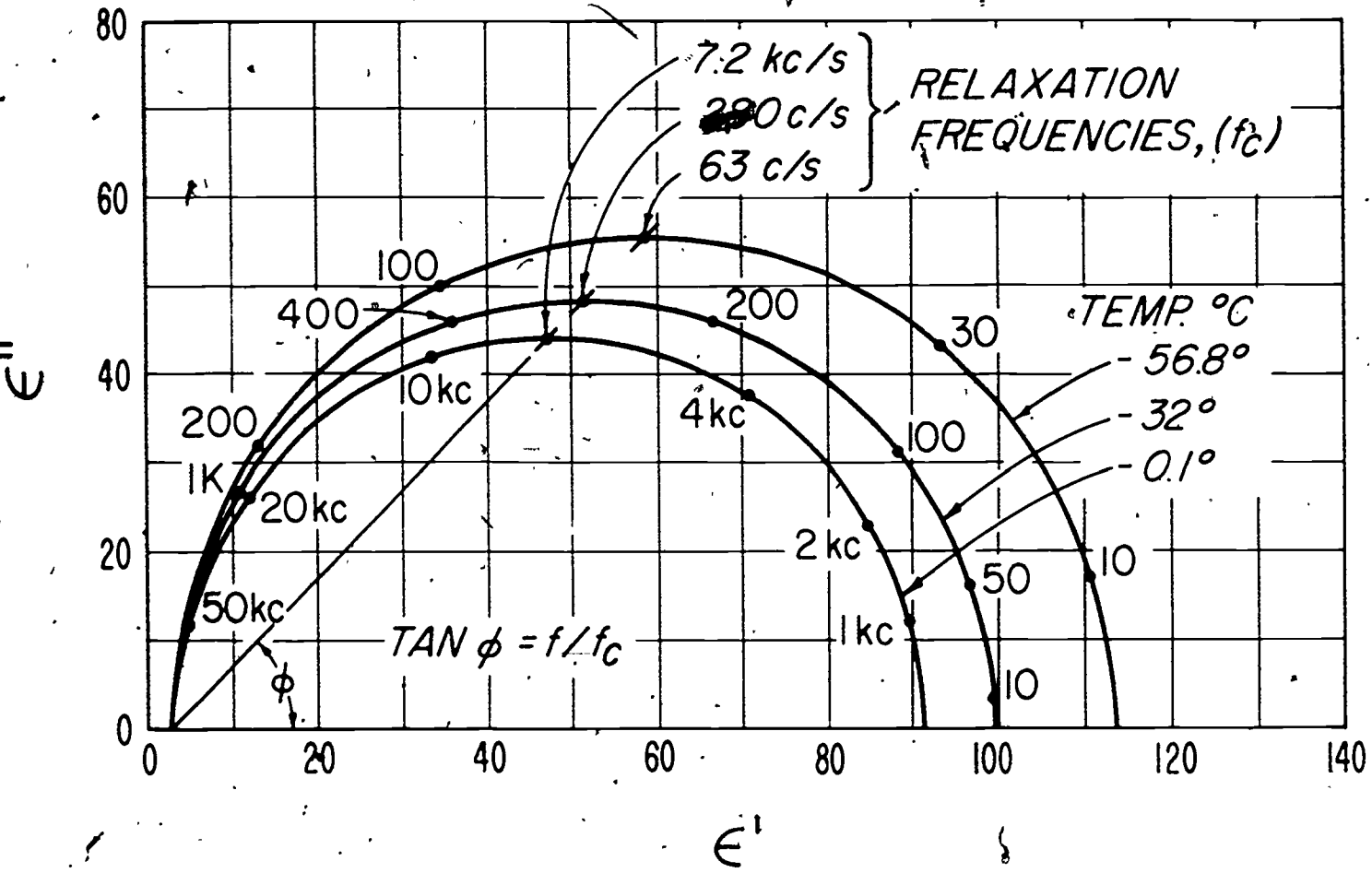

FIGURE 6-3: Electrical Properties of Pure Ice. From Auty and Cole.

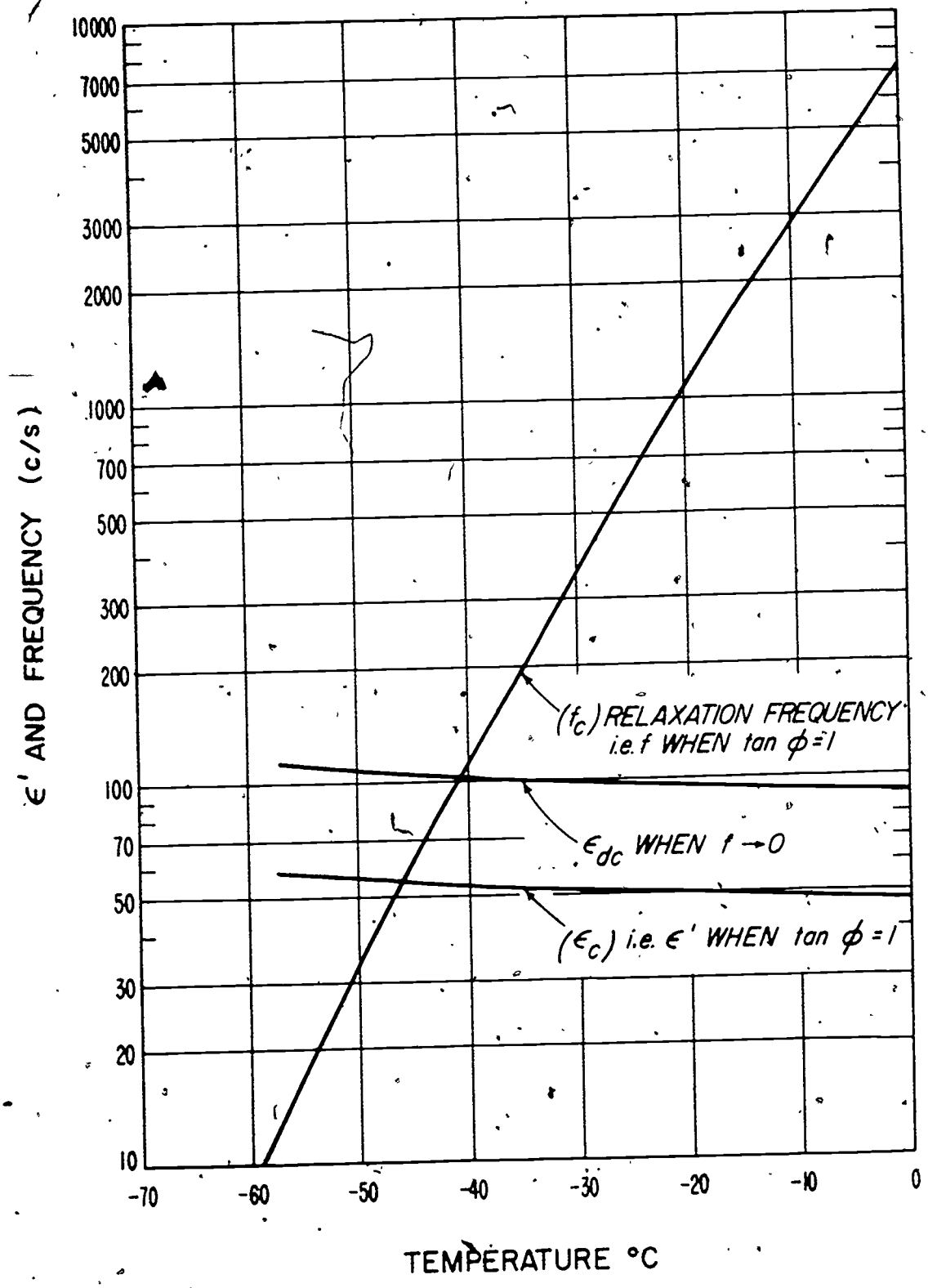

FIGURE 6-4: Pure Ice -- Frequency and Relative Permittivity when Tan ϕ = 1 - vs - Temperature. From Auty and Cole.

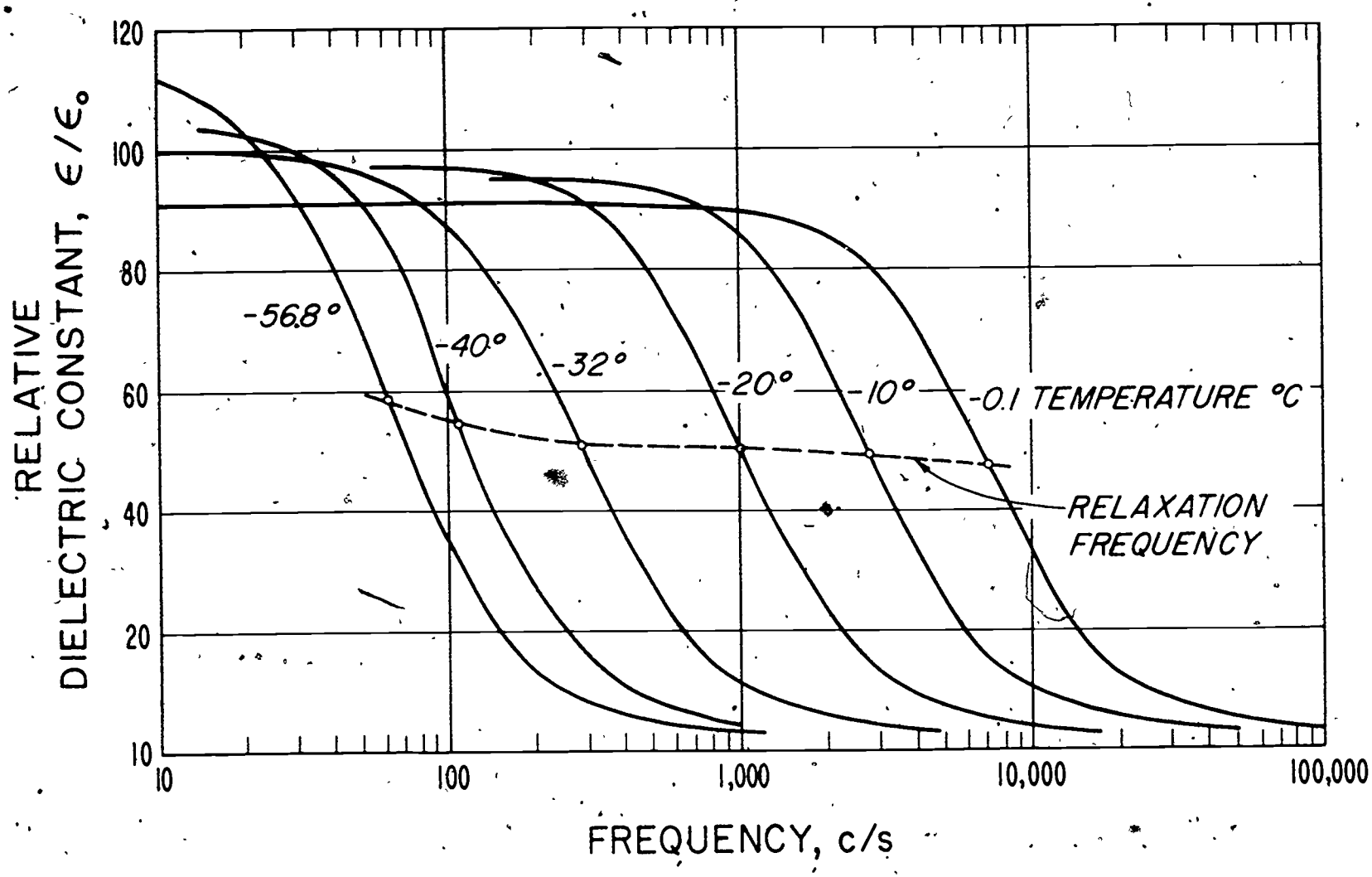

FIGURE 6-5: Relative Dielectric Constant of Pure Ice. Calculation based on Auty and Cole.

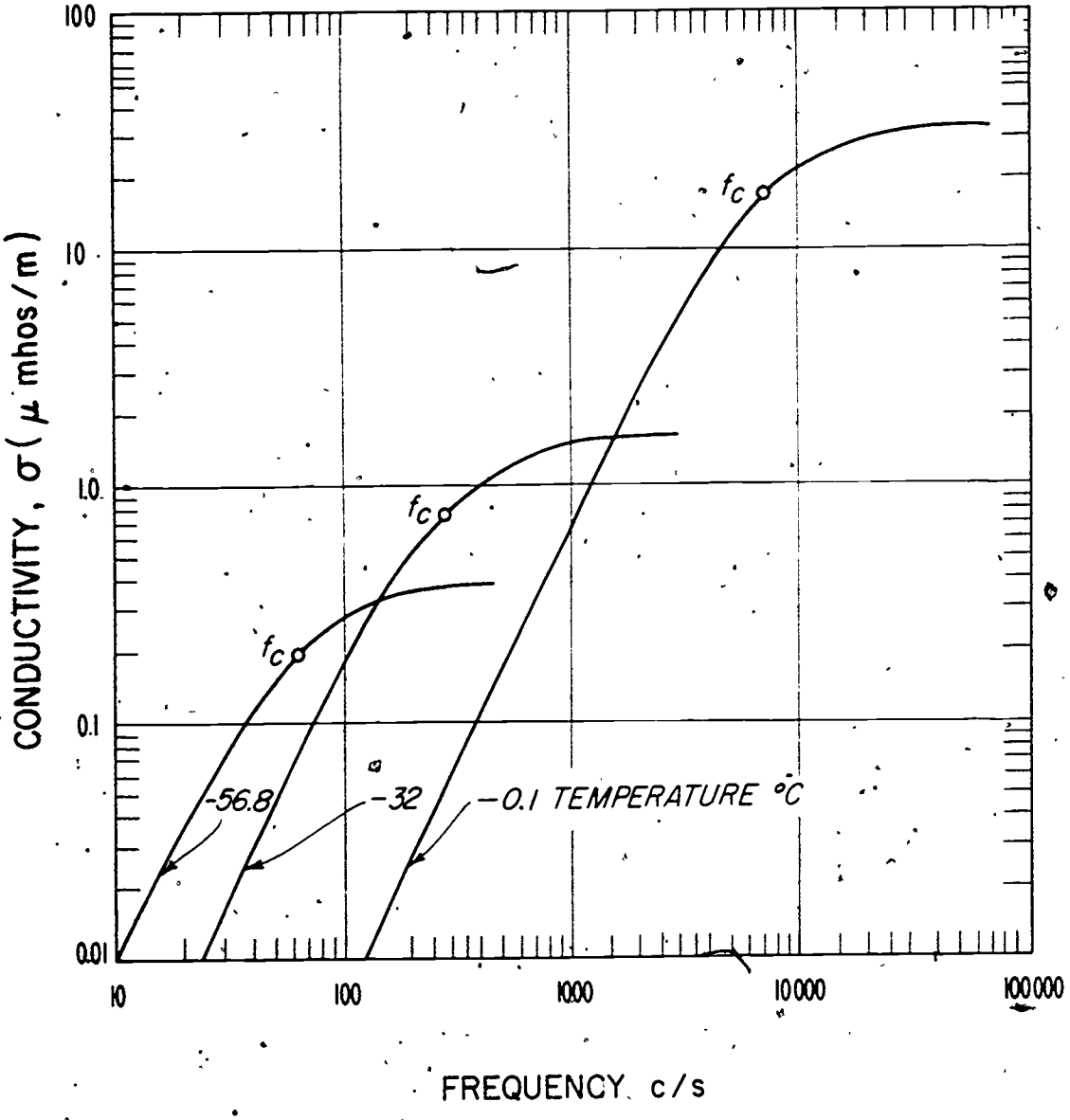

FIGURE 6-6: Conductivity of Pure Ice. Calculations based on Auty and Cole.

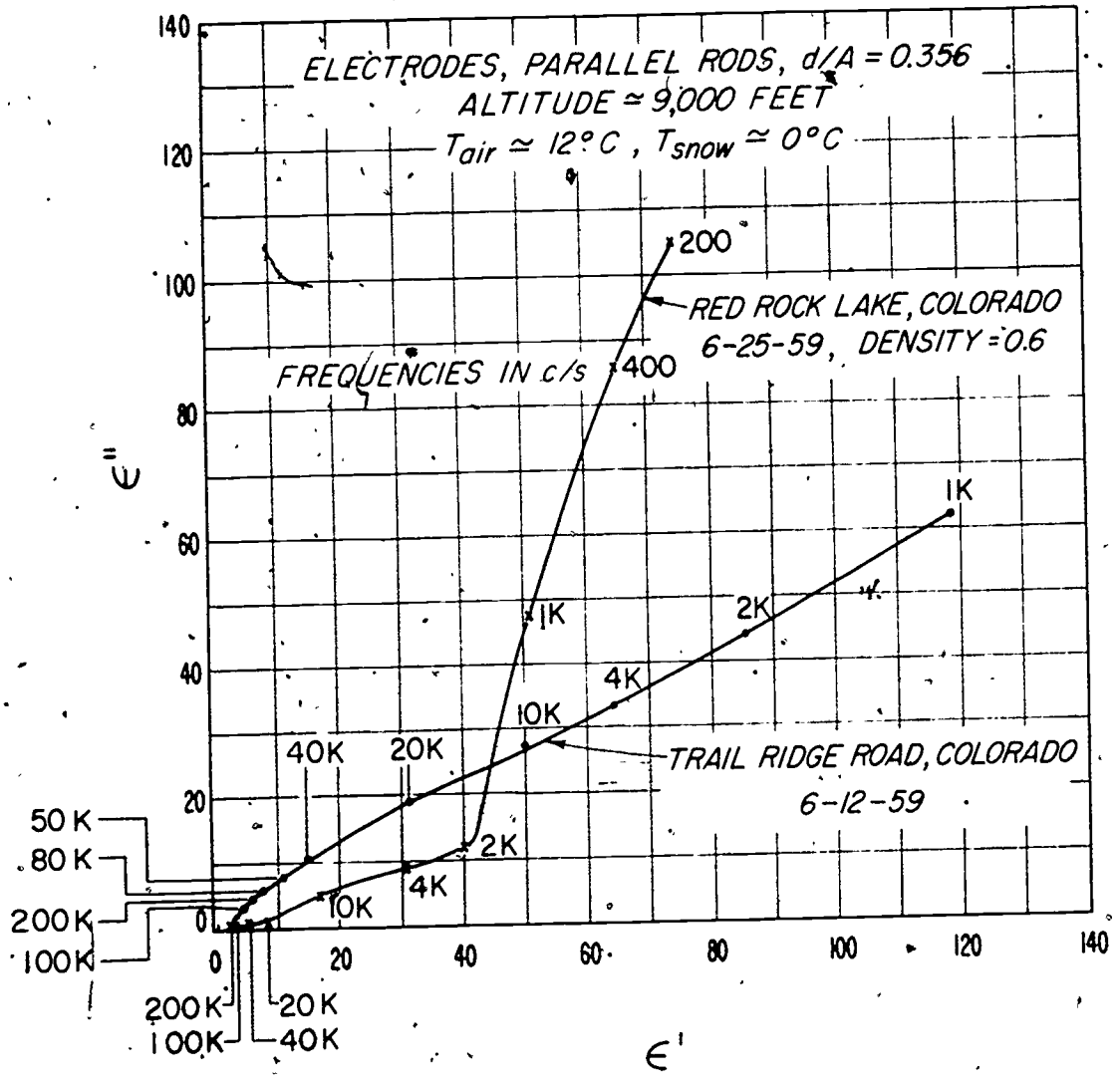

FIGURE 6-7: Electrical Properties of Spring Drift Snow. Compact and Wet.

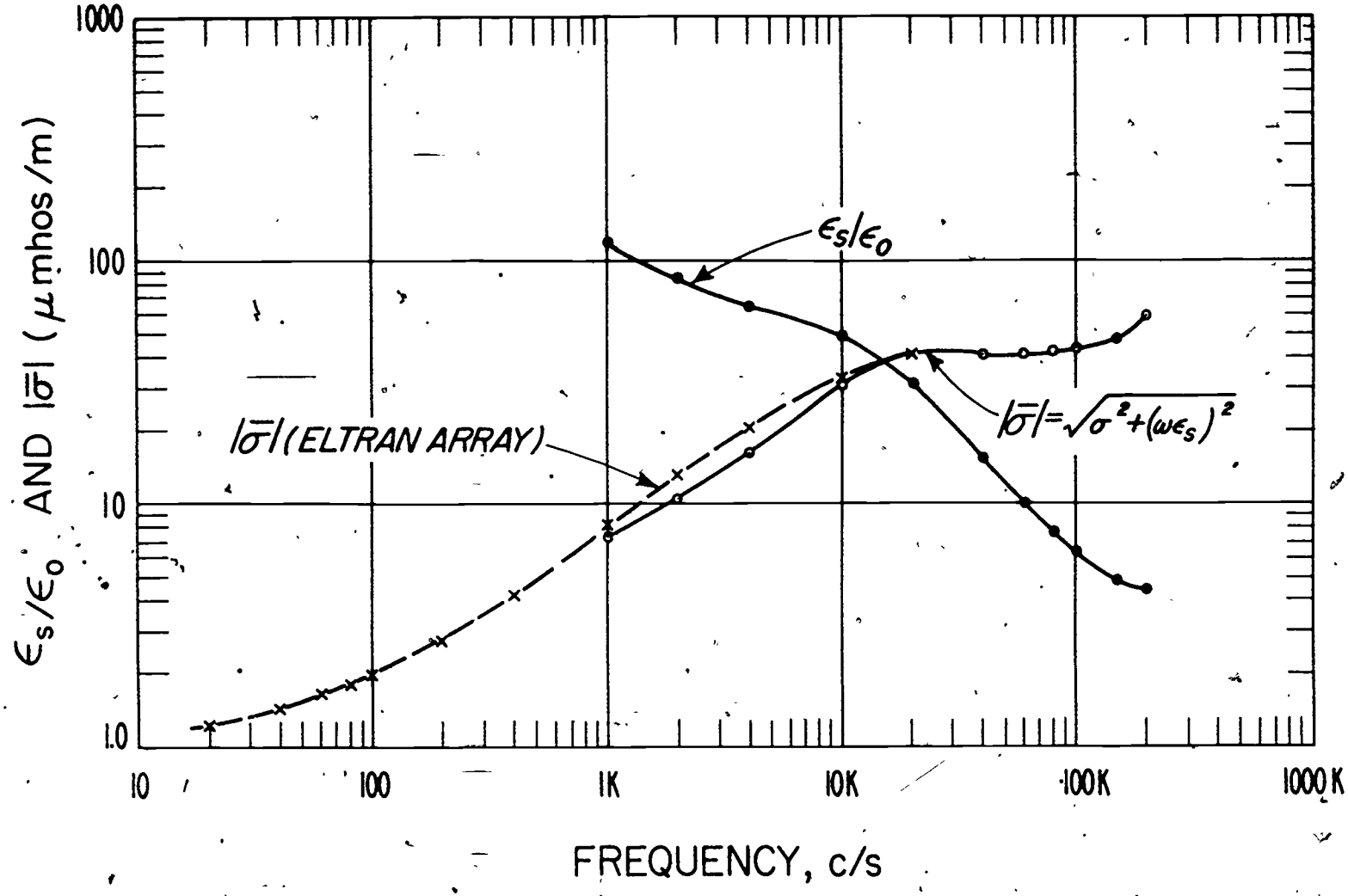

FIGURE 6-8: Electrical Properties of Wet Snow. Trail Ridge Road, Colorado, 6/12/59.

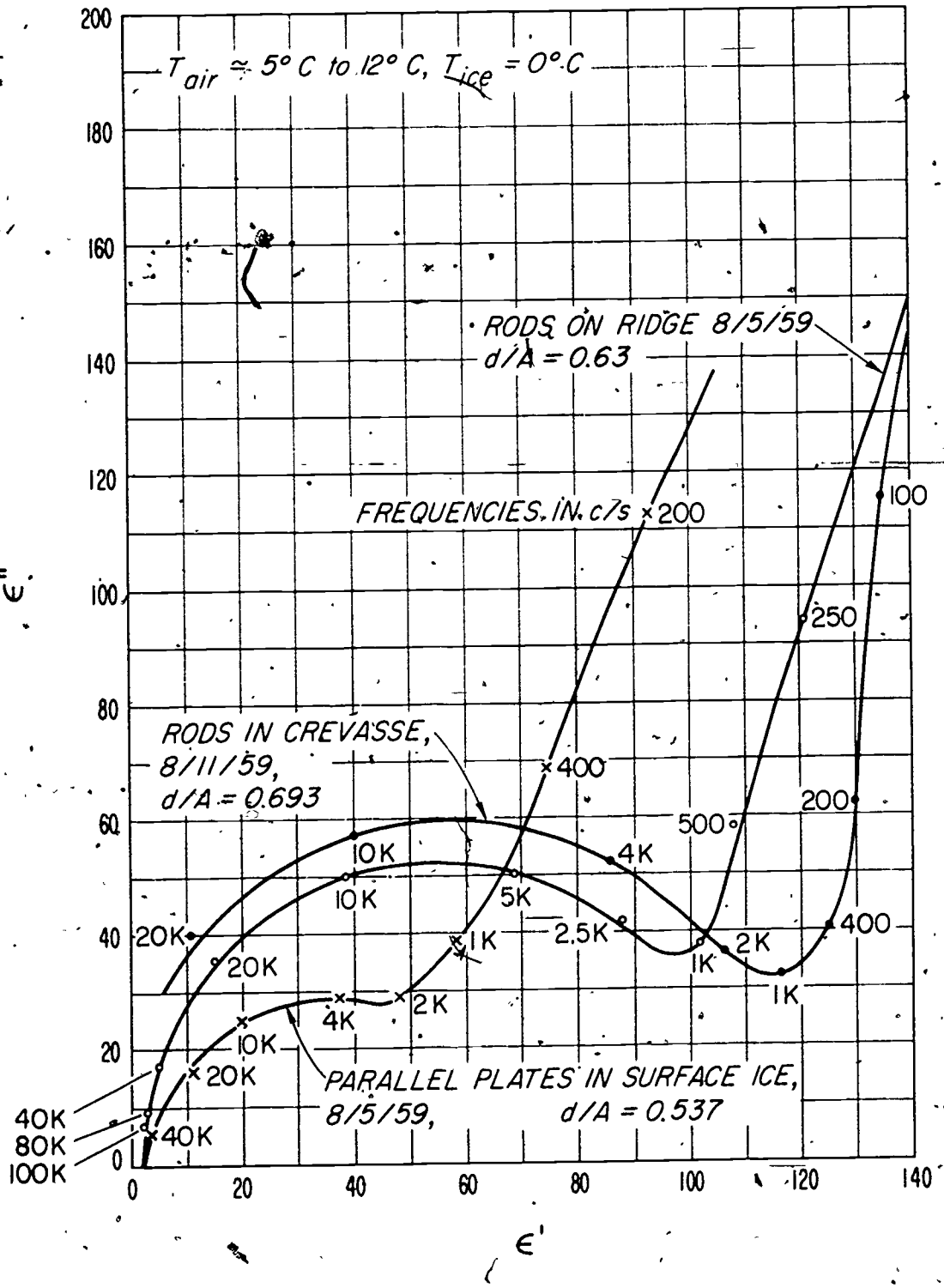

FIGURE 6-9: Electrical Properties of Glacial Ice. Athabasca Glacier, Alberta, Canada.

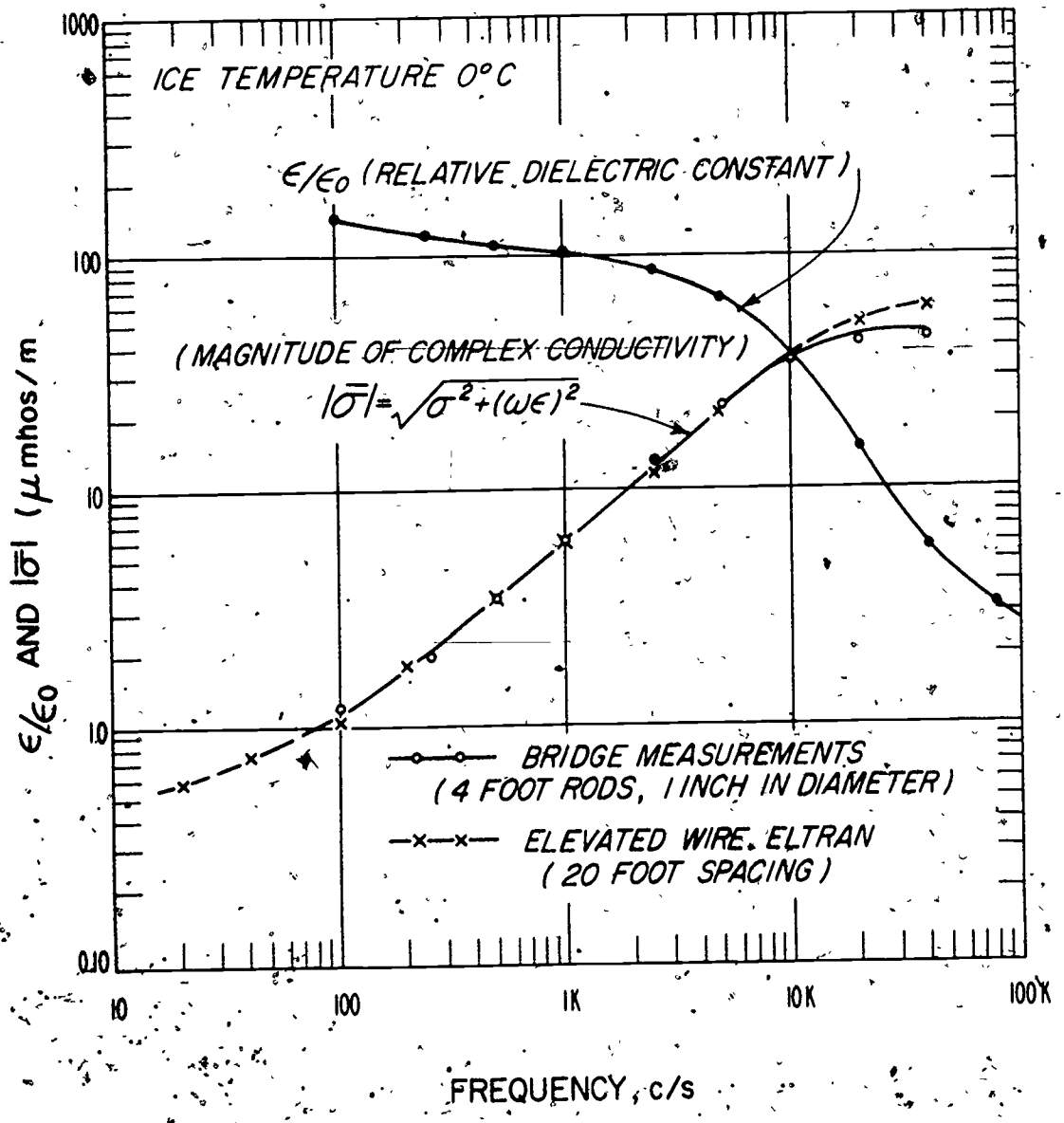

FIGURE 6-10: Electrical Properties of Glacial Ice. Athabasca Glacier, Alberta, Canada, 8/5/59.

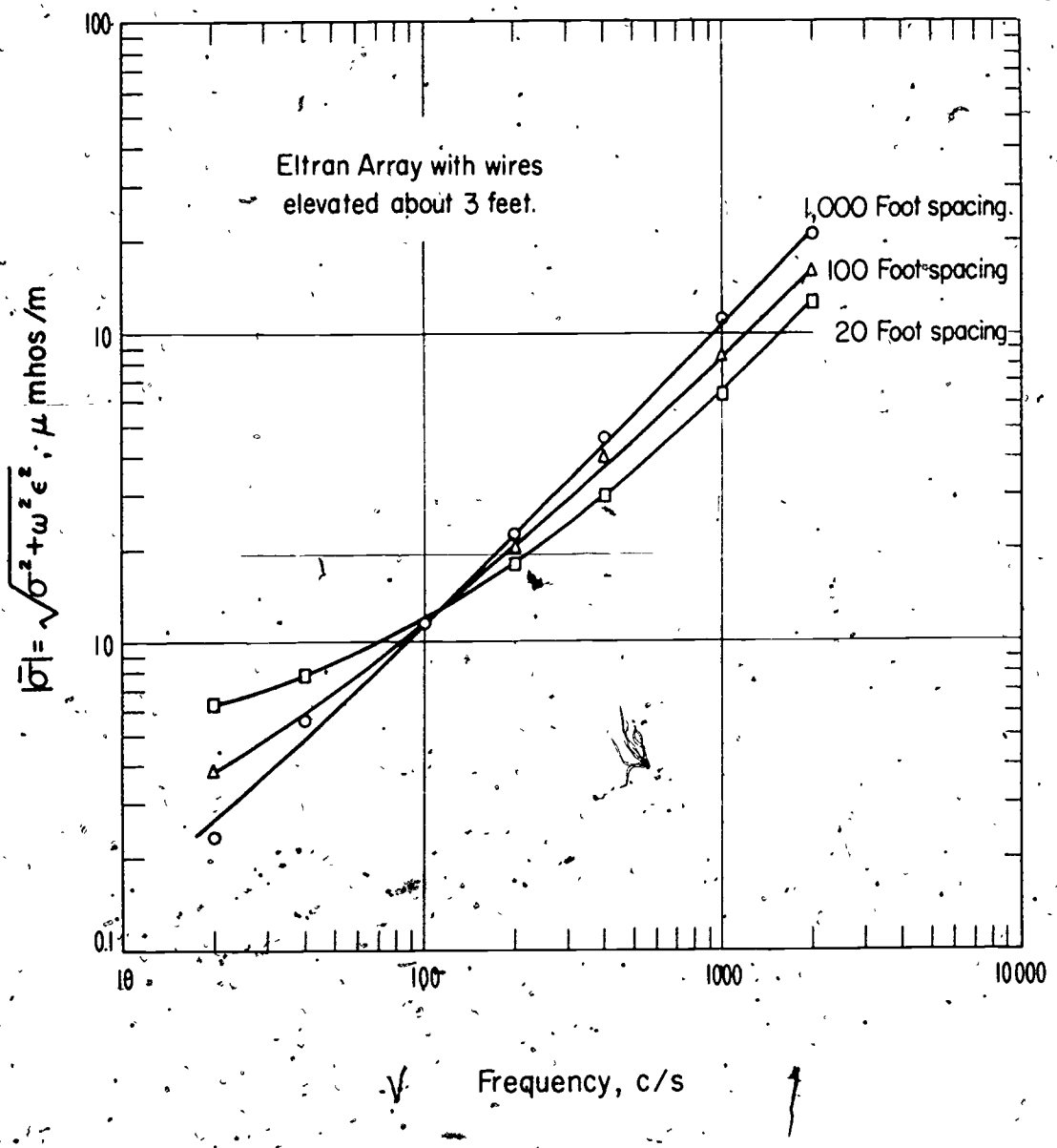

FIGURE 6-11: Magnitude of Complex Conductivity vs. Frequency at Three Electrode Spacings. Athabasca Glacier, Alberta, Canada, Aug., 1959.

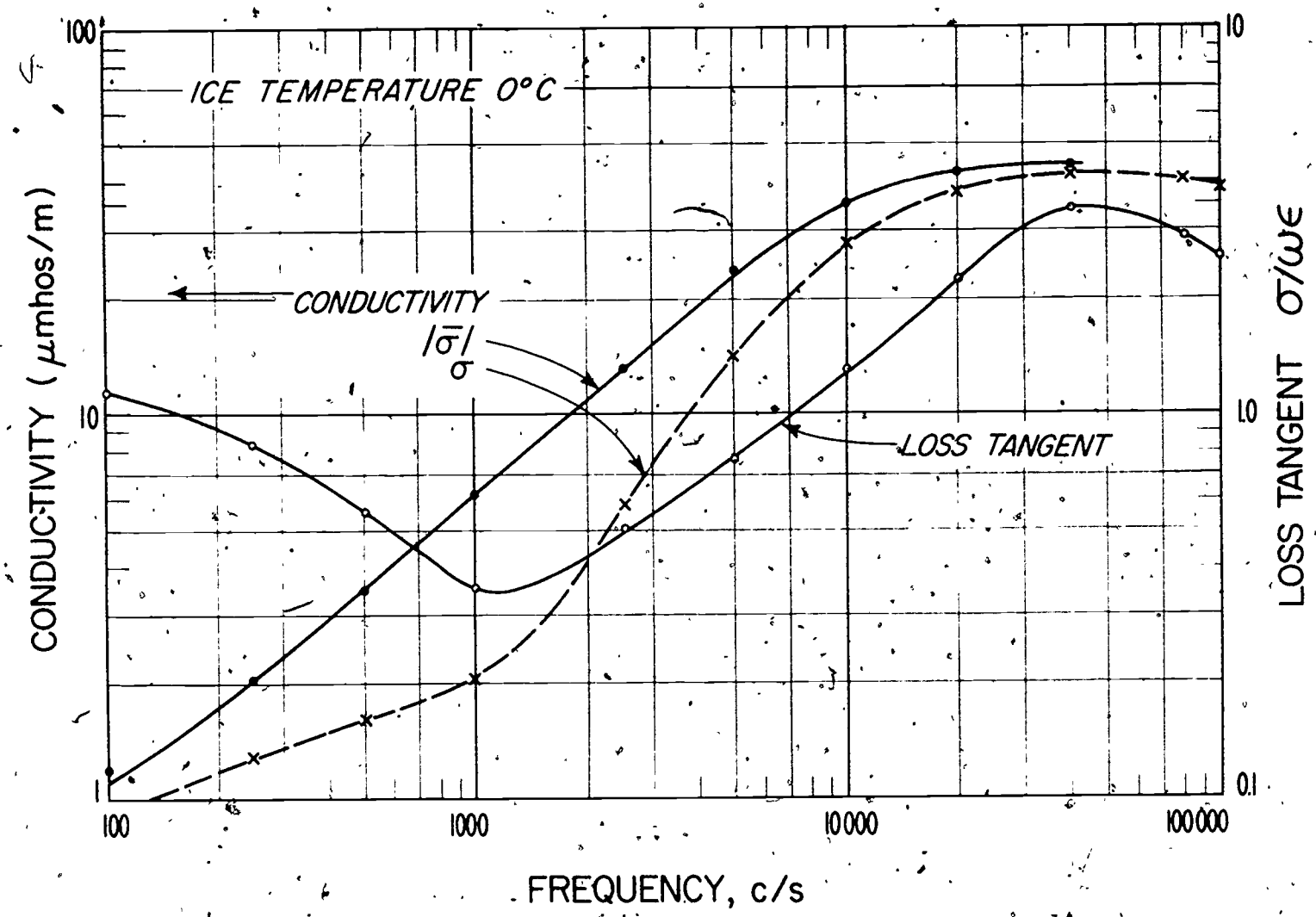

FIGURE 6-12: Electrical Properties of Glacial Ice. Athabasca Glacier, Alberta, Canada, 8/5/59.

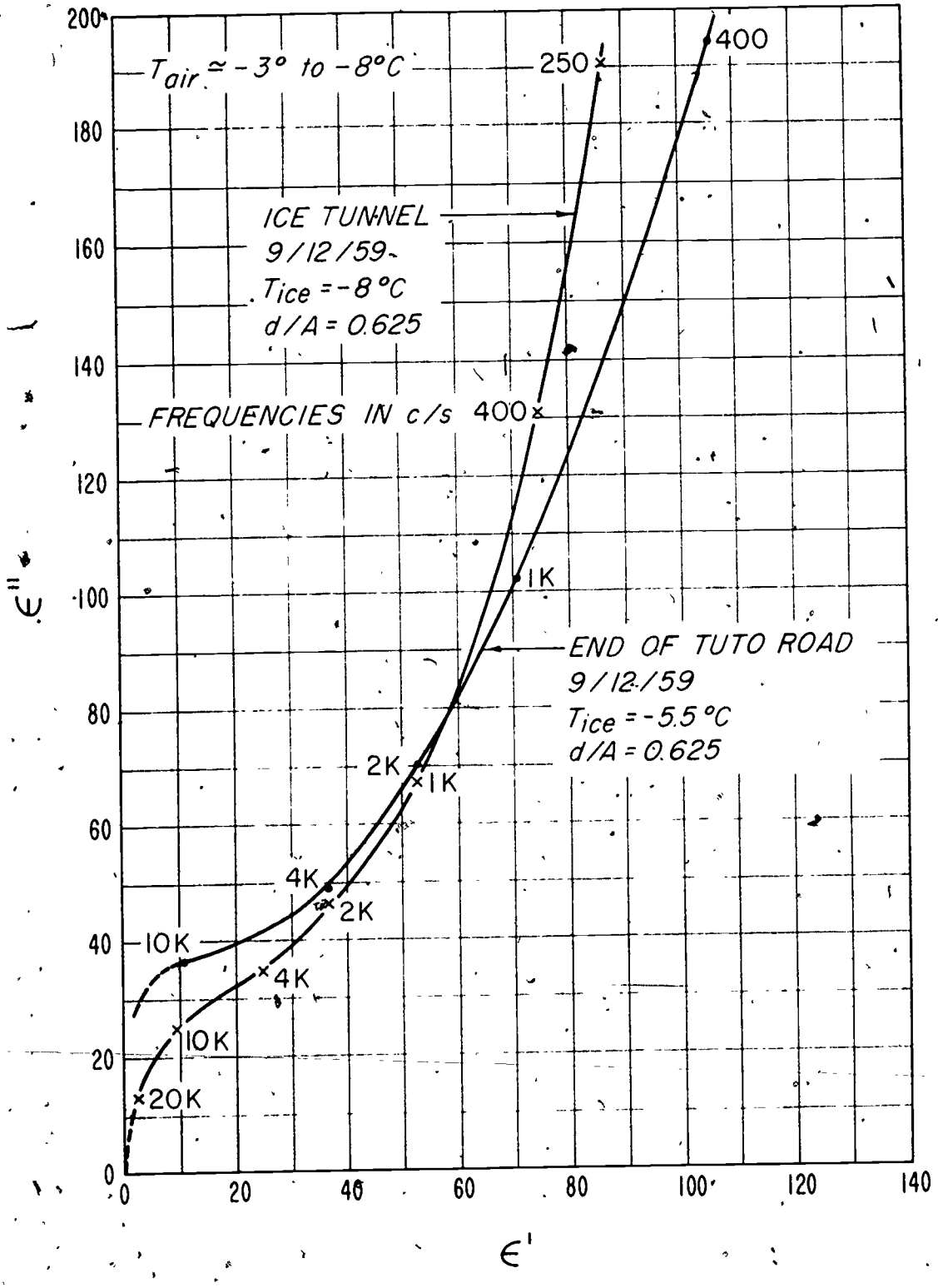

FIGURE 6-13: Electrical Properties of Glacial Ice at Tuto, Greenland, ten miles in from coast at Thule.

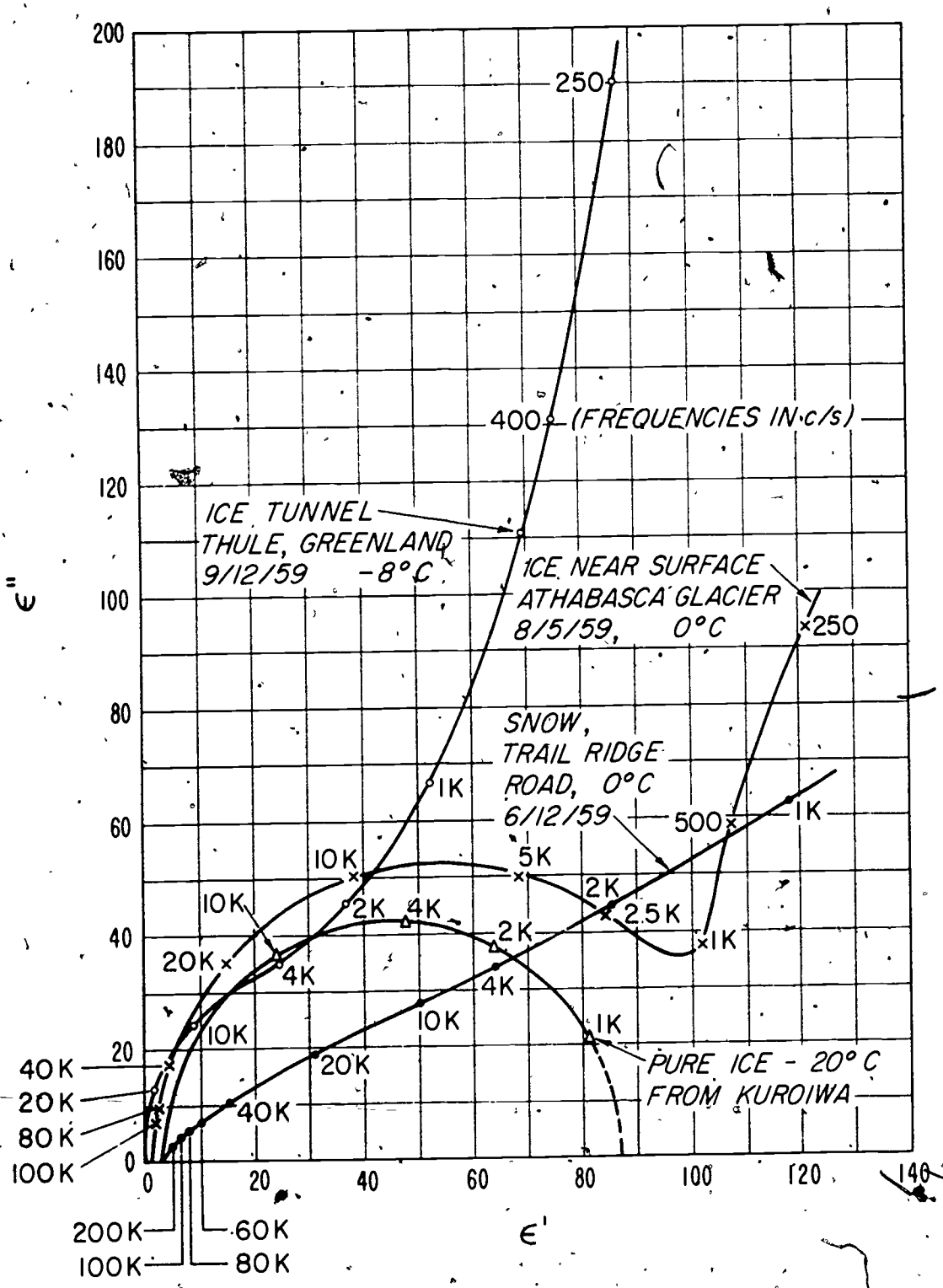

FIGURE 6-14: Comparison of Electrical Properties of Snow and Ice.

REFERENCES

Thomas, B. D., T. G. Thompson, and C. L. Utterback, 1934. "The Electrical Conductivity of Sea Water," Conseil Perm Inter p l'Explor de la Mer, Journal du Conseil, Vol. 9, pp. 28-35.

R. P. Auty and R. H. Cole, 1952. "Dielectric Properties of Ice and Solid D_2O," Journal of Chemical Physics, Vol. 20, No. 8, pp. 1309-1314.

A. D. Watt and E. L. Maxwell, 1960. "Measured Electrical Properties of Snow and Glacial Ice," Journal of Research of the National Bureau of Standards, Vol. 64D, No. 4, pp. 357-363.

N. E. Dorsey, 1940. "Properties of Ordinary Water-Substance," Reinhold Publishing Corporation, New York, N. Y.

Pounder, E. R. and E. M. Little, 1959. "Some Physical Properties of Sea Ice," I, Canadian Journal of Physics, Vol. 37, pp. 443-473.

Cook, J. C., 1960. "Electrical Properties of Salty Ice and Frozen Earth," Journal of Geophysical Research, Vol. 65, No. 6, pp. 1767-1771.

Dichtel, W. J. and G. A. Lundquist, 1951. "An Investigation into the Physical and Electrical Characteristics of Sea Ice," NAVORD Report 1769, ASTIA No. ATI 122 496.

PROBLEMS

6. 1. Discuss briefly (a few short sentences) the physical difference between relaxation time for the free electron model for metals and the relaxation time for the water molecule.

6. 2. Based on the data given in this section, estimate the relaxation time for the water molecule at -10° C.

6. 3. Calculate the skin depth for typical glacial ice at 10^4 H_z.

7. The Electrical Properties of Rocks and Soils

The electrical conductivity (resistivity) and dielectric constant of most rocks is determined by:

1. Amount of water in the rock.
2. Salinity of the water.
3. Distribution of the water.

Few rocks contain enough conductive material to appreciably affect their conductivity. Exceptions are Native Copper Ore and Native Silver Ore.

The distribution of conductive minerals is very important. The ores mentioned above tend to form interconnected veinlets and boxworks of metal which yield a high conductivity. Pyrite, galena, graphite, and magnetite may have a high content of metal or conducting mineral, but they are formed in discrete crystals, separated by insulators. Thus, may yield a high interfacial ε, but a low σ.

7. 1. Conduction Processes in Rock

The electrical conductivity of a rock will be a function of the concentration of charge carriers and the mobility of these charge carriers. These charge carriers can be electrons, ions in solution or ions in the rock material. Electrons and ions in the rock material are significant charge carriers only in metallic ores or very dry rocks. With the exception of metallic ores, the conduction within rocks in the upper several kilometers of the earth's crust is due almost entirely to the motions of ions in the water contained within the rocks. Since we are primarily concerned with the effective conductivity of the upper several kilometers of the earth's crust, we will consider

only conduction due to ions in solution.

To estimate the conductivity of a rock we would like to know the concentration of charge carriers, their mibility, and their distribution within the rock. With this information we could use equation (5.18) to compute the conductivity or resistivity of the infilling water. Occasionally, we may use such information to compute estimates of infilling water resistivity. More often we deal with estimates of water resistivity itself and then proceed as follows.

The amount of water which a rock will contain is, of course, a function of the porosity and permeability of the rock. The number of ions in solution will be determined by the impurities in the infilling water and the minerals within the rocks which go into solution and are dissociated. Figure 7-1 shows the relationship between porosity and resistivity, as determined by Zablocki, 1962. He also gives the following equations for bulk resistivity based on the assumption that the rocks are water saturated. For a granular rock such as sandstone,

$$\rho_r = 0.6\ \rho_w\ \phi_i^{-2} \qquad (7.1)$$

For jointed rocks,

$$\rho_r = 1.4\ \rho_w\ \phi_f^{-1.4} \qquad (7,2)$$

and since most igneous rocks contain both kinds of porosity

$$\rho_r = \rho_w\ (0.71\ \phi_f^{1.4} + 1.67\ \phi_i^{2})^{-1} \qquad (7.3)$$

where

ρ_r = rock resistivity

ρ_w = infilling water resistivity

ϕ_i = granular porosity

ϕ_f = fracture porosity.

For non-saturated rocks (most) we must multiply ϕ_i and ϕ_f by S_i^{-n} and S_f^{-n}. S_i represents the fraction of granular porosity filled with water and S_f the fraction of fracture porosity filled with water. Then (7.3) becomes,

$$\rho_r = \rho_w \left(0.7\ \phi_f^{1.4}\ S_f^n + 1.67\ \phi_i^2\ S_i^n\right)^{-1} \qquad (7.4)$$

For most rocks, n = 2. For a rock in which the water does not wet the grains (oil bearing rocks), however, n may be as high as 10.

If porosity data were available for rocks in general, we would still need information on the percentage saturation of the rock and the conductivity of the infilling water. The various factors which we might expect to influence the moisture and ionic content of rocks are, therefore, discussed in the next section. With sufficient knowledge of these secondary factors, we may be able to determine reasonably accurate values for the primary factors of moisture content, ionic content, and finally, conductivity.

7. 2. 1. Geology

Lithology, structure and age are the geologic factors of prime importance in determining the conductivity of a

rock. Tables 1, 2, and 3 provide a fairly comprehensive picture of the range of conductivity of crustal materials. Although mineralogy is not called out separately in these descriptions, it is inherent in the lithologic description. More detailed information on minerals which may provide free ions in solution would undoubtedly permit descriptions more closely related to the conductivity. Dakhnov gives some information on the resistivity of minerals. Water content is, for the most part, unspecified and this results in the rather wide range of cunductivities noted for most materials. Tables 1 and 3 indicate conductivity ranges for materials as they are normally found in situ, whereas the lower conductivity limits indicated in Table 2 include values for laboratory samples made virtually free of water by drying.

The variation of conductivity with age is primarily related to the compactness of older rocks and other factors which reduce the water content. Although the connate waters contained in older rocks is likely to be saltier than the water within more recent rocks, the reduced percentage content results in an over-all lower conductivity.

It is obvious from Tables 1, 2, and 3 that accurate estimates of electrical conductivity of rocks will require more data than that typically contained in geological descriptions. The important role played by past and present weather conditions will be discussed next.

7. 2. 2. Weather

The connate and juvenile waters of deposition and formation can be determined only from laboratory measurements. It might generally be expected, however, that similar rocks formed during the same period of time might have approximately the same water content with the same order of magnitude of free ions. Of considerably more importance for near surface rocks, however, are the effects of weather upon water content.

The present rainfall and the rainfall estimated to have fallen in a given region during the past several thousand or tens of thousands of years are important factors in determining moisture content, ion content, and conductivity. At first thought, one might think that areas having extremely high rainfall would be the regions where surface conductivities would be the highest and conversely that in desert regions we might expect to find very low conductivities. More often than not the exact opposite is closer to the truth. In jungles and other areas such as our pacific coastal regions, which have extremely high rainfall and have had high rainfall for many, many years as evidenced by vegetation and erosion, it is very common to find that most of the salts have been leached out of the rocks by the heavy rainfall. Thus, these regions generally have low conductivities. In other words, the water contained in the rocks in these regions is relatively pure water having a conductivity

somewhere between 10^{-2} and 10^{-4} mhos per meter. In desert regions, however, we find that water is drawn to the surface by capillary attraction where it evaporates, leaving behind the salts which had been in solution. The salts in these surface layers become very concentrated resulting in high salinity and high conductivity. Desert regions sometimes exhibit conductivities from 10^{-1} to 10 mhos per meter. Knowledge of weather conditions over thousands or tens of thousands of years are obviously necessary to obtain a true picture of expected conductivities.

The prominent role which water content plays in the conductivity of crustal materials would lead one to expect considerably lower conductivities when these materials have been frozen. Such is exactly the case and, of course, this becomes a very important factor in arctic and antaractic regions. Permafrost or perennially frozen ground is found in over half the land area of Alaska and Canada and about one-fifth the land area of the world is subject to permafrost, Brown and Johnston, 1964. One of the classical works on electrical conductivity in frozen rocks was done by M. A. Nesterov and L. Ya. Nesterov, 1947, in the Geological Survey Institute of Russia. Tables 4 and 5 from Dostovalov, 1947, and Dumos, 1962, show the effects of temperature on a variety of materials. Figure 7-2 from Semenov, 1937, gives somewhat more detailed and definitive information as it shows conductivity as a function of temperature for a medium grain sand for

various concentrations of infilling salt solution. It is evident from this Figure that the freezing process does not produce a step change in conductivity. This is due, at least in part, to the increased concentration of the salt solution as the water begins to freeze and to the increased pressure within the rock pores as the freezing water expands. Semenov indeed did find that rocks containing sands of different grain sizes, shales, and peats all had different conductivity versus temperature characteristics.

It should also be noted that dielectric constants change with freezing as might be expected from the characteristics of ice and snow. This change in dielectric constant can be of importance at all radio frequencies.

7. 2. 3. Topography and Pedology

Compared to geology and weather, topography and pedology are of lesser importance for estimating ground conductivities. At high frequencies, however, topographical features and soil will have an important effect upon effective conductivity. Topography can be a very important indicator of climatic conditions which, as indicated above, are extemely important. Also, very rough terrain can cause additional losses to an electromagnetic wave propagating across it due to the scattering of energy. This has the effect of lowering the effective conductivity of the region.

The thin layer of soil covering most of the surface of

the earth is also an indicator of past weather conditions and will be a controlling factor of effective conductivity for high frequencies which do not penetrate beneath the soil layer. In a manner similar to the study of rocks, the soil type and recent weather conditions will be the prime factors in determining the effective conductivity of the soil layer.

7. 3. True, Apparent, and Effective Conductivities

7. 3. 1. True σ -- Mineral or Rock Unit

Cube of homogenous sample, cm size.

Formation

Cube of homogenous sample, one meter to one km size, direction may be important due to anisotropy.

Region

Geoelectric or geologic section, anisotropy quite important.

$$\rho_T = \frac{\Sigma \rho_i h_i}{\Sigma h_i} \qquad (7.5)$$

$$\rho_L = \frac{\Sigma hi}{\Sigma (hi/\rho i)} \qquad (7.6)$$

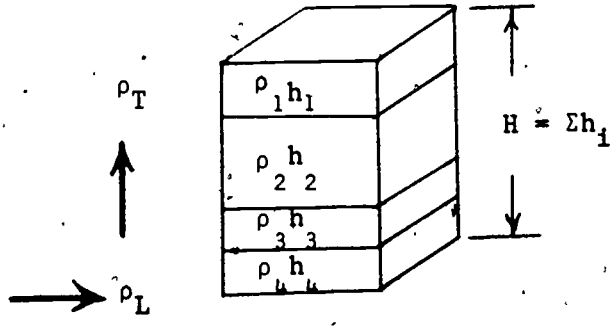

(Must be square column, not necessarily one meter)

Coefficient of anisotropy, λ,

$$\lambda = \sqrt{\rho_T/\rho_L} \qquad (7.7)$$

Typical Values

Rock type	λ
Volcanic tuff	1.1 to 1.2
Alluvium, thick	1.02 to 1.1
Interbedded limestone and shale	2.0 to 3.0
Massive shale beds	1.02 to 1.05
Interbedded anhydrite and shale	4.0 to 7.5
Graphitic slate	2.0 to 2.8

7.3.2. Apparent σ

Usually related to measured σ where homogeneity and anisotropy are assumed. Becomes true σ when assumption is true.

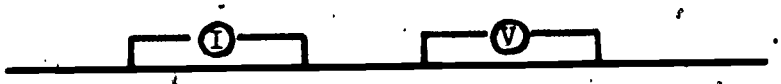

$\sigma_{constant}$ (homogeneous and isotropic)

Apparent = true

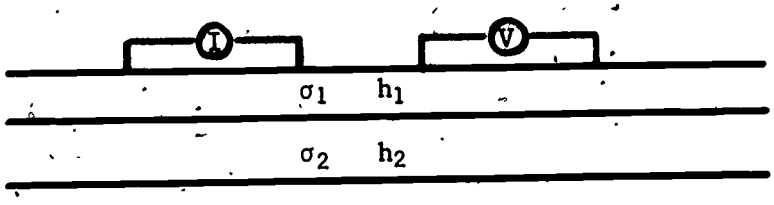

Apparent ≠ true

7. 3. 3. Effective σ

Usually related to effect of medium on a propagating, plane EM wave. Determined from α, γ, δ, and η. The expression for effective conductivity for a two layer earth as obtained from Wait, 1962, is,

$$\sigma_e = \sigma_1 \frac{\gamma_1 + \gamma_2 \tanh \gamma_1 h_1}{\gamma_2 + \gamma_1 \tanh \gamma_1 h_1} \qquad (7.8)$$

where

σ_e = is the effective conductivity at frequency of interest,

σ_1 = is the conductivity of the first layer,

γ_1 = is the propagation constant for the first layer,

γ_2 = is the propagation constant for the second layer, and

h_1 = is the thickness of the first layer.

Effective conductivity for a layered earth becomes very complex due to the partial reflection of energy at the boundaries between rock layers.

Figure 7-3 gives the skin depth for conductivities typically found for rocks, over a frequency range of interest for geologic investigations. Figure 7-4 is a map of North America showing the effective conductivity at a frequency of 10 kHz. Note variability and confidence factors also given on this map.

REFERENCES

Dakhnov, V. N., "Geophysical Well Logging," Quarterly of the Colorado School of Mines, Vol. 57, No. 2, Translated into English by G. V. Keller.

Zablocki, C. J., 1962, "Electrical Properties of Igneous and Metamorphic Rocks," Part 6 of Electrical Properties of the Earth's Crust prepared by USGS.

Brown, R. J. E. and G. H. Johnston, 1964, "Permafrost and Related Engineering Problems," Endeavor, Vol. 23, No. 89.

Dostovalov, B. N., 1947, "Electrical Characteristics of Frozen Rocks," Proceedings of the V. S. O. Breechev Permafrost Institute, Vol. V., Electrometry and Ondometry of Frozen Rock Strata (in Russian).

Dumas, Michel, 1962, "Electrical Resistivity and Dielectric Constant of Frozen Rocks," Thesis for MSC, Colorado School of Mines, Golden, Colorado.

Wait, J. R., 1962, "Electromagnetic Waves in Stratified Media," Pergamon Press, London.

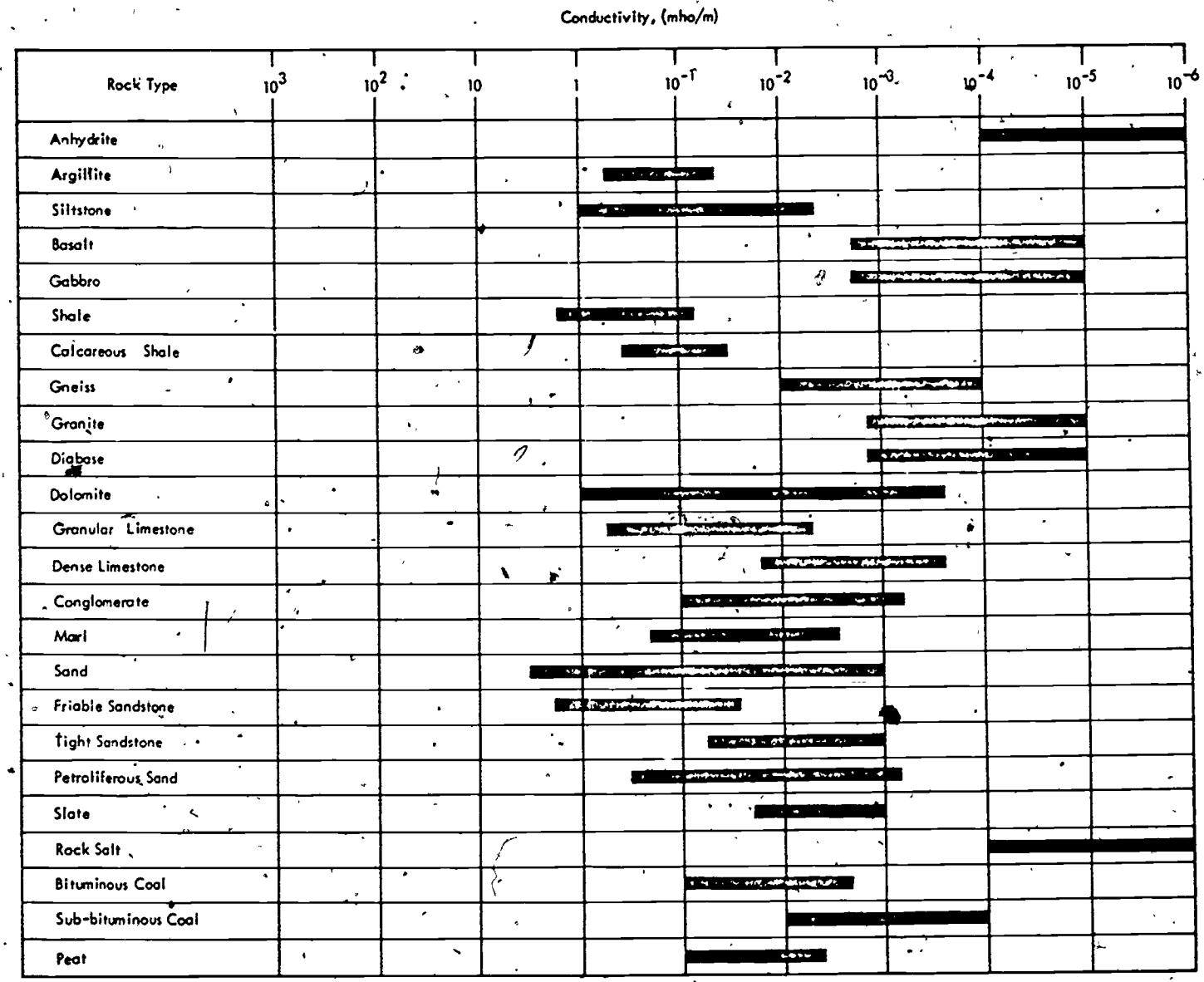

Table 1 Conductivity Ranges for Some Common Rock Types.
(Dakhnov, 1959)

TABLE 2

APPROXIMATE ELECTRICAL CONDUCTIVITIES OF EARTH'S MATERIALS (AT NORMAL SURFACE TEMPERATURE AND PRESSURE)

Material	Approximate σ (mho/m)	Comments
soils: good	10^{-2} to 10^{-1}	relatively nondispersive.
soils: average	10^{-3} to 10^{-2}	
soils: poor	10^{-4} to 10^{-3}	
water: sea	4 to 5	
water: connate, in rocks*	10^{-1} to 1	
water: fresh	10^{-4} to 10^{-3}	
snow (drifted, wet)	2×10^{-6} @10 cps to 3×10^{-6} @10 kc	values very dependent upon temperature, frequency, and impurities.
ice (glacial)	10^{-6} @100 cps to $\blacksquare\times10^{-6}$ @ 10 kc	
permafrost	10^{-6} to 10^{-4} estimates	likely to have variations similar to glacial ice.
sediments†: marine sands and shales	10^{-1} to 1	
sediments†: marine sandstones	10^{-2} to 1	
sediments†: clay	10^{-2} to 10^{-1}	relatively frequency independent.
sediments†: sandstone (wet)	10^{-4} to 10^{-2}	
sediments†: sandstone (dry)	10^{-7} @100 cps to 10^{-4} @10 kc	
sediments†: limestone	10^{-4} to 10^{-8}	
sediments†: rock salt	10^{-4} to 10^{-7}	
igneous rock‡: granite	10^{-6} to 10^{-3}	very dependent on water content
igneous rock‡: basalt	10^{-6} to 10^{-3}	
igneous rock‡: gabbro	10^{-7} to 10^{-4}	
igneous rock‡: peridotite	10^{-6} to 10^{-7} @300°C	
metamorphic‖: slate	10^{-6} to 10^{-3}	
metamorphic‖: marble	10^{-8} to 10^{-3}	
metamorphic‖: gneiss	10^{-7} to 10^{-3}	
metamorphic‖: serpentine	10^{-7} to 10^{-3}	
ore bodies§: native silver	5×10^{7}	
ore bodies§: native copper	3×10^{6} to 5.7×10^{7}	
ore bodies§: galena (PbS)	20 to 200	
ore bodies§: hematite (Fe_2O_3)	10^{-7} to 10^{-6}	

Note: lower conductivities are found for dense, dry, rock samples believed to be of oldest geological age such as the Precambrian. The values quoted are for frequencies in the 10- to 100-cps region. σ for dry rocks generally increases with frequency and in many cases follows a relation $\sigma \simeq kf^m$ where m can vary with frequency f, and ranges from 0.1 to 1 in the 10- to 10^5-cps frequency region. The actual manner in which σ varies with frequency can be quite complex and depends upon the material involved. Wait [7], p. 33, indicates that the conductivity can be approximated by the relation $\sigma \simeq k_1 + k_2 \log f$ in the frequency region of 1 to 100 cps.

* R. H. Card, "Earth resistivity and geological structure," *Elec. Engrg.*, pp 1153–1161; November, 1935.

† C. A. Heiland, "Geophysical Exploration," Prentice-Hall, Inc., New York, N. Y.; 1946.

‡ G. V. Keller, private communication.

‖ K. Noritomi, "The electrical conductivity of rock and the determination of the electrical conductivity of the earth's interior," *J. Min. Coll. Akita Univ.*, vol. 1A, p. 27; 1961.

§ H. A. Wheeler, *Electronics*, vol. 32, p. 59; September, 1941.

Table 3 Probable resistivity ranges of rocks as a function of lithology and age.

Rock Type / Age	Marine sand and shale, graywacke	Terrestrial sands and claystones, arkose	Extrusive, volcanics, basalt, ryolites, tuffs, etc.	Intrusive, igneous rocks, granite, gabbro	Chemical precipitates limestone, dolomite, anhydrite, salt
Quarternary Tertiary	1 - 10 Ω m	15 - 50	10 - 200	500 - 2000	50 - 5000
Mesozoic	5 - 20	25 - 100	20 - 500	500 - 2000	100 - 10,000
Garboniferous Paleozoic	10 - 40	50 - 300	50 - 1000	1000 - 5000	200 - 100,000
Precarboniferous Paleozoic	40 - 200	100 - 500	100 - 2000	1000 - 5000	10,000 - 100,000
Precambrian	100 - 2000	300 - 5000	200 - 10,000	5000 - 100,000	10,000 - 100,000

Table 4 Changes in soil conductivity with freezing.

TYPE SOIL	σ, (mhos/m) t = + 14°C	σ, (mhos/m) t = - 5°C
1. gray clay with layers of ice	1.4×10^{-1}	1.6×10^{-2}
2. clay, gray, gravelly	5×10^{-2}	6×10^{-3}
3. clay, heavy, dark gray	2×10^{-2}	8.7×10^{-4}
4. clay, dark gray with gravel to 1 cm in diameter	1.2×10^{-1}	1.3×10^{-3}
5. clay, gray, gravelly with layers of ice	5.7×10^{-2}	2.0×10^{-3}
6. clay, light, with fine gravel	1.2×10^{-1}	4.5×10^{-3}
7. quartzy, fine grained sand, with slate particles	6.8×10^{-2}	2.4×10^{-3}
8. clay sand, with quartz admixture	2.3×10^{-2}	9.1×10^{-4}
9. limestone, fine grain with admixture of quartz and slate particles	5.6×10^{-2}	1.8×10^{-3}
10. clayey fine grain sand with admixture of quartz particles	1.7×10^{-1}	5.9×10^{-3}

Sample No.	Porosity of Sample	Molarity of Solution	Temperature = 0°C			Temperature = -5°C			Temperature = -11°C			Temperature = -20°C		
			ϵ/ϵ_o	$\omega\epsilon$ @ 10 kHz	σ	ϵ/ϵ_o	$\omega\epsilon$ @ 10 kHz	σ	ϵ/ϵ_o	$\omega\epsilon$ @ 10 kHz	σ	ϵ/ϵ_o	$\omega\epsilon$ @ 10 kHz	σ
1	3.5	0.10	138	7.6×10^{-5}	4.5×10^{-3}	72	4.0×10^{-5}	8.2×10^{-4}	72	4.0×10^{-5}	3.5×10^{-4}	53.7	3.0×10^{-5}	1.3×10^{-4}
2	6.5	0.10	239	1.3×10^{-4}	1.2×10^{-2}	95	5.3×10^{-5}	1.1×10^{-3}	103	5.7×10^{-5}	4.6×10^{-4}	69	3.8×10^{-5}	1.6×10^{-4}
3	17.5	0.020	393	2.2×10^{-4}	1.3×10^{-2}	130	7.2×10^{-5}	2.1×10^{-3}	134	7.5×10^{-5}	7.6×10^{-4}	103	5.7×10^{-5}	2.7×10^{-4}
4	17.5	0.1	640	3.5×10^{-4}	3.2×10^{-2}	[illegible]	9.2×10^{-5}	6.5×10^{-3}	170	9.5×10^{-5}	2.3×10^{-3}	122	6.8×10^{-5}	7.8×10^{-4}
5	17.5	0.2	800	4.4×10^{-4}	5.4×10^{-2}	228	1.3×10^{-4}	1.3×10^{-2}	189	1.0×10^{-4}	5.1×10^{-3}	149	8.3×10^{-5}	1.8×10^{-3}
6	17.5	0.5	1030	5.7×10^{-4}	1.1×10^{-1}	1150	6.4×10^{-4}	8.7×10^{-2}	222	1.2×10^{-4}	2.3×10^{-2}	157	8.7×10^{-5}	8.2×10^{-3}

Table 5 Values of σ and $\omega\epsilon$ (measured values) for sandstone samples at 10 kHz. Note that $\omega\epsilon$ is small compared to σ in every case from 0°C. down to -11°C. (Data adapted from Dumas [1962].)

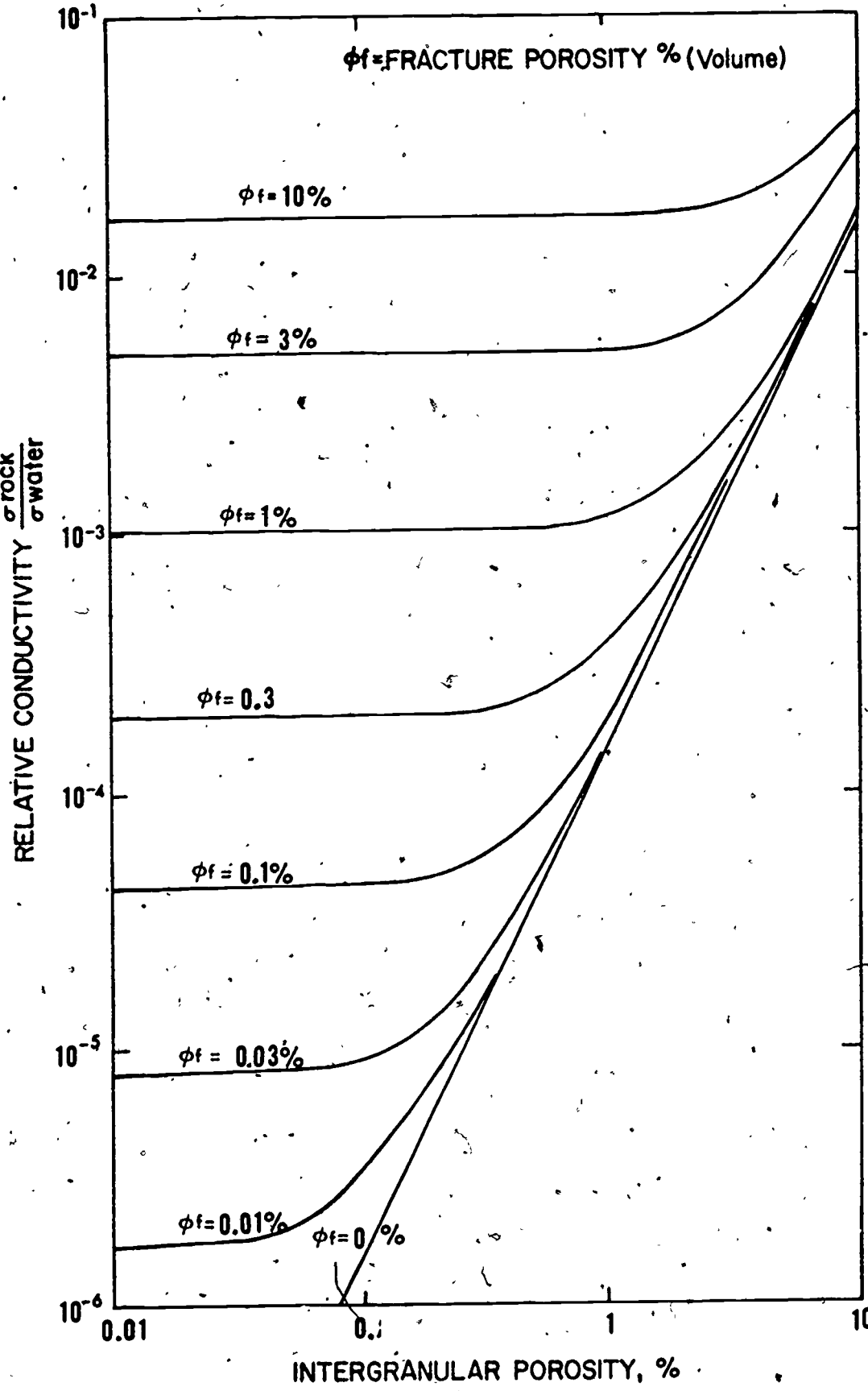

FIGURE 7-1: Relotionship Between Conductivity of o Rock and Intergranular Porosity Combinedwith Fracture Porosity.

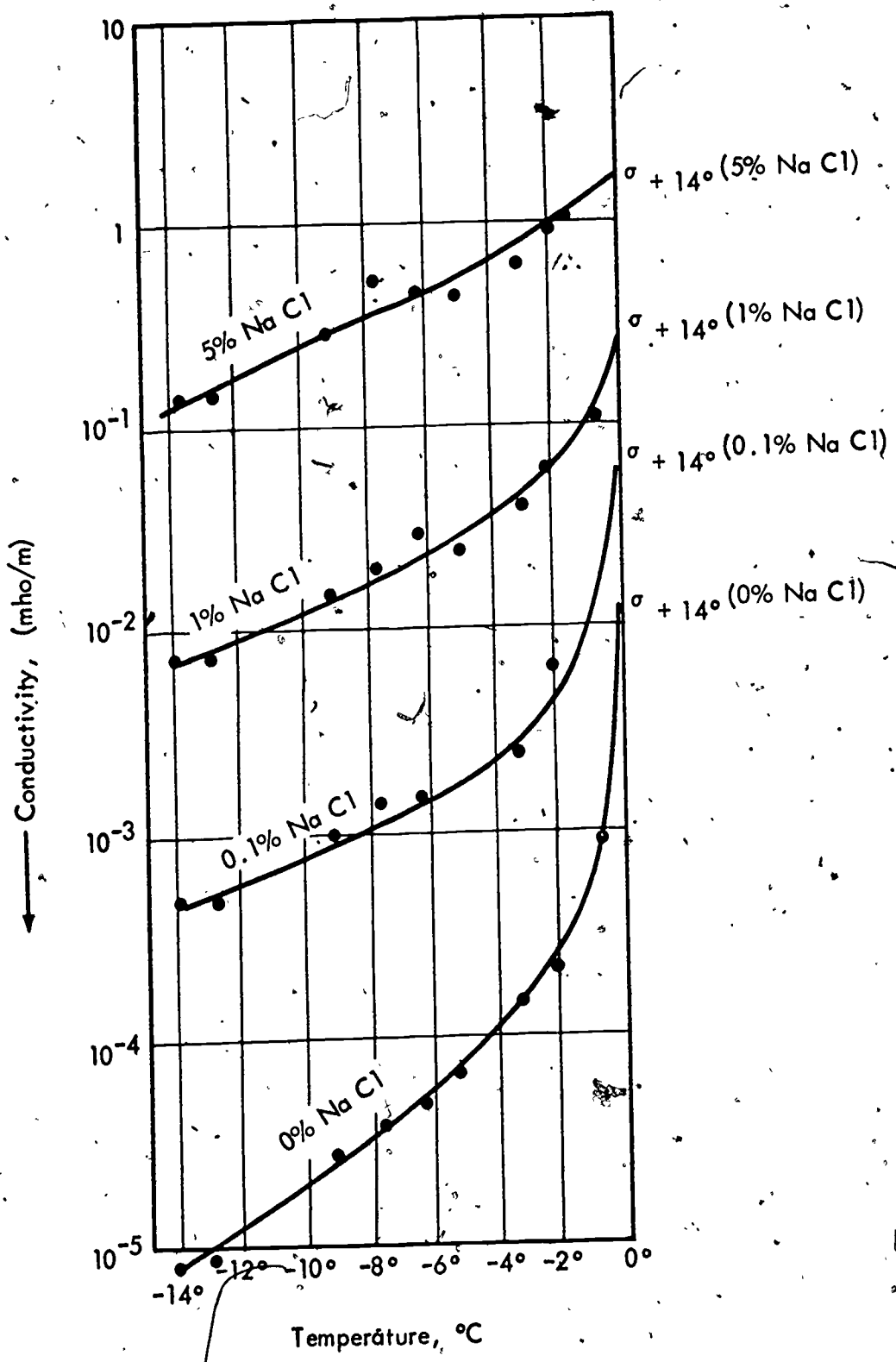

FIGURE 7-2. Conductivity as a Function of Temperature for a Medium Grained Sand for Various Concentrations of Infilling Na Cl Solution

$$\delta = \left(\frac{2}{\omega \mu_o \sigma}\right)^{1/2} \left\{ \left(\frac{\omega^2 \epsilon^2}{\sigma^2} + 1 \right) - \frac{\omega \epsilon}{\sigma} \right\}^{-1/2} \text{ or}$$

$$\delta = \frac{1}{\alpha} = \frac{1}{\omega} \left\{ \frac{\mu_o \epsilon}{2} \left[\left(1 + \frac{\sigma^2}{\omega^2 \epsilon^2} \right)^{1/2} - 1 \right] \right\}^{-1/2}$$

For Homogeneous Material, $\mu_{rel} = 1$

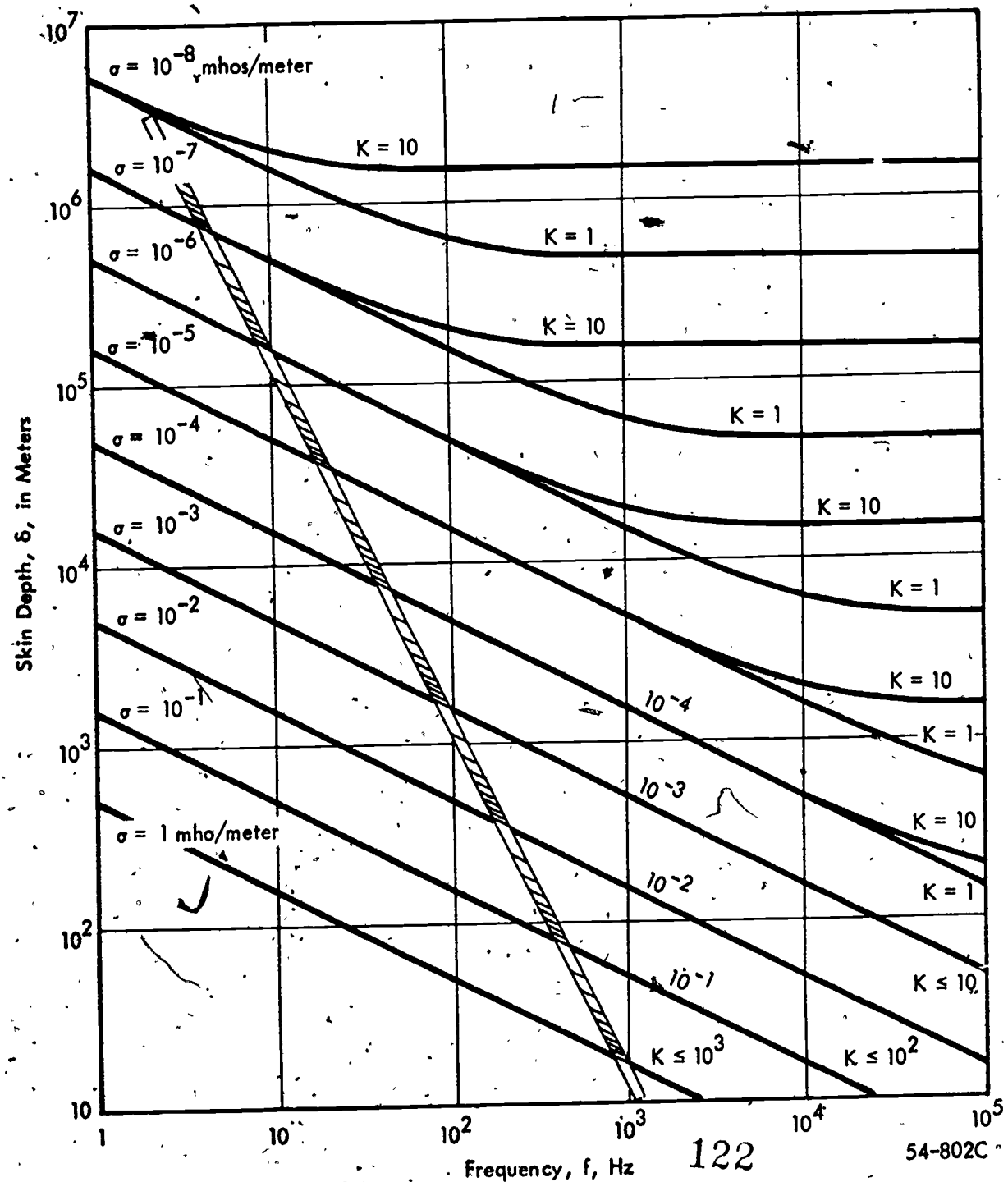

122

FIGURE 7-3 Skin Depths as Function of the Frequency of Electromagnetic Waves for Various Conductivities and Permittivities, Where $k = \epsilon/\epsilon_o$

FIGURE 7-4 10 kHz Conductivity Map of N. America

PROBLEMS

7. 1. Given an igneous rock with granular porosity of 5 percent and fracture porosity of 10 percent. If the rock is saturated with sea water, determine the rock conductivity. Also, determine the conductivity if we assume the rock is saturated with typical fresh water from a lake.

7. 2. From Figures 7-4 and 7-3, estimate the depth of penetration (skin depth in the earth) of radio waves at Fort Collins from WWVL (north of Fort Collins), f = 20 kHz and KCOL, f = 1.410 mHz. How accurate are these estimates likely to be?

8. Electrical Properties of Living Matter

Conduction in living materials results from the transportation of ions in solution. Polarization is from all five possible processes including the effect of dipolar protein molecules. A very simplified description of living tissues, adequate for discussing the electrical properties of such, is indicated in Figure 8-1. We are primarily concerned with the cell wall or membrane, the cytoplasm inside the cell, and the intercellular media which tends to separate one cell from another. The properties of these three types of living materials are given on Figure 8-1. It is apparent that the cell wall would tend to act as an insulator, producing interfacial polarization and low dc conductivity. Keeping this general picture in mind, we will proceed to discuss the electrical properties of animal and plant materials.

8. 1. Electrical Properties of Animal Tissues

The following material was taken for the most part from Pressman, 1970, chapters 3 and 4. Figure 8-2, from Pressman, shows the dielectric constant and resistivity of muscle tissues as a function of frequency. Pressman takes particular note of those regions where the electrical properties are changing rapidly with frequency, i.e., the dispersion ranges. The student should be advised not to confuse the α, β, γ dispersion ranges with the propagation parameters, which we denote with the same Greek letters.

The α dispersion range probably relates to relaxation of the charging processes on the cell wall. The apparent resistivity decreases as the capacitive reactance of the cell wall becomes lower with increasing frequency. Capacitive reactance, X_c is given by the expression:

$$X_c = \frac{1}{2\pi fC}$$

The β dispersion range probably relates to relaxation processes within the cell wall itself. From 10^8 to 10^{10} Hertz, the small dispersion noted is probably associated with relaxation of protein molecules.

The γ dispersion range is undoubtedly related to the relaxation of the water molecule. Except for this γ range, the above interpretation of the variation of electrical properties with frequency should all be considered subject to question.

In general, data for the electrical properties of animal tissue shows these tissues to have relatively high conductivities increasing with frequency. Dielectric constants are also quite high, particularly at low frequencies, and remain large even in the Gigahertz range. The very high dielectric constants at low frequencies are undoubtedly due to interfacial and electrochemical effects, whereas the dielectric constant at the Gigahertz frequencies is undoubtedly due to the dipolar protein and water molecules.

8. 2. The Electrical Properties of Plants

The electrical properties of plants, similar to the properties of rocks and soil, are directly related to the moisture content within the plant, the physical distribution of this moisture, and the electrical properties of the solutions.

Figure 8-3 from Henson and Hassler, 1965 gives the electrical properties of cured tobacco leaves as a function of frequency and moisture content. The dispersion of dielectric constant over five

decades indicates a variety of polarization processes at work. It should be noted that the authors measured the conductivity at dc as well as the frequencies indicated and found that the dc conductivity was essentially zero. This indicates that the effective conductivity measured can probably be associated with movement of ions for short distances within the cells. Other losses or conductivity effects are probably associated polarization processes. It is interesting to note that the dielectric constant changed approximately linearly with density as the leaves were compacted, whereas the apparent conductivity changed very little. This would indicate that the space between the cells containing the moisture was being reduced (this is analogous to the reduction of the spacing between capacitor plates). Apparently the cell walls were not being crushed since this would have resulted in an increase in conductivity.

The 600 percent moisture for uncured tobacco leaves indicates that these are percentage moisture content by weight. The relative dielectric constant, ε', of uncured leaves was too high to show on the Figure. The values obtained for $\varepsilon/\varepsilon_0$ varied from 5800 at dc to 800 at 10^6 Hertz.

The measurement of the dielectric constant of tobacco leaves provides a non-destructive means for monitoring the curing of the leaves.

8.2.2. Electrical Properties of Grain and Seed

The electrical properties of corn and wheat are shown in Figure 8-4 over the frequency range of 1 to 50 Megahertz. This data was obtained from Nelson, 1965. We find a variation of electrical properties with moisture content similar

to those noted for tobacco leaves. The variation of the properties with frequency cannot be compared very well, however, since the data overlap for only a small part of the frequencies. The increase in conductivity with frequency for the seeds probably results from the essentially zero conductivity between the individual grains. In other words, the conduction process takes place within each seed and is effective only at very high frequencies.

These data relate to the non-destructive measurement of moisture content. Long term storage of grain or seed requires careful control of the moisture content.

8. 2. 3. The Electrical Properties of Wood

Two basic classifications are appropriate for the moisture contained in wood.

1. Water which is bound up or absorded in the cell walls.
2. Free water inside the cells.

The fiber saturation point refers to the saturation of cell walls. This apparently occurs at about 20 to 30 percent moisture content (by weight) for most wood. This is evident from Table 8-1 taken from the wood handbook, Agricultural Handbook #72, 1955. The resistivity or conductivity of wood changes quite rapidly until the cell walls become saturated; but as more water is added the conductivity changes very little. Wood tends to be anisotropic, with resistivity being greater across the grain.

At 16 percent moisture content, the resistivity of a particular type of wood was 10^6 ohm meters. This is indicative of the very rapid change in electrical properties as the cell walls are saturated. In general, oven dry wood is a very good insulator, the resistivity being approximately 10^{16} ohm meters. At one time, wax-impregnated wood dowels were often used for insulators for radio station transmission lines.

The resistances given in Table 8-1 can be used to obtain approximate values for resistivity from the relation:

$$V = \frac{I}{2\pi r \sigma_a} \tag{8.1}$$

where r is the radius of a hemispherical electrode placed in a media having conductivity, σ_a. The resistance of this electrode contact is given by Ohm's law and we may write:

$$\rho_a = 2\pi r R \tag{8.2}$$

where ρ_a is the apparent resistivity of the wood and R is the resistance measured between hemispherical electrodes. The data given in Table 8-1 was not obtained with hemispherical electrodes. Long stakes or needles, however, act as if they were a hemispherical electrode having a radius approximately equal to their length. Since the data for Table 8-1 was obtained with electrodes 5/16th of an inch long, we can replace r in equation (8.2) with the value 7.5×10^{-3} meters.

Therefore, the resistances in Table 8-1 may be converted to resistivities with the expression:

$$\rho = 2.5 \times 10^{-2} R \qquad (8.3)$$

The values thus obtained are in general agreement with other measurements noted in the literature.

The relative dielectric constant of wood is generally found to vary from 3 to 5 for quite dry wood and is approximately equal to 80 for wet woods. This would indicate that the polarization processes for wet wood are primarily due to the dipolar water molecule and that dry woods are polarized from electronic and ionic processes. The dielectric constant of woods is also anisotropic with the greatest values being found parallel to the grain. This anisotropy noted for both conductivity and dielectric constant is consistent with a concept suggesting greater freedom of motion for ions along the grain of the wood.

TABLE 8-1 - The average electrical resistance along the grain in megohms. Measured at 80° F. between 2 pairs of needle electrodes 1 & 1/4 inches apart, driven to a depth of 5/16th inch. Several species of wood at different values of moisture content.

Species	Electrical resistance in megohms when the moisture content in percent is																		
	7	8	9	10	11	12	13	14	15	16	17	18	19	20	24	28	32	40	60
Hardwoods:																			
Ash, commercial white	12,000	2,190	690	280	105	55	28	14	8.3	5.0	3.2	2.0	1.32	0.89	0.63	0.50	0.44	0.40	0.40
Basswood	36,300	1,740	470	180	88	45	27	16	9.6	6.2	4.1	2.8	1.86	1.32	.98	.69	.51	.39	.31
Birch	87,000	19,000	4,470	1,200	470	220	96	53	30.2	18.2	11.5	7.6	5.13	3.56	2.51	1.78	1.32	.95	.70
Elm, American	18,200	3,000	880	110	45	20	12	7	3.9	2.3	1.5	1.0	.68	.48	.42	.40	.40	.40	.40
Gum, red	36,000	6,400	2,000	815	344	160	91	45	25.7	15.1	9.3	6.0	3.98	2.63	1.78	1.26	.87	.66	.46
Hickory, true	.....	21,000	2,100	840	118	80	21	11	6.3	3.7	2.3	1.5	1.00	.71	.52	.44	.40	.40	.40
Khaya [1]	44,000	16,200	6,310	2,750	1,260	630	340	180	106.0	60.2	35.5	21.9	14.10	9.33	6.16	4.17	2.82	1.98	1.44
Magnolia	48,700	12,600	5,010	2,040	910	485	206	105	58.2	29.5	16.2	9.1	5.25	3.09	1.86	1.17	.74	.50	.32
Mahogany, American	20,900	6,700	2,200	870	380	180	86	48	22.4	12.3	7.2	4.4	2.69	1.86	1.07	.72	.49	.35	.26
Maple, sugar	77,400	13,200	3,100	690	250	104	53	29	16.6	10.2	6.8	4.5	3.16	2.24	1.62	1.23	.88	.78	.60
Oak: Commercial red [1]	14,400	4,700	1,200	690	265	125	63	32	18.2	11.3	7.3	4.6	3.02	2.08	1.45	.95	.80	.63	.50
Commercial white	17,400	3,500	1,100	415	170	80	42	22	12.9	7.2	4.3	2.7	1.70	1.16	.79	.60	.49	.44	.41
Sheoak [1]	9,000	600	220	90	55	30	18	8	5.0	3.1	2.1	1.5	.45	.30	.21	.16	.10	.08	.07
Tupelo, black [1]	31,700	12,000	5,000	1,820	736	275	120	66	27.9	13.0	6.9	3.7	2.19	1.38	.95	.68	.46	.33	.25
Walnut, black	81,200	9,770	2,430	880	356	155	78	41	22.4	12.9	7.3	4.9	3.16	2.14	1.48	1.02	.72	.51	.36
Yellow-poplar [1]	24,000	8,320	3,170	1,200	526	280	140	76	43.7	25.2	14.5	8.7	5.76	3.91	2.64	1.91	1.39	1.10	.84
Softwoods:																			
Baldcypress	12,600	3,980	1,410	600	265	120	60	33	18.9	11.2	7.1	4.6	3.09	1.78	1.26	.91	.66	.51	.42
Douglas-fir (coast type)	28,600	4,780	1,000	630	258	120	60	33	18.9	11.2	7.1	4.9	3.09	2.14	1.51	1.10	.79	.60	.46
Fir: California red	31,000	6,700	2,000	725	318	150	83	48	28.3	18.2	11.8	7.6	5.07	3.31	2.29	1.66	1.15	.86	.66
White	57,000	15,500	3,900	1,120	415	190	88	46	26.9	16.6	11.0	6.6	4.47	3.02	2.14	1.55	1.12	.86	.66
Hemlock, western	22,900	5,630	2,040	880	400	188	98	51	28.2	16.2	10.0	6.0	3.89	2.82	1.86	1.08	.72	.51	.37
Larch, western	39,800	11,200	3,000	1,445	600	230	120	63	33.9	19.9	12.3	7.6	5.02	3.39	2.29	1.62	1.20	.87	.66
Pine: Eastern white	20,000	5,630	2,000	880	406	200	102	56	33.1	19.9	12.3	7.9	5.01	3.31	2.19	1.51	1.06	.74	.52
Longleaf	36,000	6,700	3,100	1,320	578	270	135	74	41.7	24.0	14.4	9.9	6.76	3.72	2.46	1.66	1.15	.79	.60
Ponderosa	20,000	5,010	3,310	1,410	645	300	150	81	44.7	28.1	14.8	9.1	6.62	3.56	2.34	1.62	1.15	.87	.66
Shortleaf	45,000	11,700	3,720	1,380	660	265	130	66	36.9	22.4	13.8	8.7	5.76	3.80	2.63	1.82	1.29	.98	.66
Sugar	20,000	5,200	1,000	645	280	140	78	44	26.7	15.9	10.9	6.9	4.26	3.02	2.09	1.48	1.06	.78	.56
Redwood	22,400	4,000	1,585	915	380	180	88	42	12.9	7.2	4.7	3.2	2.29	1.74	1.22	1.06	.85	.71	.60
Spruce, Sitka	28,400	5,000	2,140	880	365	168	82	44	23.1	15.5	9.8	6.3	4.27	3.08	2.14	1.58	1.17	.91	.71

[1] Known in the trade as "African mahogany."

[2] A Philippine hardwood, identified as tanguile or some similar species.

[3] The values for this species were calculated from measurements on veneer.

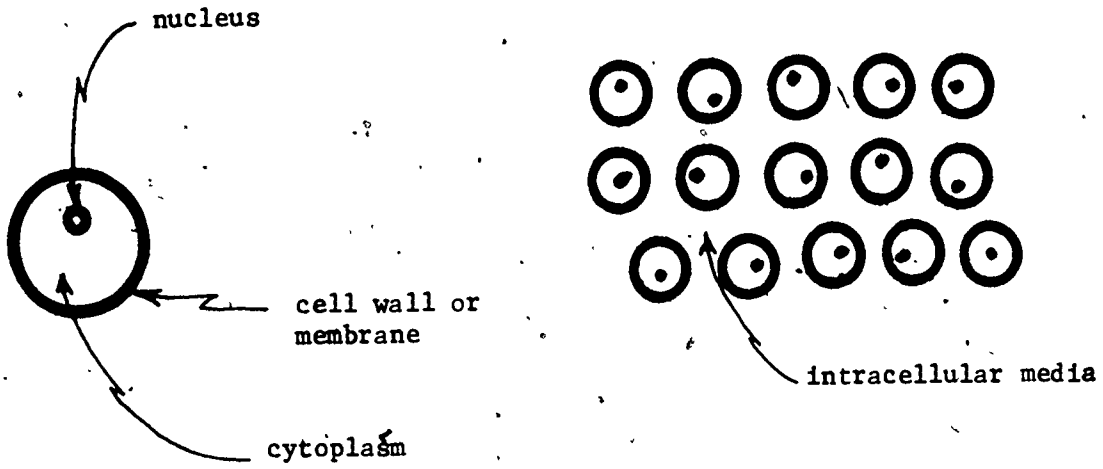

The following properties apply to animal tissue:

Cell Part	ε'	ρ
membrane	1.1 to 3.3	100 to 250 ohm-meters
cytoplasm	∿80	1 to 3 ohm-meters
intercellular media	∿80	1 to 3 ohm-meters

FIGURE 8-1 - Electrical Model of the Cell

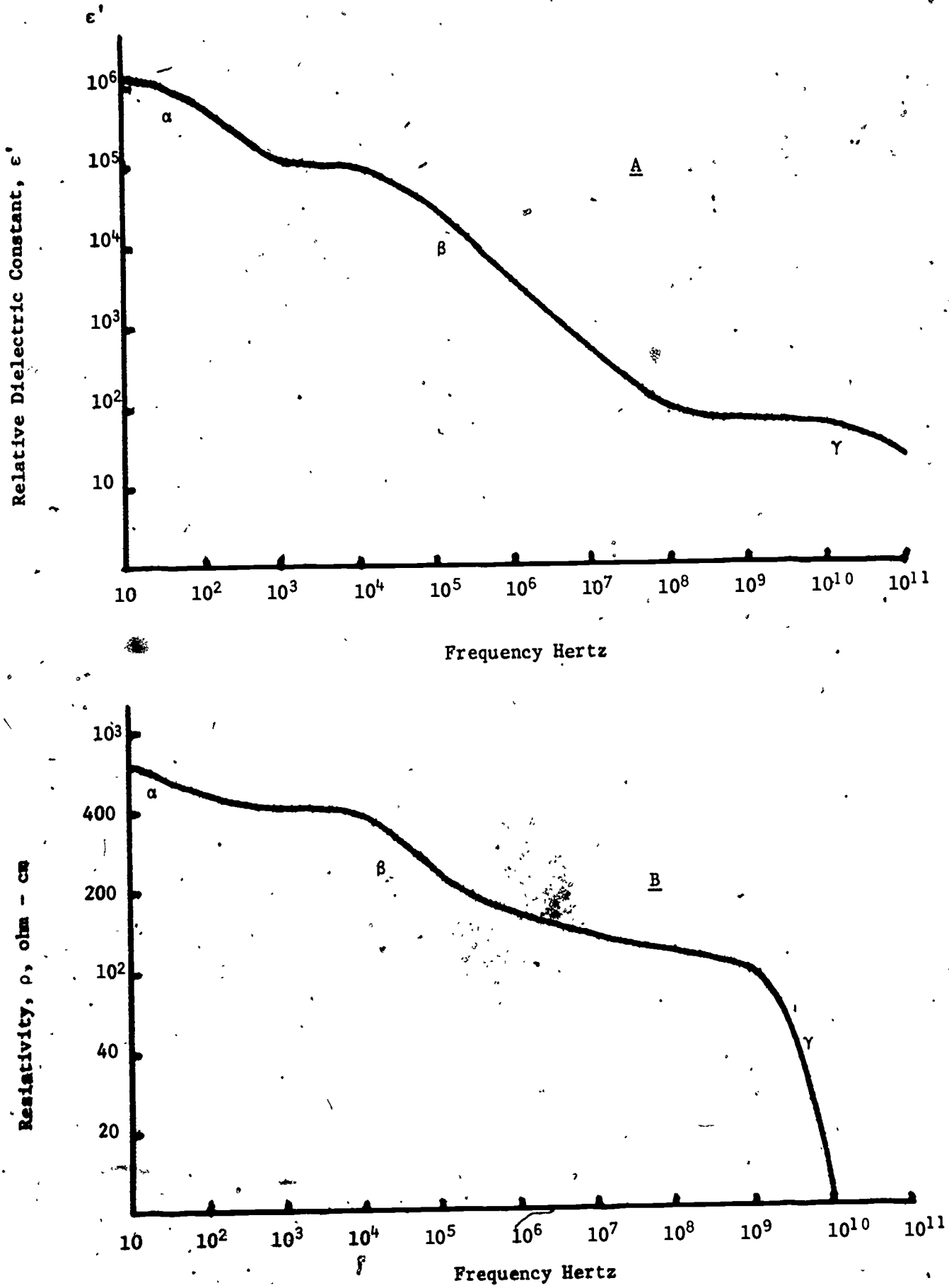

FIGURE 8-2 - Dielectric constant (A) and resistivity (B) of muscle tissue as a function of frequency.

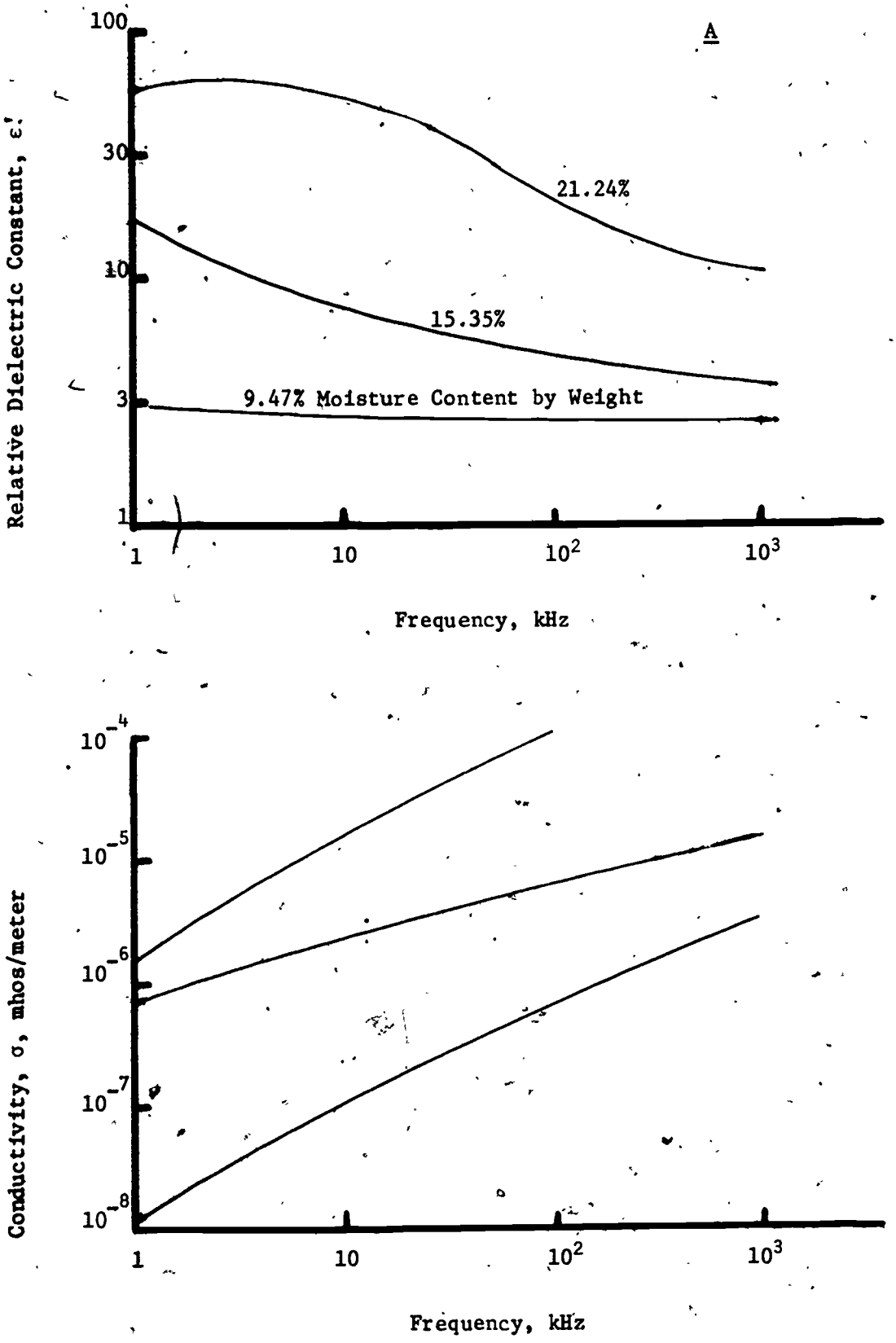

FIGURE 8-3 - Dielectric Constant (A) and Conductivity (B) of Cured Tobacco Leaves.

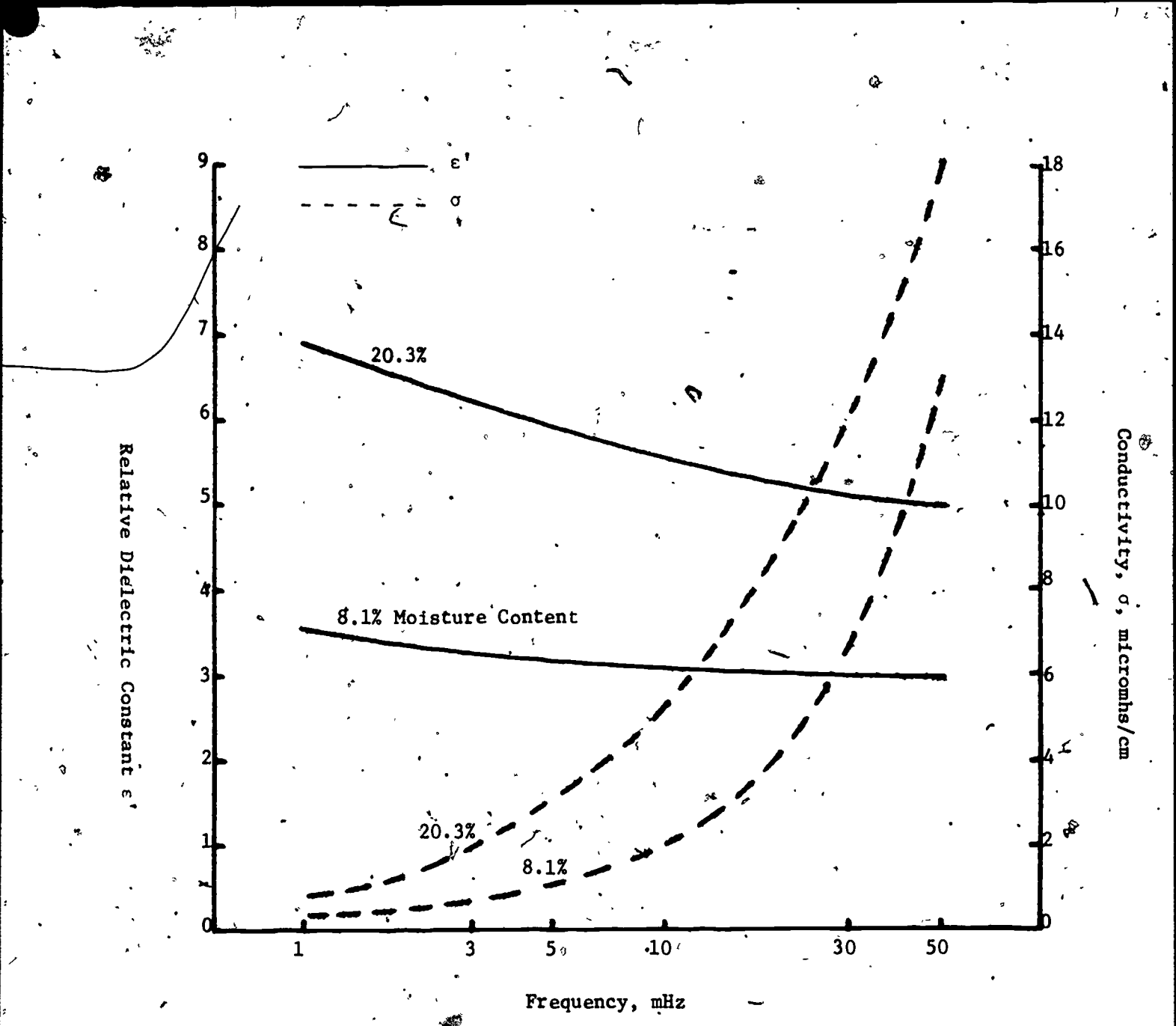

FIGURE 8-4 - Electrical Properties of Corn and Wheat

REFERENCES

A. S. Presman, 1970. Electromagnetic Fields and Life. Plenum Press, New York and London, pp. 336.

W. H. Henson, and F. J. Hassler, 1965. "Certain Dielectric and Physical Properties of Intact Tobacco Leaves," Transactions of the ASAE, 1965, pp. 524-527.

S. O. Nelson, 1965."Dielectric Properties of Grain and Seed in the 1 to 50 MHz Range," Transactions of the ASAE, 1965, pp. 38-43.

9. Introduction to Scattering

9. 1. Definitions

Scattering and diffraction are variations on the same phenomena or physical process.

I. A scattered field is defined as the difference between the total field with the scattering object and the field that would exist without the scattering object. Or,

$$E_S = E_T - E_I$$

II. A diffracted field is defined as the total field in the presence of the scattering object. Or,

$$E_D = E_T = E_I + E_S$$

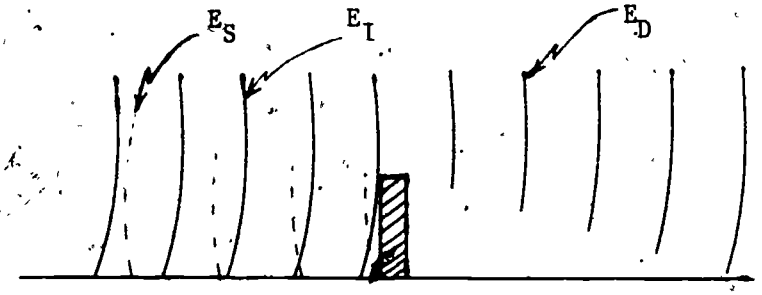

III. Reflection is usually used in reference to scattering from a smooth, often planar, surface. An image of the light source results.

IV. Specular reflection is defined as reflection when the angle of incidence equals the angle of reflection.

V. Backscattering is defined as that process or phenomena which scatters energy back toward the source.

VI. Radar cross section is a measure of the ability of an object

to scatter energy. It is equivalent to the area of an isotropic radiator which would produce a radar echo equal to that from the target. It is defined mathematically as,

$$\sigma_S = \lim_{R \to \infty} 4\pi R^2 \left| \frac{W_r}{W_i} \right|$$

where W_r is the scattered power flux density at a distance R from the scatterer and W_i is the power flux density in an incident plane wave field.

VII. Polarization refers to the directional properties of the electromagnetic field. Polarization is the orientation of the field vectors of an electromagnetic wave. In radio physics, polarization refers to the direction of the electric field vector $\overline{E}$; in optics, it usually refers to the direction of the magnetic field vector $\overline{H}$.

VIII. A linearly polarized wave has constant polarization, at a given point, with time.

IX. Depolarization is the process, always associated with scattering, whereby the polarization of the scattered energy is altered from that of the incident energy.

9. 2. Concepts

1. Scattering occurs because of an abrupt change in the electrical properties of the media through which a wave is propagating. The mass of the object does not produce electromagnetic scattering.

2. Scattering may be correctly considered as the reradiation of energy, produced by currents induced by the incident field.

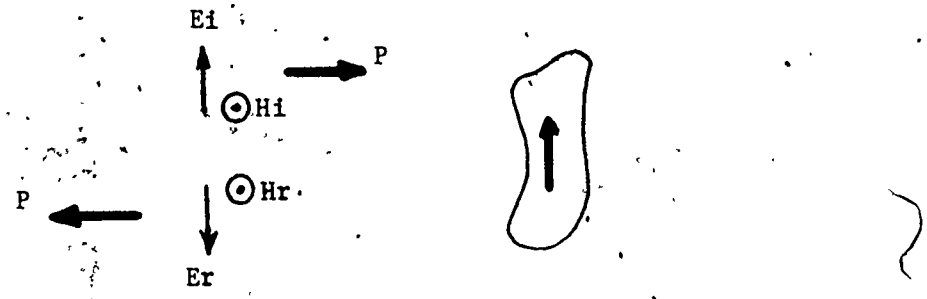

3. Depolarization occurs whenever scattering occurs.

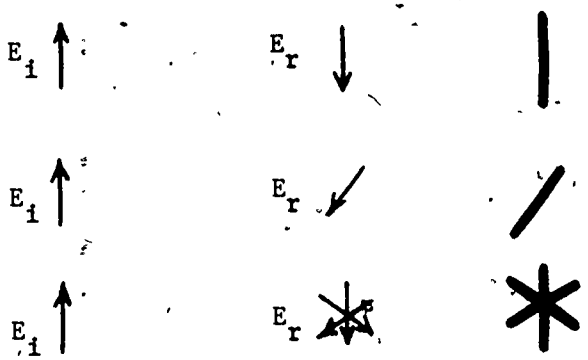

4. Radar cross section, or scattering efficiency, is a function of,

   a) Frequency

   b) Target size

   c) Target shape

   d) Electrical properties of the target

   e) Angle of incidence (except for the sphere).

5. There are three size/frequency or size/wavelength ratio ranges of interest,

   a) $d/\lambda < 1$, Rayleigh Scattering $\sigma_S \propto 1/\lambda^4$

   e.g., when $\pi D \simeq \lambda/4$, (sphere) $\sigma_S \simeq \frac{\pi r^2}{30}$

   and when $\pi D \simeq \lambda/8$, $\sigma_S \simeq \frac{\pi r^2}{480}$.

b) $d/\lambda \simeq 1$, resonance scattering, σ oscillates around πr^2.

c) $d/\lambda > 1$, optical scattering $\sigma_S = \pi r^2$

The above are specifically for a sphere.

6. Roughness effects are important at dimensions equivalent to a wavelength. Roughness is not a useable concept when referring to Rayleigh Scattering.

7. Why is the sky blue?

λ Blue $\sim$ 0.4 micrometers

λ Red $\sim$ 0.7 micrometers

$$\sigma_S \propto \frac{1}{\lambda^4}$$

Molecule sizes $\sim$ 0.03 micrometers.

8. The mathematical complexity of all but the simplest situations limits our ability to treat many of the interesting cases rigorously. However, we can usually approximate the real world with some situation we can handle.

9. 3. Boundary Value Problems

Scattering occurs because of a change in the electrical characteristics of the media through which the energy is propagating. There is usually an identifiable boundary or boundaries between the different media.

Even in those situations where a boundary is difficult to identify we can usually make approximations and reduce the situation to a boundary value problem.

The solution of boundary value problems requires the satisfaction of: 1. EM field equations in both media; and 2) boundary conditions.

The following boundary conditions apply at any surface of discontinuity:

a) The tangential component of E is continuous at the surface.

b) The tangential component of H is continuous at the surface, except at the surface of a perfect conductor.

c) The normal component of B is continuous at the surface.

d) The normal component of D is continuous if there is no surface change density. Otherwise D is discontinuous by an amount equal to the surface change density.

10. Reflection of Plane Waves from Plane Surfaces

10.1. For Perfect Conductors

We will consider first, normal incidence.

(a) For time varying fields, neither E nor H can exist in a perfect conductor. From:

$$\delta = \left[\frac{2}{\omega\mu\sigma}\right]^{1/2}$$

and for $\sigma = \infty$,

$$\delta = 0$$

(b) Also, there can be no energy loss within a perfect conductor, $P = I^2 R = 0$. Therefore, all the energy must be reflected.

(c) From the first boundary condition, $E_{tang.}$ continuous, the field just outside the conductor must = 0, therefore:

$$E_r = - E_i$$

To show direction of propagation we write:

$$E_r e^{j(\omega t + \beta X)} = - E_i e^{j(\omega t - \beta X)} \qquad (10.1)$$

(d) For a continuous wave E_i and E_r combine to form a total field, a standing wave or,

$$E_T = E_i (e^{j(\omega t - \beta X)} - e^{j(\omega t + \beta X)}) \qquad (10.2)$$

This forms a standing wave as shown below:

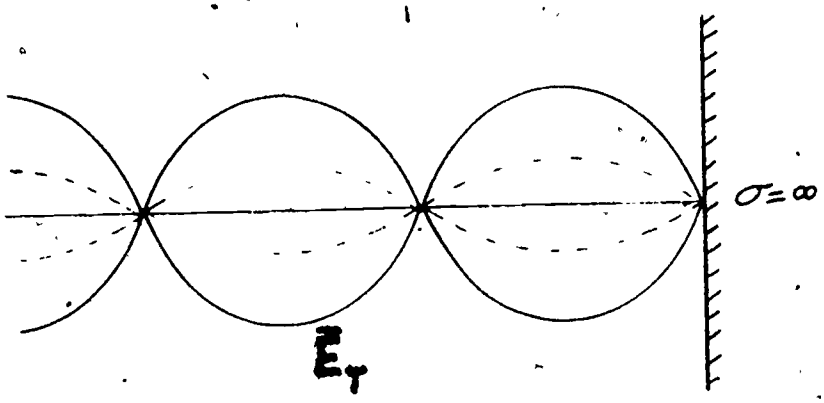

(e) For a radar pulse, a standing wave is not established, but the pulse is reflected with its polarization exactly reversed.

(f) To determine $\bar{H}$, we note that since $\bar{E}$ is reversed, $\bar{H}$ must maintain the same polarization in order to effect a reversal in propagation (from $\bar{E}X\bar{H}$). Since:

$H_i = H_r$, then,

$$H_T = H_i \left[e^{j(\omega t - \beta X)} + e^{j(\omega t + \beta X)}\right] \quad (10.3)$$

This forms the standing wave,

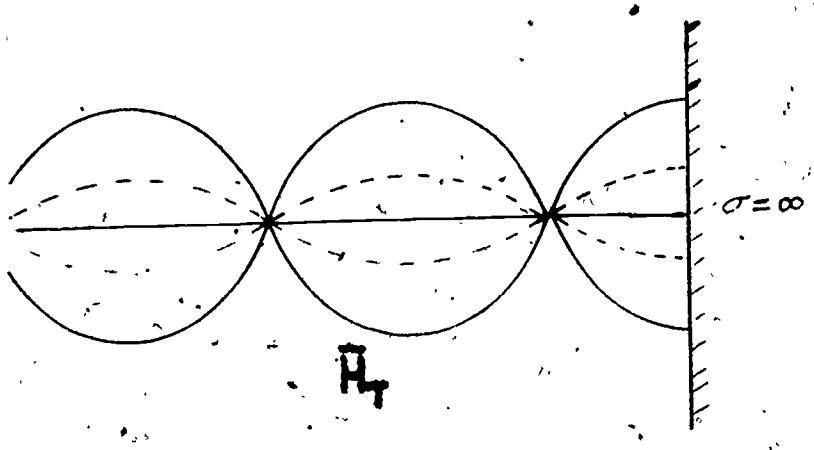

(g) To satisfy boundary conditions, H = 0 within the conductor, and twice H_i outside it, there must be a surface current flowing such that the amperes per meter equals the magnetic field intensity.

(h) Note that equations (10.2) and (10.3) may be put in the form,

$$E_T = -2jE_i \sin\beta X \, e^{j\omega t} \qquad (10.4)$$

$$H_T = 2H_i \cos\beta X \, e^{j\omega t} \qquad (10.5)$$

The factor j shows E_T and H_T to be 90^o out of phase, indicating no power loss at the interface or elsewhere, which is consistant with $\sigma = \infty$ and perfect reflection. The standing wave patterns also show a 90^o phase difference between the $\bar{E}$ and $\bar{H}$ fields.

10.2. Reflection by a Perfect Dielectric Normal Incidence - Infinite Plane

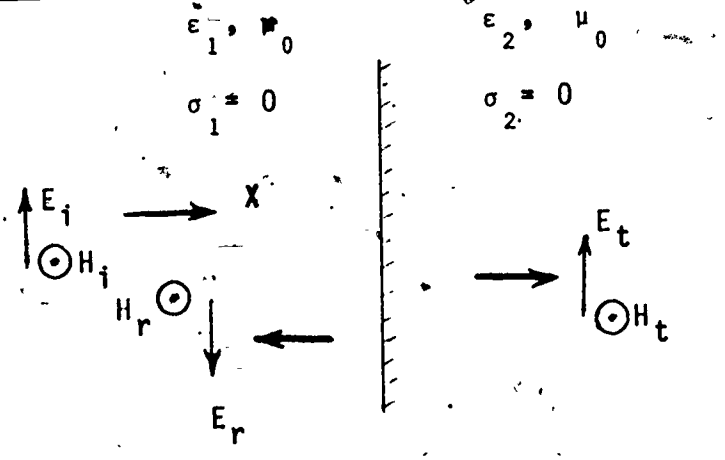

(a) For a perfect dielectric, $n = \sqrt{\mu/\varepsilon}$, hence, $n_1 = \sqrt{\mu_0/\varepsilon_1}$, $n_2 = \sqrt{\mu_0/\varepsilon_2}$

Therefore, we may write,

$$E_i = n_1 H_i \qquad (10.6)$$

$$E_r = -n_1 H_r \qquad (10.7)$$

$$E_t = n_2 H_t \qquad (10.8)$$

which satisfy the space relationships in each medium.

(b) The boundary condition, E and H tangential are continuous, requires that,

$$H_i + H_r = H_t \qquad (10.9)$$

$$E_i + E_r = E_t \qquad (10.10)$$

Combining these five equations we get,

$$H_i + H_r = \frac{1}{n_1}(E_i - E_r) = H_t = \frac{1}{n_2}(E_i + E_r)$$

and then by multiplying through by n_1 and n_2 we have,

$$n_2 (E_i - E_r) = n_1 (E_i + E_r)$$

$$E_i (n_2 - n_1) = E_r (n_2 + n_1)$$

$$\text{and } \frac{E_r}{E_i} = \frac{n_2 - n_1}{n_2 + n_1} \qquad (10.11)$$

$$\text{Similarly } \frac{H_r}{H_i} = \frac{\eta_1 - \eta_2}{\eta_1 + \eta_2} \qquad (10.12)$$

Also note that,

$$\frac{E_t}{E_i} = \frac{2\eta_2}{\eta_2 + \eta_1} \qquad (10.13)$$

These solutions for reflection at normal incidence, on perfect conductors and dielectrics, of infinite extent, are of limited interest, but they do form a basis for comparison with the solutions of greater interest which follow.

If $\mu = \mu_0$, equations (10.11) and (10.12) become,

$$\frac{E_r}{E_i} = \frac{\sqrt{\epsilon_1} - \sqrt{\epsilon_2}}{\sqrt{\epsilon_1} + \sqrt{\epsilon_2}} \qquad (10.15)$$

$$\frac{H_r}{H_i} = \frac{\sqrt{\epsilon_2} - \sqrt{\epsilon_1}}{\sqrt{\epsilon_2} + \sqrt{\epsilon_1}} \qquad (10.16)$$

From (10.15) and (10.16) we see that for the dielectric class of materials, a high dielectric constant will result in good reflection or scattering. You will find many references to SLR detection of dielectric constant differences; they are referring to the effect apparent in these equations and they are assuming the materials are poor conductors (good dielectrics).

10.3. Reflection from a Smooth, Plane Surface of a Medium Having Arbitrary Constants. Normal Incidence.

The same approach used for a perfect dielectric will give us the same general answer:

$$\frac{E_r}{E_i} = \frac{\eta_2 - \eta_1}{\eta_2 + \eta_1} \tag{10.17}$$

$$\frac{H_r}{H_i} = \frac{\eta_1 - \eta_2}{\eta_1 + \eta_2} \tag{10.18}$$

Now, however:

$$\eta_1 = \left[\frac{j\omega\mu_1}{\sigma_1 + j\omega\epsilon_1}\right]^{1/2} \tag{10.19}$$

$$\eta_2 = \left[\frac{j\omega\mu_2}{\sigma_2 + j\omega\epsilon_2}\right]^{1/2} \tag{10.20}$$

For the perfect dielectric:

$\sigma_2 = 0$ and if

$\sigma_1 = 0$,

$\eta = \sqrt{\frac{\mu}{\epsilon}}$

and we have the same result we obtained earlier.

For the perfect conductor case:

$\sigma_2 = \infty$

$\eta_2 = 0$

and $\therefore \frac{H_r}{E_i} = -1$

$$\frac{H_r}{H_i} = +1$$

which is also in agreement with our previous answer.

10.4. Reflection from Smooth, Plane Surfaces at Oblique Incidence

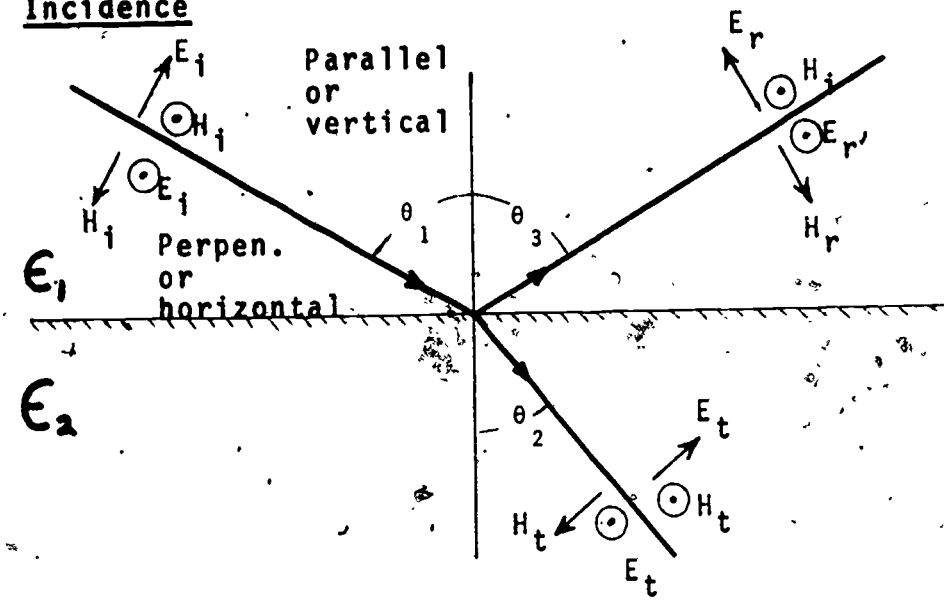

FIGURE 10-1

For a perfectly smooth, plane surface, there will be no backscattered energy. This is obvious from the geometry of the situation given in Figure 10-1. Reflection is now a function of polarization of the incident energy as well as the angle of incidence. From Snell's Law we have the relation,

$$\frac{\sin \theta_1}{\sin \theta_2} = \sqrt{\frac{\epsilon_2}{\epsilon_1}} \qquad (10.21)$$

and from Ray Theory,

$$\theta_1 = \theta_3 \tag{10.22}$$

For a propagating plane electromagnetic wave, the power transmitted per square meter is given by,

$$P = \bar{E} \times \bar{H} \tag{10.23}$$

For a plane wave in an homogenous isotropic media,

$$P = \frac{E^2}{\eta} \tag{10.24}$$

Therefore, the power incident/meter^2 on the surface of the boundary will be,

$$P_i = \frac{E_i^2}{\eta_1} \cos \theta_1 \tag{10.25}$$

and at $\theta = 0^o$, normal incidence,

$$P_i = \frac{E_i^2}{\eta_1}$$

It follows, of course, that

$$P_t = \frac{E_t^2}{\eta_2} \cos \theta_2 \tag{10.26}$$

and

$$P_r = \frac{E_r^2}{\eta_1} \cos \theta_3 \tag{10.27}$$

Now, from the conservation of energy we get,

$$\frac{1}{\eta_1} E_i^2 \cos\theta_1 = \frac{1}{\eta_1} E_r^2 \cos\theta_1 + \frac{1}{\eta_2} E_t^2 \cos\theta_2 \qquad (10.28)$$

and finally if we divide through by $\frac{1}{\eta_1} E_i^2 \cos\theta$, we arrive at the desired result,

$$\frac{E_r^2}{E_i^2} = 1 - \frac{\eta_1 E_t^2 \cos\theta_2}{\eta_2 E_i^2 \cos\theta_1} \qquad (10.29)$$

and for a perfect dielectric we have,

$$\frac{E_r^2}{E_i^2} = 1 - \frac{\sqrt{\epsilon_2} E_t^2 \cos\theta_2}{\sqrt{\epsilon_1} E_i^2 \cos\theta_1} \qquad (10.30)$$

In order to eliminate the E_t and E_i terms in the right hand side of the equation, we must consider the polarization of the incident energy.

Case I. <u>Polarization Perpendicular (Horizontal) to the Plane of Incidence</u>

From the boundary condition, $E_{tangential}$ continuous we get,

$$E_i + E_r = E_t \quad \text{or} \qquad (10.31)$$

$$\frac{E_t}{E_i} = 1 + \frac{E_r}{E_i}$$

Inserting (10.25) and (10.24) we get,

$$\frac{E_r^2}{E_i^2} = 1 - \sqrt{\frac{\epsilon_2}{\epsilon_1}} \left(1 + \frac{E_r}{E_i}\right)^2 \frac{\cos\theta_2}{\cos\theta_I}$$

$$\text{or } 1 - \left(\frac{E_r}{E_i}\right)^2 = \sqrt{\frac{\varepsilon_2}{\varepsilon_1}} \left(1 + \frac{E_r}{E_i}\right)^2 \frac{\cos\theta_2}{\cos\theta_1}$$

Dividing through by $\left(1 + \frac{E_r}{E_i}\right)$ results in,

$$1 - \frac{E_r}{E_i} = \sqrt{\frac{\varepsilon_2}{\varepsilon_1}} \left(1 + \frac{E_r}{E_i}\right) \frac{\cos\theta_2}{\cos\theta_1}$$

$$\text{or } \frac{E_r}{E_i} = \frac{\sqrt{\varepsilon_1}\cos\theta_1 - \sqrt{\varepsilon_2}\cos\theta_2}{\sqrt{\varepsilon_1}\cos\theta_1 + \sqrt{\varepsilon_2}\cos\theta_2} \qquad (10.32)$$

From Snell's Law we can write the following,

$$\frac{\sin\theta_1}{\sin\theta_2} = \sqrt{\frac{\varepsilon_2}{\varepsilon_1}}$$

$$\frac{\sin^2\theta_1}{\sin^2\theta_2} = \frac{\varepsilon_2}{\varepsilon_1}$$

$$\text{or } \sqrt{\varepsilon_2}\cos\theta_2 = \sqrt{\varepsilon_2 - \sin^2\theta_1\,\varepsilon_1} \qquad (10.33)$$

Substituting (10.27) into (10.26), we get,

$$\frac{E_r}{E_i} = \frac{\sqrt{\varepsilon_1}\cos\theta_1 - \sqrt{\varepsilon_2 - \sin^2\theta_1\,\varepsilon_1}}{\sqrt{\varepsilon_1}\cos\theta_1 + \sqrt{\varepsilon_2 - \sin^2\theta_1\,\varepsilon_1}}$$

$$\text{or } \frac{E_r}{E_i} = \frac{\cos\theta_1 - \sqrt{(\varepsilon_2/\varepsilon_1) - \sin^2\theta_1}}{\cos\theta_1 + \sqrt{(\varepsilon_2/\varepsilon_1) - \sin^2\theta_1}} \qquad (10.34)$$

Note that for normal incidence, equation (10.28) reduces to,

$$\frac{E_r}{E_i} = \frac{1 - \sqrt{\varepsilon_{2/\varepsilon_1}}}{1 + \sqrt{\varepsilon_{2/\varepsilon_1}}} = \frac{\sqrt{\varepsilon_1} - \sqrt{\varepsilon_2}}{\sqrt{\varepsilon_1} + \sqrt{\varepsilon_2}}$$

Case II. Polarization Parallel to the Plane of Incidence (Vertical)

The solution for this case is:

$$\frac{E_r}{E_i} = \frac{(\varepsilon_{2/\varepsilon_1})\cos\theta_1 - \sqrt{(\varepsilon_{2/\varepsilon_1}) - \sin^2\theta_1}}{(\varepsilon_{2/\varepsilon_1})\cos\theta_1 + \sqrt{(\varepsilon_{2/\varepsilon_1}) - \sin^2\theta_1}} \qquad (10.35)$$

Note that equation (10.28) and (10.29) are generally known as the Fresuel Reflection Coefficients (he first worked out the expression for specular reflection). When considering medium 1 (the source region) to be air or a vacuum we may write these equations as:

$$R_h = \frac{\cos\theta_1 - (\varepsilon'_2 - \sin^2\theta_1)^{1/2}}{\cos\theta_1 + (\varepsilon'_2 - \sin^2\theta_1)^{1/2}} \qquad (10.36)$$

and

$$R_v = \frac{\varepsilon'_2\cos\theta_1 - (\varepsilon'_2 - \sin^2\theta_1)^{1/2}}{\varepsilon'_2\cos\theta_1 - (\varepsilon'_2 - \sin^2\theta_1)^{1/2}} \qquad (10.31)$$

where $R_h = E_r/E_i$ for horizontal polarization and $R_v = E_r/E_i$ for vertical polarization.

Our analysis of scattering so far has dealt only with smooth, plane surfaces. Although not applicable to many real world situations, you should now have some understanding of the effect of electrical properties and angle of incidence. Of more importance, we will find these results useful for comparison with solutions for more complex cases, which require approximate solutions.

We will next be considering scattering from surfaces most useful in remote sensing:

1. Rough surfaces
2. Spheres
3. Long thin cylinders
4. Curved smooth or rough surfaces.

11.0 Scattering From Rough Surfaces and Other Objects

We have previously introduced and defined Radar (scattering) Cross Section as,

$$\sigma_s = \lim_{R \to \infty} 4\pi R^2 \left| \frac{W_r}{W_i} \right| \tag{11.1}$$

We will now simplify the writing of this equation as follows,

$$\sigma_s = 4\pi R^2 \left| \frac{W_r}{W_i} \right| \tag{11.2}$$

and will keep in mind that it is valid only for distances, $R >> \lambda$ and $R > d$, and that we are concerned here with the total magnitude of the power densities without regard to polarization or phase differences. The term we have been dealing with, E_{r/E_i}, is the reflection coefficient. The values or expressions we have determined so far should be considered specular reflection coefficients, since they apply to smooth, planar surfaces.

Note that σ_s is the scattering cross section based on power densities normal to the directions of incidence and reflection.

Cosgriff, et. al., 1960, use another scattering parameter, γ, which is related to σ_s as follows,

$$\gamma = 4\pi R^2 \frac{I_s}{I_o S \cos \theta_0} \tag{11.3}$$

where $I_s = W_r$

$I_o = W_i$

S is the area of the scattering surface,

and θ_o is the angle of incidence.

It is obvious therefore that,

$$\sigma_s = \gamma S \cos \theta_o \tag{11.4}$$

The denominator in (11.3) is the total power incident on the scattering surface (that surface which is effective in generating the scattered energy at the observers location).

We should also note that another commonly used term is, σ_o, "radar cross section/unit area of terrain.

$$\sigma_0 = \lambda S \tag{11.5}$$

$$\text{or,} \quad \sigma_0 = \sigma_s / \cos \theta \tag{11.6}$$

11.1 Reciprocity as Applied to Scattering

For notations of the form, γ_{vv} note that the first subscript refers to the polarization of the incident energy and the second subscript refers to the polarization of the scattered energy.

Noting the geometry of the scattering problem, Figure 11-1, we can obtain from the reciprocity theorem.

1. $\cos \theta_o \gamma_{hh} (\theta_o \phi_o; \theta_s \phi_s) = \cos \theta_s \gamma_{hh} (\theta_s \phi_s; \theta_o \phi_o)$

2. $\cos \theta_o \gamma_{vv} (\theta_o \phi_o; \theta_s \phi_s) = \cos \theta_s \gamma_{vv} (\theta_s \phi_s; \theta_o \phi_o)$

3. $\cos \theta_o \gamma_{vh} (\theta_o \phi_o; \theta_s \phi_s) = \cos \theta_s \gamma_{hv} (\theta_s \phi_s; \theta_o \phi_o)$

4. $\cos \theta_o \gamma_{hv} (\theta_o \phi_o; \theta_s \phi_s) = \cos \theta_s \gamma_{vh} (\theta_s \phi_s; \theta_o \phi_o)$

11.2. Scattering From a Rough Surface

Using the geometry of Figure 11-1 and considering a rough surface, the altitude, z, of the surface may be described through a Fourier series expansion, resulting in a series of sine waves which may be treated mathematically. For instance, for a square wave we obtain the Fourier series,

$E = A_o [\sin \omega t + 1/3 \sin 3 \omega t + 1/5 \sin 5 \omega t + \ldots]$ (11.7)

We are interested, however, in aperiodic, random surfaces. If $z = f(X,Y)$, then we shall define $\bar{z}$ as the mean amplitude of the surface roughness and $\bar{z}^2$ as the mean square of surface roughness.

To establish a roughness figure for concrete and asphalt surfaces (Cosgriff, et.al.,1960), plaster casts were made of representative surface areas. The casts were sliced into sections to expose surface profiles as shown below.

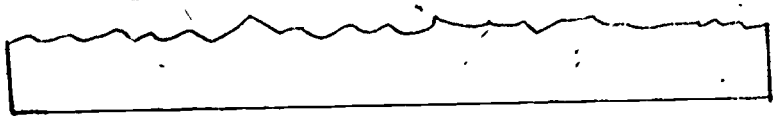

The surface height was measured every 0.25 mm. Numerical techniques were then used to obtain a Fourier expansion and to determine $\overline{z}^2$ and correlation coefficients for surface variations. The solution for scattering from a slightly rough surface is given for backscattering only ($\theta_0 = \theta_s$) by Cosgriff, et al., 1960, as,

$$\gamma = 8 \sin^3 \theta \, T \, \overline{z}^2 \, K^4 \int_0^\infty \rho(r) \, J_0 \, (2 K_r \cos \theta) \, r dr \quad (11.8)$$

where,

θ is angle of incidence

$\overline{z}^2$ is mean surface roughness

$K = \beta = 2\pi/\gamma_0$

$\rho(r) = \rho(\sqrt{X^2 + Y^2})$ where X and Y are positions on the surface and $\rho(r)$ is the autocorrelation function for the surface.

J_0 is a Bessel Function of argument $(2 K_r \cos \theta)$.

T is a function similar to Fresnel Reflection and contains polarization, angle of incidence, and dielectric constant dependences. See Equation (11.9) and (11.10)

The reader should note particularly:

1. The direct dependence on $\overline{z}^2$
2. The inverse dependence on $\frac{1}{\lambda^4}$
3. The similarity between T and Fresnel Coefficient as evidenced by the equations for T,

$$T_h = \left[\frac{(\varepsilon_1 + j\,\varepsilon_2 - 1)}{[\sin\theta + \sqrt{\varepsilon_1 + j\,\varepsilon_2 - \cos^2\theta}]^2}\right]^2 \qquad (11.9)$$

$$T_v = \left[\frac{(\varepsilon_1 + j\varepsilon_2 - 1)[(\varepsilon_1 + j\varepsilon_2)(1 + \cos^2\theta) - \cos^2\theta]}{(\varepsilon_1 + j\,\varepsilon_2)\sin\theta + \sqrt{\varepsilon_1 + j\,\varepsilon_2 - \cos\theta}]^2}\right]^2 \qquad (11.10)$$

11.2.1. Approximations of a Rough Surface

Even though random roughness $\bar{z}^2$ may be different or impossible to compute for many applications, a good estimate may be obtained by noting the following.

(a) For a sine wave

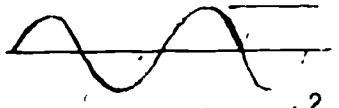

The mean square value = 1/2 (Peak)^2

(b) For a random surface,

Note that we have three ranges of dimensions (X and z) indicated on this drawing. Because of the $1/\lambda^4$ term, it is probable that only one of the three may be treated as a rough surface scatterer at any one frequency. The other size ranges would either have no effect or they would appear as terrain features or have large object effects (to be treated as cylinders, spheres, planes, etc.).

Peak average values for each of the surface features illustrated appear to be:

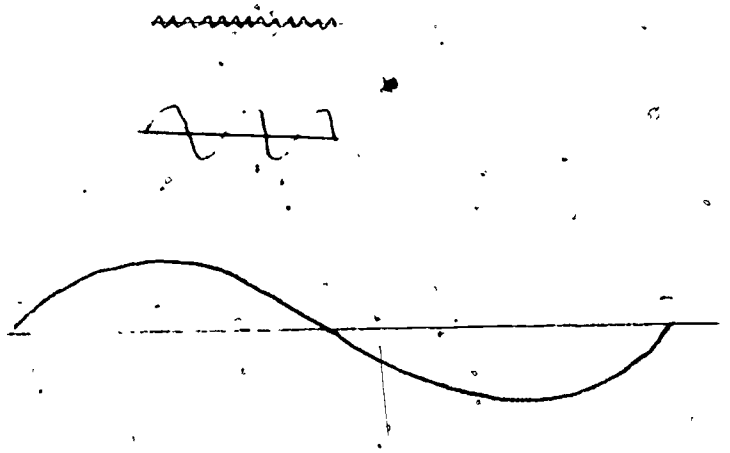

From these, mean square values may be estimated as,

$$MS \approx \overline{z}^2 \approx 1/2\ (peak)^2 \qquad (11.11)$$

for each frequency or size range indicated.

Note that the frequency effect will relate to dimensions parallel to the electric field. For a truly random surface, $\overline{z}^2$ will have the same value for each frequency or wavelength range of equal bandwidth. $\overline{z}^2$ in equation (11.8) should be evaluated relative to the wavelength of interest.

When evaluating roughness we must be careful to consider skin depths. Materials which the energy sees through will not seem as rough as their physical dimensions would indicate.

Resonance effects will be set up for periodic roughness such as occurs for water waves. HF scatter from sea waves may be very useful in measuring predominant periods.

At normal incidence, the fraction of total incident power specularly reflected from a rough surface is

$$\frac{W_r}{W_i \text{ (specular)}} = \exp -2\left[\frac{2\pi(\overline{Z^2})^{\frac{1}{2}}}{\gamma}\right]^2 \qquad (11.12)$$

when $(\overline{z^2})^{1/2} = \lambda/2\pi$, only 13.5 percent of the incident power is specularly reflected ($\sigma = \infty$).

when $(\overline{z^2})^{1/2} = \frac{\lambda}{\sqrt{2}\ 2\pi}$, only 1.8 percent reflected.

11.3. Scattering From Mathematically Describable Shapes

Figure 11-2 through 11-6 give equations and results for scattering from various shapes of interest. All of these results assume a perfectly conducting material.

REFERENCES

Mentzner, J. R., 1955. Scattering and Diffraction of Radio Waves Pergamon Press.

Corgriff, R. L., W. H. Peake, and R. C. Taylor, 1960. Terrain Scattering Properties for Sensor System Design , Ohio State University, Bulletin 181.

Moore, Richard K., 1969. Radar return From the Ground, University of Kansas, Bulletin of Engineering, No. 59.

Senior, T. B. A., July, 1965. Surface Roughness and Tolerances in Model Scattering Experiments, IEEE Transactions on Ant. and Propagation (PGAP), Vol. AP-13, No. 4.

Peake, William A., 1959. The Interaction of Electromagnetic Waves With Some Natural Surfaces, Ohio State University, Research Report 898-2.

Oliver, T. E., et.al., 1969. Radar Backscattering Data for Agricultural Surfaces, Ohio State University, Report 1903-9, Cleaninghouse N 69-23435.

Crispin and Siegel, 1968. Methods of Radar Cross Section Analysis, Academic Press.

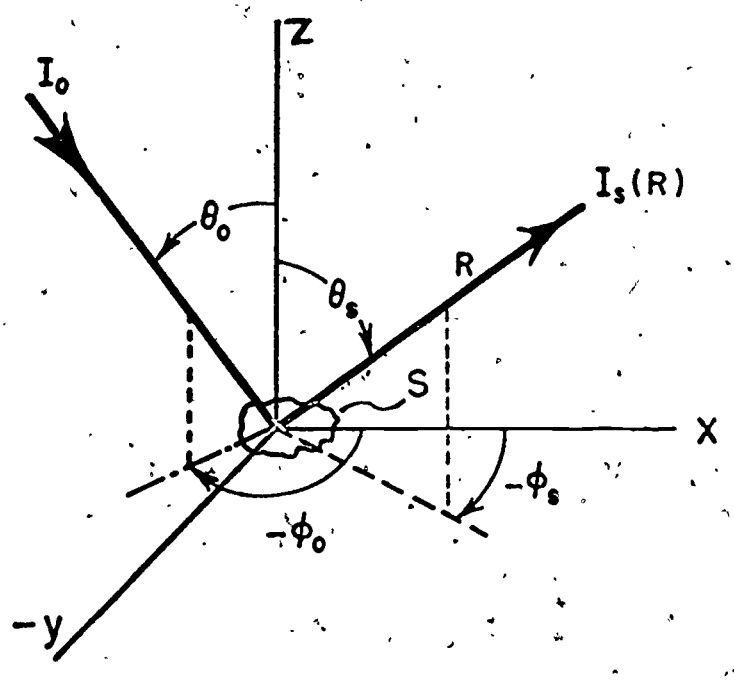

FIGURE -11-1 Geometry of the scattering problem.

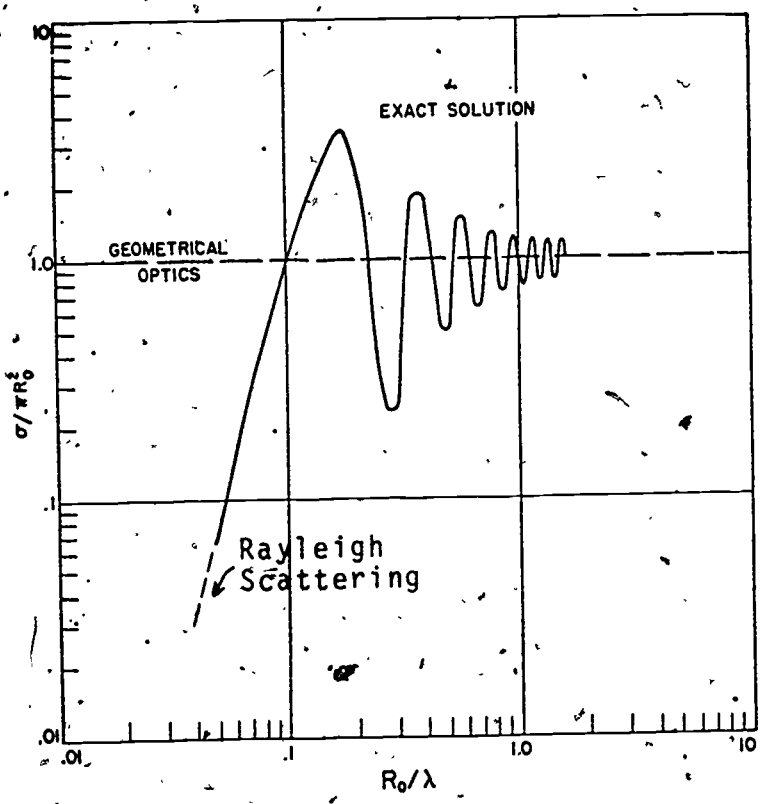

FIGURE 11-2 Normalized radar cross sections of perfectly conducting spheres of radii R_0

Reference: Mentzner, 1955

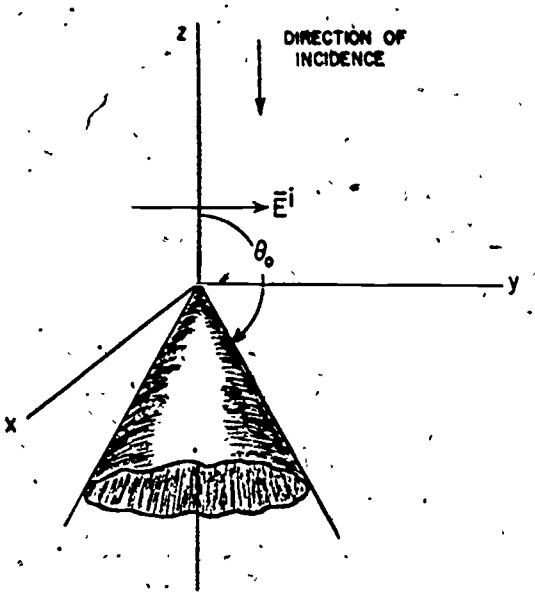

FIGURE 11-3 Plane wave incident axially on infinite conducting cone.

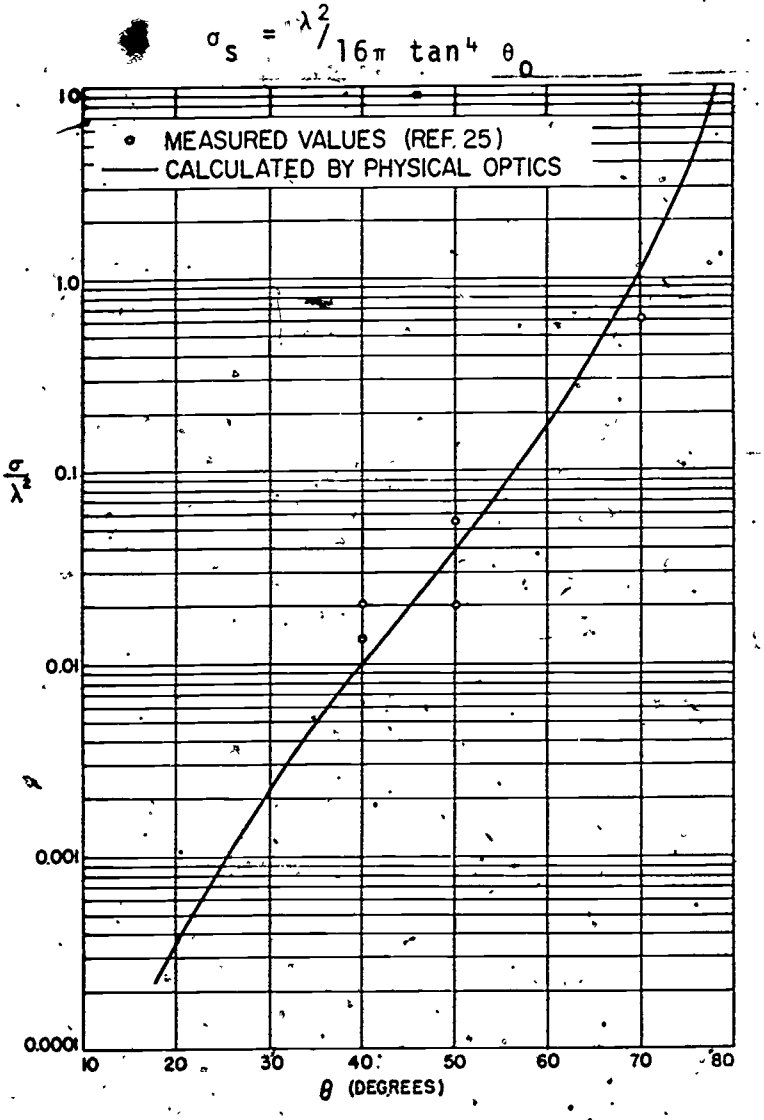

Normalized radar cross section of cone of half-angle θ.

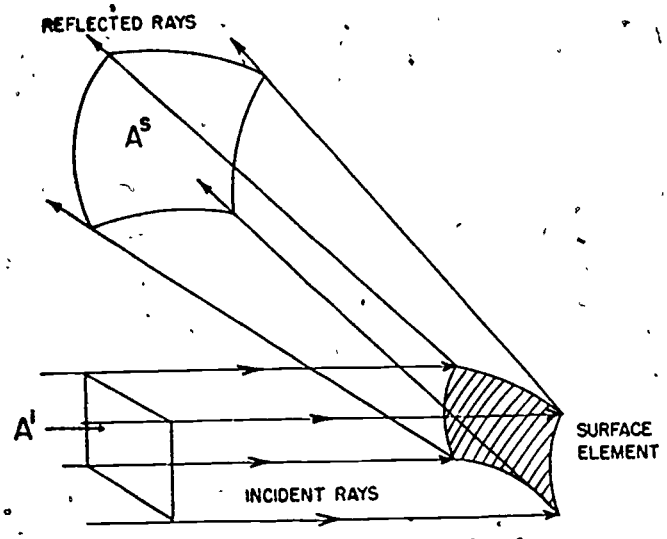

Diverging rays scattered from curved surface.

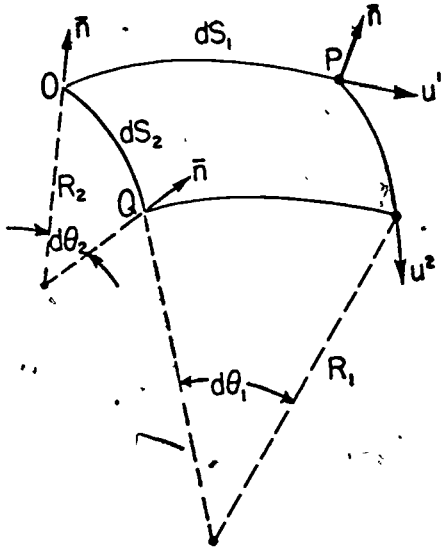

Scattering element with two different principal radii.

FIGURE 11-4

$$\sigma_s = \pi R_1 R_2$$

$$\sigma_{abs}(cond) = \infty$$

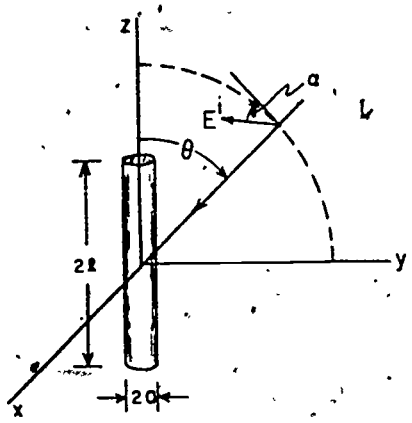

Thin wire with incident plane wave.

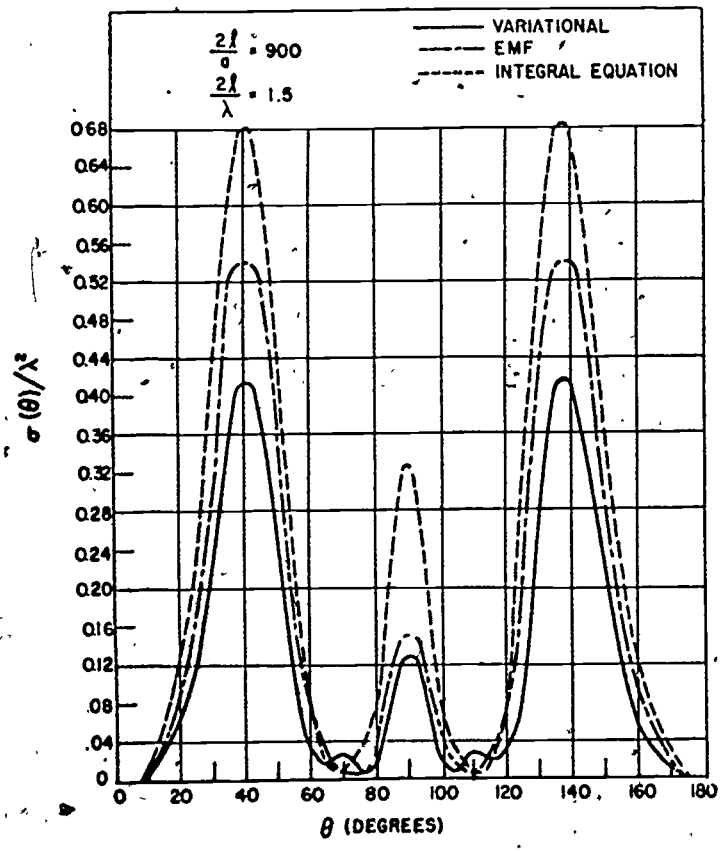

Angular response of wire (after TAI).

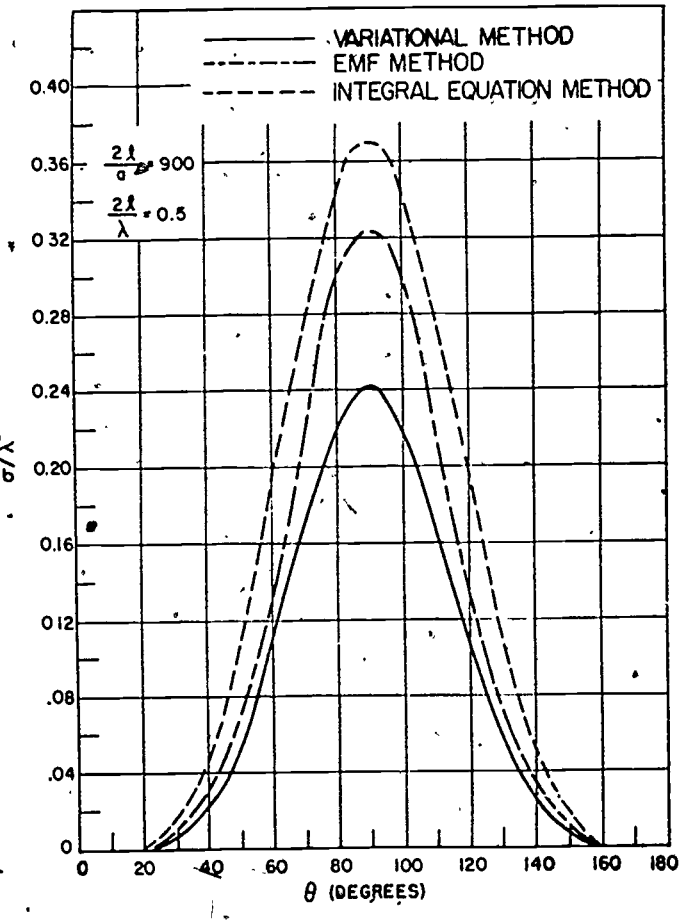

Angular response of wire (after TAI).

FIGURE 11-5

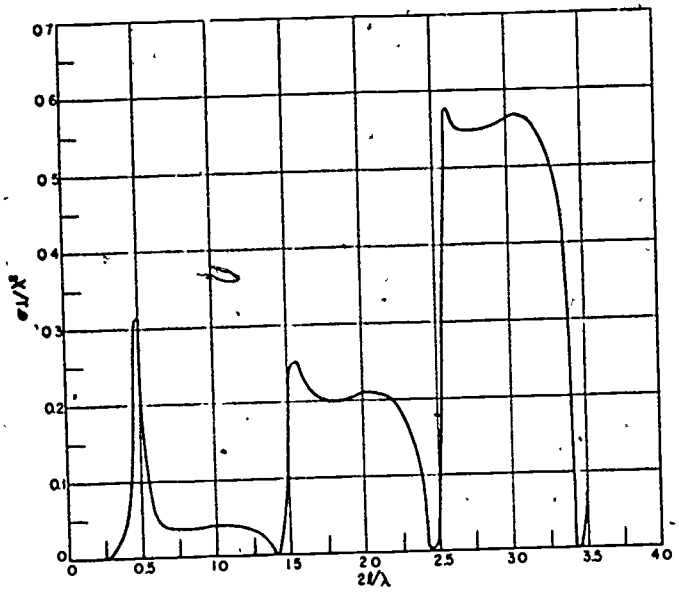

FIGURE 11-6 Broadside response of wires (after TAI).

APPENDIX

Formulas for radar cross sections of scatterers of large characteristic dimensions

Scatterer	*Aspect*	*Radar cross section*	*Definition of symbols*
Sphere	—	$\sigma = \pi a^2$	a = Radius
Cone	Axial	$\sigma = \frac{\lambda^2}{16\pi} \tan^4 \theta_0$	θ_0 = Cone half-angle
Paraboloid	Axial	$\sigma = 4\pi\xi_0^2$	$2\xi_0$ = Apex radius of curvature
Prolate spheroid	Axial	$\sigma = \pi b_0^4/a_0^2$	a_0 = Semimajor axis b_0 = Semiminor axis
Ogive	Axial	$\sigma = \frac{\lambda^2}{16\pi} \tan^4 \theta_0$	θ_0 = ½ angle of tangent nose cone
Circular plate	Incidence at angle θ to normal	$\sigma = \pi a^2 \cot^2 \theta J_1^2\left(\frac{4\pi a}{\lambda} \sin \theta\right)$	a = radius of plate
Large flat plate of arbitrary shape	Normal	$\sigma = 4\pi A^2/\lambda^2$	A = Plate area
Circular cylinder	Incidence at angle θ to broadside	$\sigma = \frac{a\lambda}{2\pi} \frac{\cos \theta \sin^2 (kL \sin \theta)}{\sin^2 \theta}$	a = radius L = cylinder length

PROBLEMS

11.1 The power density incident ($\theta = 60^0$) on the earth is given as 100 watts/m^2. The energy received at the radar receiver input terminals is one microwatt. If the airplane is at an altitude of 15,000 feet and if the radar antenna has an area of 10 square meters, compute σ_s.

11.2 Consider a lake with waves averaging 6 inches in height. What is the highest frequency at which the lake may be represented as a smooth surface? Over what frequency range can it be treated as a rough surface?

12.0 Side Look Radar

We are going to consider the Side Look Radar Systems in terms of system effects on system performance. We will not be concerned with the details of system design. We will examine:

1) Resolution
2) Dynamic range
3) Propagation effects
4) Image quality
5) Overall specifications

12.1 Slant Range Resolution

For a short pulse, propagation time to and from the target, Δt, is given by,

$$\Delta t = \frac{2R}{C} \tag{12.1}$$

where R is range and C is velocity (3×10^8 m/sec.)

If return pulses are non-overlapping (in time), resolvable, then differences in range must be,

$$\Delta R \geq \frac{C\tau}{2} \tag{12.2}$$

where τ is pulse width. Let ΔR = slant range resolution = $\rho_{R_S} = \frac{C\tau}{2}$. Then, ground range resolution is,

$$\rho_{R_G} = \frac{C\tau}{2} \sec \phi \quad \text{(See Figure 12-2)} \tag{12.3}$$

Ultimately then, the range resolution is limited by the system ability to generate a very narrow pulse of energy.

In the limit:

$$\tau_{min} = \frac{1}{f}$$

at K_a band $\tau_{min} = \frac{1}{33 \times 10^9}$

$= 3 \times 10^{-11}$ sec.

$\rho_{R_S}{}_{min} = (3 \times 10^8)\ (3 \times 10^{-11})/2$

$= 4.5 \times 10^{-3}$ meters

This would be a Monopulse Radar such as is proposed for snow depth measurements. This is very difficult to achieve. The Westinghouse AN/APQ - 97 system has a pulse width of 0.07 microsecond. Therefore,

$$\rho_{R_S} = (3 \times 10^8)\ (7 \times 10^{-8})$$

$= 10.5$ meters

It is specified as 12 meters.

Narrow pulse width requires a wideband transmitter and receiver, i.e.,

$$BW = \frac{0.159}{\tau} \qquad (12.4)$$

This limits or sets transmitter power requirements because noise power is proportional to the square root of bandwidth.

12.2 Azimuth Resolution

Antenna beamwidth, θ, for a

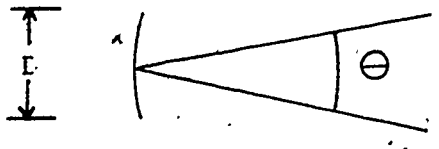

Parabolic dish antenna is given by,

$$\theta = \frac{50\lambda}{D} \text{ (Uniform illumination)} \qquad (12.5)$$

For k_a band, $\lambda = 10^{-2}$ meters and if D = 5 meters,

$$\theta = \frac{50 \times 10^{-2}}{5}$$

$$= 0.1^0$$

The antennas used for Side Look Radar systems are not parabolic dishes but are long linear arrays. The focusing of these antennas is accomplished by proper phasing of the signal received from each portion of the antenna. The resolution obtained for an antenna 5 meters long is equivalent to that obtained for a parabolic dish having a diameter of 5 meters. The Westinghouse AN/APQ -97 Side Look Radar system specifies an antenna beam width pattern of 0.1^0. This results in an azimuth resolution of approximately 21 meters at a 16 kilometer range. Obviously, the pulse width for the system has been adjusted such that the range and azimuth resolutions are approximately equal, resulting in an illumination of a square patch of terrain.

12.3 Synthetic Aperture Systems

The physical limitations imposed by operation from an aircraft has suggested the development of synthetic or electronic means of improving the resolution of Side Look Radar systems. The Goodyear AN/APQ -102 Side Look Radar System makes use of the Doppler phenomena to obtain a synthetic aperture. The Doppler effect is, of course, the apparent

with respect to the source of the waves. The source in this case is the reradiated or reflected energy from the target. Figure 12-3 illustrates the concept associated with a Doppler Synthetic Aperture system. In position 1, the aircraft is approaching the target and signals returned from the target will be shifted a known amount depending on the aircraft speed, the range R, and the angle θ. Signals having a frequency shift consistent with this position are stored for later processing. In position 2, the aircraft is now directly opposite the target and signals returned from the target will exhibit no frequency shift. Signals exhibiting zero frequency shift are stored for processing with the signals received from this same location when the aircraft was in position 1. When the aircraft reaches position 3, it is now moving away from the target and the signals returned from the target will exhibit a negative frequency shift consistent with that location, range and angular position. These signals are also stored and will be processed with the signals stored for the same target location when the aircraft was in positions 1 and 2. It should be intuitively obvious that this system now has a synthetic or apparent aperture equivalent to the distance between positions 1 and 3 on Figure 12-3. For small angles then, we can express the aperture, L, according to the relation,

$$L = \theta R \qquad (12.6)$$

where θ, R, and L are defined on Figure 12-3. From equation (12.5) it would appear that the system resolution would improve with smaller antennas, i.e., smaller D. There are practical system limitations to this however, and in practice, antennas 3 to 5 feet long are used.

The actual resolutions obtained with synthetic aperture systems is not known since system specifications have been classified up to this time. For a more rigorous and technical description of sythetic aperture systems, the reader is referred to Brown and Porcello, 1969.

12.4 Other Resolution Limits

The cathode ray tube (CRT) and the film used for permanent recording of the imagery are not presently a limitation in overall system resolution, although they could be for future systems. A minimum spot size for advanced CRTs is about 0.0007 inch. For a 4 inch tube, we can obtain 5700 spots per sweep. If this is related to a ground sweep of 21 kilometers, then each spot is equal to 4 meters on the ground. Obviously therefore, the CRT is capable of accurate reproduction of imagery obtained from Side Look Radar systems today. The resolution of the film is about 4 times better than that of the CRT.

12.5 The Classical Radar Equation

The radar equation may be written in the form,

$$S = \underbrace{\frac{P_t G}{4\pi R^2}}_{(a)} \times \underbrace{\frac{\sigma_S}{4\pi R^2}}_{(b)} \times \underbrace{\frac{G\lambda^2}{4\pi}}_{(c)} \quad \text{(Watts)} \qquad (12.7)$$

where the first term in the equation, (a) represents transmitted power density at range R, i.e., it is equal to W_i,

$$G = \frac{4\pi A_e}{\lambda^2} \text{ (antenna gain)} \tag{12.8}$$

where A_e is antenna effective area in meters^2. The gain of an antenna is defined as the increase in power density radiated in a given direction compared to the power density which would be radiated by an isotropic antenna, assuming the same total power is radiated. The second part of the equation, (b) is, from the definition of σ_S, $\frac{Wr}{Wi}$. The third part of the equation, (c) is the effective receiving aperture in meters^2, A_r. We see, therefore, that

$$S = W_r A_r \text{ (watts)} \tag{12.9}$$

The radar equation is usually given in the form,

$$S = \frac{P_t G^2 \lambda^2 \sigma}{(4\pi)^3 R^4} \tag{12.10}$$

Then substituting (12.8) into (12.10), we get,

$$S = \frac{P_t A_e^2 \sigma}{4\pi \lambda^2 R^4} \tag{12.11}$$

Actually, when the target fills the beam of the antenna, S tends to vary as $\frac{1}{R^3}$ (no longer have point source and $\frac{1}{R^2}$) This is the condition found for most remote sensing applications of radar. Further information on radar systems can be obtained from Berkowitz, 1965, Crispen and Siegel, 1968, and Wheeler, 1967.

12.6 Attenuation of Radar Waves

The attenuation of electromagnetic energy in the gigahertz range is given in Figure 12-4 for a clear, non-cloudy atmosphere. At the Ka band frequency of 33 gHz, the total attenuation for a range of 20 kilometers would be just slightly more than 2 DB. It is apparent from this curve that frequencies above the ka band must be carefully selected to avoid excessive attenuation.

Additional attenuation will result from the presence of clouds and precipitation. Prior to the formation of the precipitation, water drop sizes in clouds are generally less than .1 millimeter. From Figure 12-5, it is apparent that the effective cross-section and therefore the scattering and attenuation will be negligible. As the drop sizes increase and precipitation begins, attenuation will become significant. Figure 12-6 gives drop size distributions for several rain rates from Mitchell, 1966. Based on this information, calculations of attenuation rates as a function of rain rate have been made. The results of these calculations are given in Figure 12-7 from LeFande, 1968. More accurate attenuation rates can be obtained for Ka band radar by reference to Figure 12-8 from Oguchi, 1964. He has computed the effect on attenuation of the disortion in the shape of a falling raindrop.

In conclusion, the attenuation of Side Look Radar energy will be negligible in the absence of any precipitation.

Precipitation will cause appreciable attenuation of the energy however, with the resultant degradation of image quality.

12.7 Dynamic Range Requirements

The dynamic range for reflected signals from radar targets may be as great as 70 to 90 DB. This dynamic range is beyond the capability of most receivers and is certainly beyond the capability of the cathode ray tube or film recording system. In order to maintain a reasonable range of gray scales on the film, an automatic gain control system is used. The receiver senses the average energy being received and adjusts the gain of the system to obtain an optimum range of gray scales. The gain of the system will change therefore, as the general characteristics of the terrain change. For instance, if the aircraft were passing from a mountainess region to flat prairies or farmlands, one would expect the gain of the system to change considerably. A gain change of 10 to 30 DB could be anticipated for this situation. It is impossible therefore, to make quantitative comparisons of image brightness (one region compared to another) unless a record is maintained of changes in system gain.

12.8. Image Quality

A variety of factors can affect the quality of the imagery obtained. These include excessive motion of the aircraft, the effects of precipitation, mountain shadowing, flight direction, and other factors associated with the operation of the total system. These kind of problems can be anticipated, and the individual contracting for radar imagery should specify the

quality of images which will be considered acceptable.

12.9 Image Interpretation

Most detailed interpretations today depend heavily on prior interpreter knowledge of the relations between terrain features, vegetation types, and the climate and geology of the region. This apriori information allows the interpreter to relate changes in the brightness and texture of the image to changes in terrain, vegetation, and geology. In effect, the interpreter relates a variation in the image to a change in roughness or electrical properties and further relates this variation to known vegetation, topographic, and geologic conditions of the region.

Automatic interpretation of data must wait for digital or analog magnetic tape recording to be effectively used. Bi-frequency, multi-polarization systems would obviously be very valuable in separating roughness and electrical property effects.

The effective interpretation of radar imagery for Panama and for certain parts of Columbia is ample evidence of the present value of this system. Significant improvements and enhancement of this value can be expected in the near-future.

Many articles are now available in the open literature which describe the effective use of radar imagery for topographic, geological, and vegetation analyses.

REFERENCES

Berkowitz, R. S., 1965. Modern Radar, Wiley

Crispin and Siegel, 1968. Methods of Radar Cross-Section Analysis, Academic Press

Wheeler, Gershon J., 1967. Radar Fundamentals, Prentice Hall

Mitchell, R. L., June, 1966. Radar Meterorology at Millimeter Wavelengths, Aerospace Corporation Report TR-669 (6230-46)-9.

LeFande, R. A., November, 1968. Attenuation of Microwave Radiation for Paths Through the Atmosphere, Naval Research Laboratory Report 6766.

Oguchi, I., January, 1964. Attenuation of Electromagnetic Waves Due to Rain With Distorted Raindrops (Part II), Journal of the Radio Research Laboratories, Vol. 11, No. 53 (Japanese).

Rosenblum, E. S., March, 1961. Atmospheric Absorption of 100-400 KMCPS Radiation: Summary and Bibliography to 1961, Microwave Journal, p. 92.

Brown, William M., and Leonard J. Porcello, 1969. An Introduction to Synthetic-Aperture Radar, IEEE Spectrum, Vol. 6, No. 9

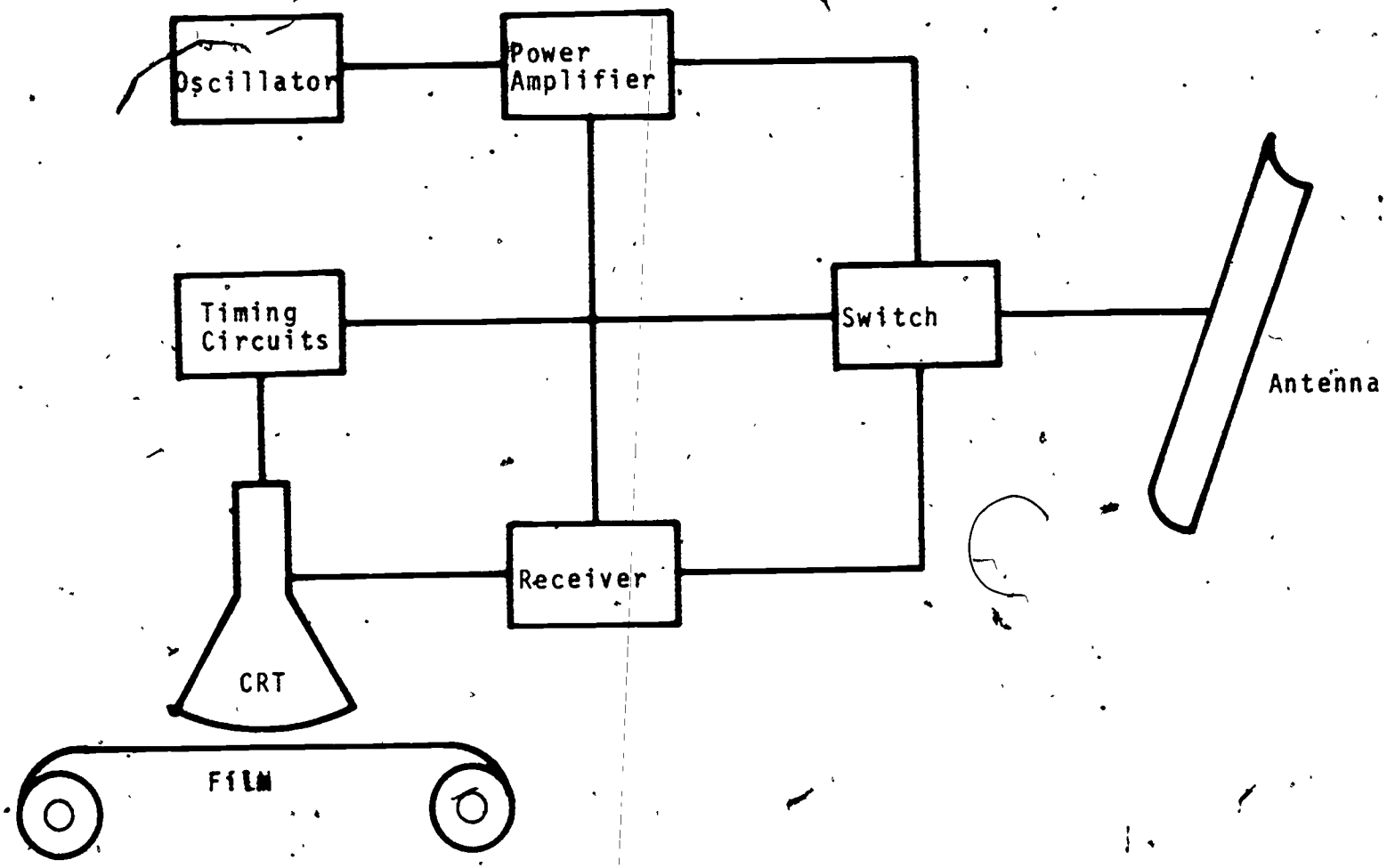

FIGURE 12-1: Side-Look Radar System

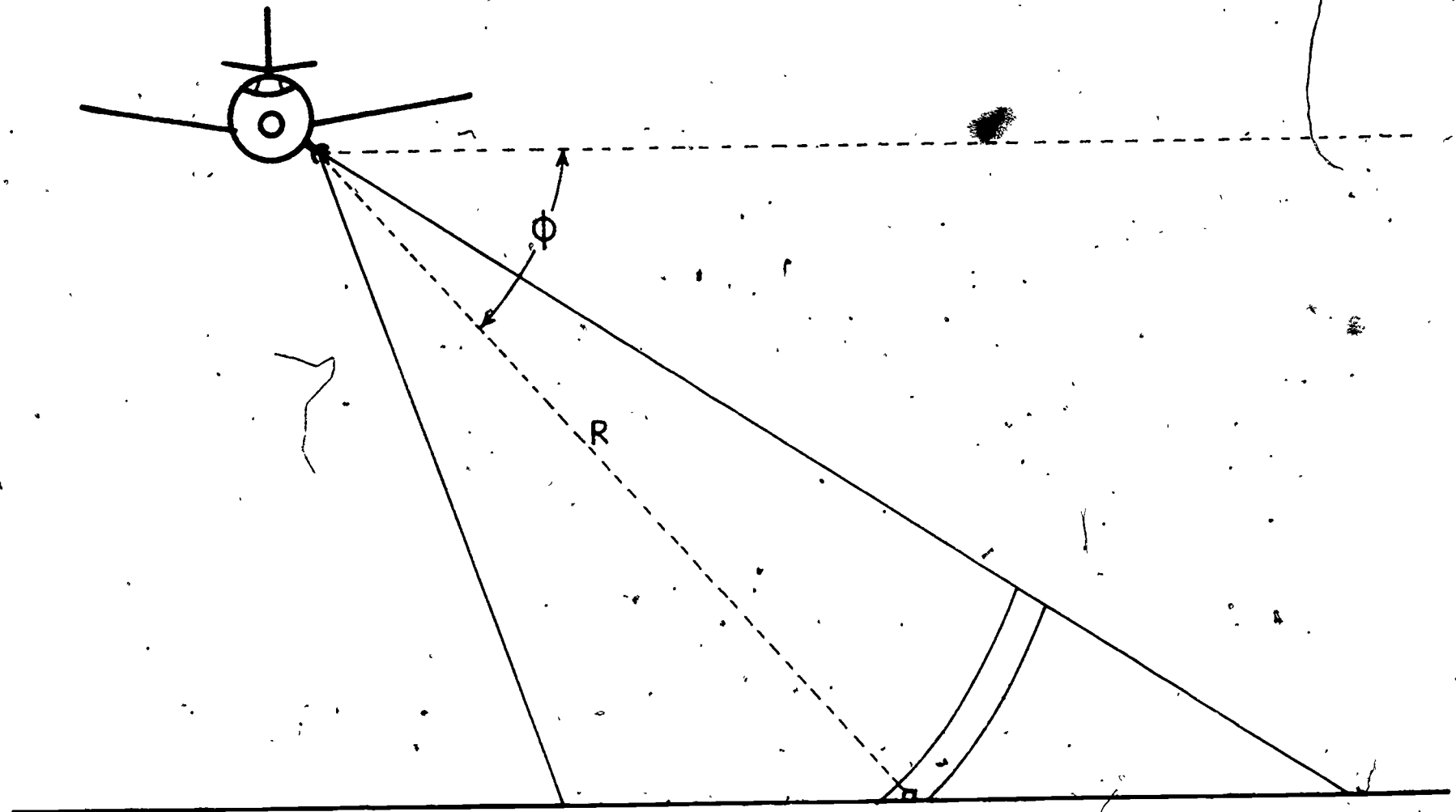

FIGURE 12-2: Side-Look Radar Geometry

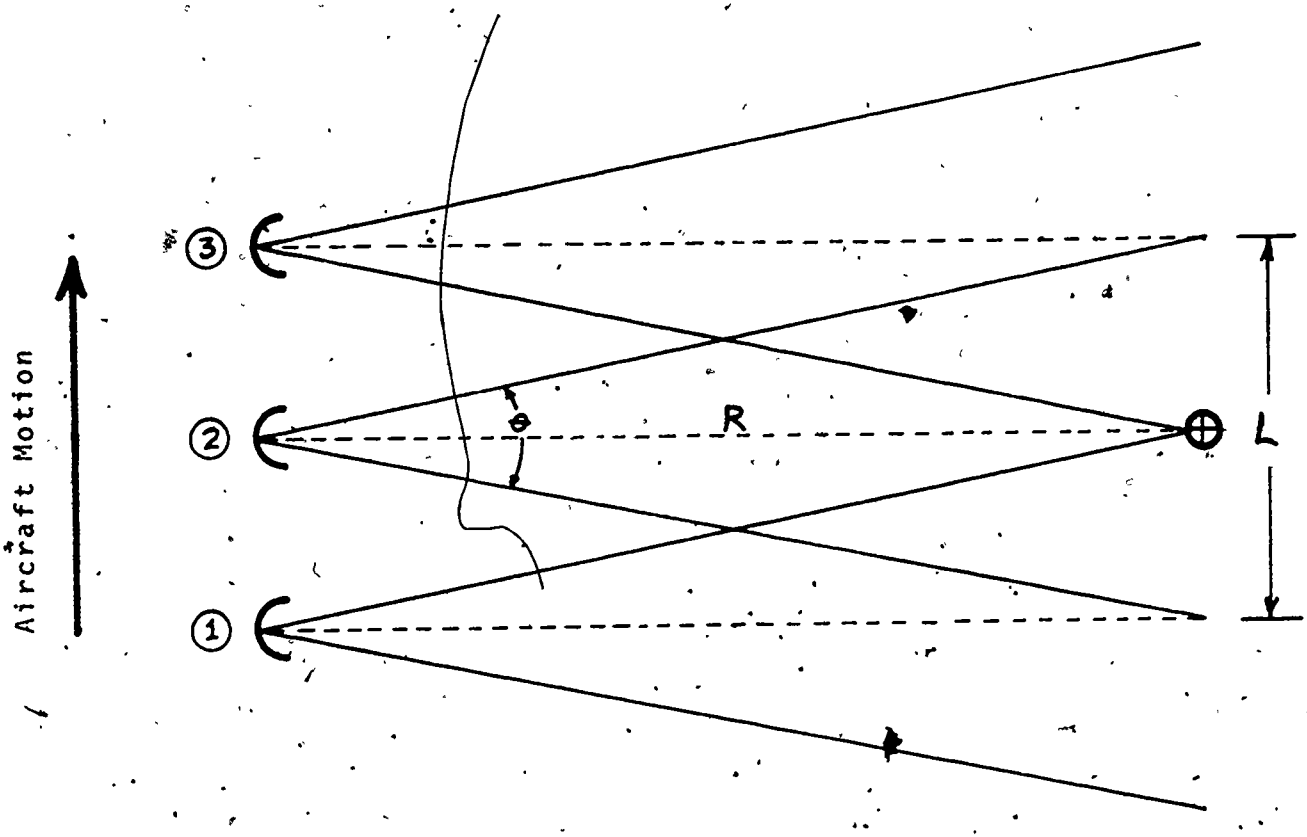

FIGURE 12-3: Synthetic Aperture (L) For Doppler System

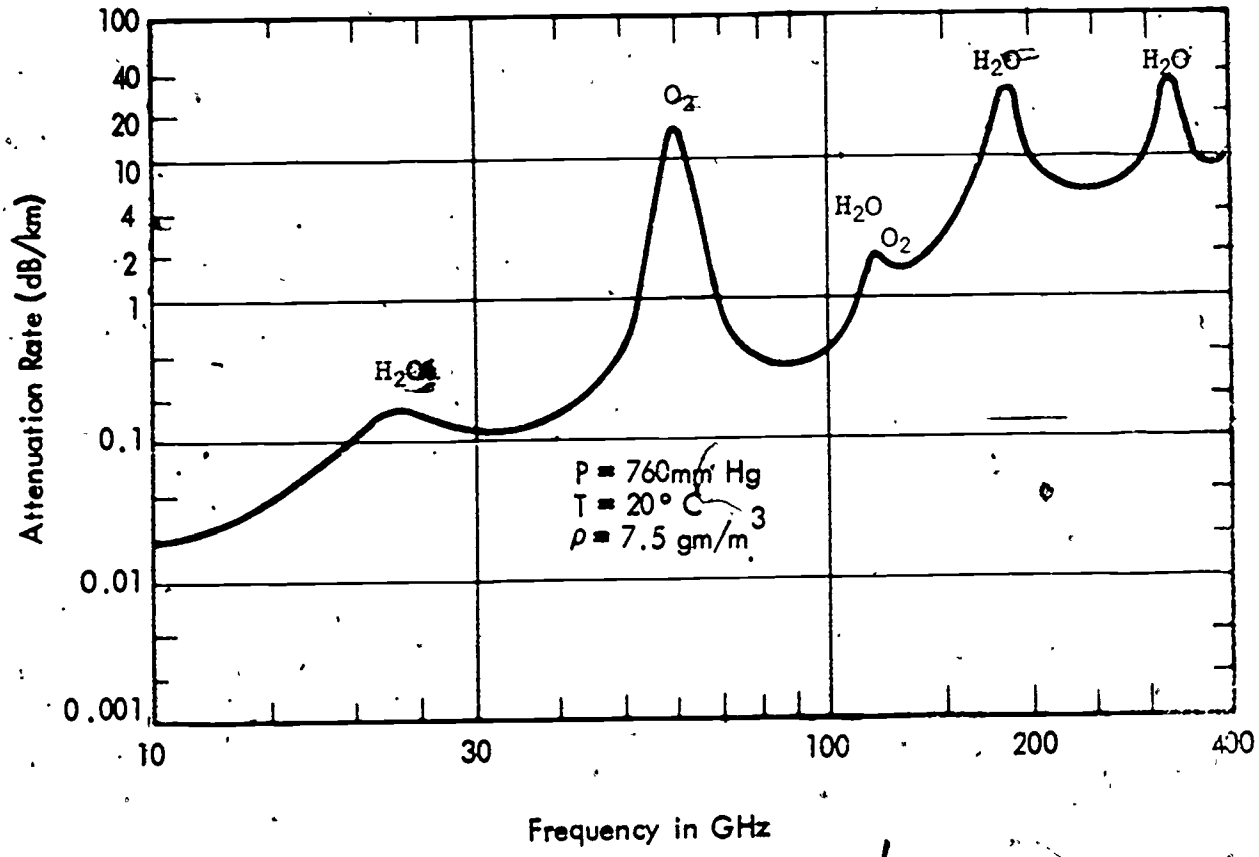

FIGURE 12-4: Atmospheric Attenuation Rate for the 10 to 400 GHZ Frequency Region from Rosenblum, 1961.

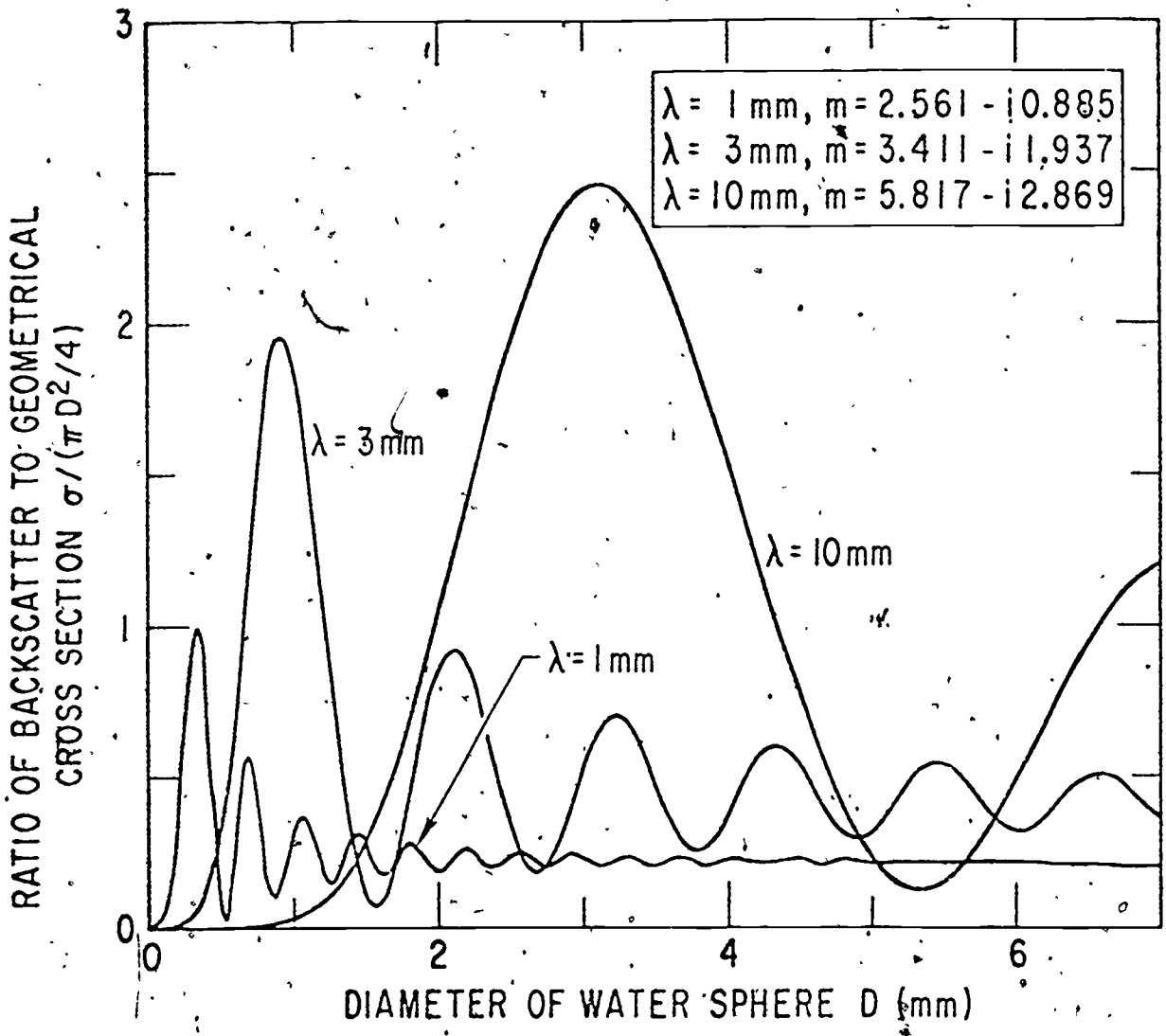

FIGURE 12-5: Backscatter cross section of water spheres from Mitchell, 1966.

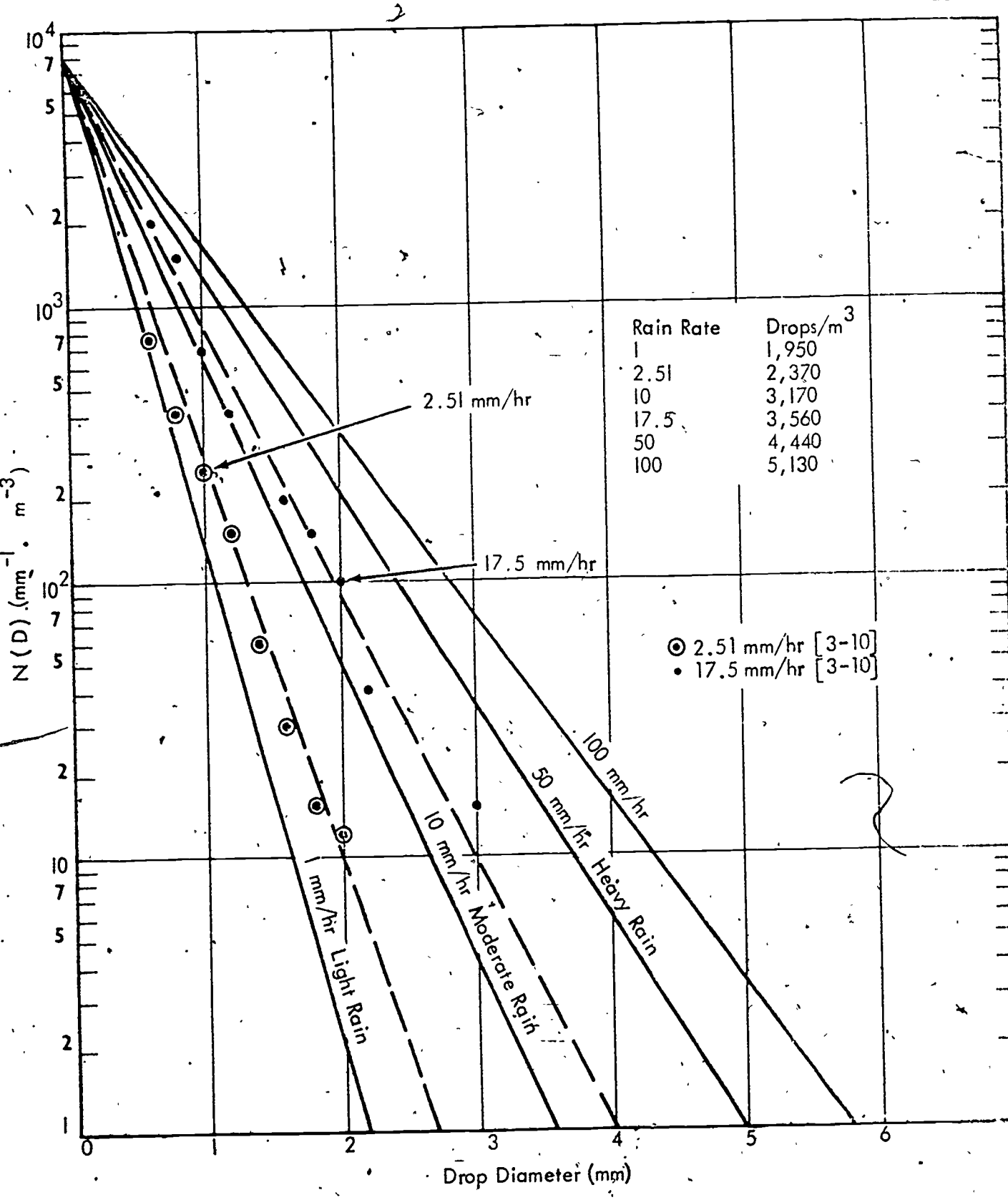

Figure 12-6 The Marshall - Palmer and Measured Drop Size Distributions for Several Rain Rates

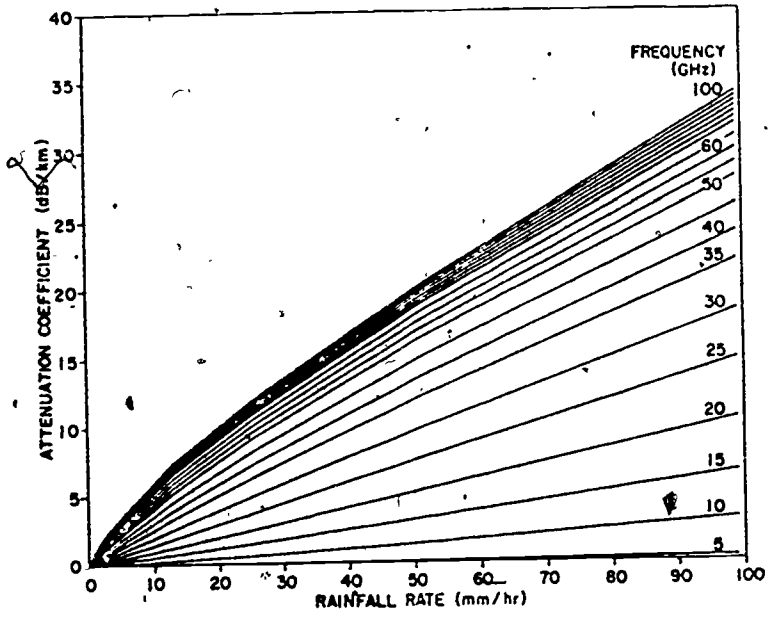

FIGURE 12-7: Calculated Attenuation Rates as a Function of Rain Rate from LeFande, 1968.

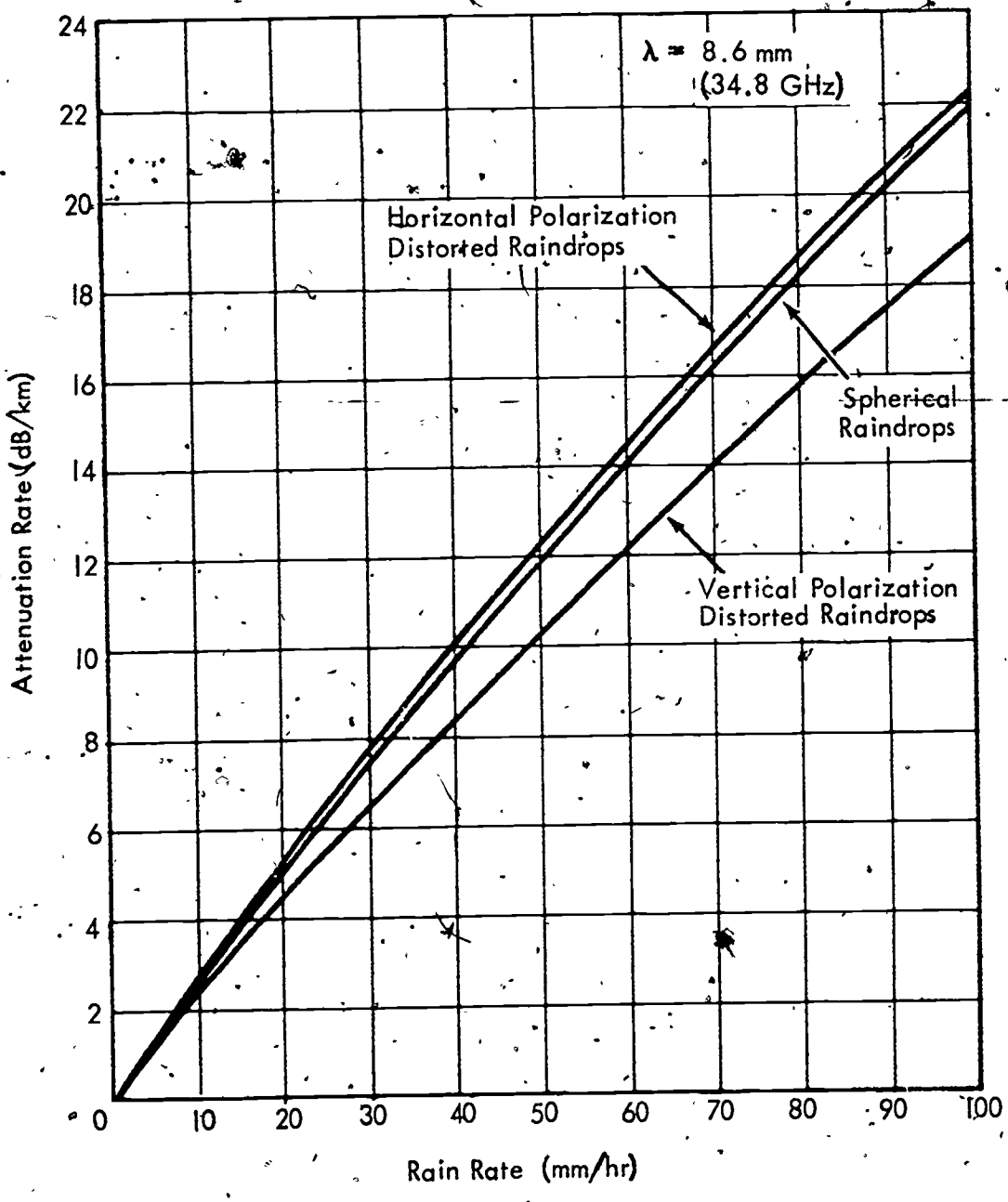

FIGURE 12-8: Attenuation Rates as a Function of Rain Rates from Oguchi, 1964.

13.0 LOW-FREQUENCY SYSTEMS (SURFACE)

By low-frequency, we mean frequencies from 100,000 Hz down to fractions of one Hertz. Surface systems are those systems which must be operated on the ground. They qualify as remote sensors because they are used primarily to detect subsurface objects or conditions. Low-frequency systems (surface) include:

(1) Four-terminal arrays.

(2) Induced polarization (IP).

(3) Wave-impedance (also known as intrinsic impedance, magneto-tellurics, and audio magnetotellurics).

(4) Wave-tilt.

(5) Loop coupling systems.

(6) Well logging.

This section will discuss in detail only the first three, since (4) is really a variation of (3), (5) is considered partially under airborne systems and (6) does not really qualify as a remote sensor.

13.1 FOUR-TERMINAL ARRAYS

Ground conductivity measurements have been made with four-terminal arrays since the turn of the century. Their important advantage is that the contact resistance of the probes does not enter into the calculation of the apparent conductivity of the ground.

General Case

Referring to Figure 13-1, a d. c. current source I produces a current density J at radius r when the current sink is located at infinity.

$$J_r = \frac{I}{\text{area of hemisphere}} = \frac{I}{2\pi r^2} \tag{13.1}$$

and since $$J_r = \frac{E_r}{\rho_a} = E_r \sigma_a \tag{13.2}$$

then $$E_r = \frac{I}{2\pi r^2 \sigma_a} \tag{13.3}$$

where ρ_a = apparent resistivity in ohm-meters.

σ_a = apparent conductivity in mhos/meter.

E_r = potential gradient at point P in volts/meter.

The potential distribution in the ground is:

$$V_r = \int_r^\infty E_r \, dr = \int_r^\infty \frac{I \, dr}{2\pi r^2 \sigma_a} = \frac{I}{2\pi r \sigma_a} \Big]_r^\infty \tag{13.4}$$

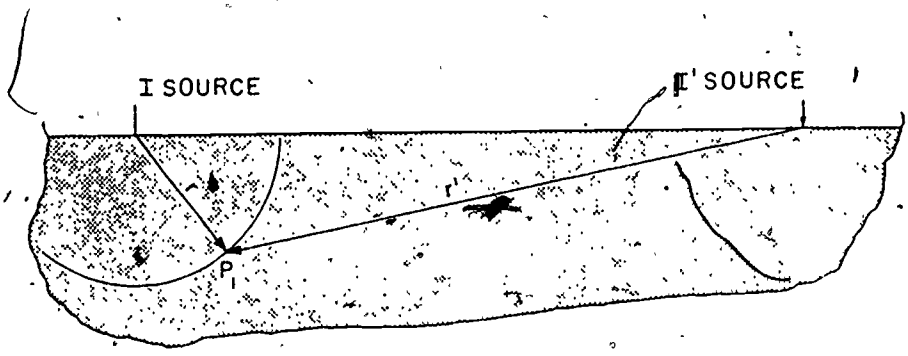

Figure 13-1. CURRENT SOURCES AND POTENTIAL

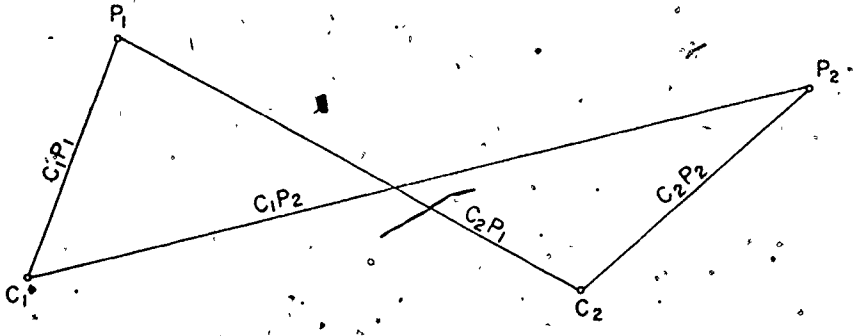

Figure 13-2. GENERAL FOUR-TERMINAL ARRAY

Then the potential at the surface of a hemisphere of radius r is:

$$V_r = \frac{I}{2\pi r \sigma_a} \qquad (13.5)$$

also at radius r' from current source I',

$$V_{r'} = \frac{-I'}{2\pi r' \sigma_a}$$

where $I = -I'$.

At any point P, the potential due to both current sources is

$$V_p = V_r + V_{r'} = \frac{I}{2\pi \sigma_a}\left(\frac{1}{r} - \frac{1}{r'}\right) \qquad (13.6)$$

Now consider the general four terminal case in Figure 13-2 C_1 and C_2 are current sources. P_1 and P_2 are potential measurement points.

Then
$$V_{(P_1P_2)} = V_{P_1} - V_{P_2}$$

$$= \frac{I}{2\pi \sigma_a}\left[\left(\frac{1}{C_1P_1} - \frac{1}{C_2P_1}\right) - \left(\frac{1}{C_1P_2} - \frac{1}{C_2P_2}\right)\right]$$

$$= \frac{I}{2\pi \sigma_a}\left[\frac{1}{C_1P_1} + \frac{1}{C_2P_2} - \frac{1}{C_1P_2} - \frac{1}{C_2P_1}\right] \qquad (13.7)$$

and then apparent conductivity,

$$\sigma_a = \frac{I}{2\pi V}\left[\frac{1}{C_1P_1} + \frac{1}{C_2P_2} - \frac{1}{C_1P_2} - \frac{1}{C_2P_1}\right] \qquad (13.8)$$

Where σ_a = apparent conductivity in mhos/meter.

I = current flowing between C_1 and C_2 in amperes.

V = voltage between P_1 and P_2 in volts.

C_1P_1 = distances between named points in meters.

C_2P_2 = distances between named points in meters.

C_1P_2 = distances between named points in meters.

C_2P_1 = distances between named points in meters.

This general case equation is valid for all arrays if direct current is used and the ground is homogeneous and isotropic. It can be simplified according to the geometry of each array. In Figure (13-3) some common arrays are shown, for which we give the simplified formulas below.

The Wenner Array.

$$\sigma_a = \frac{I}{2\pi a E} \text{ mhos/meter.} \qquad (13.9)$$

Average current to potential electrode spacing, $b = 1.5a$.

The Dipole Array.

$$\sigma_a = \frac{I}{\pi E}\left[\frac{a^2}{b(b^2 - a^2)}\right] \text{ mhos/meter} \qquad (13.10)$$

Where b = average spacing between dipoles.

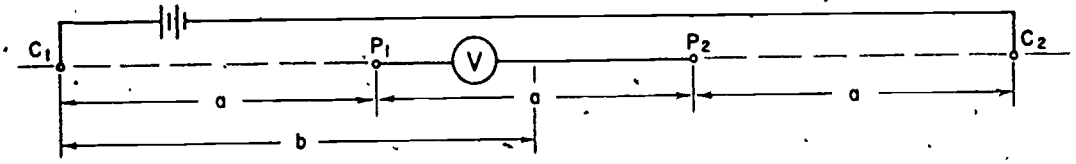

WENNER ARRAY

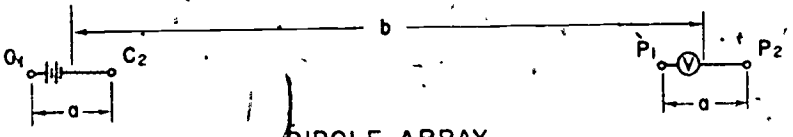

DIPOLE ARRAY

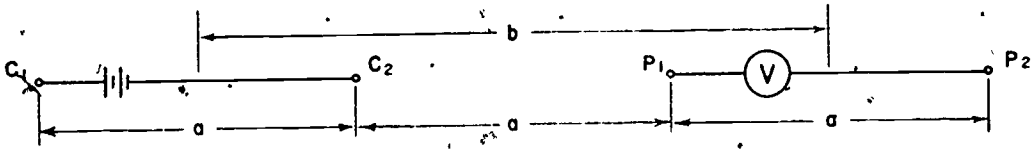

ELTRAN ARRAY

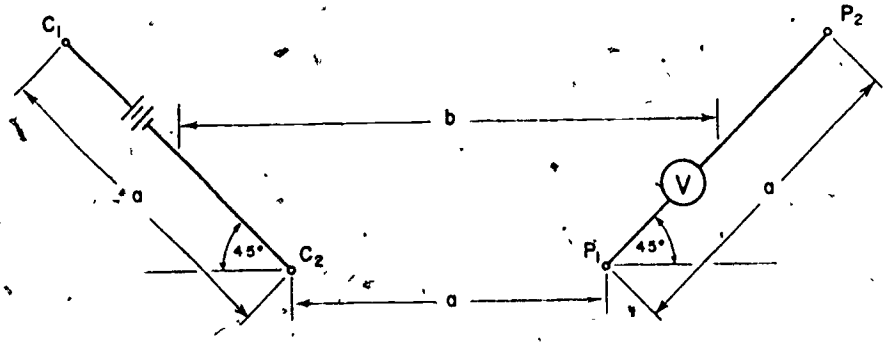

RIGHT ANGLE ARRAY

Figure 13-3 . COMMON FOUR-TERMINAL ARRAYS

If $b \geq 10a$, then

$$\sigma_a = - \frac{I a^2}{\pi E b^3} \text{ mhos/meter.} \qquad (13.11)$$

The negative sign indicates opposite polarity of E with respect to I.

The Eltran Array. (A Special Case of the Dipole Array).

$$\sigma_a = - \frac{I}{6\pi a E} \text{ mhos/meter} \qquad (13.12)$$

Average current to potential electrode spacing, $b = 2a$.

The Right Angle Array.

This array is used effectively for a. c. measurements because it eliminates inductive coupling between the wires.

$$\sigma_a = \frac{0.05284\, I}{a E} \text{ mhos/meter} \qquad (13.13)$$

The average current to potential electrode spacing, $b = 1.707a$.

It is possible to spread the array apart for deeper soundings without changing the probe distances. It then becomes a dipole array with its dipoles at right angles to each other.

The dimension "b" given for each array indicates the relative depth of sounding.

13.1:1 Two and Three Layer Interpretations

The data obtained by any of the methods described previously is plotted as σ_a (mhos/meter) versus b (meters). Since σ_a is the apparent conductivity of any number of layers, interpretive methods are used to arrive at the conductivity of each layer.

Universal Theoretical Curve Development

This derivation is fully developed by G. V. Keller, 1966.. We only propose to give its basic structure so that the reader may know the background of the theoretical curves mentioned below.

To determine the current distribution in a two layer earth model, we will use an analogy to the light distribution in a two medium optical model. Looking at the optical model, Figure 13-4, we see a point light source at A in a semi-infinite half-space of air overlaying a semi-infinite half-space of reflective transparent glass whose coefficient of reflection is K. At M_1 the light intensity is the sum of a ray directly from A and a ray reflected from the boundary which has an image source at A'. Then we can say that at

$$M_1 \text{ the light intensity} = \frac{S}{4\pi}\left[\frac{1}{(AM_1)^2} + \frac{K}{(A'M_1)^2}\right]$$

where S = source intensity and (AM_1) and $(A'M_1)$ are distances from the sources.

Now in the electrical model, Figure 13-4 also, we will establish a point current source at A in a medium of conductivity σ_1, overlaying a medium of conductivity σ_2. Following the optical analogy, the total current at M_1 is:

$$I_{(M_1)} = \frac{I}{4\pi}\left[\frac{1}{(AM_1)^2} + \frac{K_{12}}{(A'M_1)^2}\right] \qquad (13.14)$$

where

$$K_{12} = \frac{\sigma_1 - \sigma_2}{\sigma_1 + \sigma_2} \qquad (13.15)$$

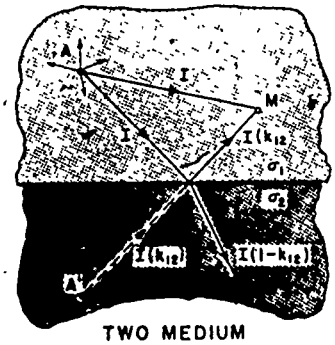

TWO MEDIUM
ELECTRICAL MODEL

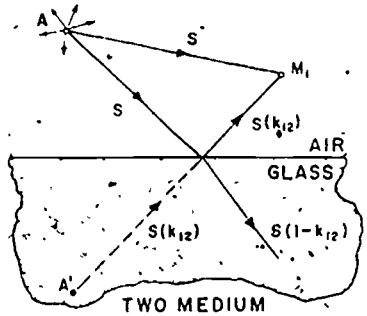

TWO MEDIUM
OPTICAL MODEL

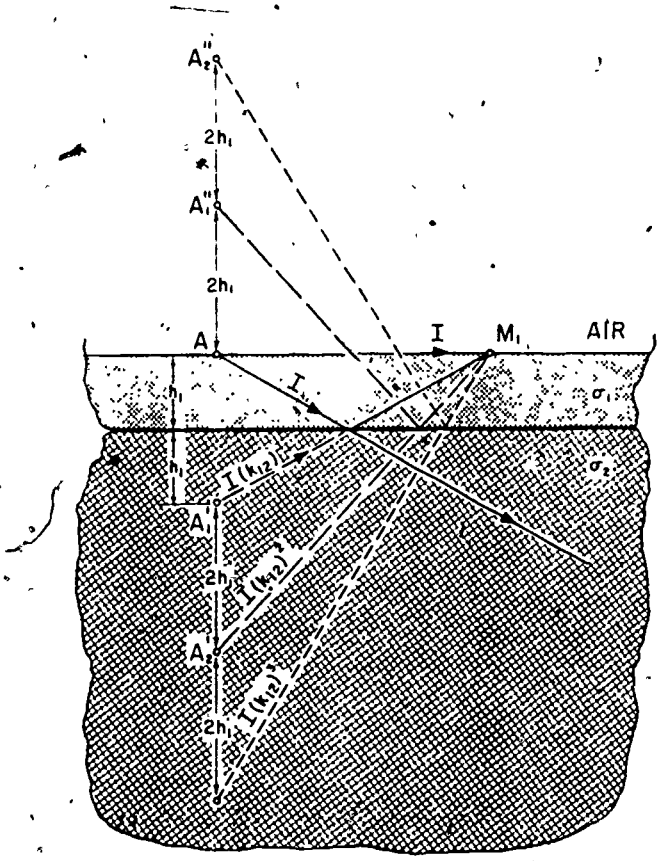

THREE MEDIUM
ELECTRICAL MODEL

Figure 13-4 OPTICAL AND ELECTRICAL MODELS

Two conditions that must be met are (1) the potential function must be continuous across the boundary between the media, and (2) the normal component of current flow across the boundary must be continuous.

For the three layer electrical model shown in Figure 13-4, the first medium will be air, the next two will be mediums of conductivities σ_1 and σ_2. The current source is on the first boundary as is the observation point. As before, there is current at M_1 direct from A and reflected current from image source A'_1 of a magnitude $I K_{12}$. In this case, since A is on the first boundary, in order to satisfy the boundary conditions, we must put an image source at A''_1. This necessitates another image source below the boundary at A'_2 and so on, an infinite number of times; each current being diminished by the factor K_{12}. Then the current observed at M_1 is the sum of all the currents from sources A to A'_∞.

It is from this model that Keller derives an expression for apparent conductivity in terms of first layer conductivity. For the polar dipole array this expression is

$$\sigma_a = \sigma_1 \left\{ 1 - \sum_{n=1}^{\infty} \frac{(K_{12})^n}{\left[1 + \left(\frac{2n\,h_1}{b}\right)^2\right]^{3/2}} + 3 \sum_{n=1}^{\infty} \frac{(K_{12})^n}{\left[1 + \left(\frac{2n\,h_1}{b}\right)^2\right]^{5/2}} \right\}^{-1} \qquad (13.16)$$

This may be expressed as a dimensionless ratio of σ_a/σ_1 in terms of a dimensionless ratio, b/h_1, or

$$\frac{\sigma_a}{\sigma_1} = \left\{ 1 - \sum_{n=1}^{\infty} (K_{12})^n \left[1 + \left(\frac{2n}{b/h_1} \right)^2 \right]^{-3/2} + 3 \sum_{n=1}^{\infty} (K_{12})^n \left[1 + \left(\frac{2n}{b/h_1} \right)^2 \right]^{-5/2} \right\}^{-1}$$

(13:17)

where:

σ_a = apparent conductivity measured at the surface of the earth in mhos/meter.

σ_1 = conductivity of the first layer in mhos/meter.

K_{12} = reflection coefficient at the interface between layers 1 and 2, defined by $\frac{\sigma_1 - \sigma_2}{\sigma_1 + \sigma_2}$.

n = 1, 2, 3, 4, ... ∞ = number of image sources of current.

h_1 = thickness of the first layer in meters.

b = average electrode spacing.

From this equation a family of curves may be plotted which will be used in curve matching to arrive at the conductivity and thickness of each layer in a two layer earth. Such a family of curves for a polar dipole array is shown in Figure 13-6. Other formulas for different arrays have been developed but are not included here.

Curve Matching

The purpose of field surveys is to determine the apparent conductivity of the earth to various depths, to determine the average conductivity of the layers, and to determine the thickness of the layers.

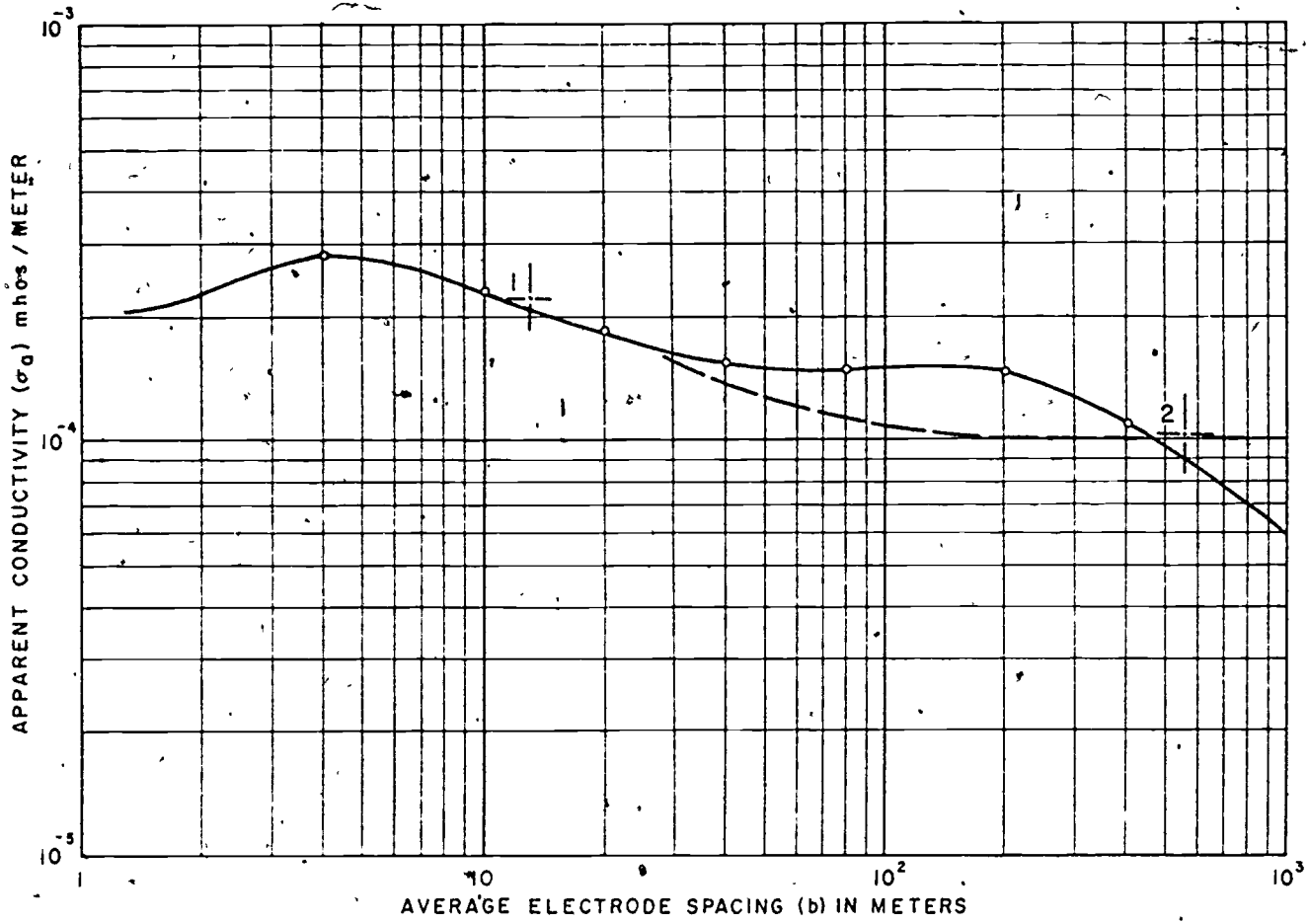

Figure 13-5 APPARENT CONDUCTIVITY vs SPACING

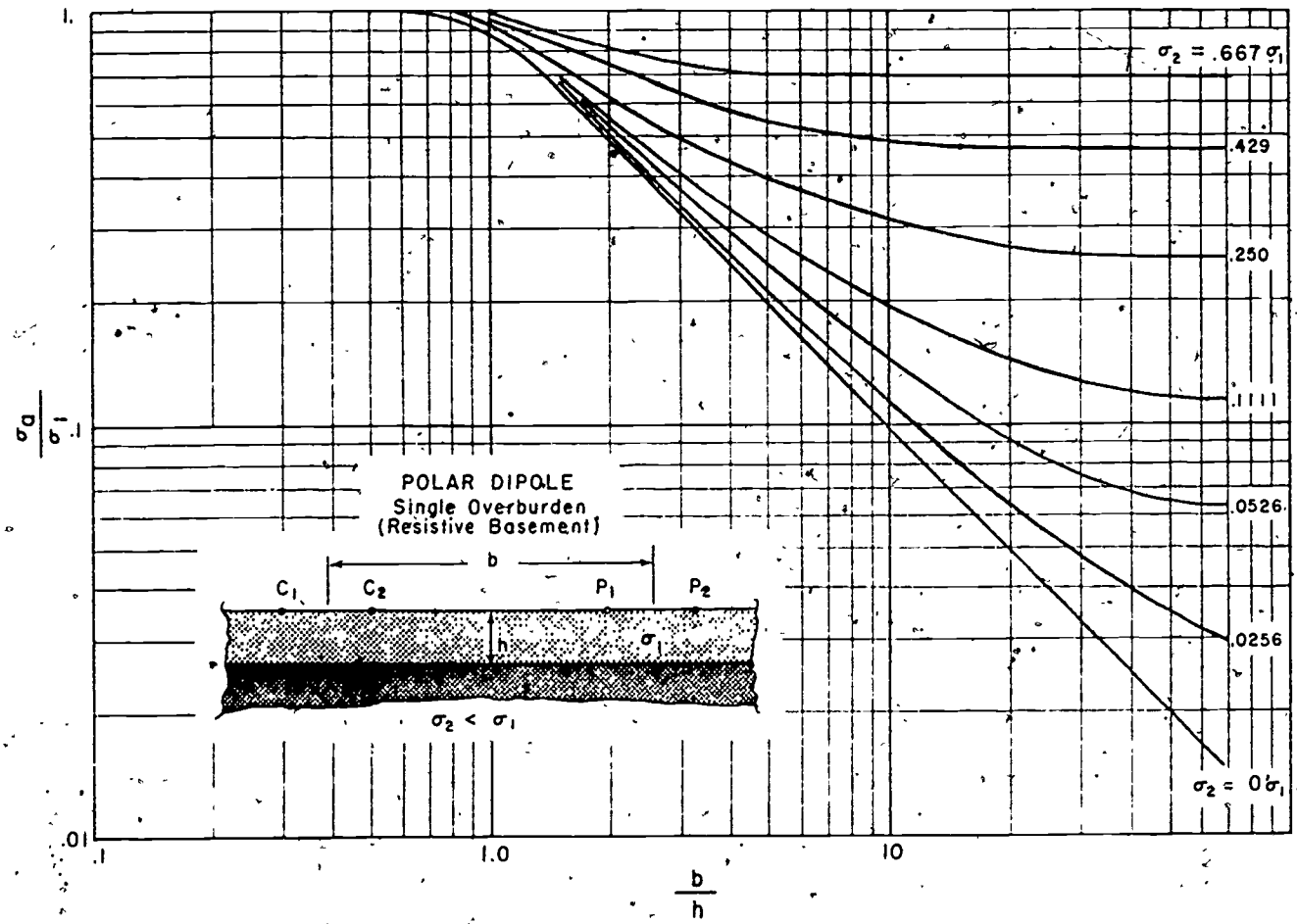

Figure 13-6 THEORETICAL TWO LAYER CURVES

From reduced field data we have apparent conductivities, σ_a for corresponding electrode spacings (b). The coordinates of any point on the theoretical curves are b/h_1 and σ_a/σ_1. The field data is also plotted as functions of σ_a/σ_1 and b/h_1, with σ_1 and h_1 given values of 1. The technique of curve matching to determine the actual values of σ_1 and h_1 will now be demonstrated.

Figure 13-5 is a fictitious field curve which from inspection must be for a three layer earth because of its three inflection points. It is assumed the data was taken with a dipole array. Since the dipole theoretical curves in Figure 13-6 are for a two layer earth, we will attempt to match only that portion of the field curve preceding the third inflection point to a curve in Figure 13-6. The field and theoretical curves must, of course, be plotted on identical paper.

Figure 13-5 is placed on top of Figure 13-6 and positioned for a best match of curves with the axes of the two figures parallel. Now a cross is marked on the field curve (see cross #1 on Figure 13-5) at the point overlaying the (1, 1) coordinate of the theoretical curve. The location of this point on the field curve must also be the point where the ratios b/h_1 and σ_a/σ_1 equal 1 for the field data. Reading the values from Figure 13-5 for the location of cross #1, we have $b = h_1 = 13$ meters and $\sigma_a = \sigma_1 = 2.2 \times 10^{-4}$ mhos per meter.

We can also determine the conductivity of the second layer (σ_2) since the theoretical curves are families of curves with the ratio σ_2/σ_1 as a parameter. From our curve matching above, we see that the field curve corresponds to a theoretical curve for $\sigma_2/\sigma_1 = 0.429$. Therefore, $\sigma_2 = 0.429\,\sigma_1 = 0.94 \times 10^{-4}$ mhos per meter.

To find h_2, the thickness of the second layer and σ_3, the conductivity of the third layer, we must extend our theoretical development. One obvious method would be to construct theoretical curves for three layer earths. But to do this for all possible conductivity and layer thickness ratios would involve a prodigious amount of work even with computers. An alternate, simpler solution is given here. If we replace the first two layers with an equivalent fictitious layer, we then have reduced a three layer problem to a two layer problem which we can solve as above. This is basically what we do. The defining equations for fictitious conductivity, σ_f and fictitious depth, h_f, are

$$\sigma_f = \frac{\sigma_1 h_1 + \sigma_2 h_2}{h_f} \tag{13.18}$$

and

$$h_f = h_1 + h_2 \tag{13.19}$$

Figure 13-7 is a family of curves of σ_f/σ_1 plotted as a function of h_f/h_1 with σ_2/σ_1 and h_2/h_1 as parameters. This "A" curve is used if $\sigma_1 > \sigma_2 > \sigma_3$. Three other families may be calculated for $\sigma_1 < \sigma_2 < \sigma_3$, $\sigma_1 > \sigma_2 < \sigma_3$ and $\sigma_1 < \sigma_2 > \sigma_3$. We may now complete the interpretation of the fictitious field curve in Figure 13-5.

The field curve is placed over the A curves with cross #1 directly over the (1, 1) coordinate of the A curves. Then a line is traced on the field curve from the curve on the A set which has the same conductivity ratio σ_2/σ_1 as was determined by the previous two layer interpretation. This is the dashed line on Figure 13-5. We may now match the portion of the curve beyond the third inflection point to an appropriate two layer theoretical curve with the one additional requirement that the cross (cross #2 on Figure 13-5) must fall on the dashed line. The coordinates of cross

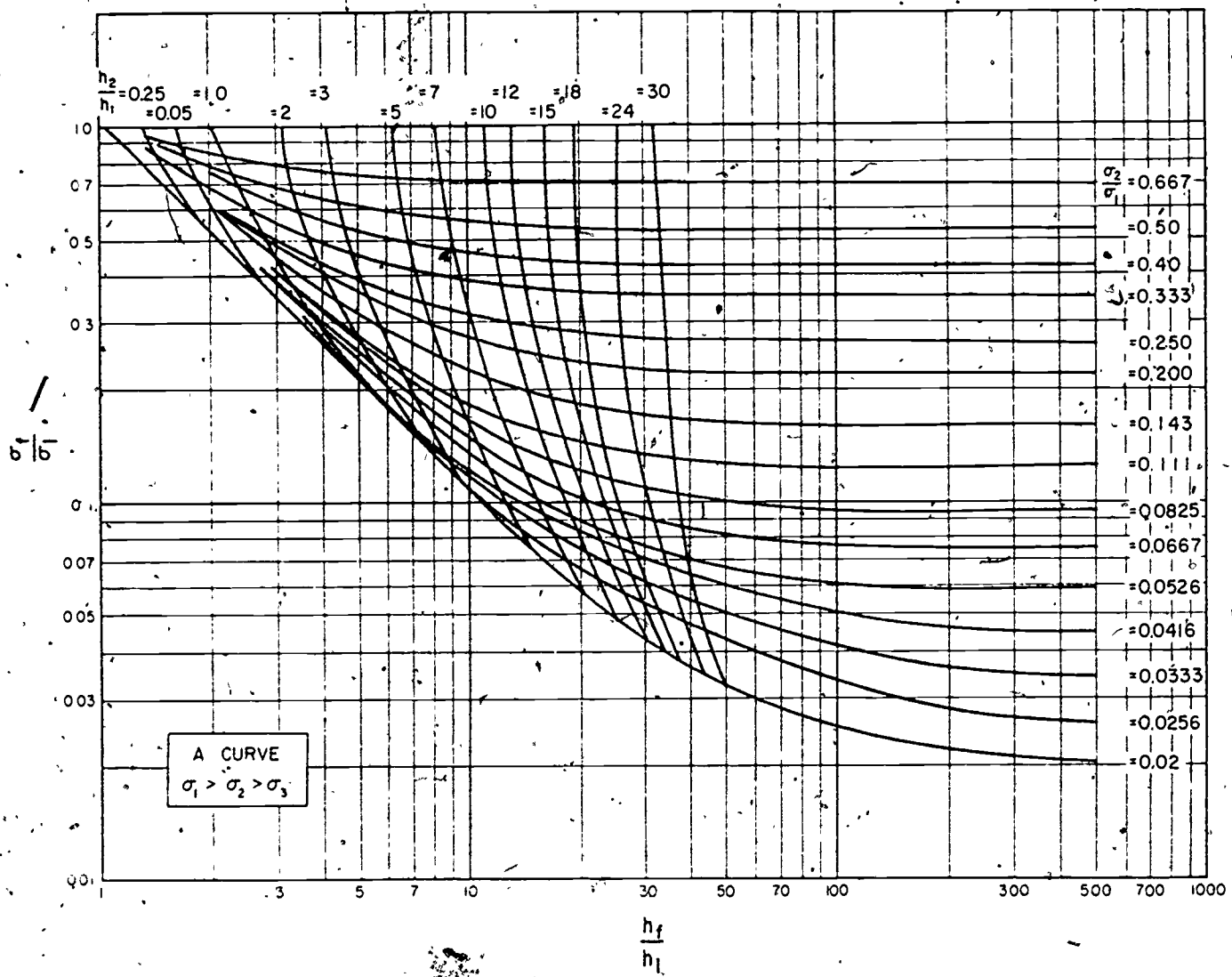

Figure 13-7 THREE LAYER INTERPRETATION CURVE

#2 on the field curve give us the values of σ_f and h_f. From Figure 13.5, $\sigma_f = 1 \times 10^{-4}$ mhos/meter and $h_f = 550$ meters. Now from equation (13.19) we may calculate h_2. Thus $h_2 = h_f - h_1 = 550$ m - 13 m = 537 meters. Since we had reduced the three layers to a two layer problem composed of a fictitious layer and the actual 3rd layer, the conductivity ratio obtained in the second two layer interpretation can be used to calculate σ_3. Thus

$$\sigma_3 = \sigma_f \times \text{conductivity ratio}$$

There is such a small portion of field curve beyond the third inflection point that we can only say that probably $\sigma_3 < 5.6 \times 10^{-6}$ mhos/meter for this sample problem. If additional data were obtained at larger electrode spacings, we could obtain a more accurate value for σ_3.

It must be stressed that to use the curves given here we are assuming horizontal layers composed of homogeneous, isotropic material. For conditions other than these considerable error would result. Furthermore, the theory used here is strictly valid only for DC current. The results are good, however, as long as $\sigma >> \omega\varepsilon$ and dipole dimension b is small compared to a skin depth (δ) at the frequencies used.

13.1.2 Experimental Results

Apparent Conductivity as a Function of Geology and Depth

The interpretation of data obtained at Boulder, Colorado is given on Figure 13-8. This is in general agreement with results from wells drilled in this area which show a layer of soil as thin as 3 feet with sandstone extending from that depth down to 386 feet, the depth of the deepest well in the immediate area. The high conductivity of the third layer could be caused by a general water table at a 70 meter depth. It is well known, of course, that high conductivity in non-metallic bearing rocks is largely due to their water content. The effect of water saturation is clearly shown in Figure 14-9-A, B, and C which are profile plots of conductivity. This type of data is obtained by maintaining a fixed electrode spacing while moving across an area of interest. Such procedures are extensively used in exploration and prospecting.

Ordinarily it is extremely difficult, if not impossible, to interpret results from a four layer case. We were very fortunate to be able to make an interpretation of data obtained at Pole Mountain, Wyoming. After making a two layer interpretation for the curve out to an electrode spacing of 400 meters, it was noted that the apparent conductivity had approached the actual conductivity of the second layer. This allowed us to interpret the remaining portion of the curve as a separate three layer problem, since we could assume the first layer had negligible effect on apparent conductivity for spacings greater than 400 meters.

The data presented thus far was all obtained at 20 Hz. Measurements were made, however, up to 16,000 Hz. and as long as the electrode spacings were short compared to a skin depth in the earth, the results showed no variation in conductivity with frequency. This supports the original assumption that $\sigma >> \omega\varepsilon$.

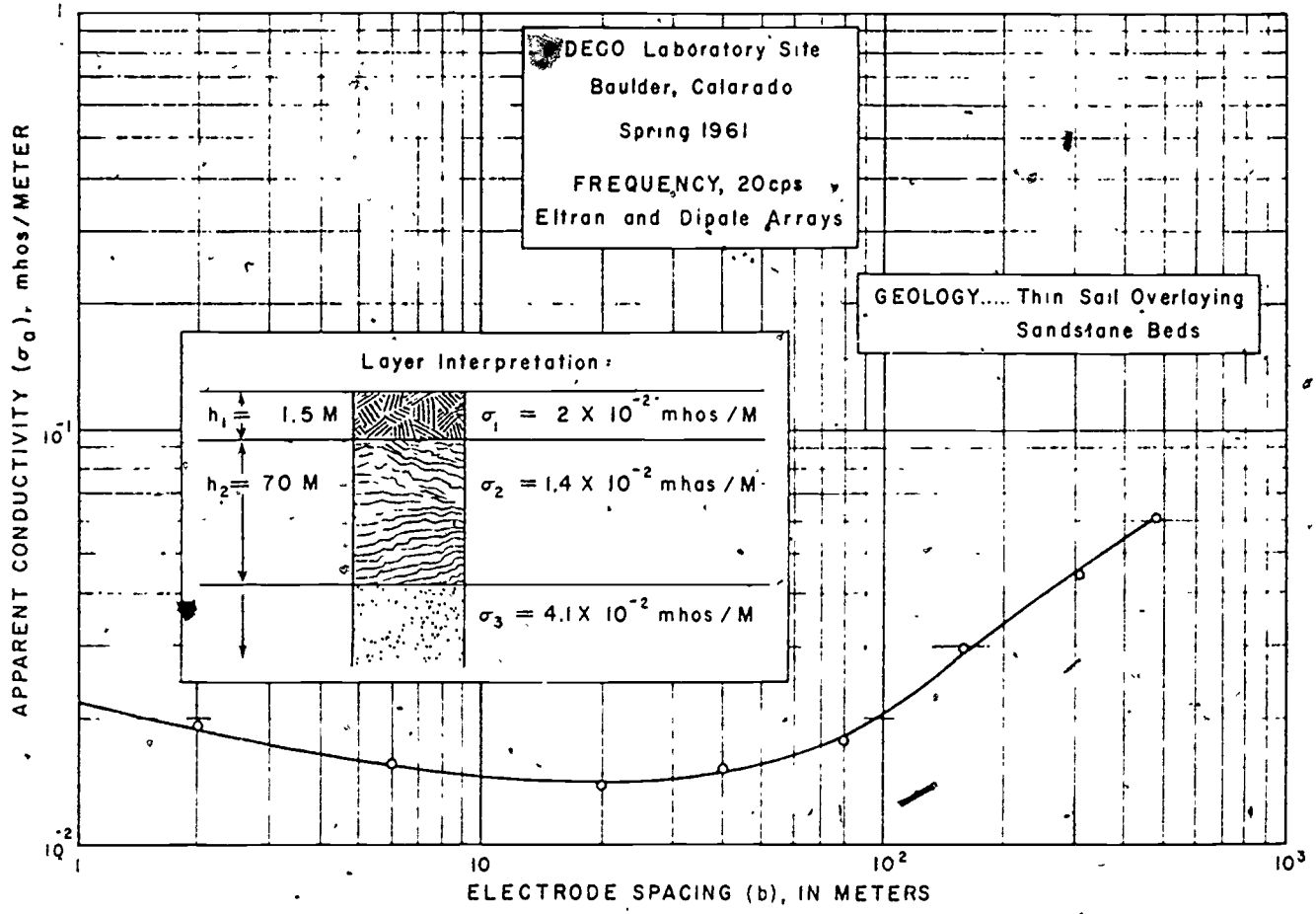

Figure 13-8 APPARENT CONDUCTIVITY vs ELECTRODE SPACING

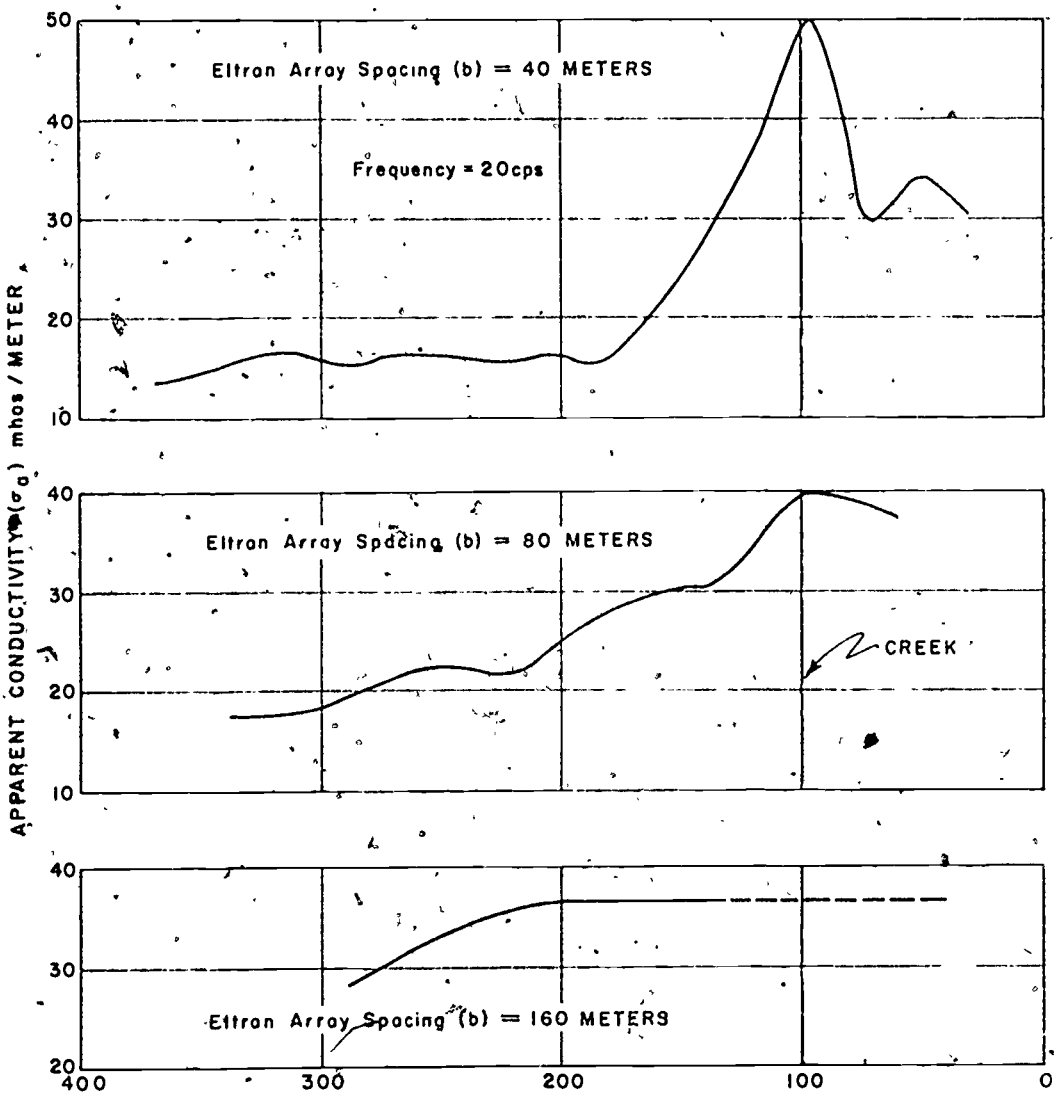

FIGURE 13-9. APPARENT CONDUCTIVITY PROFILES AT BOULDER, COLORADO SITE

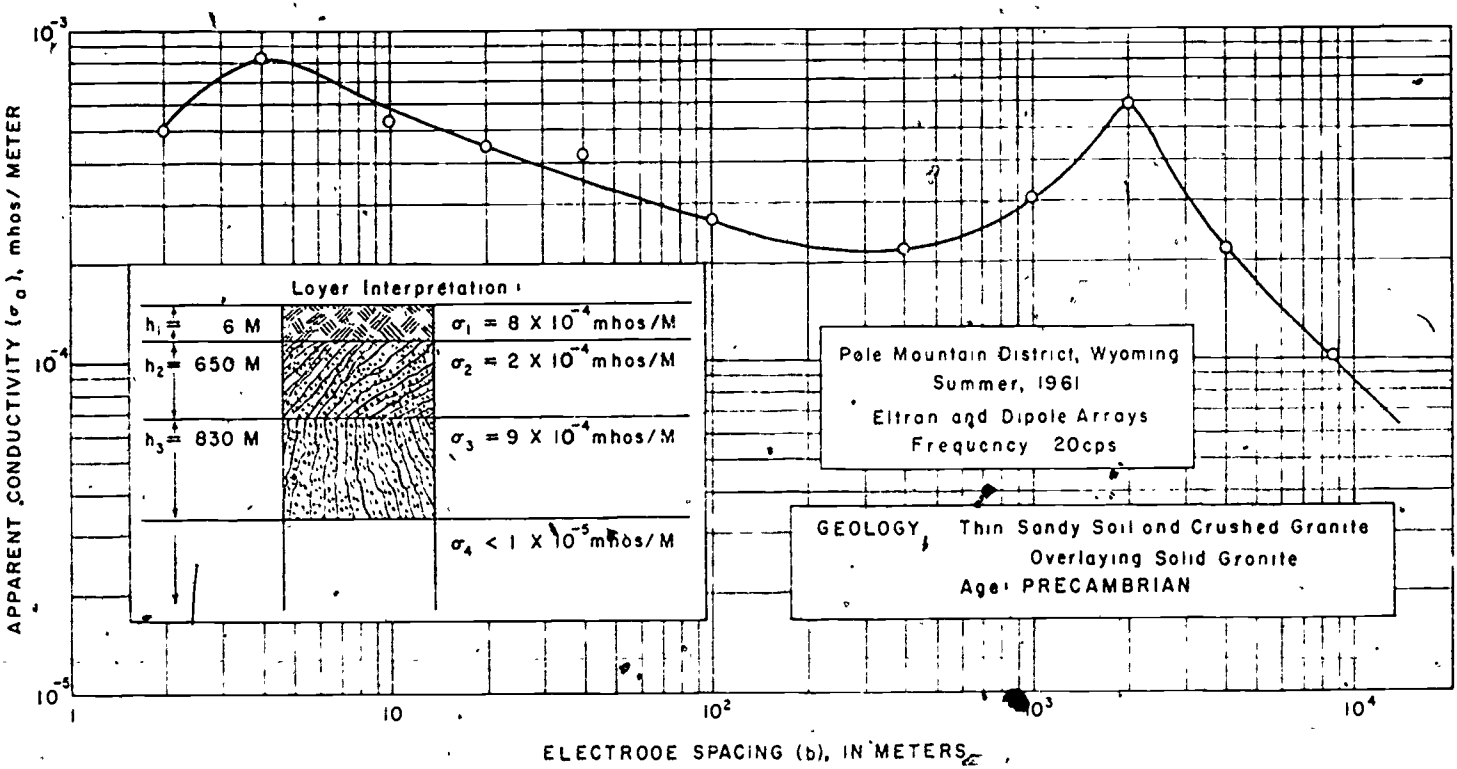

Figure 13-10 APPARENT CONDUCTIVITY vs ELECTRODE SPACING

13.2 WAVE-IMPEDANCE MEASUREMENTS

In Section 3.2.5, we established the equation for intrinsic impedance in a good conductor as,

$$\frac{E}{H} = \sqrt{\frac{j\omega\mu}{\sigma}} \tag{13.20}$$

which can be solved for apparent conductivity

$$\sigma_a' = (8\pi^2 \times 10^{-7})\, f\, \frac{H^2}{E^2} \tag{13.21}$$

where σ_a' is apparent conductivity as observed from measurement of horizontal E and H fields to distinguish it from σ_a (apparent conductivity observed from four-terminal array measurement). Now by measuring horizontal components of the fields at the earth's surface, E_h and H_h, at different frequencies, we may obtain a plot of σ_a' versus frequency. This does not, however, indicate a variation of the conductivity of the material with frequency. This is a variation of conductivity as seen by electromagnetic waves incident on the surface. That is, the lower the frequency of the wave, the greater is the depth of penetration; therefore, if the real conductivity σ_r changes with depth, the apparent conductivity will change with frequency. Needless to say, if σ_r were a function of both frequency and depth it would be impossible to interpret the curves unless one of the functions were known.

Assuming σ_r is not a function of f, then a plot of apparent conductivity versus frequency may be interpreted by using Cagniard, 1953, Universal curves to determine σ_r and thickness, h, for 2 or 3 layer problems.

To obtain accurate interpretations of field curves, it is necessary to obtain data over 2 or 3 frequency decades. Since useful data presented here was obtained over only a little more than 1 decade, no interpretation will be attempted. We can, however, compare field measurements with a predicted

σ_a' vs. f curve based on the layer conductivities and depths as obtained from four-terminal array measurements.

To obtain a predicted or calculated σ_a' from a given layered earth, we proceed as follows. Figure 13-11 shows a plane electromagnetic field propagating downward into a single layered semi-infinite earth. The solution to Maxwell's field equations if we assume $\sigma_1 \gg \omega\epsilon_1$ and $\mu_1 = \mu_0$ are,

$$E_{X_1}(\omega, Z) = E^+_{X_1}(\omega, 0)e^{-\gamma_1 Z} + E^-_{X_1}(\omega, 0)e^{\gamma_1 Z} \qquad (13.22)$$

and

$$H_{Y_1}(\omega, Z) = H^+_{Y_1}(\omega, 0)e^{-\gamma_1 Z} + H^-_{Y_1}(\omega, 0)e^{\gamma_1 Z} \qquad (13.23)$$

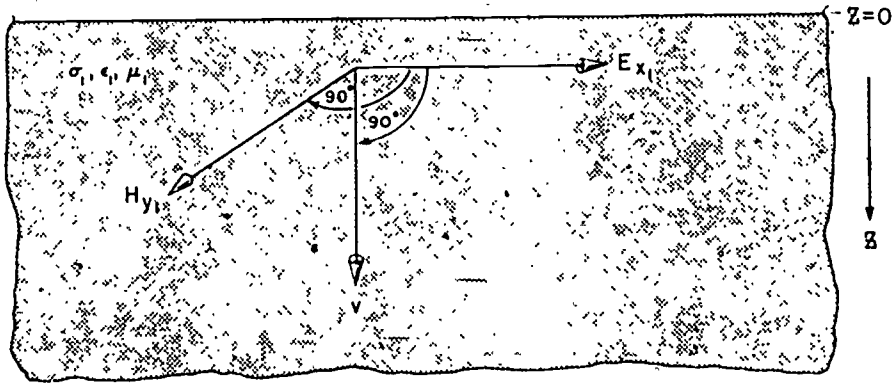

A. SINGLE LAYER OF SEMI-INFINITE EARTH

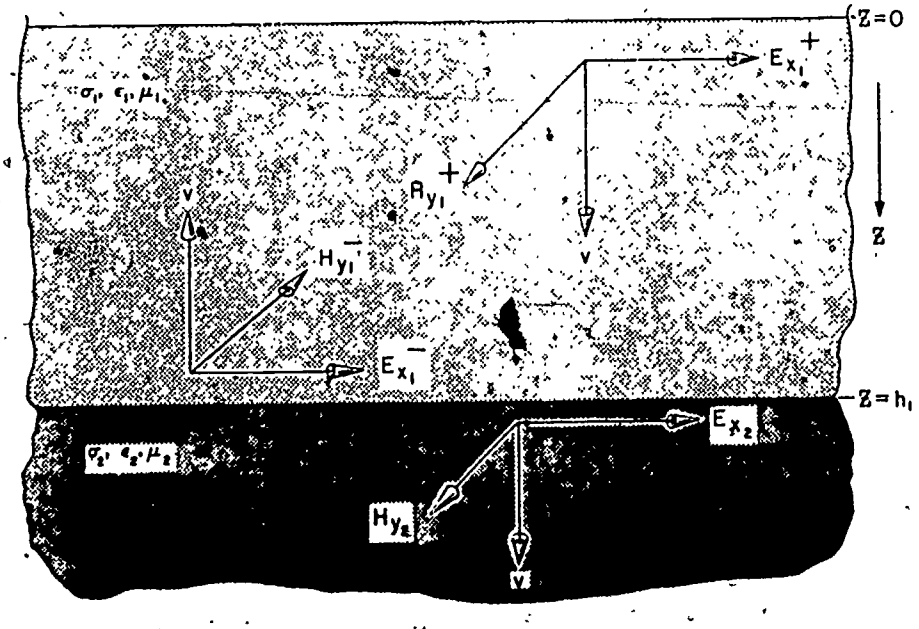

B. TWO LAYERED EARTH, SECOND LAYER SEMI-INFINITE

Figure 13-11 PLANE ELECTROMAGNETIC FIELD IN THE EARTH FROM A SOURCE ABOVE THE EARTH

where $E^{+}_{X_1}(\omega, 0)$ and $H^{+}_{Y_1}(\omega, 0)$ are the transmitted (downward propagating) electric and magnetic fields at $Z = 0$ and $E^{-}_{X_1}(\omega, 0)$ and $H^{-}_{Y_1}(\omega, 0)$ are the reflected electric and magnetic fields at $Z = 0$. For a semi-infinite earth of finite conductivity, however, $E^{-}_{X_1}(\omega, 0)$ and $H^{-}_{Y_1}(\omega, 0)$ are equal to zero and we may write

$$E_{X_1}(\omega, Z) = E^{+}_{X_1}(\omega, 0)e^{-\gamma_1 Z} \tag{13.24}$$

and

$$H_{Y_1}(\omega, Z) = H^{+}_{Y_1}(\omega, 0)e^{-\gamma_1 Z} \tag{13.25}$$

Then at $Z = 0$, we have

$$E_{X_1}(\omega, 0) = E^{+}_{X_1}(\omega, 0) \tag{13.26}$$

and

$$H_{Y_1}(\omega, 0) = H^{+}_{Y_1}(\omega, 0) \tag{13.27}$$

Then by definition the intrinsic impedance, η_1, is

$$\eta_1 = \frac{E_{X_1}(\omega, Z)}{H_{Y_1}(\omega, Z)} \tag{13.28}$$

and for the conditions given above

$$\eta_1 = \left[\frac{j\omega\mu_0}{\sigma_1}\right]^{1/2} \tag{13.29}$$

The apparent impedance as seen from the surface is

$$\eta_a = \frac{E_{X_1}(\omega, 0)}{H_{Y_1}(\omega, 0)}$$

$$= \frac{E^+_{X_1}(\omega, 0)}{H^+_{Y_1}(\omega, 0)}$$

$$= \eta_1$$

and from (13.29) it is obvious that,

$$\sigma'_a = \sigma_1 \tag{13.30}$$

for a single layered semi-infinite earth.

For a two layered earth with the second layer semi-infinite, as shown in Figure 13-11B, we may write

$$E_{X_1}(\omega, Z) = E^+_{X_1}(\omega, 0)e^{-\gamma_1 Z} + E^-_{X_1}(\omega, 0)e^{\gamma_1 Z} \tag{13.31}$$

and

$$H_{Y_1}(\omega, Z) = H^+_{Y_1}(\omega, 0)e^{-\gamma_1 Z} + H^-_{Y_1}(\omega, 0)e^{\gamma_1 Z} \tag{13.32}$$

where $E^-_{X_1}(\omega, 0)$ and $H^-_{Y_1}(\omega, 0)$ are now finite and may be expressed as

$$E^{-}_{X_1}(\omega, 0) = E^{+}_{X_1}(\omega, 0)e^{-2\gamma_1 h_1}\frac{\eta_2 - \eta_1}{\eta_2 + \eta_1} \qquad (13.33)$$

and

$$H^{-}_{Y_1}(\omega, 0) = H^{+}_{Y_1}(\omega, 0)e^{-2\gamma_1 h_1}\frac{\eta_1 - \eta_2}{\eta_2 + \eta_1} \qquad (13.34)$$

where $\frac{\eta_2 - \eta_1}{\eta_2 + \eta_1}$ and $\frac{\eta_1 - \eta_2}{\eta_2 + \eta_1}$ are the reflection coefficients.

Substituting (13.33) and (13.34) into (13.31) and (13.32), we get

$$E_{X_1}(\omega, Z) = E^{+}_{X_1}(\omega, 0)\left[e^{-\gamma_1 Z} + e^{\gamma_1(Z - 2h_1)}\frac{\eta_2 - \eta_1}{\eta_2 + \eta_1}\right] \qquad (13.35)$$

and

$$H_{Y_1}(\omega, Z) = H^{+}_{Y_1}(\omega, 0)\left[e^{-\gamma_1 Z} + e^{\gamma_1(Z - 2h_1)}\frac{\eta_1 - \eta_2}{\eta_2 + \eta_1}\right] \qquad (13.36)$$

Then at $Z = 0$, we get

$$E_{X_1}(\omega, 0) = E^{+}_{X_1}(\omega, 0)\left[1 + R e^{-2\gamma_1 h_1}\right] \qquad (13.37)$$

and

$$H_{Y_1}(\omega, 0) = H^{+}_{Y_1}(\omega, 0)\left[1 - R\, e^{-2\gamma_1 h_1}\right] \tag{13.38}$$

where

$$R = \frac{\eta_2 - \eta_1}{\eta_2 + \eta_1}$$

$$= \frac{\sqrt{\sigma_1} - \sqrt{\sigma_2}}{\sqrt{\sigma_1} + \sqrt{\sigma_2}} \tag{13.39}$$

We can now solve for the apparent intrinsic impedance as

$$\eta_a = \frac{E_{X_1}(\omega, 0)}{H_{Y_1}(\omega, 0)} = \frac{E^{+}_{X_1}(\omega, 0)}{H^{+}_{Y_1}(\omega, 0)}\left[\frac{1 + R\, e^{-2\gamma_1 h_1}}{1 - R\, e^{-2\gamma_1 h_1}}\right] \tag{13.40}$$

$$= \eta_1\left[\frac{1 + R\, e^{-2\gamma_1 h_1}}{1 - R\, e^{-2\gamma_1 h_1}}\right] \tag{13.41}$$

Equation (13.41) may be solved for σ'_a which gives

$$\sigma'_a(\omega) = \sigma_1\left[\frac{1 - R\, e^{-2\gamma_1 h_1}}{1 + R\, e^{-2\gamma_1 h_1}}\right]^2 \tag{13.42}$$

Now let

$$\gamma_1 = \sqrt{j\omega\mu_0\sigma_1}$$

$$= \sqrt{\frac{\omega\mu_0\sigma_1}{2}} + j\sqrt{\frac{\omega\mu_0\sigma_1}{2}}$$

and

$$K_1 = \sqrt{2\omega\mu_0\sigma_1}\ h_1$$

Then we may write

$$\sigma'_a(\omega) = \sigma_1\left[\frac{1 - 2R\,e^{-K}\cos K + R^2 e^{-2K}\cos 2K}{1 + 2R\,e^{-K}\cos K + R^2 e^{-2K}\cos 2K}\right] \qquad (13.43)$$

With this formula we may calculate σ'_a as a function of frequency for any two layered earth.

Figure 13-12 shows field data obtained by measuring the horizontal components of E and H at the DECO Site near Boulder, Colorado along with a calculated curve of σ'_a vs. f for the two layered earth determined from four-terminal array measurements. Obviously the two methods did not yield identical results although the general shape of the curves are the same. The displacement of the curves could conceivably be caused by anisotropies in the earth which would affect the two methods differently. This is evident when one considers that the conductivity as measured by four-terminal arrays is $\sigma = \sqrt{\sigma_V \sigma_H}$ where σ_V is the conductivity in a vertical plane and σ_H is the apparent conductivity in a horizontal plane. Whereas only the conductivity in a horizontal plane σ_H will affect the attenuation of a downward propagating wave.

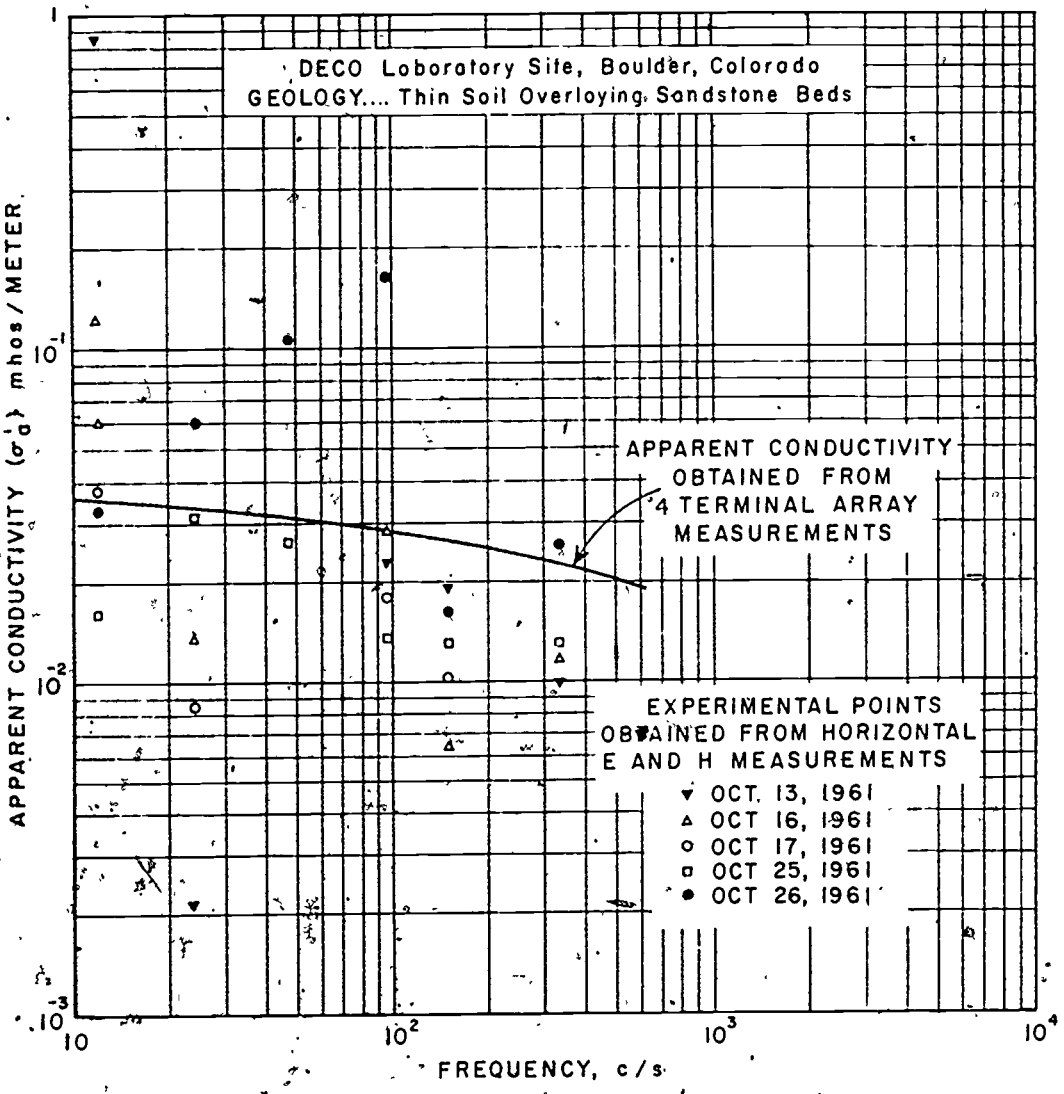

Figure 13-12 APPARENT CONDUCTIVITY vs FREQUENCY

13.3 INDUCED POLARIZATION (IP)

In the methods previously described for measuring the electrical properties of the earth, it has been assumed that these properties did not change with frequency. For most earthen materials, this assumption is essentially correct. It has been discovered however, that certain rock types, in particular sulfide ore minerals, exhibit a marked change in electrical properties with frequency. This effect takes place at frequencies from 0.1 Hertz to 100 Hertz. The detection of this change in electrical properties with frequency presented itself as an obvious technique for exploration for sulfide minerals. The primary method for accomplishing these measurements is known by the name of induced polarization or over-voltage measurements. This method has been discussed in detail by Wait, 1959.

For the induced polarization method, variations in the electrical properties are studied. These variations cannot be explained in terms of the atomic or molecular characteristics of the material, but appear to be pinned on the overall structure and crystaline makeup of the rock. The term induced polarization, of course, refers to the polarization of the materials induced by an electric field or an electric current. The polarization processes important to this effect at these frequencies are the inter-facial and electrochemical processes referred to in Section 5. The electrochemical processes contributing to induced polarization appear to be electrode reactions between electrolytes and metallic mineral grains in rocks. Providing the metallic grains are distributed through the rock, rather than forming a continuous filament, current must flow part of the time through the the electrolyte and part of the time through the metallic grains. At the boundary between the electrolyte and the metal, charge is transferred from ions in solution to the metal or from the metal to ions in solution. If the charge gained by an ion happens to be an electron, the process contitutes reduction; if the ion loses an electron, the process is oxidation.

If a mineral is relatively insoluble, the tendency for ions to go into solution from the mineral is quickly balanced by the tendency for the ions to precipitate out of solution. When an electric current is forced through the materials, this condition of balance is destroyed and the transfer of ions into and out of solution is radically altered.

The oxidation process at one face and the reduction process at the other face of a metallic grain usually does not require the same amount of energy. One process will tend to go faster and easier than the other. Since the current going in one side of the grain must equal the current going out the other side, there must be a potential gradient established across the grain or across the face where the slower reaction is taking place. The extra voltage or potential gradient required to force the current across the face of the mineral grain is called over-voltage. The response time of these reactions results, of course, in a variation of the over-voltage or polarization effect as a function of frequency. Since these processes are relatively slow, the induced polarization effect is greatest at frequencies from .1 Hertz to 10 Hertz. Any system capable of accurately measuring the electrical properties as a function of frequency in this frequency range can be used as an induced polarization system.

13.3.1 Measurement and Interpretation Techniques

Four-terminal arrays as described previously formed the primary technique for measuring induced polarization effects. Since this technique is used primarily in the search for minerals, it was important to device an interpretation scheme which would locate the ore body in depth and in horizontal positions. Measurements are usually made, therefore, along one or more lines crossing the area being explored. Measurements are made at a variety of spacings, to obtain depth penetration, along each of the survey lines. The data is plotted as shown in Figures 13-13 through 13-16. These figures, prepared by McPhar Geophysics Limited, were prepared from

scale models to be used in interpreting field results. Although computer modelling has been done for mathematically describable objects, most of the interpretation case studies have been accomplished through scale models. The resistivity for both the model and the surrounding material is given in units of ohm feet/2π.

The frequency effect (fe) and metal factor (Mf) shown on these figures are defined by the equations,

$$fe = \frac{\rho_2 - \rho_1}{\sqrt{\rho_2 \rho_1}} \times 100 \qquad (13.44)$$

where fe is frequency effect in percent,

ρ_1 is the resistivity at the lower frequency, and

ρ_2 is the resistivity at the higher frequency.

$$Mf = \frac{fe \times 10^5}{\sqrt{\rho_2 \rho_1}} \qquad (13.45)$$

Most systems use a lower frequency of 0.1 Hertz and a high frequency of 1.0 to 2.5 Hertz.

Hundreds, if not thousands, of scale model cases are available for interpretation of field results. Although field data are rarely as well behaved as the results from scale model measurements or theoretical calculations, they can usually be related to a model situation sufficiently accurate for an initial interpretation.

The results of an induced polarization survey is never considered adequate to identify and define an ore body. One of the key problems in using this technique results from a similar induced polarization effect associated with certain clays such as montmorillonite. A subject of considerable on-going research seeks to determine methods for recognizing the frequency effects associated with clays as compared to the frequency effects produced by sulfide minerals. Since these research efforts are as yet unsuccessful, the location of a significant IP anomaly

is followed up by a drilling program to determine exactly what caused the effects measured.

13.4 SUMMARY

In addition to exploration for minerals, low frequency systems on the surface are being used and have been used extensively in the search for subsurface ground water. The U. S. Geological Survey in the State of Illinois has conducted extensive surveys over the entire State in the search for ground water to obtain municipal supplies. The Canadian Geological Survey is studying the use of four-terminal and wave-impedance measurements for this purpose.

The electrical measurements of the properties of the earth may also be used to effectively locate fault systems which have resulted in displacement of rock units such that the electrical properties on each side of the fault are different. The faults may often also be located due to the tendency for water to collect in the crushed rock zone of the fault itself.

Four-terminal arrays and a three-terminal modification of this technique are also used extensively in well logging. Virtually all wells drilled in the search for petroleum products are logged from the bottom of the well to a near surface location. These well logs are used primarily to locate the elevation or horizon of the contacts between different rock strata. This is a very effective method when the rock types of interest have differing electrical properties.

Cost data for 1971 shows that an induced polarization crew with equipment will cost approximately $250 to $350 per day. An efficient crew can cover one to five line miles per day depending on the terrain and weather conditions. This cost would also cover the expense involved in plotting the results for interpretation. Well logging costs range from $.15 to $.20 per foot depending on the type of system and variety of measurement required.

The user of these techniques must never forget that these techniques and

their interpretation are valid only when array dimensions are less than a skin depth for the frequency being used in the materials of interest.

Theoretical Induced Polarization and Resistivity Studies

Scale Model Cases

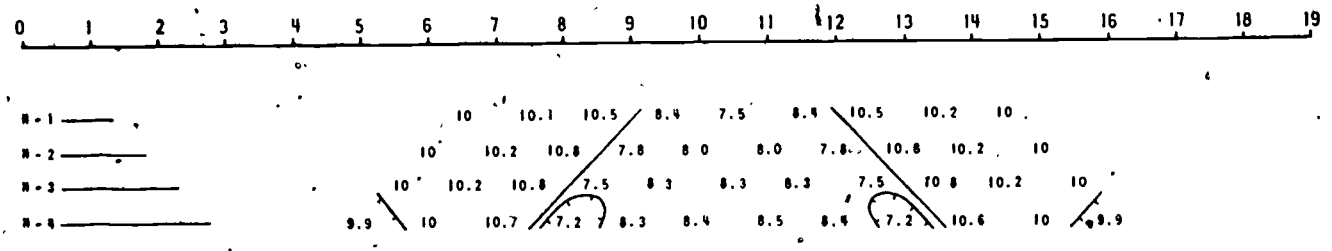

$(P/2\pi)a$

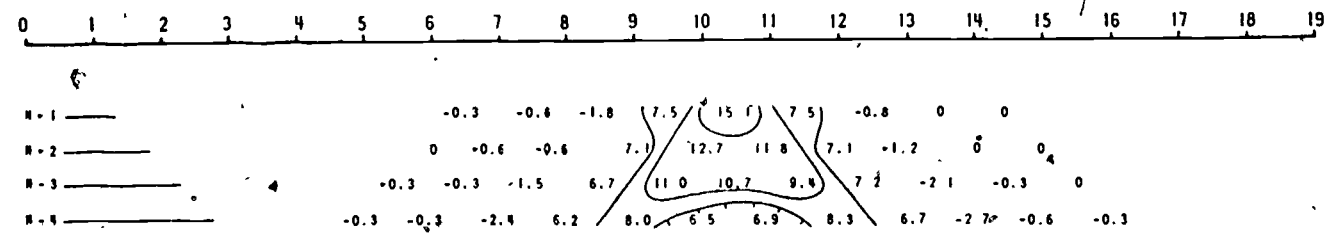

$(fe)a$

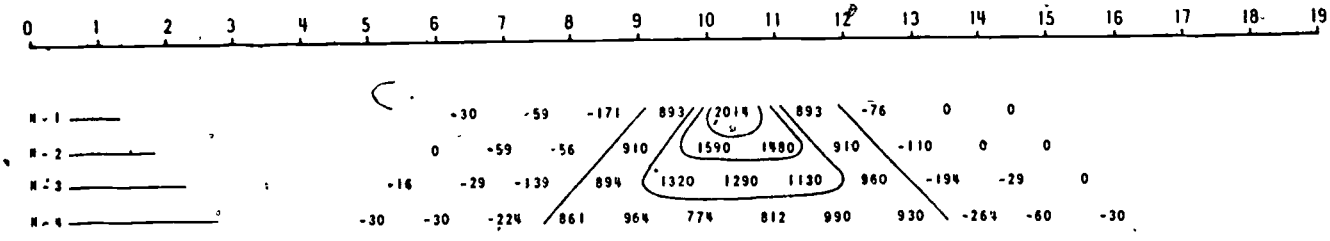

$(Mf)a$

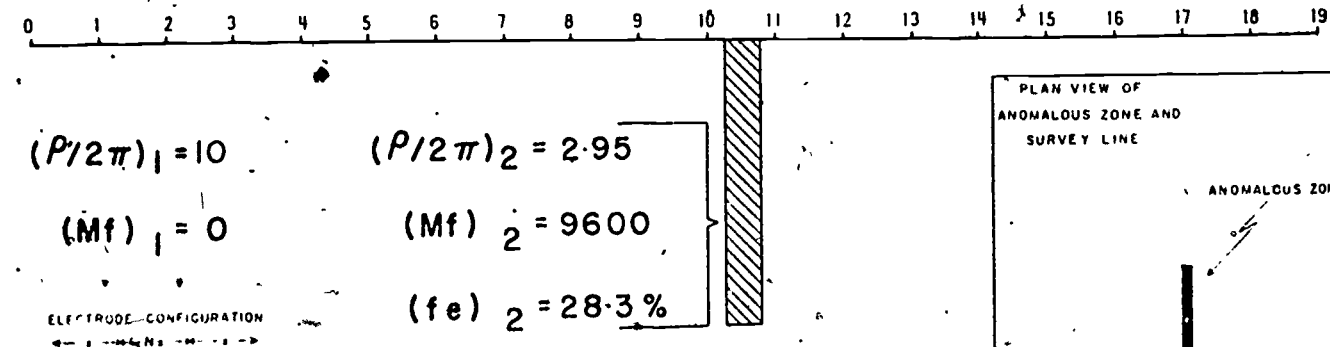

$(P/2\pi)_1 = 10$ $(P/2\pi)_2 = 2.95$

$(Mf)_1 = 0$ $(Mf)_2 = 9600$

$(fe)_2 = 28.3\%$

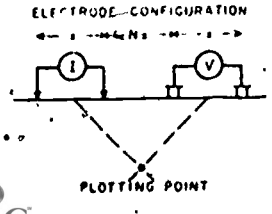

Figure 13-13

CASE 1-0-0-BV-10-a

McPHAR GEOPHYSICS LIMITED

Theoretical Induced Polarization and Resistivity Studies

Scale Model Cases

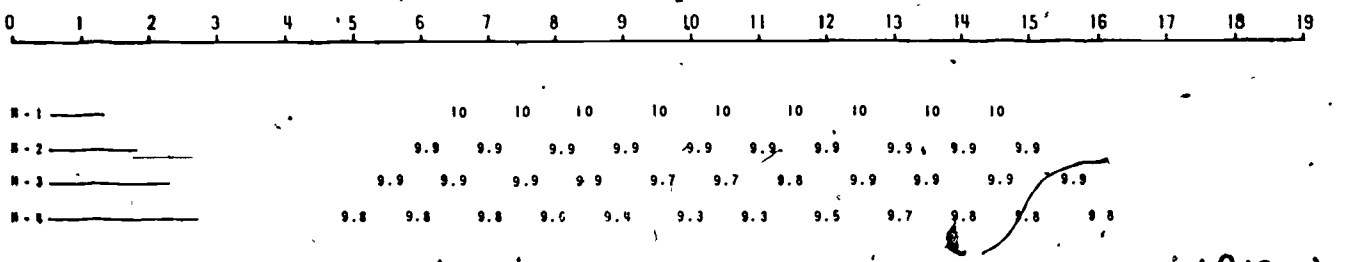

$(P/2\pi)a$

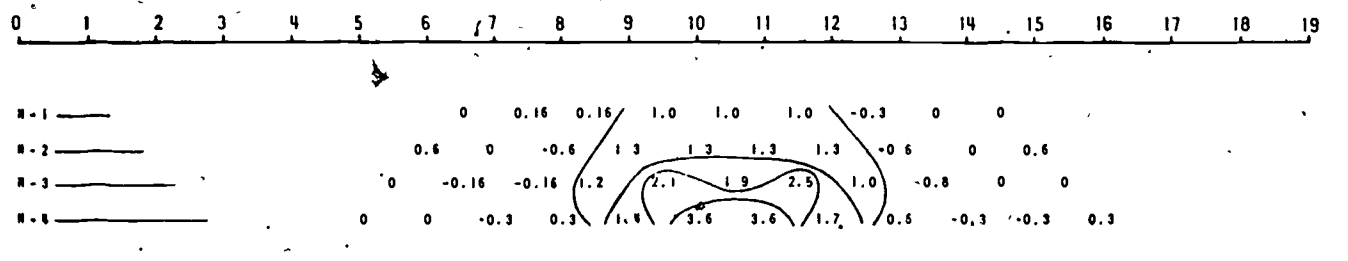

(fe)a

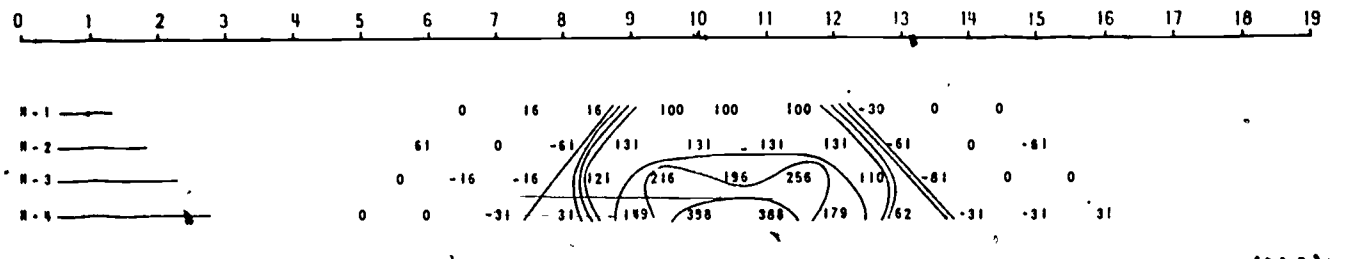

(Mf)a

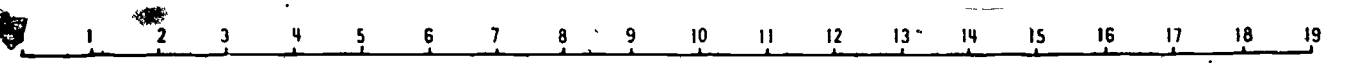

$(P/2\pi)_1 = 10$ $(P/2\pi)_2 = 4.03$

$(Mf)_1 = 0$ $(Mf)_2 = 6810$

$(fe)_2 = 27.4\%$

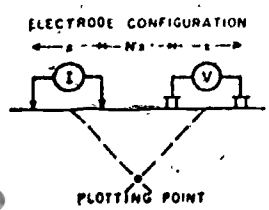

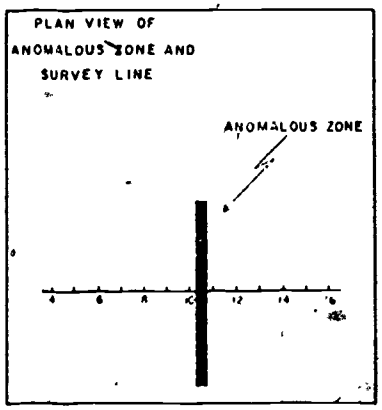

Figure 13-14

225 CASE 1-2-0-BV-10-a

McPHAR GEOPHYSICS LIMITED

Theoretical Induced Polarization and Resistivity Studies

Scale Model Cases

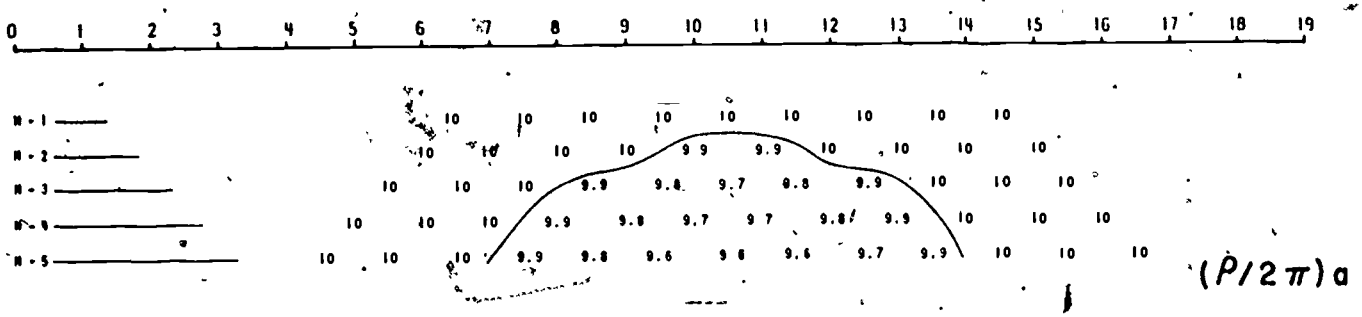

$(P/2\pi)a$

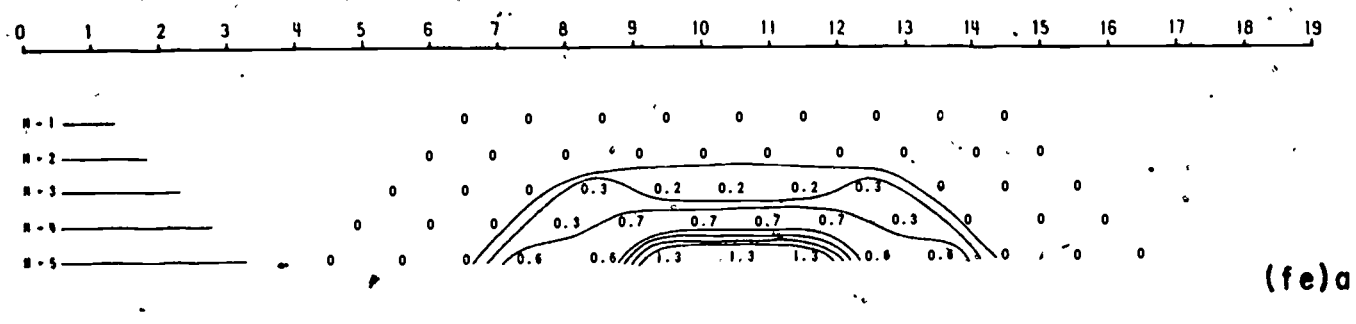

(fe)a

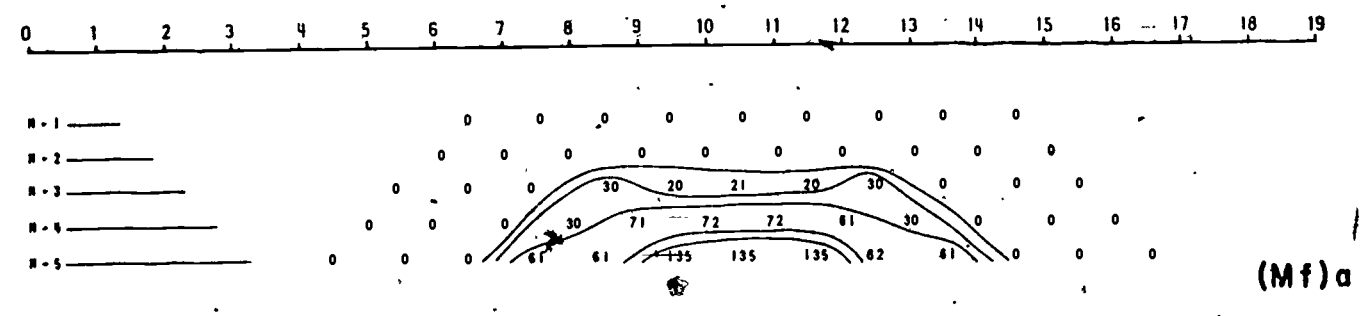

(Mf)a

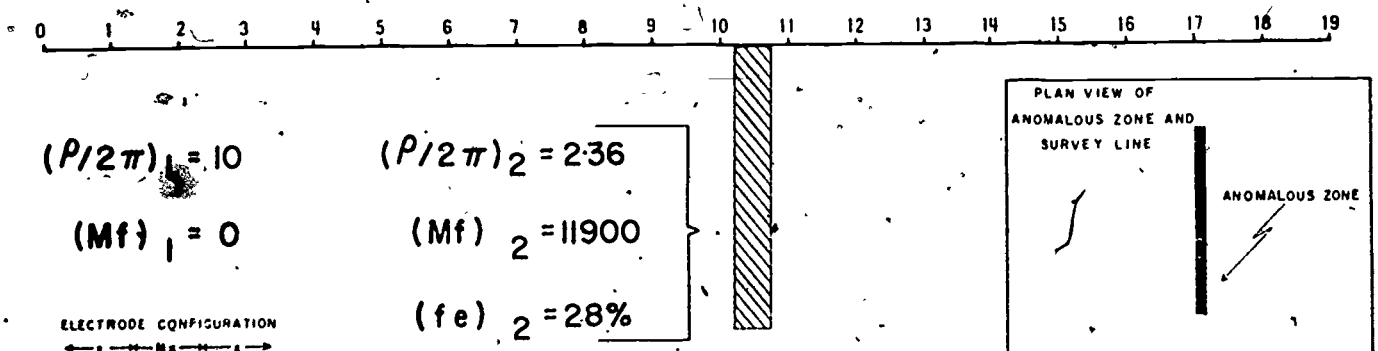

$(P/2\pi)_1 = 10$

$(Mf)_1 = 0$

$(P/2\pi)_2 = 2.36$

$(Mf)_2 = 11900$

$(fe)_2 = 28\%$

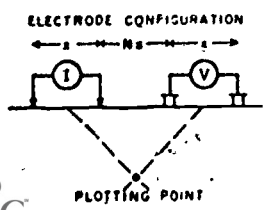

Figure 13-15

CASE I-0-0-BV-10-d

McPHAR GEOPHYSICS LIMITED

Theoretical Induced Polarization and Resistivity Studies

Scale Model Cases

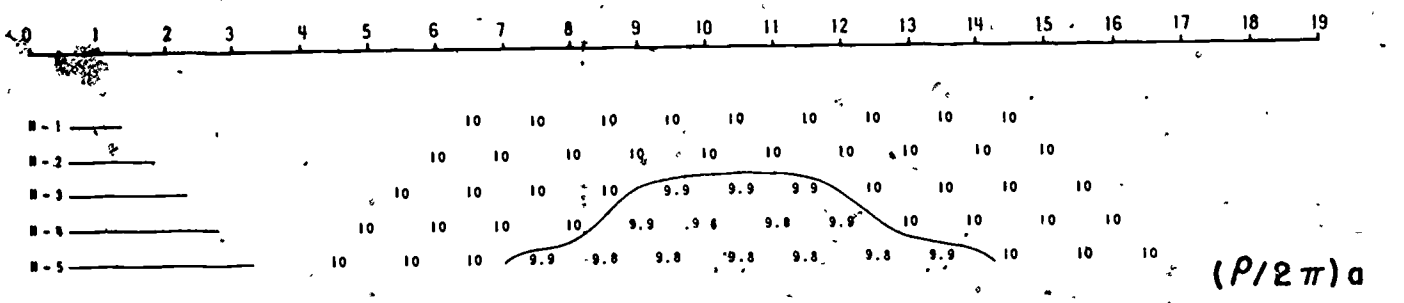

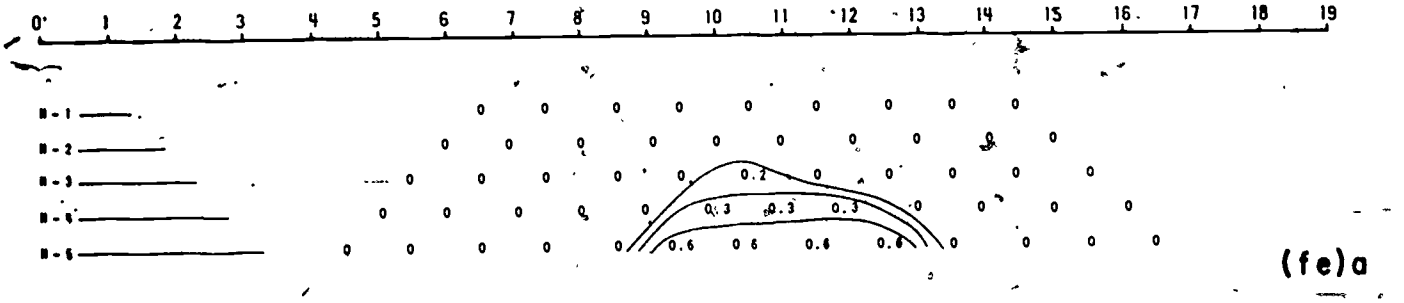

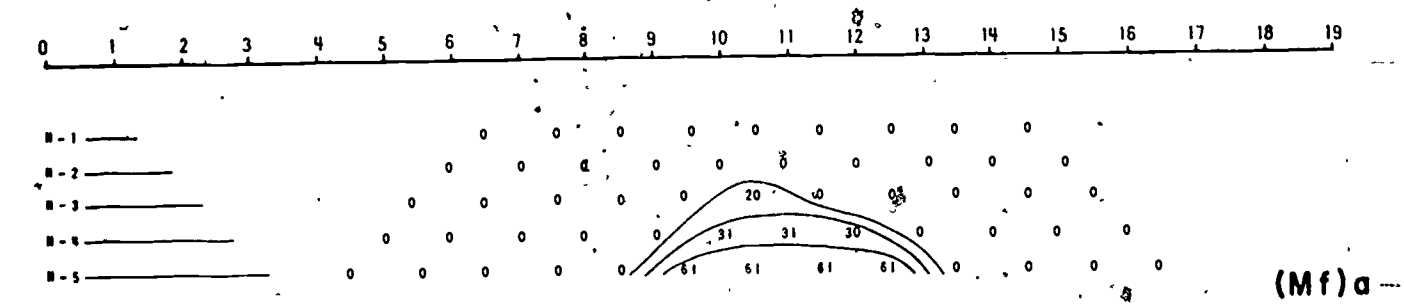

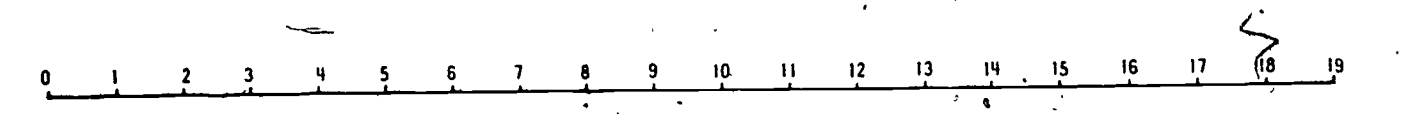

$(P/2\pi)_1 = 10$

$(Mf)_1 = 0$

$(P/2\pi)_2 = 2.5$

$(Mf)_2 = 10400$

$(fe)_2 = 26\%$

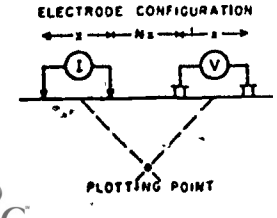

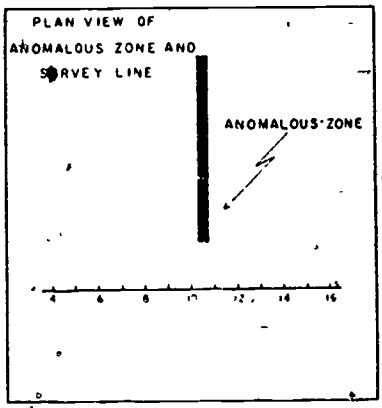

Figure 13-16

CASE I-1.5-BV-10-d

REFERENCES

Keller, G. V., 1966. Electrical Methods in Geophysical Prospecting, Pergamon Press.

Maxwell, E. L., et.al., 1961. Electrical Conductivity Measurements of the Earth at Audio Frequencies, DEC. Report 30-F-1, ONR Contract 3387(00), NR371-590, 28 November, 1961.

Wait, J. R., 1959. Overvoltage Research and Geophysical Applications, Pergamon Press.

14.0 LOW-FREQUENCY SYSTEMS (AIRBORNE)

Time did not permit the preparation of special material for this section. In lieu of this, copies of two papers by Barringer are provided. Barringer's Input System is probably the most widely used airborne geophysical system. Several companies fly the system and are normally booked up six months to two years ahead.

The Input and Radiophase Systems are anomally detectors. Under normal use, the data cannot be interpreted to obtain absolute values of conductivity. Results from the Input System are followed up by ground measurements to determine the cause of the anomally.

Note that both systems are detecting changes in electromagnetic fields caused by currents induced in the earth. The Input System carries its own source of energy and is, therefore, a truly active system. Radiophase uses energy from low frequency broadcast (military) stations and is active in the sense that the energy is man-made, even though the Radiophase System does not provide it.

Input System costs average $25 per line mile which is considerably less than the $100 to $250 per line mile for Induced Polarization surveys. If the lines are spaced about 1000 feet the cost per square mile would be about $125. Radiophase costs were not available.

Some case histories for the Input System illustrate the results to be expected.

THE INDUCED PULSE TRANSIENT AIRBORNE ELECTROMAGNETIC PROSPECTING SYSTEM

BY

A. R. BARRINGER

FEBRUARY, 1967

THE INDUCED PULSE TRANSIENT AIRBORNE ELECTROMAGNETIC PROSPECTING SYSTEM

ABSTRACT

Airborne electromagnetic prospecting is assuming increasing importance as a relatively new tool for exploring the natural resources of large areas of country at high speed and low cost. There is, however, a definite need for improved methods which are better able to cope with difficult overburden conditions. The induced pulse transient airborne electromagnetic technique has been developed in an attempt to achieve maximum depth of exploration and discrimination against spurious responses from conductive overburden. The method depends upon the generation of very high powered electromagnetic pulses and the measurement of the response of underlying terrain to these pulses. It has been found that the ground reaction exhibits a transient decay of eddy currents and the analysis of this decay provides an excellent means of identifying conductive orebodies of both the massive and disseminated sulphide type. Deep penetration is obtained by virtue of the time isolation which exists between the transmitted primary field and the secondary field received from the ground.

The method has been perfected during the past ten years and is now in widespread use. Improvements are continuing and it is hoped to develop the technique additionally as a new tool for water resource evaluation and general geological mapping.

Ancillary equipment such as airborne magnetic and gamma-ray spectrometric equipment has been developed for use with the system in order to provide an integrated approach.

GENERAL REVIEW OF APPLICATIONS OF AIRBORNE ELECTROMAGNETIC PROSPECTING SYSTEMS

Most metalliferous orebodies show a higher electrical conductivity than their enclosing rocks. This is particularly true of the massive sulphide type where the conductivity contrast may vary between 10 to 1 and 10,000 to 1. This fact has been utilized for many years as a means of prospecting for orebodies and has given rise to many ground electrical geophysical systems employing both electrode contact with the ground and non-contacting electromagnetic inductive coupling. These methods have proven most valuable in aiding in the discovery of new orebodies and the delineation of extensions to existing orebodies and mineral prospects.

During the last twenty years increasing attention has been devoted to developing airborne prospecting systems in order to provide a means of covering large areas of country at relatively high speed and low cost. The magnotometer was the first instrument to find extensive airborne use and it has proven a most powerful tool in the direct location of iron ores and in providing an aid to geological mapping. More recently airborne electromagnetic systems have been coming into use as a reconnaissance method for detecting both magnetic and non-magnetic ore deposits of the conductive type. The extensive use of airborne electromagnetic prospecting systems in Canada has resulted in the discovery of a number of important new orebodies, most of which had virtually no surface expression and some of which can be classified as major mineral deposits. It is expected that discoveries will continue in all parts of the world as

airborne electromagnetic systems see increasingly widespread use and as the techniques of discrimination and depth penetration are improved.

Whereas airborne electromagnetic systems function very effectively in prospecting areas where the surface rocks and soils are fairly resistive and overburden is shallow, they encounter trouble when the reverse conditions exist. In arid or semi-arid terrain, for example, rapid surface evaporation of rainfall creates a condition of surface salinity which in turn produces high surface conductivity. This conductivity generates almost continuous anomalous response in EM systems and tends to mask any underlying geologic conductors.

Similarly, certain types of glacial clays can form thick conductive blankets over the underlying terrain making penetration with airborne EM very difficult and creating misleading responses.

Unfortunately many potentially important mineral prospecting areas around the world suffer from these problems and it is necessary to continuously strive at improving airborne electromagnetic systems in order to make these areas more amenable to airborne prospecting. The importance of this to the development of natural resources in the less explored parts of the earth can be brought into perspective by examining the relative rates of coverage of ground and airborne methods. In forested country, a ground electromagnetic crew cannot cover more than 100 traverse miles per month and generally the mileage covered

is much smaller. An airborne electromagnetic system can cover between 2,000 and 10,000 traverse miles per month depending upon weather conditions and in addition it can survey terrain covered by swamps, lakes and rivers which are frequently impossible to explore by ground methods.

The induced pulse airborne electromagnetic technique was initially developed with the dual purpose of attempting to increase penetration whilst at the same time improving discrimination against spurious responses from surface conductivity. More recently, it has become apparent that the method has potential not only in locating sub-surface geologic conductors such as massive sulphide orebodies, but also for use as a general geological mapping tool.

The detailed analyses of terrain conductivity which can be obtained with the pulse transient approach can be used to delineate sub-surface fresh water aquifers lying beneath conductive overburden such as glacial clays or saline sands and gravels. It can also be used to trace conductive marker horizons such as shales, and map out the junction between rocks of contrasting conductivity. In other words, there appears to be a broad field of application for the method, in conjunction with other techniques such as the airborne magnetometer, as an aid in the geologic mapping of terrain and in its general evaluation for mineral, water and other natural resource potentials.

A BRIEF HISTORY OF THE INDUCED PULSE TRANSIENT TECHNIQUE

The induced pulse transient electromagnetic technique of airborne prospecting was originally conceived in 1957 as an approach to overcoming some of the inherent noise problems of continuous wave airborne electromagnetic techniques. The system was developed in Canada and commenced operational use in 1961. The original development work was sponsored by Selco Exploration Company Limited of Toronto and this work has been continued by Barringer Research Limited of Toronto. Various improvements of the system have been developed since the equipment first became operational and the most up-to-date version, which is known as the Mark V INPUT® System will be described in this paper. The system is being operated in many parts of the world by licensed survey organizations. Descriptions of earlier versions of the system have previously been published in journals (1), (2), and (3) and in the patent literature. Development work is continuing and it is hoped to fly an all digital system programmed for automatic data compilation by computer during 1968.

PRINCIPLES OF THE INDUCED PULSE TRANSIENT SYSTEM

The induced pulse transient system operates on the principle of generating eddy current pulses in the ground and analysing the amplitude and decay characteristics of these eddy currents for information regarding the composition and conductivity of the ground. The eddy currents are induced in the ground by high-powered electromagnetic field pulses of half sine wave shape. The primary field pulses have a base width of approximately 1.5 milliseconds and are spaced 2 milliseconds apart, as shown in Figure 1. They are generated by circulating current pulses of the desired half sine waveform in a large loop antenna surrounding the survey aircraft. The loop is part of a pulse-forming network. Other components of this network are mounted in the pulse transmitter located inside the aircraft. Each individual primary field pulse is followed by a short period during which transmission does not occur. The primary field is therefore discontinuous in nature and the eddy currents induced in the ground during the pulse period tend to decay approximately exponentially during the period following the pulse.

The brief gaps in the primary field are used to detect the presence of eddy currents in the ground and to measure their amplitude and waveform. The eddy currents generate a secondary magnetic field which corresponds in wave shape to the eddy currents. This secondary field is detected by means of a coil and pre-amplifier mounted in a "bird", which is towed behind the aircraft on 500 feet of cable. See Figures 2 and 3. The separation which the system achieves

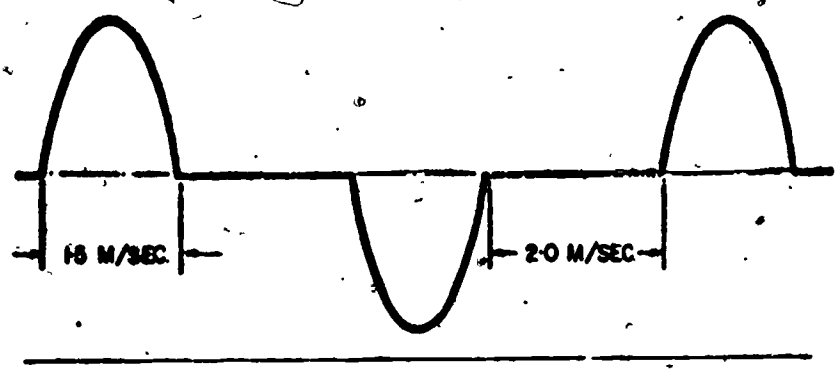

FIG. 1 Primary E.M. Field

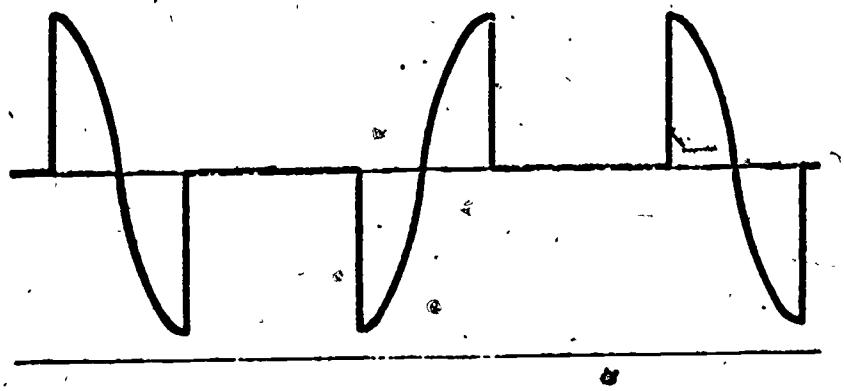

FIG. 2 Primary Field Detected in Bird

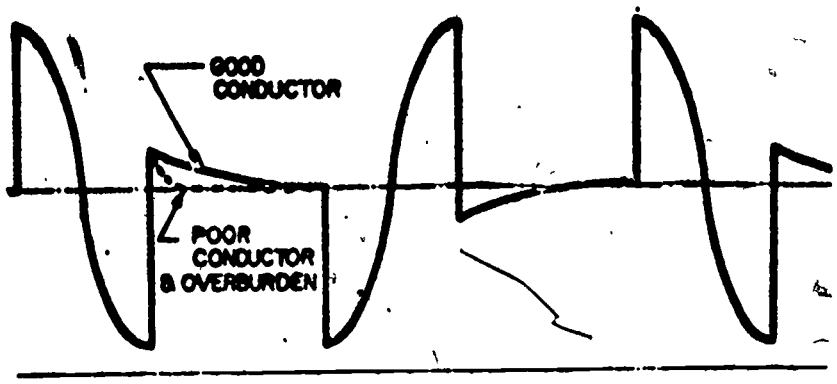

FIG. 3 Primary and Secondary Field Detected in Bird

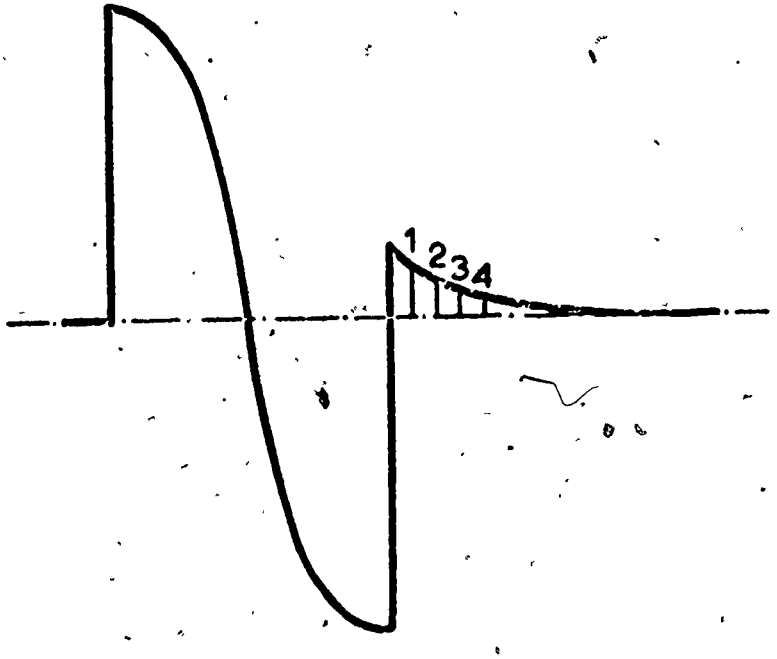

FIG. 4 Four Channel Sampling of Mark II and III Input Systems (Six Channels are used in Mark IV and V Systems)

between the primary exciting field and the received secondary field constitutes the outstanding advantage of the method, since it overcomes the orientation noise common to other airborne electromagnetic prospecting systems which employ continuous waves. The signal voltage generated in the detector coil is fed to the induced pulse transient receiver where it is sampled at several points in time as indicated in Figure 4. The sampling points have a fixed time relationship with respect to each other and with respect to the termination of the transmitted primary pulse. In current operational versions of the INPUT receiver, each sample is taken for a duration of 400 microseconds at mean delays of 300, 500, 700, 1100, 1500 and 1900 microseconds after termination of the primary pulse. The signal information contained in each sample position is subsequently processed in the receiver to produce 6 analogue output voltages, each one of which is proportional to the amplitude of the eddy current in the ground at the sample delay in question. The fixed time relationship between the sampling positions allows the time constant of the decaying eddy currents to be measured in terms of the ratios of the analogue output voltages. This time constant is proportional to the conductivity of the earth's structure under consideration. The analogue output signals produced by the induced pulse transient receiver are recorded during flight by means of a multi-channel strip chart recorder. Other data of importance for the interpretation of results are recorded simultaneously, such as the earth's total magnetic field, flight altitude, aircraft location and time.

Special techniques are utilized in the induced pulse transient system to reject interference. Current pulses are circulated in the transmitting loop in alternate directions around the aircraft, which causes the eddy current pulses in the ground to alternate in polarity. This feature, when used in conjunction with coherent sampling techniques of signal processing, constitutes a very effective digital filter and results in a high rejection of low frequency coil movement noises as well as atmospheric and man-made electromagnetic noises with frequencies components differing from the pulse repetition rate of the pulse transmitter.

THEORY OF OPERATION AND NOTES ON DESIGN FEATURES

The transmitter embodies a current-carrying loop installed around the aircraft; the wing span and length of the fuselage are used to the best advantage to obtain a loop of large area. Current is fed into the loop in pulses, each of which has the form of a half sinewave. This transmits a magnetic field of corresponding form. At reasonable distances from the aircraft the magnetic field can be considered that of a dipole with a vertical axis. The magnetic field intensity along any radius from the centre of the loop thus varies inversely as the third power of distance from the centre. The equation of total magnetic field intensity can be expressed:

$$H = (M/r^3) \sqrt{1 + 3\sin^2 \theta} \sin t/T \quad \text{for } 0 < t < T/2$$

$H = 0$ for all other values of t.

In this equation M is a magnetic moment which embodies the turns-area of the loop and the amplitude of applied current; r is distance from centre of loop; θ is the polar angle, measured from the axis normal to the plane of the loop, t is time, and T is the period of a complete sine wave. Individual pulses may follow each other at intervals of T or more, and alternate pulses are usually of opposite polarity. For analytical purposes it is sufficient to consider a single pulse and the effects which may follow it in the interval $T/2 < t < T$.

A fundamental electromagnetic principle is that a time varying magnetic field is always accompanied by an electric field proportional to its rate of change. Thus if H varies as $\sin \frac{t}{T}$

then E varies as (1/T)cos t/T.

The directions of E and H are mutually orthogonal; hence, if H eminates from a vertical dipole, the direction of E is represented by a family of horizontal circles concentric with the dipole axis. In connection with the induced pulse transient system a principal point is that at the end of a pulse, the value of E is finite. In free space electric fields will collapse to zero almost instantaneously, but in a medium having a finite electrical conductivity or magnetic permeability the collapse will be delayed by inductive effects. If the medium is conductive, there will of course be a current circulation corresponding to the electric field. During the collapse period this will generate a magnetic field of corresponding time character. This can frequently be expressed:

$$h = h_o e^{-t/T_c}$$

where T_c is the time constant of a negative exponential transient.

In theory the decay transient could be recorded by a sufficiently sensitive magnetometer, but the usual receiver employs an induction coil whose output is proportional to:

$$dh/dt = (h_o/T_c)e^{-t/Tc}$$

The above represents a very simplified expression of the form of the decay transient. In practice it is more complex and requires detailed analytical treatment to derive a more comprehensive expression. Studies on the transient

field have been published by Wait (4) and Bathacaria 6, 7 and 8.

The receiving coil is wound on a ferrite rod and is mounted in the bird with a special shock mount which provides isolation from rotational vibrations. Rotational movements in the earth's magnetic field generate large voltages in an untuned coil and must be minimized in order to reduce noise and eliminate dynamic range problems in the electronics. The receiving coil is towed in a bird on 500 feet of shielded cable and is connected to a set of coherent sampling channels in the aircraft.

The coherent detection system is comprised of 6 channels, each of which samples a different portion of the transient signal, as previously outlined. The electronics are entirely solid state and extensive use is made of integrated circuitry. Modular plug-in circuitry is used throughout to facilitate rapid servicing in the field, and survey aircraft are normally equipped with extensive spare circuit modules to ensure reliability.

ADVANTAGES OF THE INDUCED PULSE TRANSIENT SYSTEM

A principal advantage of the system is that time isolation between the transmitted and received signals eliminates the interfering effects of the primary field; this enables higher sensitivities to be obtained that can, at the present time, be achieved with continuous wave electromagnetic techniques. In addition, the quality of the records is somewhat more uniform since the system is insignificantly affected by varying air turbulence.

Recently in the Mark V system the transmitted power has been increased by a factor of 4 in relation to earlier versions and the peak ampere turns area now amounts to 2.8 million ampere turns. As far as is known this represents an electromagnetic field output which is 2 or 3 orders of magnitude greater than has been achieved with any previous airborne electromagnetic prospecting system.

The increase in power output of the system does not necessarily mean an effective increase in signal to noise ratios unless full compensation for orientation noise is achieved. Although there is a time isolation between the primary field and the received signal, transient eddy currents are induced in the aircraft when a high powered transmitter is used. It is necessary to achieve a high degree of perfection in compensating for these eddy currents, otherwise they will create a related, although much weaker, form of orientation noise of the type caused by the primary field in continuous wave systems.

The compensation technique used in the induced pulse transient system has fortunately been developed to the stage where the effects of the bird swinging can be almost entirely eliminated.

The net result of using very high powered transmission and accurate compensation for the metal in the aircraft is that exceptionally deep penetration is obtained. The effect of flat conductors can be seen at flying heights of over 2,000 feet, while lenticular orebodies have been detected at flying heights of up to 1,100 feet. Test flights carried out over a known orebody 200 feet beneath the surface have yielded clearly defined responses at flying heights of up to 800 feet.

Normal survey terrain clearance is 380 feet, so that it can be seen that penetration for large orebodies can be up to 700 feet beneath the surface. It is believed that penetrations of 400 or 500 feet can be routinely expected for moderate size conductive orebodies with strike dimensions of not less than 1,000 feet.

Another important feature of the induced pulse transient system, apart from depth penetration, is the discrimination obtained between underlying sulphide conductors and surface conductivity effects. In most cases the eddy currents induced in conductive swamp muskeg and the like will completely decay to zero within 700 microseconds from the termination of the pulse, which means that the effects will not report in the last three channels of the system. In

regions of high conductivity, such as Western U.S.A. or Western Australia, the effects of overburden may persist longer but seldom reach the last 2 channels except in broad, easily identifiable plateaus. On the other hand, sulphide bodies are generally good conductors and eddy currents collapse far more slowly. As a result, they normally give anomalies which persist right through all channels as clearly resolved anomalies. This provides an extremely simple means between overburden conductivity and sulphide conductors. Further detail is given in a subsequent section on interpretation.

The incorporation of active filtering circuits in the Mark V System has helped to increase signal to noise ratios and improve the appearance of the records. In order to ease interpretation, all 6 channels are now recorded on a common baseline and it has been found very easy to recognize anomalies and to judge their conductivity at a glance when this method of presentation is used. (See examples given.) Ratios of 6 channels can be very rapidly measured when a common baseline is used and confusion between the channels when an anomaly occurs is impossible since the signal is always decaying and the traces sort themselves out in the proper sequence.

Excellent discrimination against 50 and 60 cycle interferences is obtained with recent versions of the induced pulse transient system. It is generally possible to survey much closer to powerlines than can be achieved with ground follow-up equipment. Powerlines occasionally respond when they are grounded in a manner which creates conductive loops; even under these conditions, however,

it has been found possible to identify geologic conductors within a little more than 100 feet of major powerlines.

The use of optical recording on a direct writing ultraviolet type recorder enables a multi-channel presentation of data to be carried out. In some installations up to 13 channels have been used representing 6 induced pulse transient channels, one altitude channel, one magnotometer channel 4 gamma-ray spectrometer channels, and one channel indicating the presence of powerlines. This comprehensive range of data is conveniently cross-correlated when recorded on a single chart.

ANCILLARY MAGNETIC AND GAMMA-RAY SPECTROMETRIC EQUIPMENT

One of the major early problems with the induced pulse transient system was achieving compatibility with a suitable airborne magnetometer. Instruments such as the fluxgate magnetometer are subject to severe interference by the transmitted pulse, the harmonics of which appear to enter the signal circuits. Similarly the proton precession magnetometer, under normal circumstances, is subject to severe interference by the higher frequency harmonics of the pulse repetition rate. This problem has been overcome with the proton precession magnetometer by time-sharing. In this procedure the train of pulses from the transmitter is interupted once per second for a short period, to take a magnetometer reading. The magnetometer has been specially designed for this purpose and originally took readings at a 5 gamma sensitivity. Recent advances in the design of the magnetometer now enable a one gamma sensitivity to be achieved in a reading time of only 200 milliseconds. Loss of transmitted field due to the time-sharing operation is therefore very minor and magnetic recordings of the highest quality with direct digital readout can now be obtained simultaneously with the induced pulse transient system records.

In one of the INPUT installations a new type of gamma-ray spectrometer which features analogue correction circuits for the effects of Compton scattering in the various channels, has also been incorporated. Spectrum stabilization is employed using an internal artificial radio-isotope as a reference to eliminate system drift. This unit provides highly stable corrected outputs for uranium, potassium and thorium, as well as a total count.

FLIGHT PATH RECOVERY AND PLOTTING OF RESULTS

Standard techniques of survey flying are employed with the induced pulse transient system. Aerial photo mosaics are made of the survey area as a preliminary step and the proposed flight lines are laid out on the mosaic using a spacing of 300 metres between lines or 200 metres in high priority areas. Navigation is carried out by a navigator in the nose of the aircraft using the aerial mosaic as a guide, or alternatively a doppler navigation radar is used if the terrain is unusually featureless. A 35mm frame or strip camera is operated continuously during survey and fiducial marks and numbers are recorded simultaneously on the film and chart record every thirty seconds. The films are developed at the aircraft base and the flight lines are identified on copies of the air photo mosaics. The location of fiducial points are marked on the mosaic and reflight instructions are given to the air crew if any serious navigation errors have been made. A reproduction at the air photo mosaic is prepared on a transparent base showing all of the flight lines and fiducial points and this is subsequently used for plotting the geophysical results. At a later stage this transparent base map can be used for producing white prints for use as work maps.

INTERPRETATION OF INDUCED PULSE TRANSIENT RECORDS

One of the principal advantages of the induced pulse transient technique is the ability to make subtle discriminations between poor, medium and good conductors and to identify steeply dipping good conductors beneath flat lying overburden of medium conductivity. This feature of simple conductivity discrimination is of great value in locating sulphide orebodies under difficult conductive overburden conditions.

In general, highly resistive overburden having a resistivity greater than 1000 ohm metres does not report on the records at all. Overburden having a resistivity between 100 ohm metres and 1000 ohm metres appears only on channels 1 and 2 (ie delays of 300 microseconds and 500 microseconds after the pulse). Conductive overburden having a resistivity between 30 ohm metres and 100 ohm metres records on up to 4 channels (ie delays out to 1100 microseconds), whilst highly conductive overburden with resistivities between 10 and 30 ohm metres reports on 5 channels with a trace of response out to the maximum delay (1900 microseconds) of 6 channels.

It can be seen from the above that massive sulphide orebodies which generally have resistivities of less than 1 ohm metre, will produce six channel anomalies and can be readily identified in the presence of conductive overburden having resistivities as low as 30 ohm metres. This covers the majority of situations encountered in prospecting for massive sulphides with the exception of the arid

and semi-arid regions of the world and certain areas containing highly conductive clay and laterite zones.

The recognition of massive sulphides in conductive overburden having resistivities of 30 ohm metres or greater is very simple using the pulse transient technique. Response on those channels which are reacting to overburden is ignored in the initial scan of the records and the delayed channels such as 4, 5 and 6 are scrutinized for anomalies. The locations of anomalies are plotted in their correct positions on the flight lines using symbols indicating conductivity and magnetic correlation. Thus, different symbols are used according to the number of channels on which the anomaly appears. Where the airborne magnetometer shows an anomaly directly corresponding with the electromagnetic anomaly, this is indicated by the use of a symbol together with a number which gives the size of the anomaly in gammas. A small coincident magnetic anomaly generally indicates the presence of pyrrhotite or sulphide ore containing disseminated magnetite. A large magnetic anomaly indicates the presence of a considerable amount of magnetite. A six channel conductive anomaly associated with a magnetic anomaly of many thousands of gammas is frequently indicative of high grade magnetite ore of greater than 45% iron content, since high grade magnetite shows strong conductivity.

The relationship of conductors to geologic conditions is obviously of great importance in interpreting results. Conductors of great length which conform with the geologic strike are liable to be graphitic bands or sedimentary

sulphide bands of no value. Isolated conductors which appear to lie in favourable structural locations as indicated by a study of air photographs or contoured magnetic maps, often assume high priority for ground follow-up. Similarly, an association with igneous intrusives as indicated by ground geologic mapping, the interpretation of air photographs or contoured magnetic maps may be of great importance. The priority ratings given to conductors is very much a function of their overall relationship to known or inferred geology, and interpretations based solely on geophysical grounds are, in most cases, to be avoided.

This discussion on interpretation has so far been limited to the case of good conductors lying beneath overburden having a resistivity of 30 ohm metres or higher. Interpretation generally becomes more difficult in the case of highly conductive overburden, or when looking for medium conductivity orebodies such as disseminated sulphides of the porphyry copper type. Prospecting for disseminated sulphides in resistive terrain such as the pre-cambrian shield of northern parts of the globe, is perhaps the easiest of these special cases. Excellent response has been obtained in Sweden from an orebody containing only a few percent of sulphides. However, the overburden in this area had a resistivity of several hundred ohm metres or greater, and although the disseminated sulphides gave only a 3 or 4 channel response, the anomalies arising from the orebodies were not masked by the overburden (see Examples). Similar types of disseminated orebodies lying in conductive overburden would undoubtedly be very hard to identify.

The semi-arid and arid regions of the world present some of the most difficult problems. Erratic and heavy rainfall in conjunction with extremely rapid evaporation causes salts to be leached out and deposited in low lying depressions. Sufficient surface moisture always remains in these salts to make them extremely conductive, so that the drainage zones in arid country frequently show very high conductivity. This is particularly true in regions where salt-pan development takes place.

Generally in surveying semi-arid and arid terrain it is necessary to accept the fact that portions of the survey will be erased by too much surface conductivity. Nevertheless the development of surface conductivity is patchy and even in the worst areas, it is possible to carry out useful survey over a significant portion of the ground covered. A study of the flight records will indicate immediately those portions of a flight line which must be eliminated due to the presence of an overriding six channel response from the overburden. Experience has shown (in the desert regions of Australia for example) that stretches between salt pans can sometimes give quite good results. The salt pans themselves represent a major problem for exploration by most geophysical methods - including both airborne and ground.

These interpretation notes have been confined to a non-mathematical approach; however, research is underway at the present time on the determination of dip, strike, width and depth of conductive bodies from an analysis of anomaly profiles. Recent work has indicated that interpretive techniques of the type

prevalent in the literature, which assume that conductive bodies lie in a medium of infinite resistivity, are liable to give unrealistic and erroneous results. The circulation of eddy currents in the enclosing rocks and in the overlying cover of conductive orebodies can exercise a major influence on anomaly profiles and on the transient decay characteristics. It has been established that the effect of these peripheral eddy currents must be taken into account if meaningful estimates of key parameters such as depth and width are to be made. Modelling and mathematical studies are therefore underway to produce new interpretive techniques which will be published at a later date.

RESEARCH IN THE APPLICATION OF THE INDUCED PULSE TECHNIQUE TO GEOLOGIC MAPPING AND WATER PROBLEMS

Extensive research is currently being undertaken in conjunction with the Canadian Geological Survey on the development of the INPUT System for use as a conductivity mapping tool in the Prairie regions of Canada. Preliminary surveys carried out in 1965 and reported by Dr. L. S. Collett (5) have indicated that there is good correlation between INPUT resistivities and pleistocene geology. There are encouraging indicates that large scale resistivity mapping of this type will provide rapid information on the distribution of gravels, sands and clays up to several hundred feet in depth, depending upon conditions. The main problem in studying the results obtained in these types of surveys is the difficulty of interpretation. In multi-layered cases it is known that the decay curve is modified in a manner which should be indicative of the layering conditions.

More sampling points are required, however, on the decay curve, in order to make a meaningful study and computer techniques will be necessary in order to handle the large volume of data. For this reason the Canadian Geological Survey is, at present, sponsoring additional research in which 12 channels will be incorporated into the INPUT System and a digital recording system will provide a computer compatible output. The ultimate aim is to produce maps on a semi-automated basis in which various interpretative techniques can be employed in an attempt to obtain the maximum of information and elucidate

not only the surface resistivity patterns, but the sub-surface distribution of resistivity as well. It is hoped as a result of this work to develop the system as a new aid to tracing and mapping underground aquifers such as ancient river channels buried beneath glacial clays and silts.

An independent programme is currently being carried out by the United States Geological Survey, Regional Geophysics Branch, on the development of the INPUT System as a general geological mapping aid. This work is being directed by Mr. Jack Meuschy and Mr. Frank Frisknecht of the USGS. A Convair 240 aircraft has been equipped with an INPUT System as well as with other equipment such as a doppler navigator, high sensitivity magnetometer, and a highly sophisticated gamma-ray spectrometer. A considerable number of problems have had to be overcome in adapting the INPUT System to relatively high speed aircraft such as the Convair. A new type of bird has been designed which will tolerate high flying speeds and which, as an additional benefit, also maintains excellent stability in its geometrical relationship to the aircraft. This bird is of relatively light weight and features a towing position close to its nose and a drag skirt on the tail. Pitching manoeuvres of 10° climb and descent cause only a 1° change in the towing angle of the bird relative to the axis of the aircraft.

The bird also features a two coil system consisting of a vertical axis coil and a horizontal coil with its axis lying in the direction of flight. It has been necessary to reduce the size of the transmitting loop on the Convair aircraft in order to prevent excessive drag, but despite this good results have

been obtained in preliminary surveys. All the equipment in the Convair aircraft is connected to a digital recording system and, as in the Canadian Geological Survey Programme, it is planned to develop computerized data compilation techniques. If the performance of the system as a mapping tool meets expectations it is understood to be likely that the present six sampling channels will be increased in number in order to provide a more comprehensive conductivity analysis.

The principal application of the INPUT System as applied to geological problems appears to lie in the mapping of conductive clays, shale bands, fault zones, alteration halos, graphite zones, sulphide zones, salt pans, resistive gravels and conductive rocks in general. It seems likely that this approach, used in conjunction with magnetometry and gamma-ray spectrometry, will provide a means of mapping valuable geological information whilst at the same time prospecting for ore deposits. In the underdeveloped areas of the world such maps could greatly speed the work of geologists on the ground whilst at the same time covering the prime need of natural resources evaluation.

Ultimately it is probable that computerized data reduction techniques used in conjunction with a 3 component receiver will become the standard configuration for the INPUT System when used as a geological mapping aid. Preliminary modelling work has indicated that a wealth of information is contained in the spatial and time varying behaviour of the three components of the transient field, but a very exhaustive theoretical and modelling study will be required before full interpretive techniques can be worked out.

REFERENCES

(1) New Approach to Exploration - the INPUT Airborne Electrical Pulse Prospecting System - Barringer, Anthony R. - Mining Congress Journal, October, 1962.

(2) Recent Progress in Remote Sensing with Audio and Radio Frequency Pulses - Geleynse, M. and Barringer, Anthony R. - p. 469, Proceedings of the Third Symposium on Remote Sensing of Environment - October, 1964.

(3) The Use of Multi-Parameter Remote Sensors as an Important New Tool for Mineral and Water Resource Evaluation - Barringer, Anthony R. - p. 313, Proceedings of the Fourth Symposium on Remote Sensing of Environment - April, 1966.

(4) Transient Electromagnetic Propagation in a Conducting Medium - Wait, James R. - Geophysics V. 16, p. 213-221.

(5) The Measurement of the Resistivity of Surficial Deposits by Airborne Pulsed Electromagnetic Equipment - L.S. Collett - Presented at 35th Annual International Meeting of Society of Exploration Geophysicists, Nov., 1965 - To be published in Geophysics.

(6) Propagation of Transient Electromagnetic Waves in a Conducting Medium - Bhattacharyya, Bimal, K. - Geophysics V. 20, P. 959.

(7) Propagation of Transient Electromagnetic Waves in a Medium of Finite Conductivity- Bhattacharyya, Bimal, K. - Geophysics Vol. XXII, No. 1, 1957, pp. 75-88.

(8) Electromagnetic Fields of a Transient Magnetic Dipole on the Earth's Surface - Bhattacharyya, Bimal, K. - Geophysics Vol. XXIV, No. 1, 1959, pp. 89-108.

SUCCESSFUL DISCOVERY OF METALLIC CONDUCTION UNDER SEA WATER, GULF OF BOTHNIA, FINLAND (1965)

CASE No. 1

Perhaps the single most demanding test for the INPUT system involved the well-known Oulu magnetic anomaly lying 16 km off-shore in the Gulf of Bothnia, Finland. Lying beneath 75 feet of salt water and a further calculated 225 feet of rock/clay overburden, this anomaly presented a very formidable target for an electromagnetic method.

The problem of attempting to discriminate a target beneath a highly conductive sheet of salt water was approached by assuming that the body of sea water represented a homogenous conductivity medium. The INPUT system was first flown over deep water to avoid contributions from sea bottom materials and adjusted manually such that each channel behaved uniformly by nearly equal amounts with variations in aircraft altitude, as shown in Figure 1.

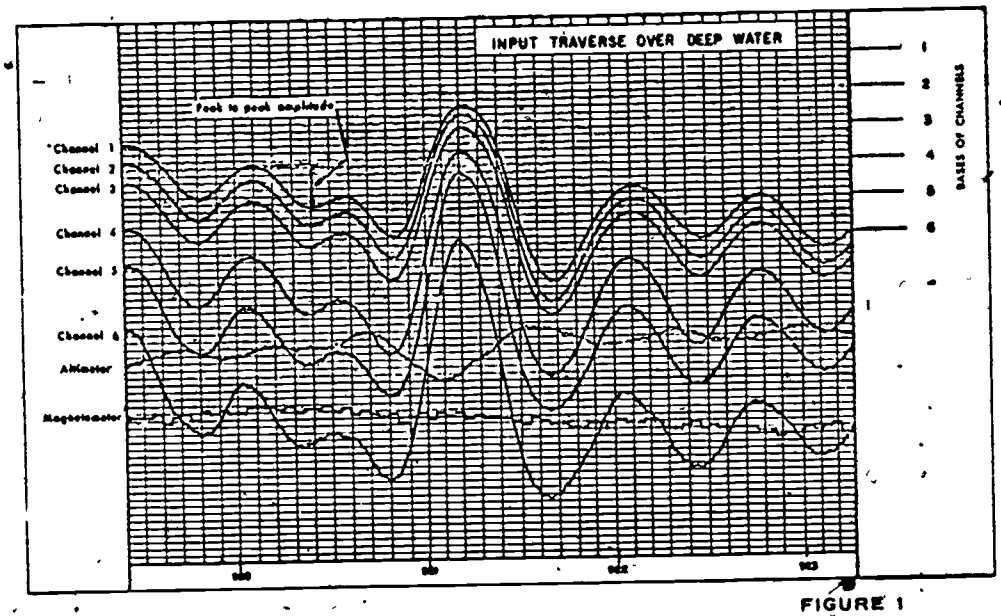

FIGURE 1

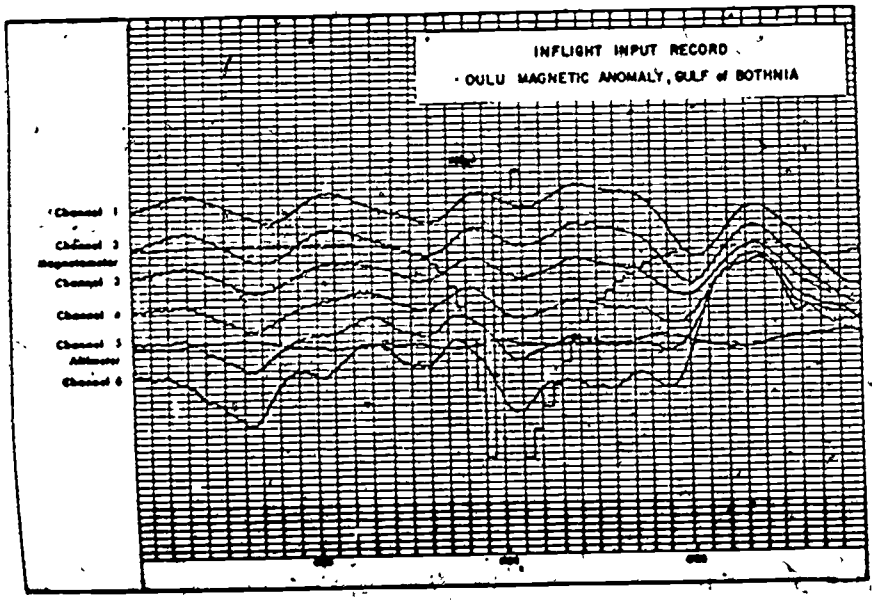

By carefully measuring amplitude variations with altitudes, an accurate average fall-off factor was established for each channel. The equipment was over-flown the target anomaly, with the result shown in Figure 2. As is immediately obvious, homogeneity is no longer present and some penetration into the sea floor has been achieved.

FIGURE 2 COURTESY OF OTANMAKI OY FINLAND

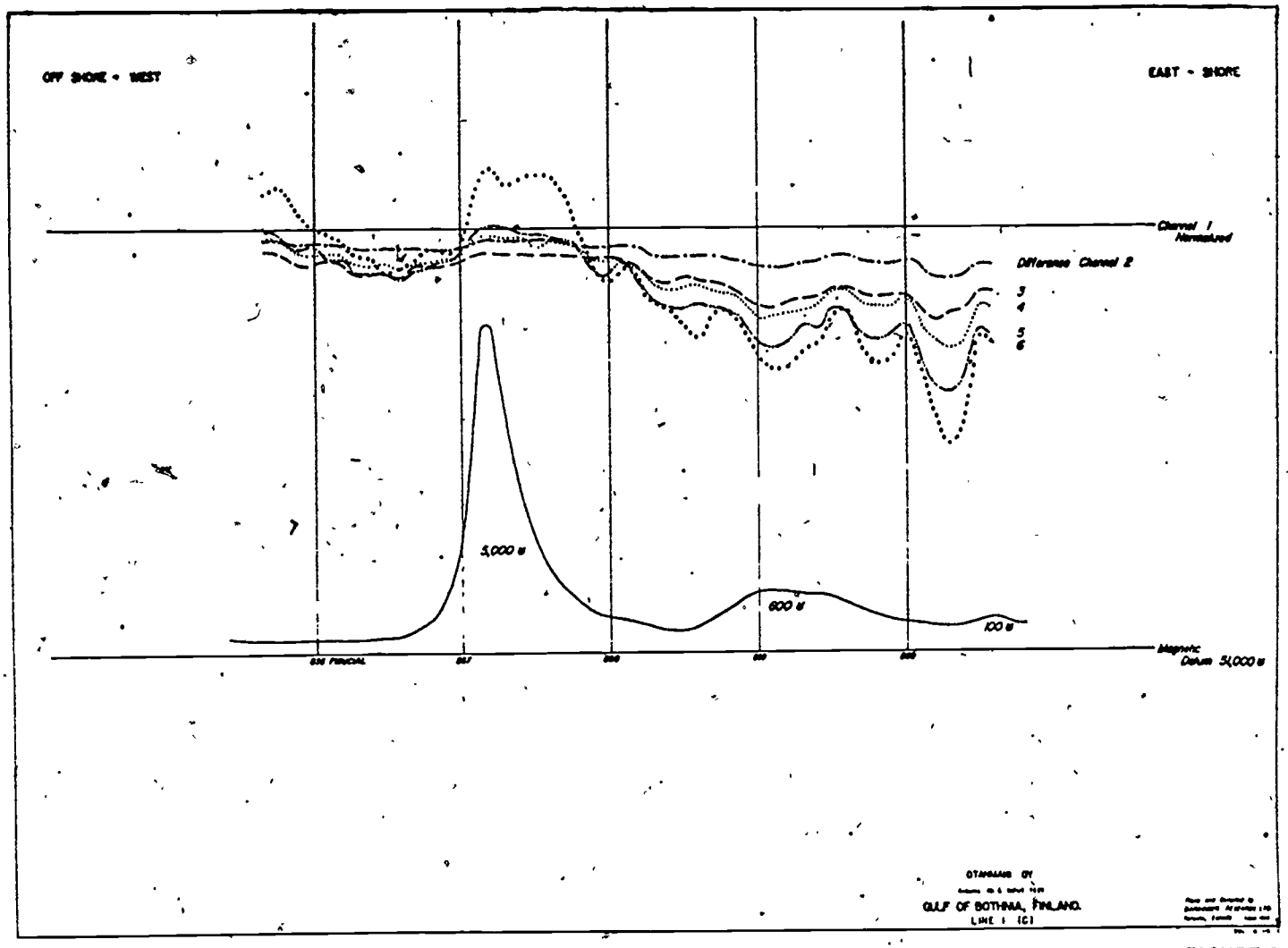

FIGURE 3

To extract pertinent responses the outputs were digitized, the established fall-off factors applied and the results normalized to Channel 1 so that in the complete absence of contrasting conductivity effects all channels would occupy the one horizontal line. Results of this processing are shown in Figure 3.

The most striking anomalous departure is the marked correlation of a precise INPUT response with a magnetic peak (positive sense now up and all time lags removed). The increasing resistivities encountered to the east reflect a shallowing of the sea floor in this direction. Several over-flights were made, and it was inferred that ore-grade magnetite underlay the magnetic expression, with perhaps a further body of hematite on its hanging wall side. Confirmation was quickly forthcoming. The following winter the Gulf of Bothnia froze over for the first time in several years. With the evidence provided by INPUT, a drill was placed on the ice on the magnetic anomaly. At the calculated depth, the first hole intersected magnetite ore running better than 40% Fe over 50 meters, with very low impurities.

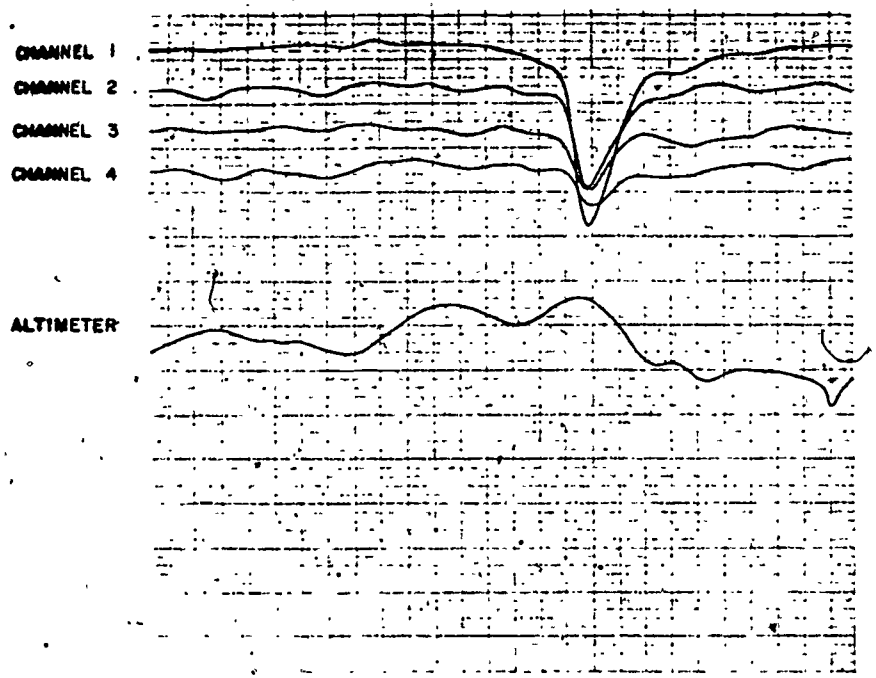

CARIBOU NEW BRUNSWICK.

MARK II

CARIBOU DEPOSIT, NEW BRUNSWICK. Massive sulphide d-zinc pyrite orebody, 4000 ft. long. Lenticular deposit in a large fold conformable with geology. A good ground conductor. Deposit originally detected by airborne E.M. and is near surface.

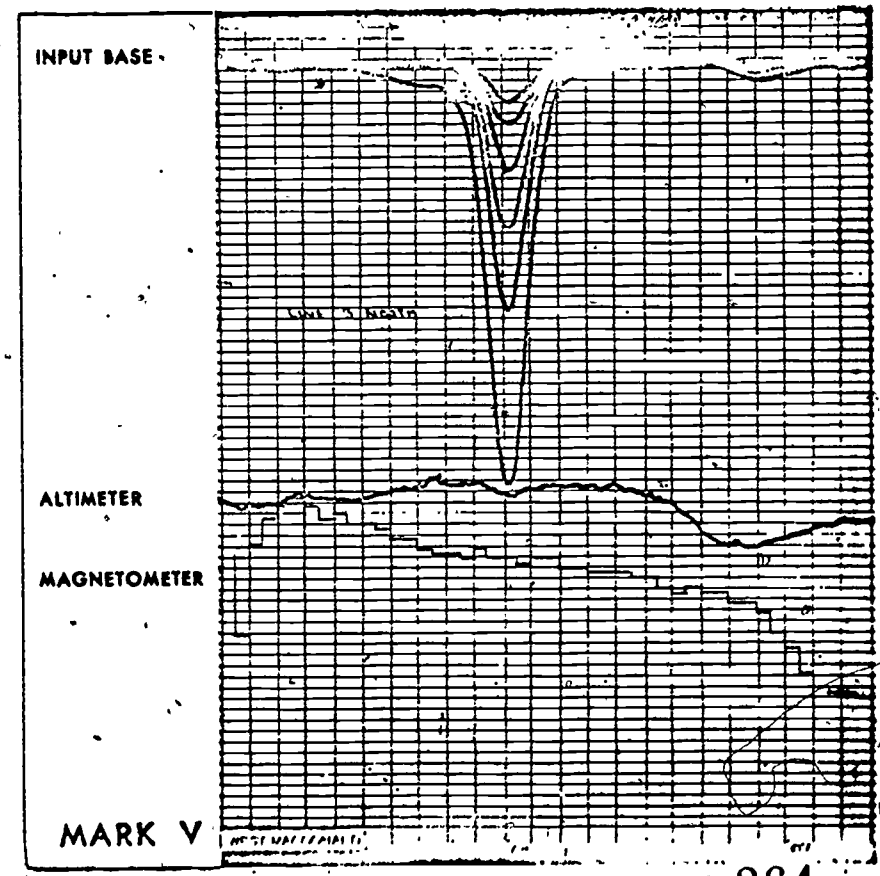

WEST MACDONALD, QUEBEC. Massive sulphide deposit, 300 ft. wide at surface with no overburden. Classic conductor on the ground, fairly homogenuous conductivity. 3.5 mg gravity anomaly, associated with body, no magnetic response.

KNOWN MASSIVE SULPHIDES

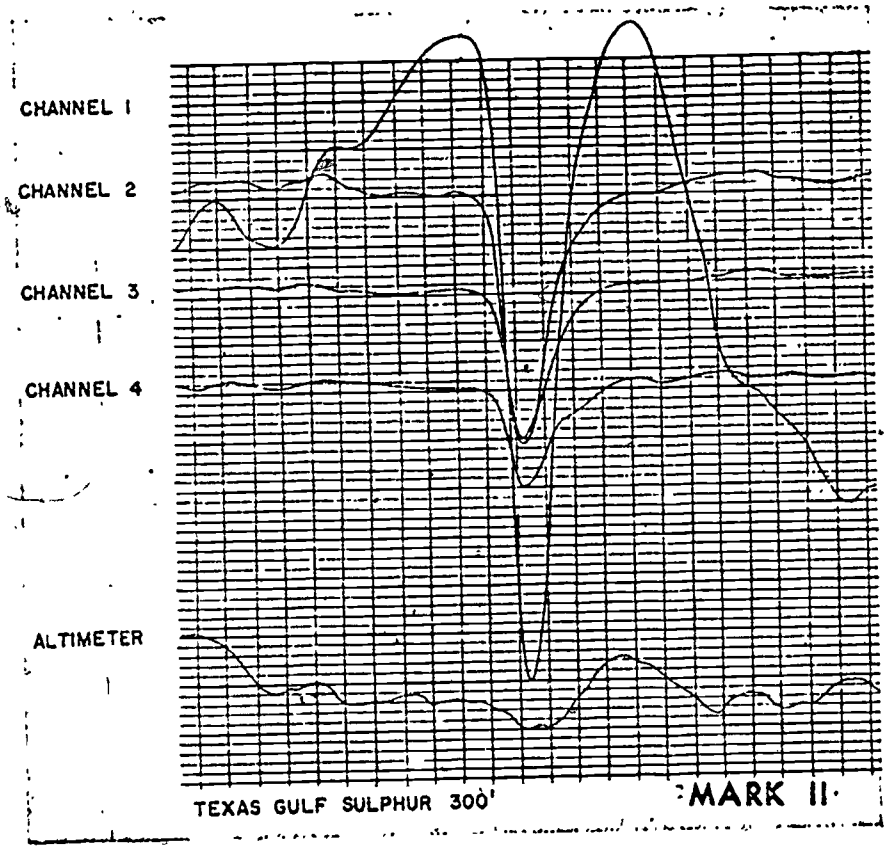

TEXAS GULF SULPHUR DEPOSIT, TIMMINS, ONTARIO. This deposit was originally found by airborne E.M. prospecting and is one of the most spectacular of geophysical finds with a value reputed to be in the vicinity of one billion dollars. A massive sulphide deposit of variable conductivity it has a strong graphitic core and a width in the order of 600 ft. Depth of burial is 35 ft. There is no magnetic association with the ore.

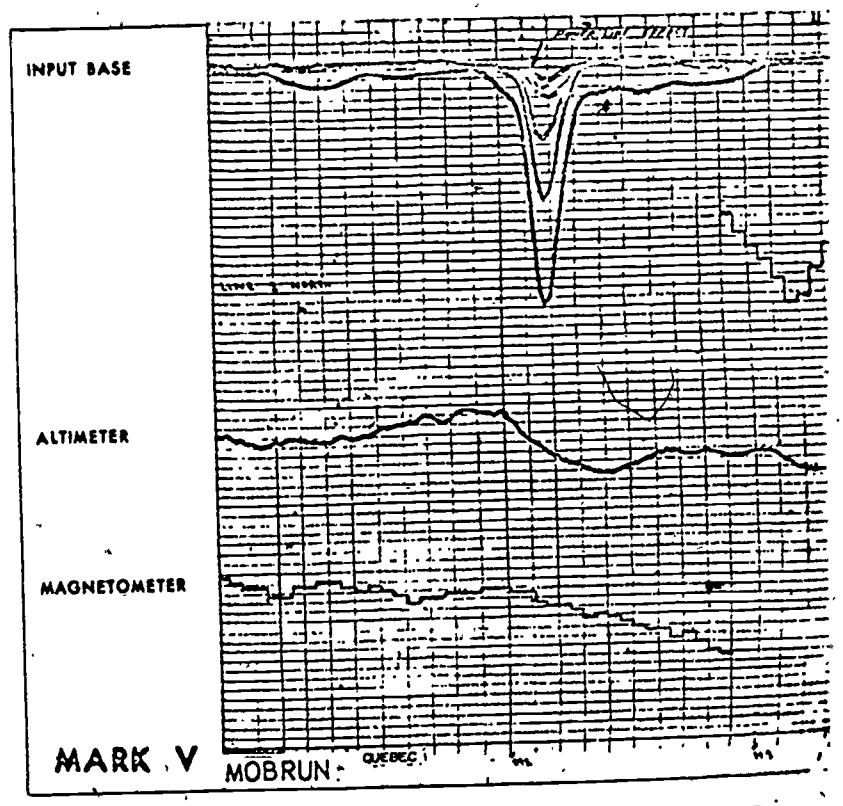

MOBRUN, NORANDA, QUEBEC. Massive sulphide deposit 100 ft. wide maximum, 1200 ft. long under clay cover 25 ft. thick. Lies under cultivated fields but angles across road with rural power-lines. Strong ground conductor and gives 1.5 mgal. gravity anomaly in local relief. No magnetic expression.

EXAMPLES OF LOW GRADE DISSEMINATED SULPHIDES (N. SWEDEN)

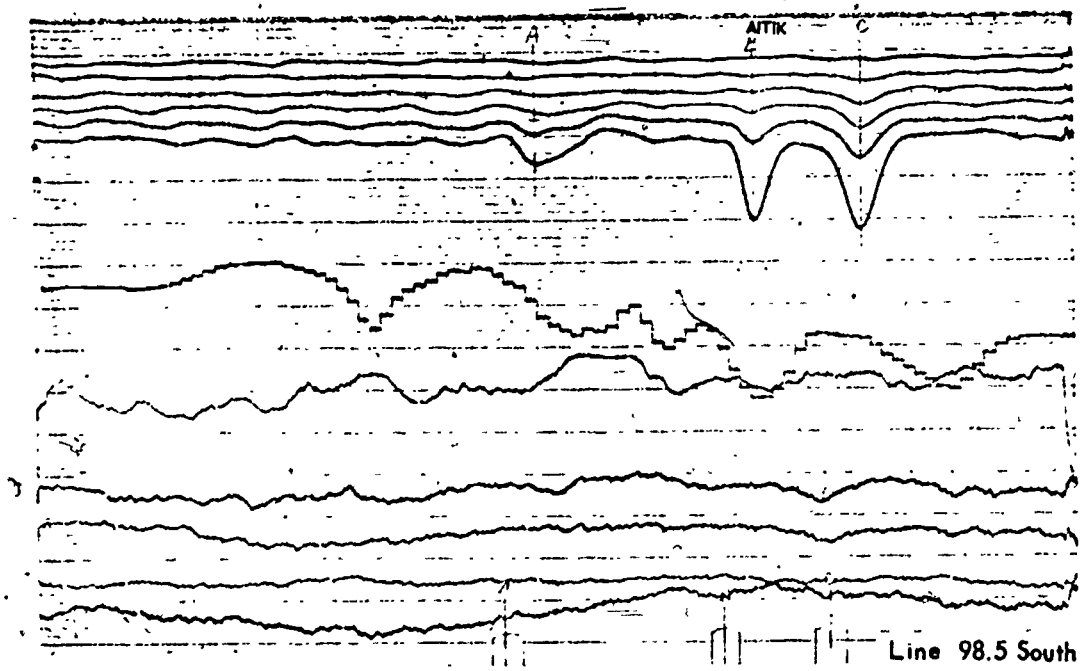

AITIK

The ore is contained within muscovite gneiss and is of the low-grade disseminated sulphide type containing only a few percent pyrite and about 1 - 2% chalcopyrite. Magnetite is also present, but there is practically no pyrrhotite.

LIIKAVARE EAST

Disseminated mineralization with about the same sulphide content as Aitik but with more pyrrhotite.

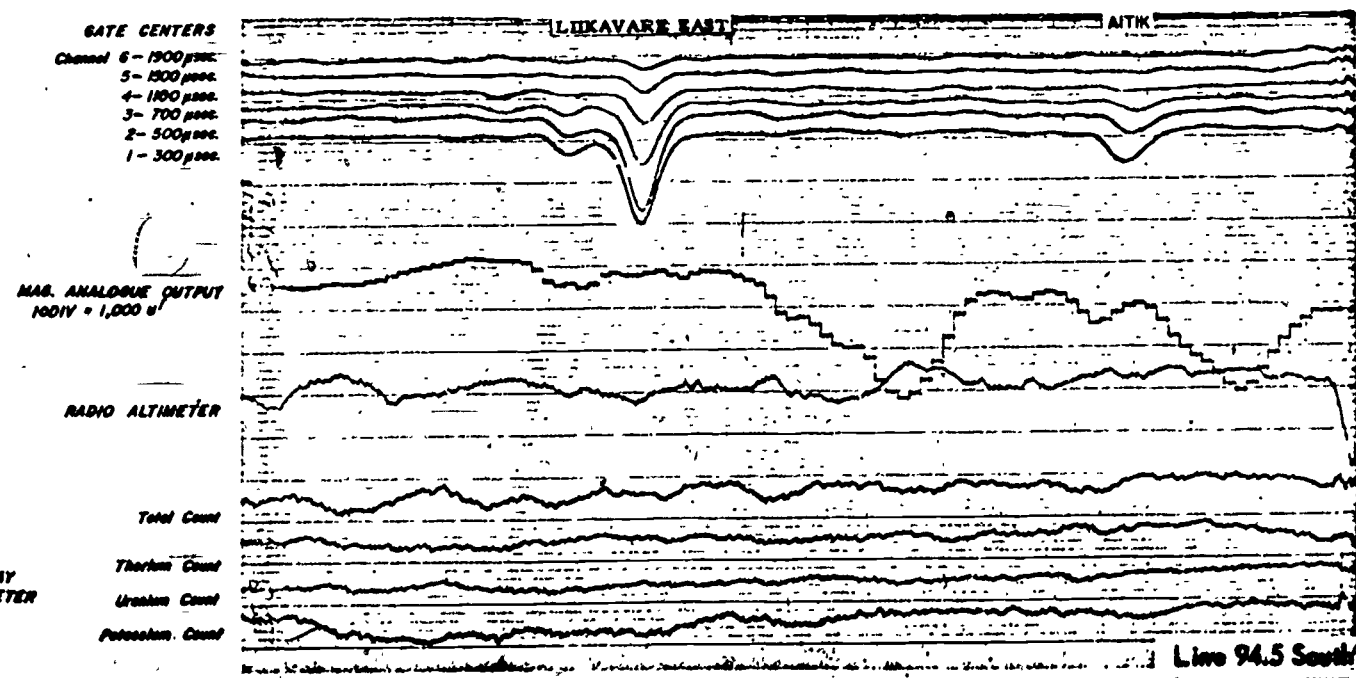

DEPTH PENETRATION WITH ALTITUDE VARIATION

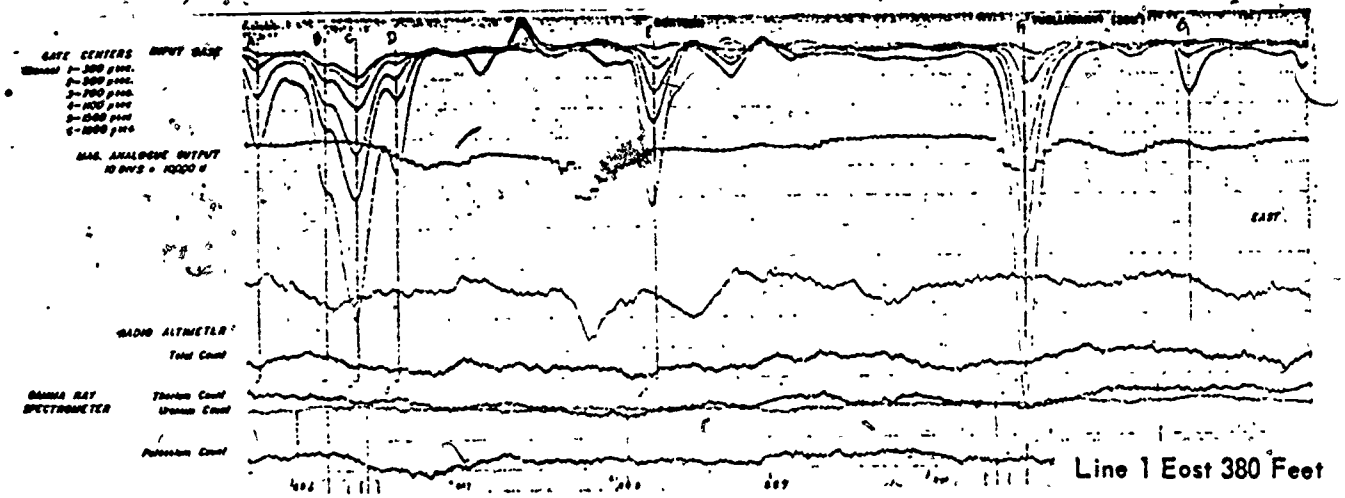

Line 1 Eost 380 Feet

REKTORN

Length 1 km. Width 20-25m. Gradual transition from West to East across strike from 100% magnetite to 100% haematite 35-40% Fe. Average 4%P.

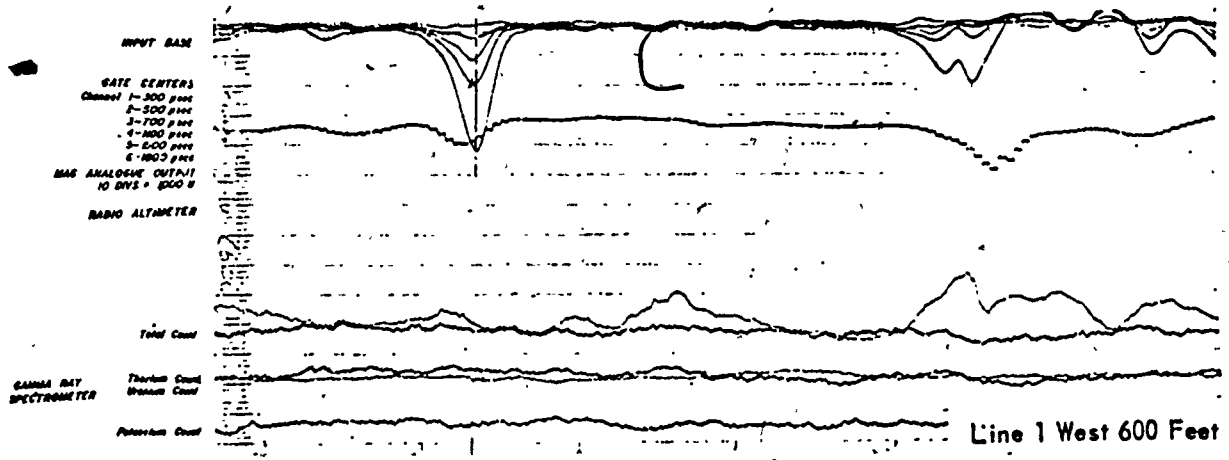

Line 1 West 600 Feet

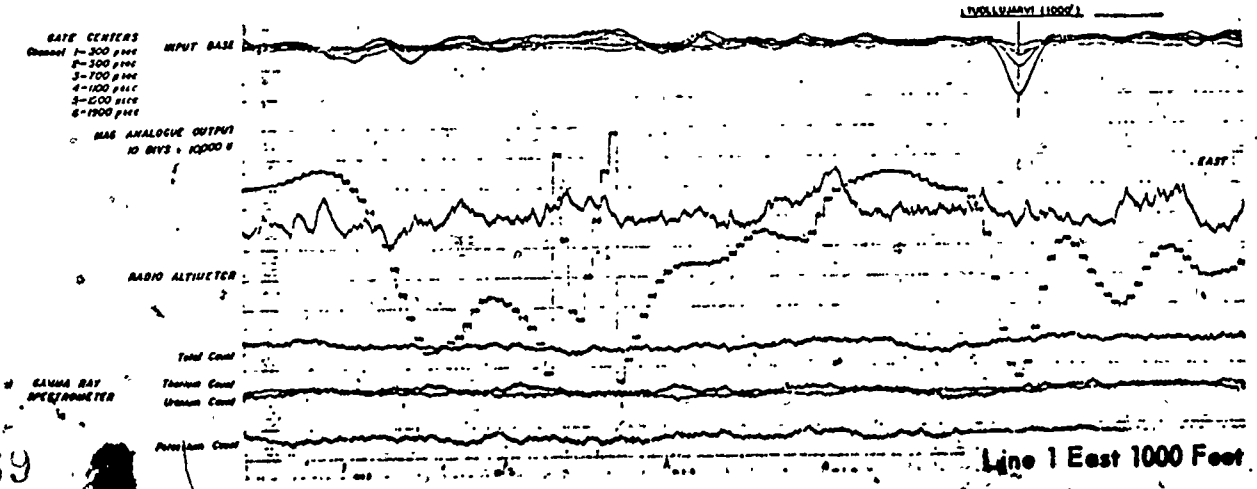

Line 1 East 1000 Feet

TUOLLUJARVI

9 drillholes drilled in 1903. Maximum ground magnetic anomaly of 10,000 gammas. Shallow drillholes indicate syenite granulite with fine veins of magnetite up to 0.2m wide, 2.5 milligal grovity anomaly.

HIGH GRADE SWEDISH IRON ORE DEPOSITS

SKARN IRON ORE

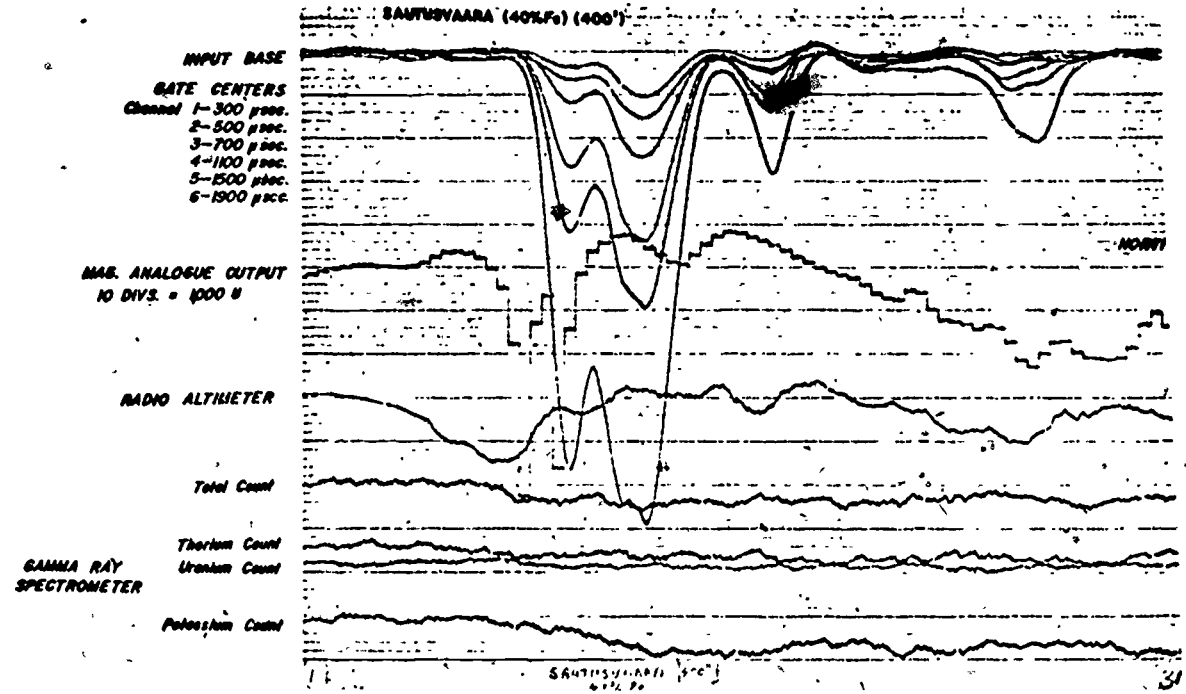

RAKKURIJOKI

1 hole only. Horizontal width of 70m. Sul-- phur content 2% due to pyrite/pyrrhotite. Average grade of ore portions better than 40%. Strike 800m. Magnetic anomaly 20,000 gammas on ground with maximum anomaly of 60,000 gammas.

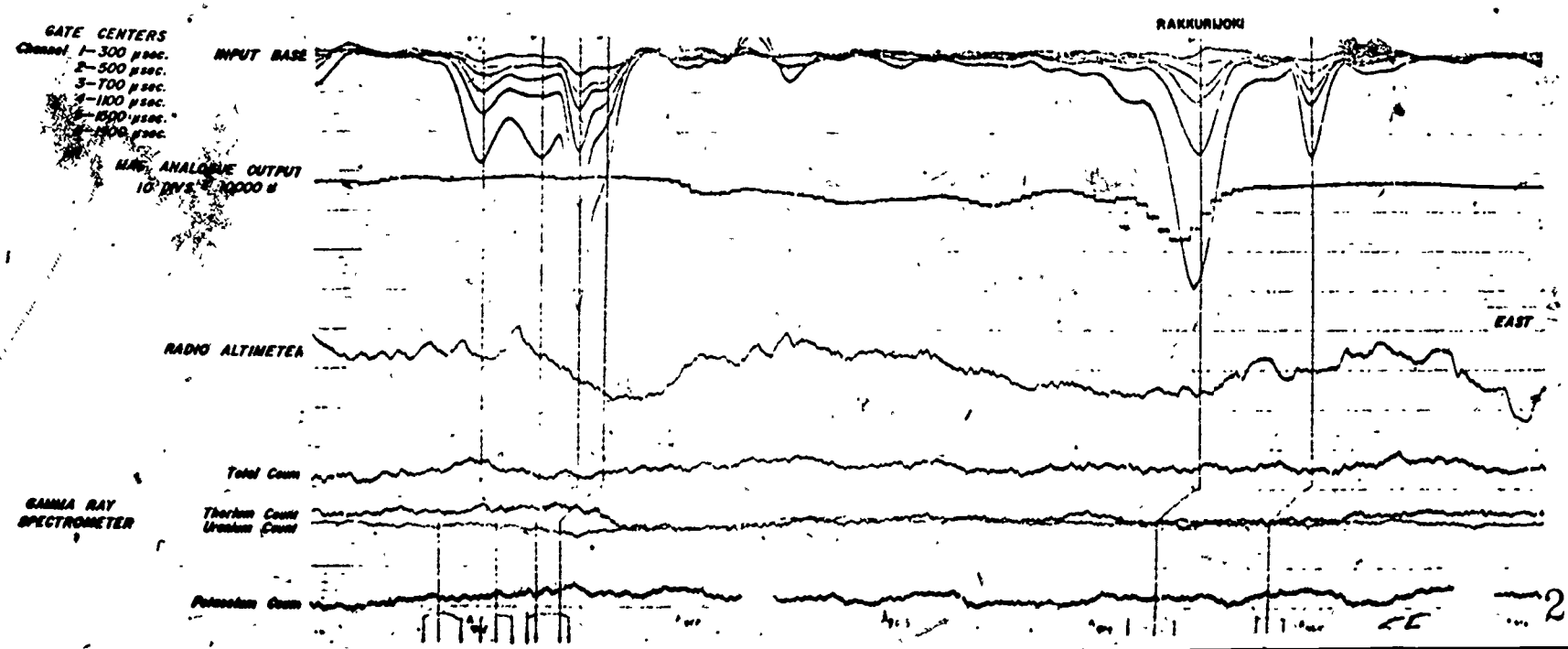

HIGH GRADE SWEDISH IRON ORE DEPOSITS

SKARN IRON ORE

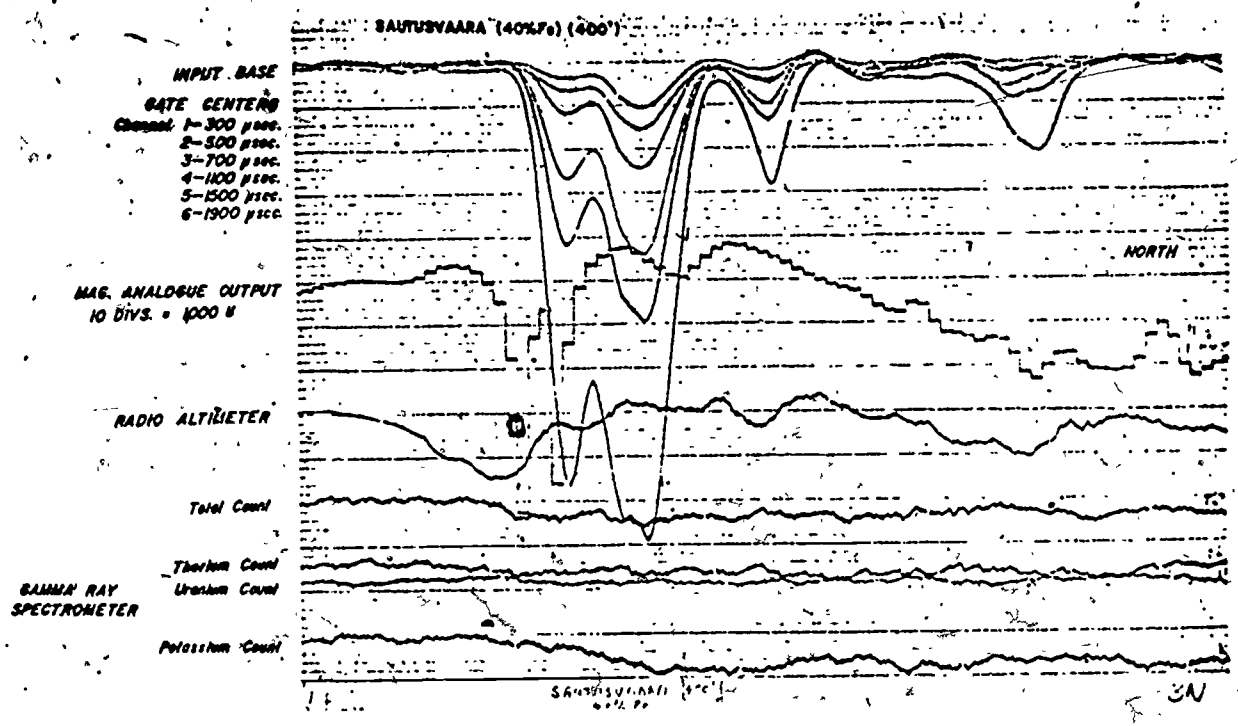

RAKKURIJOKI

1 hole only. Horizontal width of 70m. Sulphur content 2% due to pyrite/pyrrhotite. Average grade of ore portions better than 40%. Strike 800m. Magnetic anomaly 20,000 gammas on ground with maximum anomaly of 60,000 gammas.

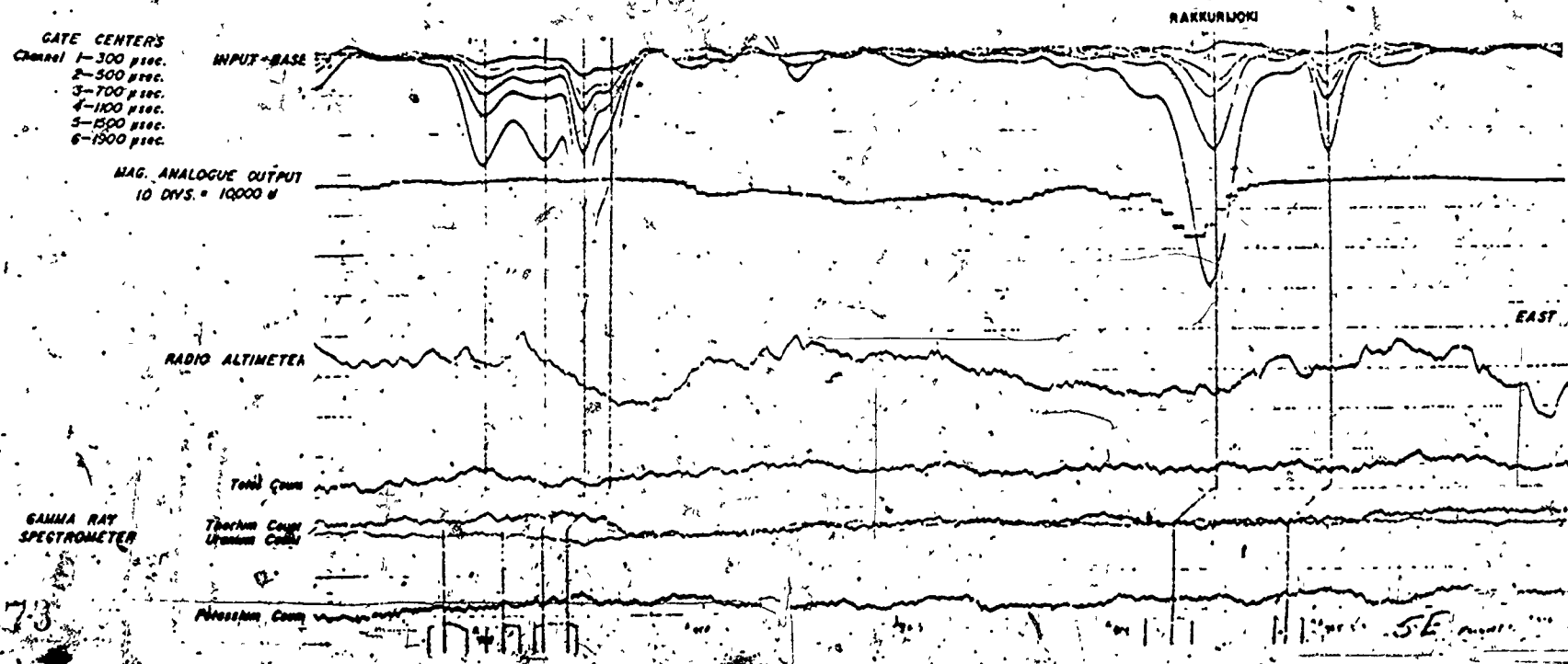

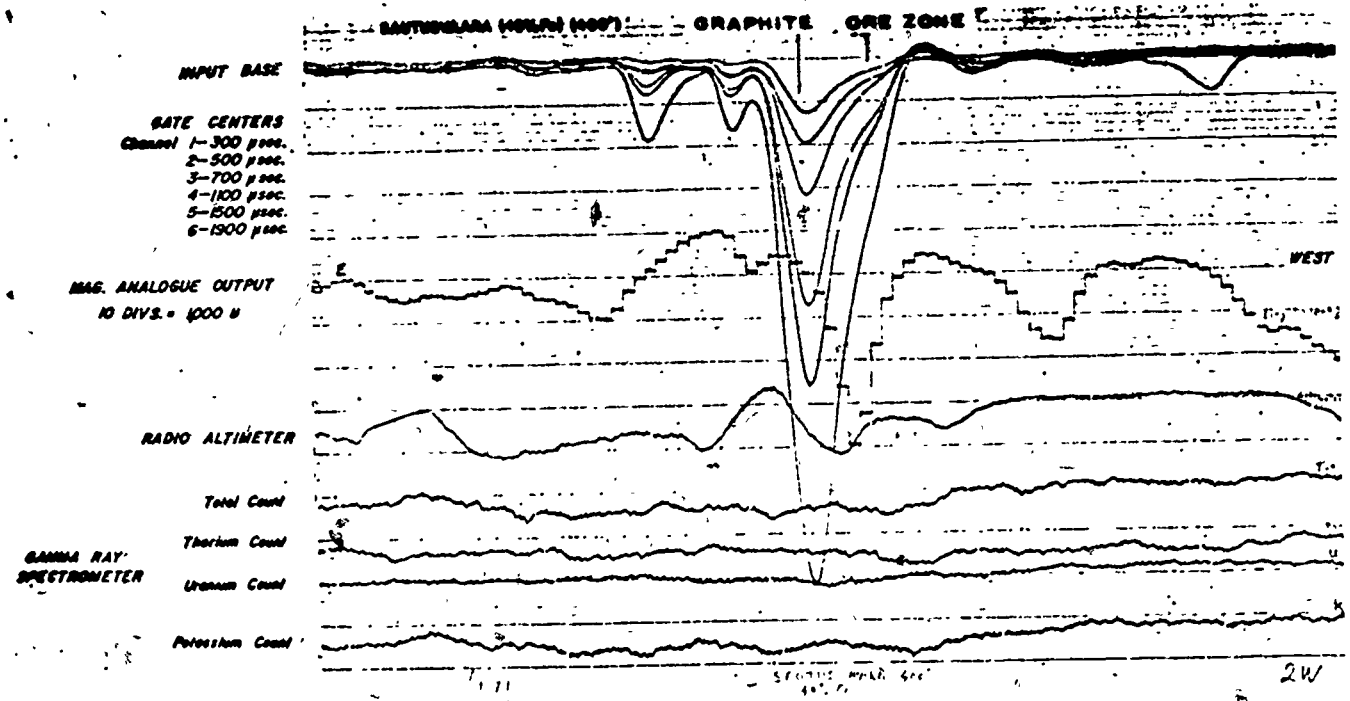

Line 2 West 400 Feet

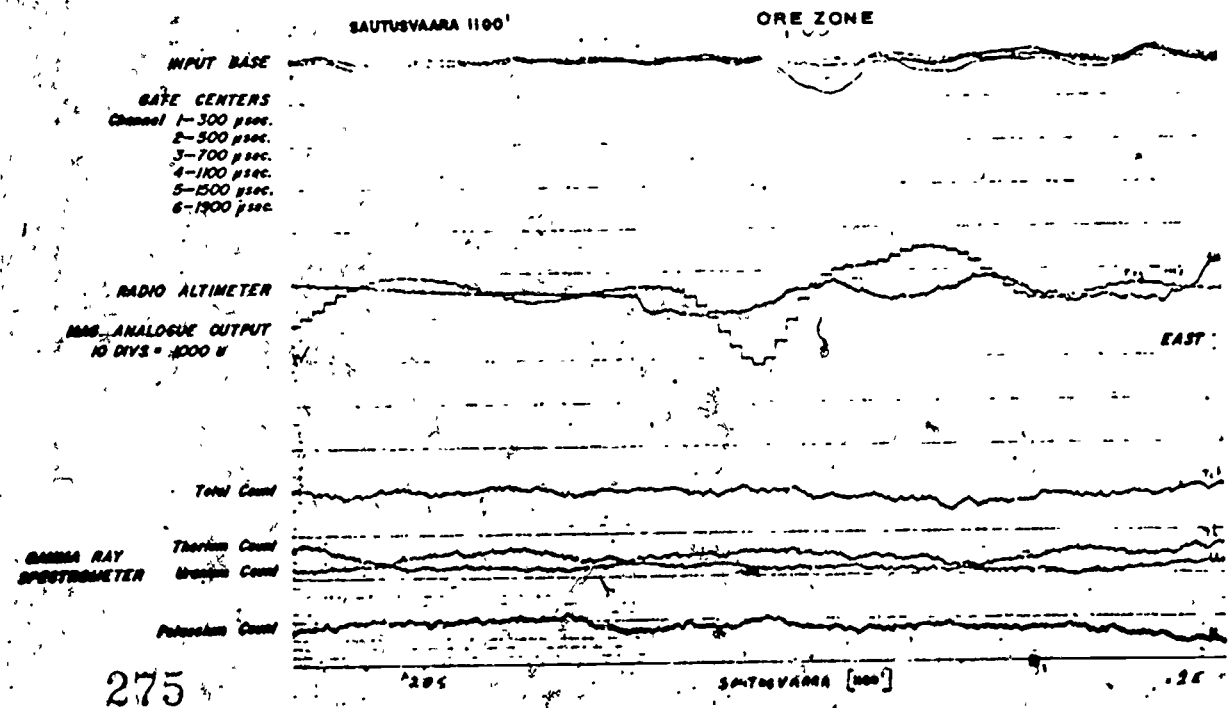

Line 2 East 1100 Feet

SAUTUSVAARA

Magnetite deposit, approximately 40% Fe. Pyrrhotite and pyrite approximately 2% S. Widths up to 150m. Possible graphite in sediments NE of ore accounting for certain adjacent bands of conductivity.

DEPTH PENETRATION WITH ALTITUDE VARIATION

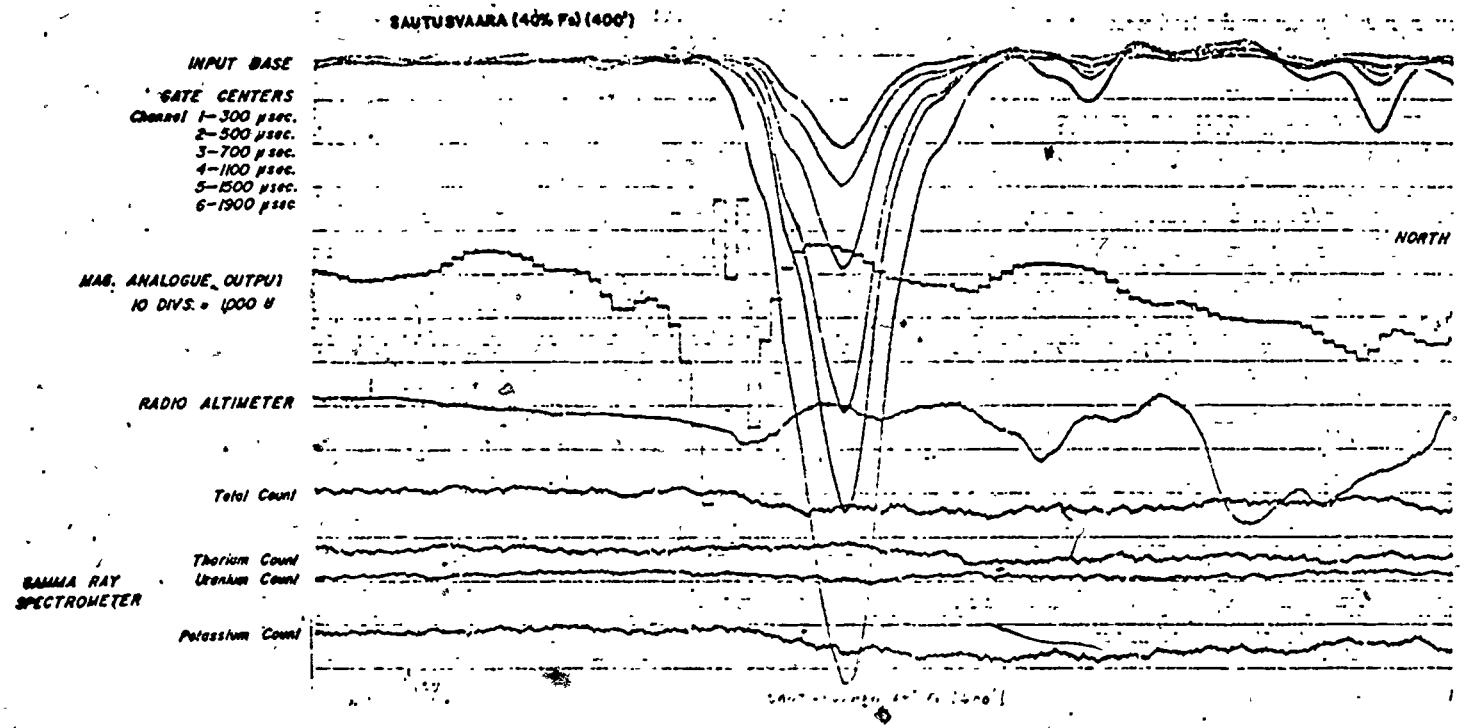

Line 1 North 400 Feet

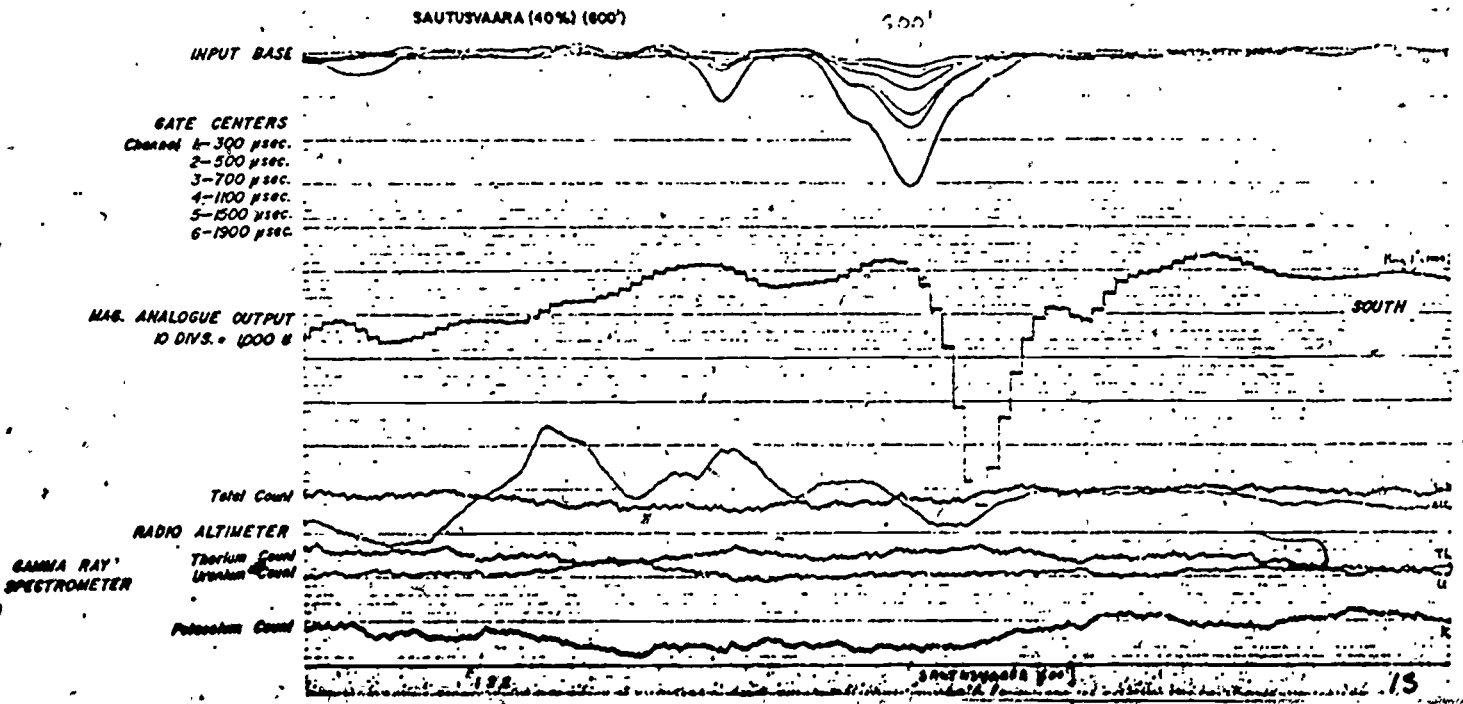

Line 1 South 600 Feet

RADIOPHASE
A NEW SYSTEM OF CONDUCTIVITY MAPPING

BY
A. R. Barringer
J. D. McNeill

ABSTRACT

A new system, called Radiophase, utilizes the signals from VLF radio stations to detect the presence of dipping conductive sheets in the ground, and to estimate the surface impedance of a homogeneous or horizontally stratified earth. Such signals propagate as ground waves for thousands of kilometers from the transmitter and penetrate to distances of hundreds of meters below the earth's surface.

The technique measures those components of the VLF horizontal magnetic and electric fields which are in phase quadrature with the vertical electric field. Both theoretical studies and modelling have demonstrated that these quadrature components are greatly influenced by the impedance of the underlying terrain.

An airborne version of the system has been flown on surveys over known mineral occurrences. Preliminary results suggest interesting correlation between the Radiophase signals and the underlying geology.

Other potential applications include the airborne mapping of water conductivity to determine the extent of pollution and estuarine salinity, and airborne mapping of ground conductivity to locate faults, shear zones, the distribution of permafrost, aquifers, etc.

1. INTRODUCTION

A number of remote sensing techniques exist for mapping terrain by means of imagery. These include photography in the ultraviolet, visible and near infrared, line scanning in the thermal infrared, and side look radar. All of these techniques record surface features, and sub-surface conditions can only be inferred by interpretation. The method we wish to describe is one which measures subtle changes in conductivity down to depths of several hundred meters, and therefore provides certain types of geological information which are unobtainable by other means. Variations in resistivity of near surface terrain is typically in the range between 10^1 ohm-meters and 10 ohm-meters, occasionally extending outside these limits at either end. It will be noted that this variation covers four decades and it is not surprising that the measurement of this parameter can be a sensitive indication of terrain conditions.

If we examine the types of geological environment associated with various conductivities, we will find that at the extremely conductive end of the scale we get desert soils and alluvium containing high concentrations of salts, and clay rich soils containing ionized clay minerals; at the other end of the conductivity spectrum we get massive unfractured rocks having low permeability and consequently only a minor water content. Between these extremes there occurs sedimentary rocks which may have a high indigenous content of salts or clay minerals which imparts an appreciable conductivity, and faulted zones which

exhibit the development of graphite or other stress minerals and channel the circulation of groundwater, thereby creating highly conductive planes in the ground. The detection of faulting and fracturing is of particular importance in considering the engineering qualities of terrain for road building, and construction activities. From the mineral prospecting point of view, faulting and fracturing forms one of the most important controls of orebody development, and the mapping of conductivity by high frequency methods enables the structural patterns of sub-surface faulting to be delineated as an aid to exploration. Simultaneous mapping by low frequency inductive electromagnetic methods enables the very high conductivity sulphide ores to be discriminated from the less conductive faults and shear zones. It is apparent that there is a wealth of information to be obtained from terrain conductivity measurements, and equipment that can map such conductivity has multiple applications in geological surveying, engineering assessments, and mineral exploration. The Radiophase technique which is described here operates in the VLF band where high sensitivities are obtained to variations in rock conductivity. It is designed to be complimentary to audio frequency inductive field electromagnetic systems which respond only to anomalously high conductivity associated with concentrations of sulphide ores in the ground.

Although stress has been laid upon the geological applications of the system, it appears also to have uses in the measurement of conductivity in saline and brackish waters. Thus it

should be possible to use the system for mapping the encroachment of the salt waters in esturine areas, a problem of considerable significance since an annual multi-million dollar marine harvest originates in these esturine areas. Similarly, problems of salt water intrusion and water pollution by effluents appears to be amenable to study by conductivity mapping. A still further application lies in the VLF mapping of conductivity contrasts associated with the distribution of permafrost in northern regions.

2. THEORY OF OPERATION

The effects of the earth on the propagation of long wave radio signals have been known since the earliest days of radio. It was not until the mid-1930s however that the theory of propagation over an earth of finite conductivity was placed on a firm basis by Norton (1). More recently the general problem of the propagation of radio waves through the shell between two concentric lossy spheres (the earth-ionosphere cavity) has been dealt with by Wait (2) who has evaluated the modes for such a cavity, particularly those excited by a vertical dipole. It can be shown from his work, and indeed it has been known for many years, that for certain cases of practical interest it is quite sufficient to consider the waves at VLF frequencies as propagating via three mechanisms, (1) multiple reflections between the earth and the ionsphere, (2) a space wave and (3) a ground wave. Figure 1 illustrates this behaviour.

Now it can be shown that, for our purposes, because of the

great distance between the transmitter and the test area, the skywave and spacewave can generally be ignored so we are left with the ground wave only. Radiophase utilizes the influence of the earth on the ground wave propagation to measure the earth's impedance.

We shall deal with two simple cases: in the first the ground wave propagates over a uniform lossy earth, which for further simplification, will be chosen as being flat. In the second case a vertical conducting sheet is assumed to be embedded in a non-conducting uniform earth. These two models, although a gross over-simplification of geophysical reality, will illustrate the main features of the Radiophase system.

2.1 Finitely Conducting Earth

It has been shown by Norton that the field propagated by a vertical dipole over a flat earth of finite conductivity can be treated as consisting of a spacewave and a groundwave. The latter propagates with a relatively low attenuation (especially at VLF frequencies) in the direction of propagation. However the field strength falls off rather rapidly with height above the earth. The passage of the wave over the earth causes small radial currents to flow in the earth and the wave front is distorted near the space-earth interface; the Poynting vector has a component directed into the earth which accounts for the power loss in that medium. Howe (3) has suggested a simple expression for establishing the reciprocal penetration depth of these currents, which is given in Equation 1.

$$P = \left[\frac{X\pi}{2}\left\{\left(1 + \frac{(\sigma \times 10^9)^2}{B^2}\right)^{\frac{1}{2}} - 1\right\}\right]^{\frac{1}{2}}$$

$X = 0.0080\ \pi^2\ f_{MHz}$

$B = 0.556 \times 10^{-6}\ \epsilon\ f_{MHz}$

ϵ = dielectric constant of the earth (1)

f_{Mlz} = frequency in Mlz

σ = earth conductivity in emu

d = depth in cm.

and $e^{-pd} = \frac{\text{current density at depth d}}{\text{current density at the surface}}$

We see that the depth of penetration is greater for low frequencies and low conductivity. This is illustrated in Table 1 which gives the penetration depth as a function of these parameters. It is seen that for low frequencies the skin depth is independent of the dielectric constant and that at 18 KHz the penetration depth is quite large; 120 meters for a ground conductivity of $\sigma = 10^{-14}$ emu which corresponds to dry rocky soil. The penetration depth decreases rapidly with conductivity becoming about 4 meters for a $\sigma = 10^{-11}$ enu, corresponding to saltwater.

Associated with these ground currents is the phenomenon of wave tilt. Near the earth's surface the electric field is no longer vertical; there is in addition a small horizontal component which is out of phase with the vertical field, producing elliptical polarization. Norton gives the following expression for the ratio of the two fields at large distances (in terms of wavelength) from the transmitter over a flat earth.

$$\frac{E_r}{E_v} = \frac{u(1 - u^2)^{\frac{1}{2}}}{1 - iku\,(1 - u^2)^{\frac{1}{2}}} \qquad (2)$$

where E_r and E_v are the horizontal and vertical field strengths respectively,

$$u^2 = \frac{1}{\epsilon + 1x}$$

ϵ = dielectric constant refered to vacuum as unity

$$x = \frac{1.8 \times 10^{18} \sigma \text{ emu}}{f_{KHz}}$$

$$k = \frac{2\pi}{\lambda}$$

z = height of receiving antenna above the ground

At nearer distances to the antenna, the ratio is not a constant with distance and it is necessary to use a more complex expression. For our purposes the above equation is entirely adequate. Furthermore, for values of z which are small compared with a free-space wavelength but still large enough to permit useful airborne prospecting, it can be shown that the ratio becomes substantially independent of z and that the horizontal field strength becomes a measure of the earth's impedance. Specifically it can be shown that at low frequencies the following relationships apply:

$$E_v = \left(\frac{\cos b}{x}\right)^{\frac{1}{2}} e^{i\left(\frac{b}{2} + \frac{\pi}{4}\right)}$$

$$E_r = \frac{\cos b}{x} e^{ib} \qquad (3)$$

$$\text{where } \tan b = \frac{\epsilon + 1}{x} << 1$$

and the ratio becomes a measure of the square root of the ground conductivity. Radiophase measures the component of E_r in phase quadrature with E_v (for reasons given below) and thus gives this quantity directly.

Should the ground be layered, i.e., have two or more strata of differing conductivities, it is possible to use two or more

frequencies to interpret the results.

2.2 Vertical Conducting Sheet Embedded in Non-Conducting Earth

Consider now the case of a vertical conducting sheet embedded in the earth as shown in Figure 2. Assuming a thin sheet for the purpose of simplicity we see that eddy currents will be induced in the sheet by the incident magnetic field but that the incident electric field will be relatively unaffected. These eddy currents will produce a secondary field which will have components both in phase and in quadrature phase with the exciting field. Their strength is a measure of the size and conductivity of the sheet. Measurements of the vector components of the secondary field will yield the strike of the conducting sheet. The response to be expected from a magnetic dipole moving over such a conductor is shown in Figure 5.

3. RADIOPHASE

Radiophase is a system which has been designed to take advantage of the series of very high power VLF radio transmitters that are now in operation (see Table 2). The present unit utilizes the signal from NAA, a station operated by the U. S. Navy in Cutler, Maine, at a frequency of 17.8 KHz. The continuous power output of about 1.0 megawatts provides a large groundwave signal many thousands of miles away.

Basically the equipment senses four variables as shown in Figure 4. The first of these is the vertical electric field strength, which is measured with a small vertical whip antenna. The phase of this signal is used to control the operation of

various synchronous detectors and the amplitude will be used to normalize other field strengths to provide impedance data. A trailing antenna is used to measure the horizontal component of the electric field. This antenna, ideally exactly located at right angles to the vertical electric field and this is null coupling to it, will in fact trail in an arc below the aircraft. Since the magnitude ratio of the two electric fields is of the order of 100 a very small amount of misalignment or curvature in the trailing antenna will result in a large pickup of the vertical field. For this reason only the quadrature phase of the horizontal electric field is recorded. Since the antenna is in maximum coupling to the horizontal electric field the aircraft attitude (pitch, etc.) will have small effect.

Finally, two horizontal magnetic dipoles are located on the aircraft so as to be orthogonal to each other. Again using the output of the vertical whip as a reference, the quadrature component of magnetic field is selected, so that the measurement is of the field induced in the conductive body rather than the primary exciting field. The output of the two dipoles can be RMS summed to give the magnitude of the resultant magnetic field and the vector direction can be determined from the knowledge of the two components, yielding the strike of the conductor. Thus the measurement is again insensitive to aircraft attitude and heading.

4. PRELIMINARY TEST RESULTS

A prototype Radiophase system has been constructed and flown

in a Beaver aircraft. Figure 5 shows the installation. The two ferrite magnetic dipoles are mounted on top of the fuselage just behind the cabin and are oriented so as to be in-line and orthogonal to the aircraft fore-and-aft axis. The six foot vertical whip is on top of the fuselage between the wings, and the trailing antenna wire, which is about 150 feet long when extended, passes from the fuselage to a ferrule located on top of the rudder. A small drag element located at the end of the wire ensures relative stability of this antenna.

Test flights were performed in the northwestern Temagami region in Ontario. The area chosen was the interface between a metadiorite still and rhyolite. Along this contact the metadiorite is intensely chloritized and base metal mineralization occurs intermittently. According to Simony (4), "three main lenticular zones of Cu-Ni-Co mineralization occur along this line, but their grade is too low to be economic. The acid volcanic band south of the sill consists of rhyolitebreccia and tuff lenses. In it, two major types of ore deposits are found; (1) lenses of high grade copper ore -- massive chalcopyrite, (2) steeply dipping, fissure filling, quartz, carbonate, chalcopyrite veins with extensive replacement of the wall rock. These are approximately parallel in strike and dip to the metadiorite-rhyolite contact".

A typical chart record for Radiophase is shown in Figure 6. It illustrates the repeatability of the system on a twice flown line measured at 200 foot altitude. It is seen that the various traces (in line and orthogonal magnetic dipoles, trailing electric

antenna) are almost identical from chart to chart. It is interesting to note that the trailing antenna is accurately picking out the islands in Lake Temagami and work is in progress to examine this relationship. Figure 7 is a composite picture of the records of eight parallel lines (shown on the map of Figure 8) spaced 1000 feet apart and flown at an altitude of 400 feet. Several interesting features are apparent. The runs were flown in a direction normal to the strike of the interface. If a vertical conductor parallel to the interface is present we should expect the in-line magnetic field dipole to be in maximum coupling and the orthogonal dipole to remain relatively inactive. That this is the case is easily seen from the chart (the two magnetic channels have approximately the same gain). The composite picture suggests that there are a number of similar features parallel to this interface since the same anomaly occurs at the same location in many of the charts. This is in agreement with the inactivity on the orthogonal trace. Furthermore, anomalies do occur in the magnetic traces over known ore deposits. It is also true that the correlation between the magnetic channels and the electric channels is not marked, once again in qualitative agreement with the simple models discussed above.

Finally, Figure 8 illustrates the benefits to be derived from using Radiophase in conjunction with other sensors. Plotted over the geological map on the left side are the contoured Radiophase results. On the right side we have added contours of the static magnetic field, plotted at 50 gamma intervals.

We see that at one location the Radiophase and magnetic highs are adjacent to each other at a geological contact and that at this location there are known ore deposits.

The picture of a basic intrusive rock (with an associated magnetic anomaly) intruding into an acid volcanic, as a potential source of mineralization is becoming rather signficant and the figure demonstrates the considerable advantage of using these two sensors simultaneously.

In summary, it appears that the correlation between the Radiophase results and the geology is signficant, and that Radiophase will become a valuable tool for geophysical and other forms of exploration. This is especially true where it is realized that it is a low cost instrument, and that the aircraft installation is quite simple and inexpensive.

BIBLIOGRAPHY

1. Norton, K. A., The Propagation of Radio Waves over the Surface of the Earth and in the Upper Atmosphere, Proc. IRE, Vol. 25; No. 9, Sept., 1937, p. 1203.

2. Wait, I. R., Introduction to the Theory of VLF Propagation, Proc. IRE, Vol. 50, No. 7, July, 1962, p. 1624.

3. Howe, G. W. O., Wireless Waves at the Earth's Surface, Wireless Engineer, Vol. 17, No. 204, Sept., 1940, p. 384.

4. Simony, P. S., Northwestern Temagami Area, Ontario Department of Mines, Geological Report No. 28, 1964, p. 26.

5. Wait, A. D., VLF Radio Engineering, Pergamon Press, 1967, pp. 123-6.

6. U. S. Naval Observatory Time Service Announcement Series 3.

TABLE 1 - PENETRATION DEPTH (METERS)

180 Khz

	$\epsilon = 5$	$\epsilon = 15$	$\epsilon = 80$
$\sigma = 10^{-15}$ emu	3760	3760	3760
10^{-14}	1187	1187(a)	1187(b)
10^{-13}	376	376	376
10^{-12}	119	119	119
10^{-11}	37.6	37.6	37.6(c)

18 Khz

10^{-15}	383	400	542
10^{-14}	119	120	124
10^{-13}	37.6	37.6	37.6
10^{-12}	11.9	11.9	11.9
10^{-11}	3.75	3.75	3.75

(a) = rocky soil (b) = fresh water (c) = salt water

10^{-11} emu = 1 mho m^{-1}

TABLE 2 - VLF STATIONS - RADIATED POWER AT LEAST 50 KW[5,6]

CALL	LOCATION	FREQUENCY (KHz)	POWER (KW)
IDO	Rome, Italy	27.2	50
LPZ	Monte Grande, Buenos Aires	23.6	72.1
NPG	Oso, Washington (after 1957)	18.6	200
NSS	Annapolis, Maryland	19.0	100
PKX	Malabar, Maya	18.98	162
ROR	Gorki, U.S.S.R.	17.0	315
UFT	Sainte Assise (near Paris)	20.7	60.8
UMS	Gorki, U.S.S.R.	17.0	315
UMS	Gorki, U.S.S.R.	15	200
NAA	Cutler, Maine	17.8	1000
NBA	Balboa, Canal Zone	24.0	150
NLK	Jim Creek, Washington	18.6	100
NPM	Lualualei, Hawaii	23.4	300
NSS	Annapolis, Maryland	21.4	85
NWC	North West Cape, Australia	15.5	1000

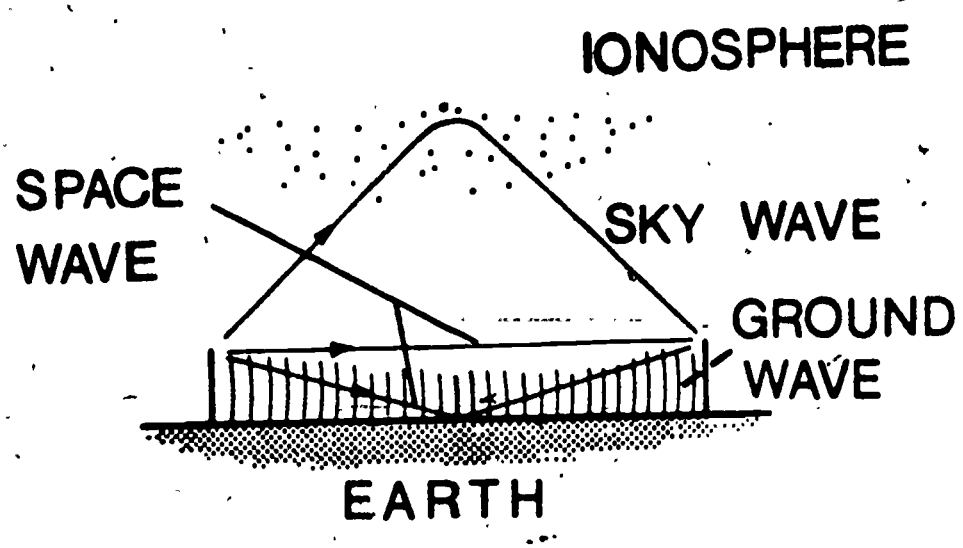

fig.1

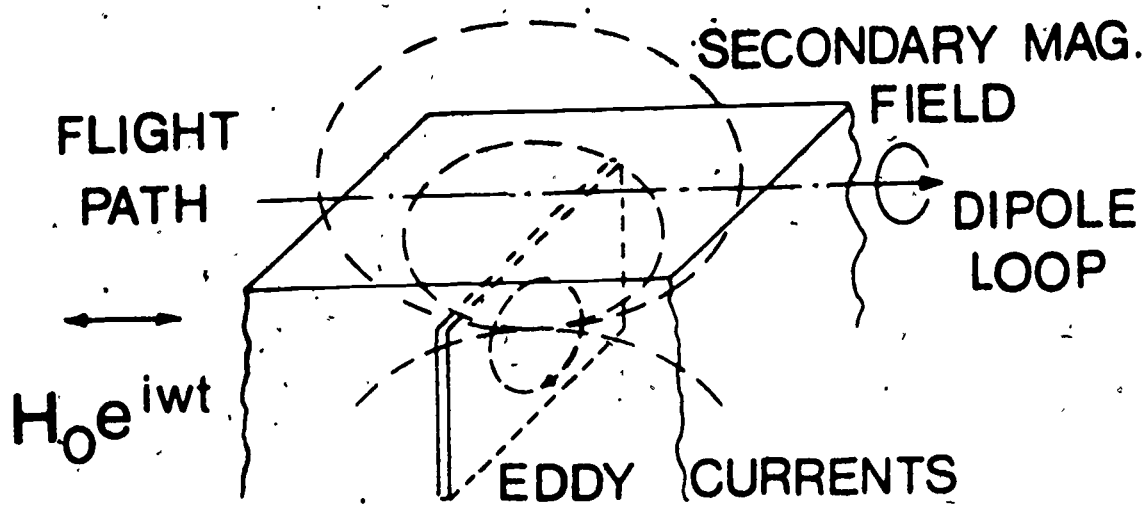

fig.2

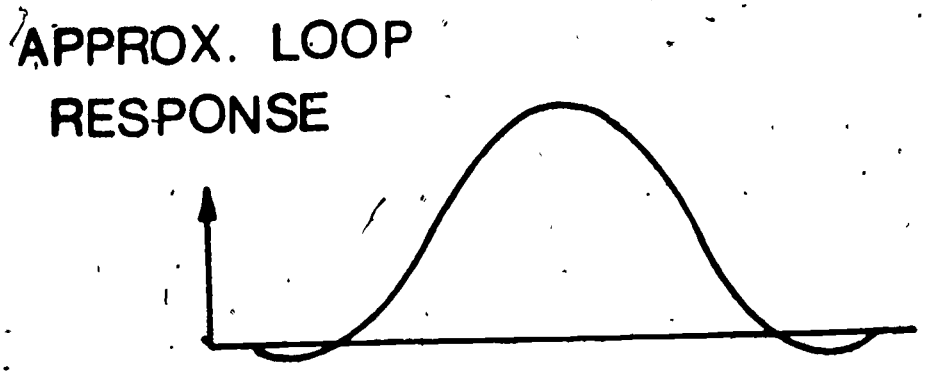

fig.3

100506

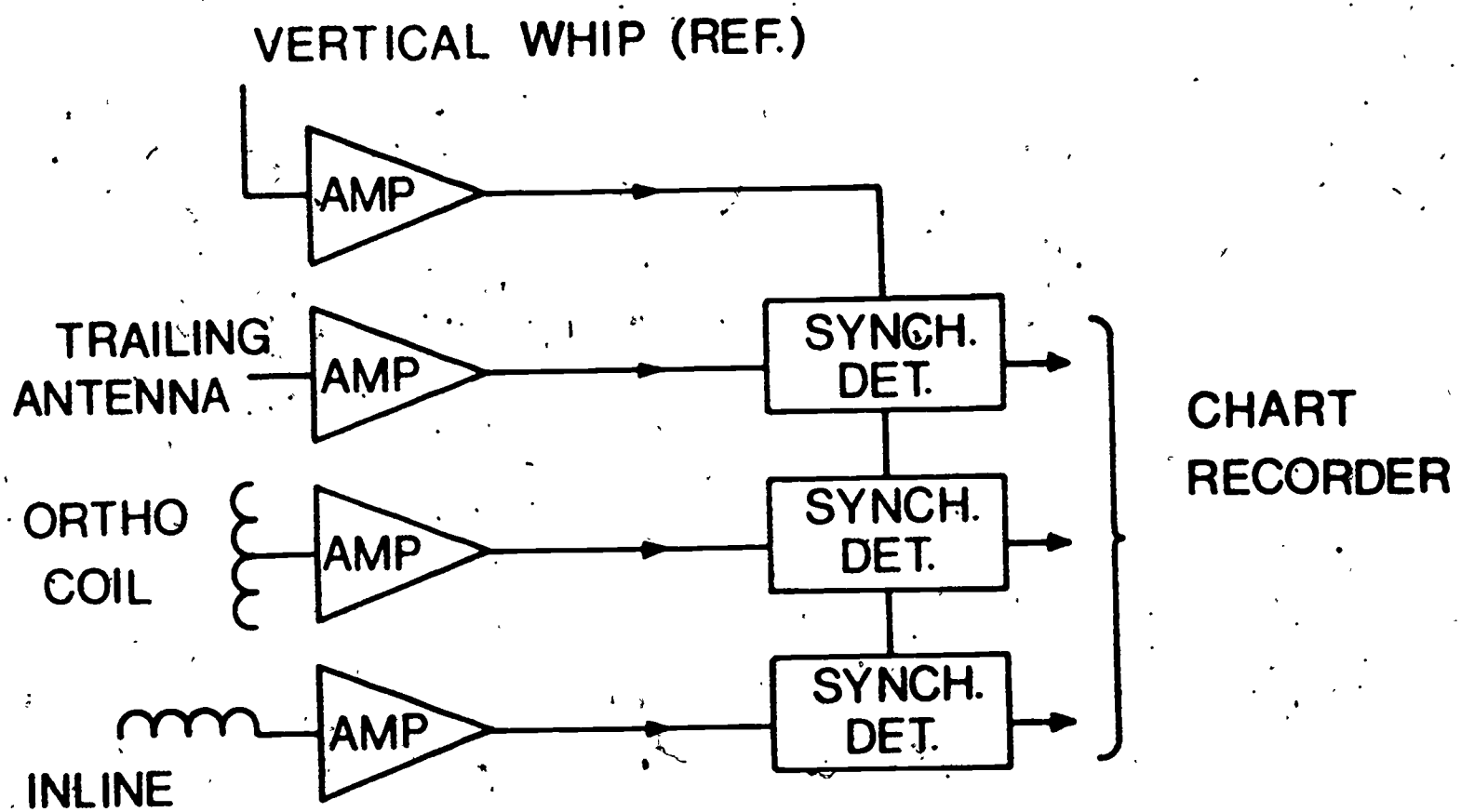

BLOCK DIAGRAM – RADIOPHASE

FIG. 4

15.0 Designing a Survey

Your author has been involved in a variety of field programs, from the Arctic to the tropics, around the world, underground, under and on the ocean and above ground. Although not all of these involved remote sensing, there are certain principles which are valid for any kind of field program. The material in this section is based on the experience mentioned above, and the experience of others.

15.1 Remote Sensing and Communications -- Past and Present

For the most part, the applicability of remote sensing techniques has been determined by cut and try methods. Radar, IR, or photographic imagery is flown, and then ground truth, comparison with maps, etc., is used to find out what was seen. There is relatively little effort made to determine the applicability of a technique from an analytical basis.

This was evident from most of the papers presented last year at the 7th International Remote Sensing Symposium.

This approach has been fostered in part by NASA and others in an attempt to sell space programs as a worthwhile business.

Very little economic analysis is done; that is, the economics of the survey techniques relative to the resource value have not been considered to any extent.

Up until World War II, communications was also a cut and try business. Low frequencies developed first, and then

were abandoned for short waves. Prediction of communications performance was almost unknown. Amateur radio operators often discovered new techniques.

During World War II, CRPL (NBS), Lincoln Laboratory (MIT), and many other government, university, and industrial laboratories brought communications from an art, to a science.

It is possible today to calculate the expected performance of a communications system at most frequencies. This includes:

(a) Atmospheric noise levels and characteristics
(b) Information rates/bandwidths
(c) Power requirements
(d) Optimum modulation systems
(e) Error rates and time availability
(f) Fading characteristics
(g) Adaptive systems
(h) Overall propagation path losses and phase shift.

Even so, much work is still going on to refine the models. This is the reason that the propagation characteristics for radar systems is relatively well known.

If remote sensing is ever to change from an art to a science, or from a researcher's plaything to an established business, we must develop models which will allow us to estimate results and economic value before the survey is performed. Progress is being made, but we still have a long way to go. We need to establish a better mix between theory and experiment to hasten advancements.

History has demonstrated that scientific advances usually follow an iterative process.

1) A theoretical advance calls for experimental verification.
2) This is followed by experimental data which shows the theory to be inadequate.
3) Then the theorists verify or question the experiment and show other possibilities.
4) Further experiments investigate the new theory and show other limitations.
5) etc.
6) etc.
7) etc.

We have had an overabundance of experimental results and too few theoretical developments.

The survey procedures which follow will meet with varying degrees of success depending on past experience and available information and theory. The simple act of following these procedures, however, will show you where further research and experience is needed.

15.2 What Are Your Survey Requirements

Before designing your survey, you must establish your requirements. For instance:

1. Do you need to establish:
   (a) Simple identification of the resource
   (b) Identification and location
   (c) Identification, location and quality, or

(d) Identification, location, quality and quantity.

2. Is it possible to detect something else and infer the presence of the desired resource.

3. Are you interested in changes with time (decades, annual, seasonal, monthly, daily, hourly).

4. Are you interested in changes with location (global, continental, regional, local, miles, 100s of feet, 10s of feet).

5. Do you need one sample or many data for statistical evaluation.

ECONOMICS

6. How much can you afford to spend on the survey.

7. What is the value of the best and worst possible results of the survey. What is the value of the natural resource.

15.3 General Procedures for Designing a Remote Sensing Survey

Now that you have determined your survey requirements, you can begin to design the survey. The nature of your survey will determine the applicability of the following procedures.

1). Establish the characteristics of the target:

Size

Shape

Orientation

Individual and group characteristics

Conductivity

Dielectric constant

Magnetic permeability

Chemical characteristics (elements present, ions present)

Physical characteristics (crystal structure, surface roughness, color, reflectance, emissivity, and temperature)

It is important to remember that many of the above characteristics will vary with season, time of day, specific location, and frequency.

2) Establish the characteristics of background materials.

The same general properties given above should be considered for background materials.

The purpose, of course, is to determine to what extent other items might be confused with the target, and to what extent the target may be obscured by background.

3) Initial selection of frequency and technique

(a) Unless you are going to design, or have designed, a unique system, you will probably not have much choice of frequency, e.g., Westinghouse SLR is Ka band and cannot be effectively changed. You may, of course, select another company or technique.

4) Weather and pollution may present problems at some locations. High energy absorption may alter your initial choice of frequency.

5) Determine the best formats for the data

Film

(a) Good for images

(b) Limited dynamic range 30 dB

(c) Difficult to convert to digital format for automatic analysis

(d) Ideal for identifying large regional trends, etc.

(e) Will aid in precomputer data handling.

Strip Chart

(a) Good for in-field visual analysis

(b) Dynamic range 30 dB

(c) Inexpensive

(d) Can be digitized.

Analog Tape

(a) Cheaper than digital tape

(b) Important if playback of original signal is desired

(c) Dynamic range 40 dB without gain ranging

(d) May be desirable for wide bandwidth, wide dynamic range data.

Magnetic Tape

(a) Best for computer analysis

(b) Wide dynamic range

(c) Multiplexing will provide many channels of data

(d) Most expensive

Punched Paper Tape

(a) Good for computer analysis

(b) Good for small amounts of data

(c) Inexpensive

(d) Good dynamic range -- multiplexing possible

(e) More reliable than magnetic tape (sometimes).

In-Field Computer Processing

(a) Gives results in-field

(b) Reduces quantity of data stored

(c) Limits further data analysis

6) Consider the importance of a visual record or preliminary processing of data in the field.

It is a very bad policy to take lots of data on digital or analog magnetic tape, or on film, with no indication in the field of the results obtained. The addition of a strip chart recorder to a digital system may be very important.

7) Scheduling the survey

You should consider:

(a) Seasonal effects (weather, vegetation, temperature, sun angle).

(b) Time of day (sun angle, weather, temperature).

(c) Aircraft availability (input system scheduled months or even years ahead).

(d) Ground truth requirements

8) Flight requirements

(a) Altitude

(b) Weight and space requirements

(c) Position location (photographs okay but may be very time consuming for analysis. Some automatic systems highly desirable; many systems to choose from.

9) Ground truth

(a) Pre-flight

To better establish survey requirements.

(b) Post-flight

To obtain absolute values. For followup, verification, more detailed analysis, sample collection, etc.

(c) Must be done during or very soon after flight to minimize changes that may occur.

(d) Be careful that localized measurements or samples are truly representative of areal measurement results.

10) Interpretation

(a) Pre-survey

What tools are available. What will you have to develop. Are consultants available.

(b) Post-survey

Hire experts. Keep flexible.

Results may not be as expected, interpretation methods may have to be different than planned.

COLLEGE OF FORESTRY AND NATURAL RESOURCES

THE DEPARTMENT OF WATERSHED SCIENCE
was formulated in 1970 to provide a framework for the undergraduate, graduate, and research investigation of the principles of watershed management, bioclimatology, and remote sensing of natural resources.

COLORADO STATE UNIVERSITY
FORT COLLINS, COLORADO